



**Antenna Design and Signal Processing for Mechanical
FMCW Coastal Surveillance Radar Systems**

Jasni E. Basuki

Supervisor:

Professor P. Brennan

A thesis submitted for the degree of

Doctor of Philosophy

Department of Electronic & Electrical Engineering

University College London (UCL)

2018

I, Jasni Basuki, confirm that the work presented in this thesis is my own. Where information has been derived from other sources, I confirm that this has been indicated in the thesis.

Abstract

The demand for highly sophisticated radar systems to be implemented along the coastal waters of the Strait of Malacca for the surveillance and tracking of vessels that travels through this narrow Strait has risen rapidly over the last few decades. Along with the technological advancements in radar systems, the increased demand is in response to the success that radars have introduced in significantly reducing some of the biggest problems contributed from security and weather condition perspectives. The existing radars implemented by Indonesian authorities to fulfil the surveillance requirements of the Strait mainly comprises of electronic scanning systems. Nonetheless, several allocated radar sites along the Strait inevitably lacks the basic infrastructure and accessibility required to install more complex systems (i.e. electronic scanning radars) that are prone to higher maintenance. This have favoured authorities to opt for the use of mechanical scanning radars, which, unlike phased array systems, are simpler, less complex, and significantly more affordable systems.

The resolution performance alongside the accuracy of the positional information of a detected target provided by the radar is highly dependent on the angular resolution of the antenna. For mechanically scanning radars, a highly directional beam is commonly produced by employing conventional parabolic reflector antennas. Reflector antennas are a popular choice for surveillance and tracking applications as it is known for producing beams with very high gain and narrow beamwidths in both planes. However, this is usually achieved by employing an undesirably large reflector, which tends to significantly increase the cost of the radar system, and most importantly its size and weight, which is critical especially for applications that highly values compact and mobile systems. To overcome this issue faced in many similar situations, several angle measurement techniques have been introduced to improve the detection performance of radars without increasing the physical size of the antenna, with the most notable and highly successful one being monopulse technique.

This research project proposes a model of a reflector antenna design for a mechanical scanning radar that is suitable to provide coastal surveillance and monitoring of vessels and low flying objects. The objective of the antenna design is to significantly improve the resolution and accuracy for target detection without utilizing a larger dish, but instead through the

implementation of amplitude monopulse and a novel post-detection processing technique that allows for the design of a more compact and cost-effective antenna system. The proposed reflector antenna system that achieves these objectives comprises of a dual-horn feed and a vertically truncated reflector of an optimal aperture shape and dimension to create a pair of simultaneous overlapping fan-shaped beams that is narrow in azimuth and several times wider in elevation. The design of the monopulse feed is modelled and simulated on a CEM tool (CST) to evaluate the monopulse patterns produced in the horizontal plane of the radar, which are optimized towards the requirements of the application. In addition, this thesis introduces a novel post-detection signal processing technique that uses priori information of the antenna response pattern to offer a substantial enhancement on the resolution and clutter resilience of any new or existing radar antenna system at a very low cost, which is especially likely to make a significant contribution to the safety at sea.

In addition to limiting the size of the antenna as much as possible while fulfilling the requirements of the application in hand, employing the proposed antenna system along the coastal shores of the Strait of Malacca would largely prioritize on keeping the effective weight and cost of the antenna to a minimum. This is achieved by manufacturing the reflector through 3D printing technology and coating its surface with a copper compound spray to achieve the properties of a metal. A prototype of the reflector antenna is manufactured accordingly using the proposed method of fabrication in order to provide an assessment of the practical antenna performance. The radiation properties of the antenna pattern are measured in an outdoor range test facility, and the measurement results allows for an accurate validation of the electromagnetic (EM) simulations of the corresponding antenna design obtained on CST. Finally, in order to assess the enhancing effect of the proposed signal processing technique on the resolution performance of an existing antenna, MATLAB based codes have been developed to demonstrate the technique on several simulated far-field patterns of antennas with common line source distributions before it is applied on the sum pattern output of the monopulse antenna designed in this project.

Impact Statement

The knowledge that can be obtained from the in-depth analysis of the research findings presented in this thesis has brought beneficial use towards areas that are inside and outside of academia. The benefits inside the academic field and within the research area is directed towards the proposed methodologies introduced in the thesis, which can lead towards an area of further research, and the method of research undertaken in this project, which is also likely to be an effective approach in other similar research areas. This project proposes several novel methodologies and techniques that would also yield significant benefits outside academia once implemented successfully. These benefits could be observed through the impact it offers on increasing the capabilities of governmental organizations in fulfilling the requirements of commercial activities, coastal surveillance and maritime security.

In conjunction with the demand and funding from private and public sectors, the impact of this research, which is likely to be the most significant on the field of radar surveillance, on the surveillance of pre-determined territorial waters of Indonesia could be realized within a short period of time, or in phases that could span over several years, ranging from a regional, national or international level. The impact could be brought about most effectively through engaging with appropriate governmental organizations, influencing ministers and collaboration with companies within the radar industry.

Acknowledgements

I would like to express my sincere gratitude to my highly distinguished supervisor, Professor Paul Brennan of the UCL Electronic and Electrical Engineering Department, who have given me outstanding advice and guidance throughout the research process. I have benefited greatly from his exceptional depth of knowledge, extensive experience on my research subject and constructive feedback given to me. His continuous support, motivation and kindness have made it more possible for me to successfully complete this multidisciplinary research project.

I would like to thank Dave Patrick in helping me set the groundwork in the first steps of experimenting and in the development of my radar. In addition, I am indebted to Ben Irvine for providing me with excellent materials and valuable help in the fabrication of my antenna system. Furthermore, I am particularly thankful to Luke Steve who has assisted me in performing the antenna measurements during my visit to QinetiQ's range facility in Funtington.

I am tremendously grateful for the support and directives given by the Indonesian Navy and in particular, Admiral Agung Pramono, for his ideas, guidance and providing me with the required data related to the site of interest for the study of my research project.

Lastly, I am hugely thankful to my parents, sisters and loved ones for their boundless support, perseverance and encouragements that have made the completion and write-up of this research project possible. Especially to my mother, who have always encouraged me to maximize my fullest potential and capabilities.

Contents

1. Introduction	1
1.1 Overview	1
1.1.1 Economic Importance	2
1.1.2 Pertaining Issues	2
1.1.3 The use of Radar Technology to Fulfil Strait Requirements	4
1.1.4 Proposed Alternatives to Existing Radar Systems	7
1.2 Scope of Research	9
1.3 Thesis Layout	10
1.4 Contributions to the Research Field	12
1.5 Author's Publications	13
2. Background and Literature Review	14
2.1 Coastal Surveillance Radars in Strait of Malacca	14
2.2 Mechanical Scanning Reflector Antenna Systems	18
2.2.1 Angle Measurement Techniques for Reflector Antennas	19
2.2.1.1 Sequential Lobing	24
2.2.1.2 Conical Scan	26
2.2.1.3 Monopulse Technique	30
2.2.2 Monopulse Feed Systems	41
2.3 Signal Processing Methods	49
3. Radar Principles	56
3.1 Friis and Radar Equation	56
3.1.1 Friis Equation	56
3.1.2 Radar Equation	57
3.2 Antenna Parameters	59
3.2.1 Field Regions	59

3.2.1.1	The Reactive Near-field Region	59
3.2.1.2	The Radiating Near-field (Fresnel) Region	59
3.2.1.3	The Radiating Far-field (Fraunhofer) Region	60
3.2.2	Radiation Pattern	61
3.2.3	Radiation Power	62
3.2.4	Impedance and Total Efficiency	63
3.2.5	Gain, Directivity and Radiation Efficiency	67
3.2.6	Polarization	67
3.2.7	Bandwidth	69
3.2.8	Noise Floor	70
3.3	Waveguide Theory	70
3.3.1	Phase Velocity of EM Waves in a Waveguide	71
3.3.2	Cut-off Frequency	71
3.3.3	Modes of Propagation in Rectangular Waveguides	73
3.3.4	Impedance in Rectangular Waveguides	75
3.4	Horn Antennas	76
3.4.1	Sectoral Horns	77
3.4.2	Pyramidal Horn	82
3.5	Coastal Surveillance Radars	84
3.5.1	Phased Array Antenna (Electronic scanning systems)	84
3.5.1.1	Beam Shaping and Steering Techniques	84
3.5.1.2	Grating Lobes	88
3.5.2	Parabolic Reflector Antenna (Mechanical scanning systems)	88
3.5.2.1	Focusing and Collimation	89
3.5.2.2	Reflector Antenna Properties	93
3.5.2.3	Reflector Illumination	97
3.5.2.4	Offset Parabolic Reflector Antenna	101
3.6	Monopulse Processing and Circuitry of 2D Monopulse Systems	104
3.6.1	Devices for Forming Sum and Difference Signals	105
3.6.1.1	Hybrid Junction	106
3.6.1.2	Digital Signal Processing	107
3.6.2	Sum and Difference Channel of a One-coordinate System	108

3.7	Summary	109
4.	Modelling and Simulation of Reflector Antenna System	110
4.1	Radar Parameters	111
4.2	Optimization of Adapter RF Performance	121
4.3	Modelling of E-plane Sectoral Horn Antenna	130
4.4	Reflector Antenna Design	133
4.4.1	Type of Reflector used and Approximated Reflector Width	134
4.4.2	Reflector Design per Specified Width and Feed Radiation Pattern	135
4.4.3	Feed Positioning Relative to the Focus of Reflector	140
4.4.4	Optimization of Illumination Taper to Maximize Antenna Gain	145
4.5	Theoretical and Simulation Results of the Antenna Radiation Properties	147
4.5.1	Theoretical Results	147
4.5.2	Comparison of Theoretical and Simulation Results	148
4.6	Summary	149
5.	Radar Scanning and Imaging Strategy	151
5.1	Amplitude Monopulse Reflector Antenna.....	152
5.1.1	Amplitude Monopulse in a Single Plane	153
5.1.2	Beam Deviation Factor for Parabolic Reflectors of Useful Shapes	155
5.1.2.1	Producing Off-axis Beam by Lateral Displacement of the Feed	160
5.1.3	Modelling of Dual-horn Feed for a 2D Monopulse System	163
5.1.3.1	Optimization of Feed Tilt	166
5.2	Signal Processing Technique.....	182
5.2.1	Pattern Selective Differential Processing	183
5.2.1.1	Aperture Theory for a One-dimensional (Linear) Aperture	184
5.2.1.2	Principles and Concept of PSDP	187
5.2.1.3	Effect of Overlap on Enhancement in Resolution Performance	192
5.2.1.4	Resolution Enhancement on Common Aperture Distributions	196
5.2.1.5	Effect of Sampling Interval on SNR of Received Signal	198
5.2.1.6	Optimum Beam Pattern	202
5.2.2	Sidelobe Reduction Technique	203
5.2.2.1	Issues with Sidelobes of a Point-target Response	204

5.2.2.2	Principles and Concept of SRT	206
5.2.2.3	Effect of n Number of Pulses on the Extent of Sidelobe Reduction	209
5.2.3	Application of PSDP to Surveillance Radar	212
5.2.4	Application of PSDP on Sum Pattern of Monopulse Antenna	214
5.3	Summary	218
6.	Experimental Measurements and Discussion of Results	219
6.1	Measurement and Validation of Horn Antenna Performance	219
6.1.1	Vector Network Analyzer	220
6.1.1.1	Sources of Measurement Errors	221
6.1.1.2	VNA Calibration	224
6.1.2	Measurement Results	226
6.2	Reflector Construction	231
6.2.1	Alternative Methods of Construction for Medium-sized Reflector	233
6.2.1.1	3D Printing Technology for Reflector Fabrication	236
6.2.2	Surface Accuracy Requirements	242
6.2.3	Feed and Reflector Support-frame and Antenna Assembly	244
6.3	Antenna Under Test (AUT) Far-field Pattern Measurements	248
6.3.1	Antenna Characterization Range (X-band)	248
6.3.2	Antenna Far-field Pattern Measurements	252
6.3.2.1	Measurement Plan and Results	252
6.3.2.2	Discrepancy Between Measurement and Simulation Results	267
6.4	Summary	267
7.	Conclusions and Future Work	269
7.1	Conclusions	270
7.2	Future Work	271
7.2.1	Field Trials of the Developed Radar System	271
7.2.2	Optimizing Scan Rate of Mechanical Scanning Radar	271
7.2.3	Pattern Selective Differential Processing in RF Hardware	273

Appendices	282
A Radar Transmit Power Budget Analysis	282
B MATLAB Based Algorithm of the Signal Processing Techniques	284
B.1 Pattern Selective Differential Processing	284
B.2 Sidelobe Reduction Technique	286
C Data Sheets	288
C.1 ValuFrame®	288
C.2 STRASYS® - ABS <i>plus</i> -P430	289
C.3 RSPRO® - Silver Plated Copper Compound (RS 247-4251)	291

List of Figures

1-1.	Geographical location of the Strait of Malacca [2]	1
1-2.	Candidate locations for radar sites surrounding the Strait of Malacca [18]	6
1-3.	The Arthur satellite at Goonhilly Earth Station [20]	9
2-1.	Surveillance radars using phased array and parabolic reflector antenna in Iran [21]	16
2-2.	Sea clutter on a PPI-scope display [27]	20
2-3.	Illustration of angular separation or distance, S_A , between two targets [27].....	21
2-4.	Two targets within a single beamwidth [24]	22
2-5.	Sequential lobing (a) Target is located on track axis. (b) Target is off track axis [24]	25
2-6.	Conical scanning beam [24]	26
2-7.	Simplified conical scan radar system [24]	27
2-8.	Received AM signal produced when target is on the boresight axis [24]	28
2-9.	Received AM signal produced when target is off the boresight axis [24]	29
2-10.	Amplitude monopulse radar block diagram [33]	32
2-11.	Monopulse antenna sum and difference beam	33
2-12.	One-coordinate phase monopulse antenna [24]	38
2-13.	Four-horn feed system of monopulse antenna [39]	41
2-14.	Multi-mode monopulse feed system with the associated propagating modes [41].....	43
2-15.	Diffraction pattern in azimuth	43
2-16.	Diffraction pattern in elevation	43
2-17.	3D model of proposed multi-mode monopulse antenna feed [40]	44
2-18.	Vertically truncated parabolic reflector - EA3462 X-band radar [43]	47
2-19.	Reflector illumination about the vertex	48
2-20.	Implementation of split-gate tracker on radar output [29]	50
2-21.	Range gate interval is aligned with the tracked-target echo pulse [44]	52
2-22.	Range gate interval is not aligned with the tracked-target echo pulse [44]	53
2-23.	Original and sharpened point-target response	54
3-1.	Illustration of the three regions surrounding a radiating antenna [50]	61

3-2. Polar plot	62
3-3. Rectangular plot	62
3-4. Polarization states of an EM wave [49]	69
3-5. Cross section of the opening of a rectangular waveguide	72
3-6. Configuration of the EM field in TE_{10} mode [63]	74
3-7. E-field variation in a waveguide for various TE modes [63]	75
3-8. Main types of horn antennas [27]	77
3-9. E-plane (y-z) cut of an E-plane sectoral horn [64]	78
3-10. A family of universal directivity curves, $\lambda D_E / a$ vs. B / λ [65]	82
3-11. Comparison of phase and time delay compensated arrays [50]	85
3-12. An electrically scannable phased array system [50]	86
3-13. Collimation of a beam using a parabolic surface [23]	89
3-14. Geometry of a parabolic reflector	90
3-15. Relationship between f/D ratio and β	92
3-16. Amplitude taper vs reflector shape - primary pattern of uniform intensity [50]	98
3-17. Tapering effect imposed on reflectors with a non-rectangular aperture outline	99
3-18. Offset parabola geometry [69]	102
3-19. Symbol of the π -hybrid [33]	106
3-20. Two-channel monopulse system	109
4-1. FMCW waveform [72]	112
4-2. Beat signal generation [73]	112
4-3. E-plane sectoral horn dimensions	118
4-4. View looking into the waveguide	118
4-5. FMCW transmit and receive pulses	119
4-6. 'Right-angle' and 'In-line' transitions [78]	122
4-7. WR90 adapter with square flange attached	124
4-8. Coax to adapter transition	124
4-9. Critical dimension parameters of transition	125
4-10. Front view of an adapter	127
4-11. VSWR of WR90 for different probe lengths	127
4-12. Return loss (S_{11}) of WR90 adapter for different probe lengths	128
4-13. S-parameters of WR90 adapter with a probe length of 5.5 mm	129
4-14. Tuning a waveguide using tuning screws [78]	130
4-15. Dimensions of a E-plane sectoral horn antenna	131
4-16. Radiation pattern of E-plane sectoral horn antenna	132

4-17. Radiation pattern (polar plot) in the a) H-plane and b) E-plane	132
4-18. Illustration of a truncated reflector as a section of a complete parabolic reflector	134
4-19. Vertically truncated reflector	134
4-20. Radiation pattern of horn antenna (polar plot) in the a) H-plane and b) E-plane	136
4-21. Relationship between f/D ratio of reflector and β	138
4-22. Vertically truncated parabolic reflector with calculated dimensions	139
4-23. Identifying the position of the feed aperture relative to the focus of reflector	141
4-24. Reflector antenna arrangement ($x = 0$)	142
4-25. Radiation pattern of reflector antenna ($f/D = 0.46$)	143
4-26. Radiation pattern of reflector antenna in horizontal plane (polar plot)	143
4-27. Radiation pattern of reflector antenna in vertical plane (polar plot)	144
4-28. Radiation pattern of reflector antenna in both principal plane (rectangular plot)	144
5-1. Reflector antenna with proposed monopulse feed	154
5-2. Pair of off-axis lobes for sum & difference monopulse [33]	155
5-3. Illuminating a plane reflector surface	156
5-4. Illumination of reflector about its vertex to produce an off-axis beam	157
5-5. Beam deviation factor of parabolic reflector as a function of reflector curvature [50]	158
5-6. Dependence of antenna gain on feed tilt and reflector curvature [50]	159
5-7. Illuminating the parabolic reflector about its vertex across a range of feed tilt, θ_i	160
5-8. Dependence of antenna gain on feed tilt for $f/D = 0.46$	161
5-9. Reflected angle vs. incident angle for a vertically truncated reflector (f/D ratio = 0.46)	162
5-10. Dual-horn monopulse feed	164
5-11. Dual-horn feed with zero feed tilt	166
5-12. Dual-horn feed with no feed tilt applied - Point of illumination ± 12.7 mm	167
5-13. Identifying the minimum feed tilt required to illuminate the reflector about the vertex	168
5-14. Feed tilt about the vertex of the reflector, for i) $\pm 1.3^\circ$, ii) $\pm 2.0^\circ$, iii) $\pm 3.0^\circ$	168
5-15. Reflector antenna employing a dual-horn feed with a feed tilt of $\pm 1.3^\circ$	169
5-16. Radiation pattern of the left beam in the a) H-plane and b) E-plane	170
5-17. Simulated pair of off-axis lobes ($\theta_i = \pm 1.3^\circ$) (power gain scale)	171
5-18. Simulated pair of off-axis lobes ($\theta_i = \pm 1.3^\circ$) (voltage gain scale)	172
5-19. Sum pattern ($\theta_i = 1.3^\circ$)	173
5-20. Difference pattern ($\theta_i = 1.3^\circ$)	174
5-21. Simulated sum pattern across the range of feed tilt applied	175
5-22. Simulated difference pattern across the range of feed tilt applied	176
5-23. Zoom in on-axis difference pattern	178

5-24. Difference-to-sum ratio pattern ($\theta_i = 1.3^\circ$)	179
5-25. Construction to calculate field at point P from a linear aperture [50]	185
5-26. Differencing to create Δ point-target response and the correlation reference pattern	189
5-27. Δ point-target response equals the correlation reference pattern in the absence of clutter ..	190
5-28. Output of correlator in the angle-domain	191
5-29. Antenna response pattern - far-field pattern of uniform line-source distribution	193
5-30. Maximum overlap ($A = 0.2$)	195
5-31. Minimum overlap ($A = 0.8$)	195
5-32. Maximum pulse sharpening	195
5-33. Reduced pulse sharpening	195
5-34. Noisy point-target response (SNR = 20 dB)	198
5-35. Original and sharpened point-target response	199
5-36. Sharpened response (noise and noise-free)	200
5-37. Noise within the sharpened point-target response	200
5-38. Optimum beam pattern for PSDP	203
5-39. Corresponding response of two closely spaced targets	205
5-40. Correlation reference pattern ($A = 0.5$)	207
5-41. Sharpened response with -6 dB negative precursor and post cursor sidelobes	207
5-42. Newly sharpened point-target response, for $n = 2$	208
5-43. Extended correlation reference pattern, for $n = 3$	210
5-44. Newly sharpened response with three precursor and postcursor sidelobes	211
5-45. Monopulse antenna response – sum pattern squared	216
5-46. Sharpened response for maximum pulse sharpening ($A = 0.2$).....	217
6-1. R&S® ZNB Vector Network Analyzer [90]	221
6-2. Major systematic errors associated with VNA measurements [91]	223
6-3. S_{11} measurement for probe length of 4 mm	227
6-4. S_{11} measurement for probe length of 4.5 mm	228
6-5. S_{11} measurement for probe length of 5 mm	228
6-6. S_{11} measurement for probe length of 5.5 mm	229
6-7. S_{11} measurement for probe length of 6 mm	229
6-8. S_{11} measurement for probe length of 6.5 mm	230
6-9. S_{11} measurement for probe length of 7 mm	230
6-10. Reflector dish manufactured out of mesh panels [93]	235
6-11. Rear view of parabolic reflector comprising of five joint panels	237
6-12. Machining process of the individual reflector parts	237

6-13. The first 3 of 5 parts of the 3D printed reflector 238

6-14. Rear view of the 3D printed reflector attached to support frame 239

6-15. Front view of the 3D printed reflector attached to support frame 241

6-16. Illustration of surface errors in a reflector antenna [50] 243

6-17. Perspective view - Aluminium profile system of radar employing reflector antenna 246

6-18. Top view - Aluminium profile system of radar employing reflector antenna 246

6-19. Side view - Aluminium profile system of radar employing reflector antenna 247

6-20. Monopulse feed and reflector attached to the designed supports 247

6-21. X-band antenna measurement range 249

6-22. Transmit parabolic reflector antenna 250

6-23. 1.2-meter antenna support 251

6-24. AUT mounted on antenna support 251

6-25. Schematic of the antenna measurement system 251

6-26. AUT – E-plane sectoral horn antenna 253

6-27. Measured principal plane pattern of E-plane sectoral horn antenna 254

6-28. Simulated and measured azimuth pattern – Sectoral horn antenna 255

6-29. Simulated and measured elevation pattern – Sectoral horn antenna 255

6-30. AUT – Center-fed reflector antenna (side) 256

6-31. AUT – Center-fed reflector antenna (perspective) 256

6-32. Measured pattern of center-fed reflector antenna in both principal planes 257

6-33. Measured pattern of center-fed reflector antenna in horizontal plane 258

6-34. Simulated and measured azimuth pattern – Reflector antenna 259

6-35. Simulated and measured elevation pattern – Reflector antenna 259

6-36. AUT – Monopulse reflector antenna 260

6-37. Mounting bracket of dual-horn feed of a monopulse reflector antenna 261

6-38. Measured off-axis beams, sum and difference patterns ($\theta_i = 1.3^\circ$) 262

6-39. Measured off-axis beams, sum and difference patterns ($\theta_i = 1.5^\circ$) 263

6-40. Measured off-axis beams, sum and difference patterns ($\theta_i = 1.7^\circ$) 263

6-41. Measured sum and difference patterns across the range of feed tilt applied 264

7-1. Two-antenna system operated by a switch after every half rotation 272

7-2. Schematic of hardware implementing pattern selective differential processing 273

List of Tables

2-1.	Comparison of a phased array antenna and parabolic reflector antenna [23] [24]	18
2-2.	Advantages of monopulse compared to other angle measuring techniques	36
2-3.	Comparison of amplitude and phase monopulse [37]	40
2-4.	Comparison of a four-horn and multi-mode feed system [39]	46
3-1.	Angle subtended by the aperture, 2β , for various f/D ratios [27]	92
3-2.	Relationship between tapering and formation of sidelobes [68]	100
3-3.	Pros and cons of offset-reflector antenna [25]	104
4-1.	Summary of radar parameters	111
4-2.	Properties of FMCW radar	114
4-3.	Rectangular waveguide adapter models [78].....	123
4-4.	Dimensions of a WR90 adapter	125
4-5.	Simulated RF performance of WR90 adapter for different probe lengths	128
4-6.	Optimizing the position of the feed aperture relative to the focus	142
4-7.	Reflector modelling for various illumination taper	145
4-8.	X dB principal plane beamwidths subtending to the reflector edges	146
4-9.	Simulated radiation properties of reflector antenna for various f/D ratios	146
4-10.	Theoretical and simulation results of reflector antenna radiation properties	149
5-1.	Properties of radiated beam across the range of feed tilt applied	161
5-2.	Radiation properties of the beams produced corresponding to each feed tilt	174
5-3.	The figure of merit $k_d s_o$ across the range of feed tilt applied	181
5-4.	Common aperture distributions of linear aperture and their Fourier Transforms [50]	187
5-5.	Original and sharpened response for different extent of beam sharpening	194
5-6.	Far-field pattern of common aperture distributions [50]	196
5-7.	Effect of the sharpening technique on different far-field distributions.....	197
5-8.	SNR of sharpened point-target response for increasing values of A	201
5-9.	SNR of sharpened point-target response for increasing sampling interval	202
5-10.	Sidelobe level of the newly sharpened response for each value of n	212

5-11. Pros and cons of differential processing on surveillance radars	214
5-12. Properties of original and sharpened response for various beam sharpening	216
5-13. Properties of sharpened response for two types of antenna	217
6-1. Summary of the various calibration properties [91]	225
6-2. Simulated and measured S_{11} of sectoral horn for varying probe lengths	231
6-3. Comparison of Copper and Aluminum properties [102]	239
6-4. Advantages of T-slotted aluminium profile system [107]	245
6-5. Far-field radiation pattern – E-plane sectoral horn antenna	254
6-6. Far-field radiation pattern – Center-fed reflector antenna	258
6-7. Measured sum beam properties across the range of feed tilt applied	264
6-8. Sum beam properties corresponding to a feed tilt of 1.3 degrees	265
A-1. Ship RCS table [108]	282
A-2. MATLAB radar equation calculator	283
A-3. Radar transmit power budget analysis	283

List of Symbols

A	Physical Area (m^2)
A_e	Effective Antenna Capture Area (m^2)
c	Propagation Velocity of EM Waves in Free Space (3×10^8 m/s)
B	Bandwidth (Hz)
BW	Beamwidth (deg)
D	Largest Dimension of an Antenna Element (m)
D_a	Horizontal Diameter (m)
D_e	Vertical Diameter (m)
D_i	Directivity (dBi)
F	Receiver Noise Figure (dB)
f/D	Reflector Focal Point to Diameter Ratio
f	Focal Point (m)
f	Frequency (Hz)
f_c	Cut-off Frequency (Hz)
G	Antenna Gain (dB)
G_r	Receiver Antenna Gain (dB)
G_t	Transmit Antenna Gain (dB)
$G(u)$	Fourier Transform of Aperture Distribution
I_g	Current in the Generator (A)
j	Unit Imaginary Number ($\sqrt{-1}$)
k	Boltzmann's constant (3.18×10^{-23} W/K/Hz)

k_m	Normalized Monopulse Slope
L	Cumulative Losses due to Propagation, Plumbing and Beamwidth (dB)
L_p	Propagation Losses (dB)
N_d	Average Noise Power in Difference Channel
p	Polarization
P_A	Available Power at the Input Terminal of a Receiver (W)
P_L	Power Dissipated as Heat (W)
P_a	Power Density at Reflector Aperture Edge (W/m ³)
P_n	Noise Power (W)
P_{norm}	Normalised Power (W)
P_o	Power Density at Center of Reflector (W/m ³)
P_r	Receive Power (W)
P_{rad}	Power Delivered to an Antenna for Radiation Purposes (W)
P_t	Transmit Power (W)
P_{target}	Reflected Power from Target (W)
P_{tot}	Total Power Radiated (W)
r	Radius (m)
R	Range from an antenna (m)
R_A	Antenna Resistance (Ω)
R_g	Resistance of Generator (Ω)
R_L	Loss Resistance (Ω)
R_f	Minimum Far-field Range (m)
R_E	Horn Apex Length (m)
R_{rad}	Radiation Resistance (Ω)
S	Sum-signal Power
S_A	Angular Resolution in Distance (m)
S_D	Power Density – Directional (W/m ³)

S_I	Power Density – Isotropic (W/m^3)
S_R	Power Density – Receiver (W/m^3)
t	Time (s)
t_d	Time Delay (s)
t_m	Modulation Period (s)
t_o	Coherent Processing Interval (s)
T_0	Noise Reference Temperature (= 290K)
T_s	Receiver Noise Temperature (K)
V_t	Target Velocity (m/s)
V_g	Peak Generator Voltage (V)
w	Spectral Width of the Beat Frequency (Hz)
W	Watt
x	Depth of Reflector (m)
X_A	Antenna Reactance (Ω)
X_g	Reactance of the Generator (Ω)
Z_A	Antenna Impedance (Ω)
Z_c	Free-space Impedance (Ω)
Z_g	Internal Impedance of Waveguide (Ω)
α	Loss Effects in Reflector Antenna
θ	Theta (deg)
θ_a	Azimuth Beamwidth (deg)
θ_e	Elevation Beamwidth (deg)
θ_s	Squint Angle (deg)
δ_s	Skin Depth (m)
λ	Wavelength at Operating Frequency (m)
λ_o	Free Space Wavelength (m)
λ_g	Waveguide Wavelength (m)

ρ	Resistivity of a Medium ($\Omega \text{ m}$)
μ	Permeability of a Medium (H/m)
σ	Radar Cross Section (m^2)
σ_θ	Standard Deviation of Angle Error
Φ	Power Density (W/m^2)
ω	Angular Frequency (Radian/s)
Ω	Ohm
Γ	Reflection Coefficient
Σ	Sum
Δ	Difference

List of Acronyms

2D	Two Dimensional
3D	Three Dimensional
ABS	Acrylonitrile-Butadiene-Styrene
ADC	Analogue to Digital Converter
AGC	Automatic Gain Control
AUT	Antenna Under Test
AWGN	Additive White Gaussian Noise
BDF	Beam Deviation Factor
CAD	Computer Aided Design
CEM	Computational Electromagnetics
CFAR	Constant False Alarm Rate
CST	Computer Simulation Technology
CNC	Computer Numerical Control
DSP	Digital Signal Processing
DUT	Device Under Test
dB	Decibel
EM	Electromagnetic
ESA	Electronically Scanned Array
FM	Frequency Modulation
FMCW	Frequency Modulated Continuous Wave
GHz	Giga Hertz
Hz	Hertz

IF	Intermediate Frequency
IMO	International Maritime Organization
K	Kelvin
LHCP	Left Hand Circularly Polarised
LHEP	Left Hand Elliptically Polarised
LNA	Low Noise Amplifier
LO	Local Oscillator
LOS	Line of Sight
LPI	Low Power Intercept
log	Logarithmic Base 10
MATLAB	Matrix Laboratory
MI	Mutual Interference
MTI	Moving Target Indicator
MWS	Microwave Studio
PEC	Perfect Electrical Conductor
PPI	Pixel Per Inch
PPS	Pulses per Second
PRF	Pulse Repetition Frequency (Hz)
PRI	Pulse Repetition Interval (s)
PSDP	Pattern Selective Differential Processing
PW	Pulse Width
RCS	Target Radar Cross Section (m^2)
RF	Radio Frequency
RHCP	Right Hand Circular Polarization
RHEP	Right Hand Elliptical Polarization
RPM	Rotation Per Minute
Rx	Receiver
SCR	Signal to Clutter Ratio (dB)

SMA	SubMiniature version A
SNR	Signal to Noise Ratio (dB)
SOLT	Short-Open-Load-Thru
Tx	Transmitter
TDM	Time-Division Multiplexing
TRL	Thru-Reflect-Line
T/R	Transmit/Receive
UCL	University College London
VNA	Vector Network Analyzer
VSWR	Voltage Standing Wave Ratio

Chapter 1

Introduction

1.1 Overview

The Strait of Malacca is a narrow, 550 miles (890 km) stretch of water between the Malay Peninsula and Indonesian island of Sumatra [1]. For decades, the geographical location of the strait was established as one of the busiest shipping lanes in the world, with Indonesia controlling majority of the sea lane [2]. From an economic and strategic perspective, the Strait of Malacca is most well known to be considered as one of the world's most important routes, linking the economies of many major Asian countries. Thus, much of the world's economy rests on the safe and efficient flow of shipping through the waterway which provides a separation between Peninsular Malaysia, Thailand, and Singapore from the Indonesian island of Sumatera. This section provides an overview of the strait from several important aspects.

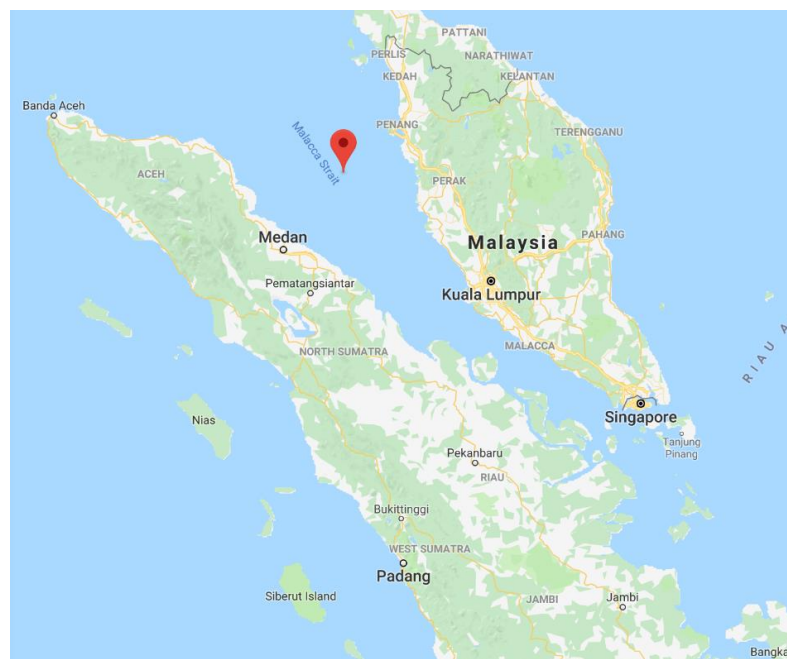


Fig 1-1. Geographical location of the Strait of Malacca [2]

1.1.1 Economic Importance

Known to be the main shipping channel between the Indian ocean and the Pacific Ocean, via the Adaman sea and the South China Sea, the Strait of Malacca provides passage to about 25% of the world's traded goods, including oil, Chinese manufactured products, coal, palm oil and Indonesian coffee [3]. For instance, some 15 million barrels of oil are transported through the strait each day, providing 90% of Japan's imports and 80% of China's [4]. Also, about a quarter of all oil carried by sea passes through the Strait, mainly from Persian Gulf suppliers to Asian markets. In 2007, an estimated 13.7 million barrels per day were transported through the strait, increasing to an estimated 15.2 million barrels per day in 2011 [5]. In 2008, an estimated 94,000 vessels passed through the Malacca straits to transport energy, raw materials, and finished goods, making it the busiest strait in the world. Due to the above activities, shipping traffic has increased by more than 60% over the past decade, and the traffic density is projected to double by 2020 [6]. These data and the future projections made proves the significance of the waterway towards the economy of many countries. In addition, due to the narrowness at certain points of the strait, such as at the Phillips Channel (close to the south of Singapore) that is only 2.8 km (1.5 nautical miles) wide, the strait has become one of the world's most congested shipping choke points [5].

The huge importance of the strait due to its strategic geographical routes and the economic dependence that many Asian countries have on it has resulted in a very busy strait that has become highly populated with ships of different sizes, although mainly large cargo vessels. Unsurprisingly, the exceptionally vast number of vessels travelling within the strait over the last few decades have caused vital problems from various human and natural causes, which would occasionally disrupt the transportation of goods, impose potential losses, and directly affect businesses. The recurring issues within the Strait of Malacca, and the various actions imposed by authorities, particularly from the technological standpoint, intended to minimize the issues encountered are highlighted.

1.1.2 Pertaining Issues

The extreme concentration of large vessels and local ship traffic within a narrow seaway with very shallow and changing bathymetry, numerous shoals, strong monsoonal winds in the northern reaches of the strait, surface currents up to 5 knots [7] and a frequent unregulated population of small fishing crafts creates a very hazardous environment that is prone to accommodate many accidents due to navigational challenges. In 1997, two oil tankers, "ORAPIN GLOBAL" and "EVOIKOS", collided in the Singapore strait, causing the worst oil

spill in the history of Singapore and east Asia. This collision resulted in about 28,500 tons of heavy marine fuel oil to be spilled into the sea [8].

In addition to the navigational dangers of collision and grounding due to traffic and strong surface currents is the annual haze due to bush fires in Sumatra, Indonesia. The haze produced due to the burning of trees within the forests of Sumatra have reportedly reduced visibility within the strait by up to 200 meters (660 ft). Moreover, the geographical location of the strait of Malacca causes the strait to be strongly influenced by the monsoons throughout the year, with the north-east winds dominating during (northern) winter and the south-west winds in summer, which frequently subjects it to recurrent high sea states and has become a common source of casualty due to the collision of vessels. Apart from their effects on the surface currents, they create distinctive wave spectra because of the fetch-limited development associated with the orientation of the strait relative to the prevailing winds [9]. Hence, particularly ships that are a few hundred meters long are forced to slow down and take extra precautions to prevent unnecessary casualty, at the expense of significantly higher traffic.

Most significantly, piracy had always been a serious problem encountered in the strait over many decades. The acts of maritime terrorism have emerged as a grave threat in recent years especially within main fishing zones and popular transport routes, which are areas with the highest incidence of piracy [10]. High incidence of piracy is regarded as the most serious issue as not only does it account for the threat to global shipping, but it also has direct impact on the global economy, safety and human lives within the strait due to frequent shipping hazards. Piracy had been high in the 2000s, with additional increase after the events of September 11, 2001 [11]. According to the international maritime bureau, after attacks rose again in the first half of 2004 the strait of Malacca was ranked as the world's most dangerous sea route. To this hazard, we must add the threat from international terrorism which the governments around the strait have identified as a serious prospect. In response, regional navies stepped up their patrols of the area in July 2004. Subsequently, attacks on ships in the Strait of Malacca dropped, to 79 in 2005 and 50 in 2006 [12]. After reaching an agreement between the governments of Malaysia, Singapore, and Indonesia to deal collectively with this issue, the port authorities of these countries had initiated coordinated air and sea patrols to tighten up surveillance requirements and encompass security, which significantly reduced attacks, to 11 in 2006 and only 2 in 2010, but with an upsurge in 2011 [13], [14]. Nonetheless, the cost of patrolling is expensive and can be defeated by pirates with access to intelligence. In addition to intervention capability, maritime awareness, here understood as obtaining knowledge of where ships are on the sea, shipping and ship traffic routes and pattern, is vital for any counter-piracy activity. In the last decade, regional coordination, cooperation and information exchange and

an increase in maritime awareness have made significant contributions to the reduction in piracy and overall safety at sea [15].

1.1.3 The use of Radar Technology to Fulfil Strait Requirements

Coastal surveillance covers a very broad range of responsibilities: law enforcement, security, and economic and safety reasons. This includes sea and lower airspace surveillance, monitoring of vessel behavior, management of incidents, and communications [16]. Organizations such as coastguards, customs and navies are responsible for overlooking large areas of water and to gather information to know what goes on, where their assets are and how to best deploy them. In addition to the information provided from a variety of sources, real-time information that is easily interpreted by the operator is critical for optimal and efficient operation. Hence, this presents the need for an integrated platform to support daily coastal monitoring activities around and within the strait.

Officials seek to detect and identify non-cooperative vessels effectively either directly during patrol duty or by recognizing vessels under threat or those possessing unusual behavior using monitoring devices. Many ship accidents, along with an increasing vessel traffic density in congested sea-lanes within the strait, have also placed a stronger requirement on monitoring and controlling the movement of ships in coastal waters. For monitoring of inland waterways close to the shore, the use of surveillance equipment, such as cameras, may be used manually by the operator for close range visual monitoring. However, visual equipment tends to be of limited use in poor weather conditions (e.g. rain, fog, or darkness) and also heavily rely on the awareness of the operator. With the advancement in modern radar technology, surveillance radars, as primary long-range sensors with the ability to operate in bad weather and null visibility conditions, have become the sensor of choice and the only proper form of efficient surveillance [17].

Following the development of maritime navigation radars and network integration systems for coastal surveillance, a wide range of coastal surveillance radars have been implemented along the coastlines of many developed countries with an objective of overlooking the safety of navigation at sea and protecting the coastline from uncooperative targets. This was followed by the emergence of Vessel Traffic Services (VTS), a marine traffic monitoring system, usually established by port authorities, that is formed through an integrated network of coherent surveillance radars. The purpose of such surveillance systems is similar to an air traffic control for aircraft. The objectives can be narrowed to notably two categories, which are, to enhance the performance of the individual radars in the detection of large cooperative and uncooperative targets at an earlier rate, over long distances and in rough weather conditions -

providing the targets Radar Cross Section (RCS) provides sufficient contrast to the background - and to monitor the active movements of these vessels. Coastal surveillance systems are also used to provide remote sensing technology for measuring waves and currents within an area of the strait, especially when bad weather conditions result in higher sea states that could affect the safety and intended direction of a ship. Measurement of the surface currents is very important to minimize any potential risks of collision or grounding through early warning systems and by providing alternative routes. Thus, navigational advice for vessels would substantially reduce the effect of sea conditions on the ships travelling in particularly confined and busy waterways. Information on sea state is of interest to the fishing industry, planning for offshore wave energy extraction, coastal development, port operation scheduling, search and rescue, tourism and recreational activities, so extraction and dissemination of environmental data would be welcomed by a wide range of user communities [18].

The implementation of a network of coastal surveillance radars consist of overlapping areas of coverage by a single or several types of radar system. Determining the most suitable radar sites along the coast to establish a network of radars surrounding chosen areas of the strait to provide surveillance and tracking of ships is critical in optimizing the results obtained. An extensive research on identifying the appropriate number of radar sites and their respective locations along the Strait of Malacca was performed by S. J. Anderson [18]. The research explains the ideal choice of sites for deploying '*N*' radars to create an optimum radar network necessary to produce accurate information of the strait. Based on the optimization processing method used in the study, Figure 1-2 displays the set of candidates of radar sites that is selected as an input to the optimization process of choosing the most suitable radar sites for optimal data collection.

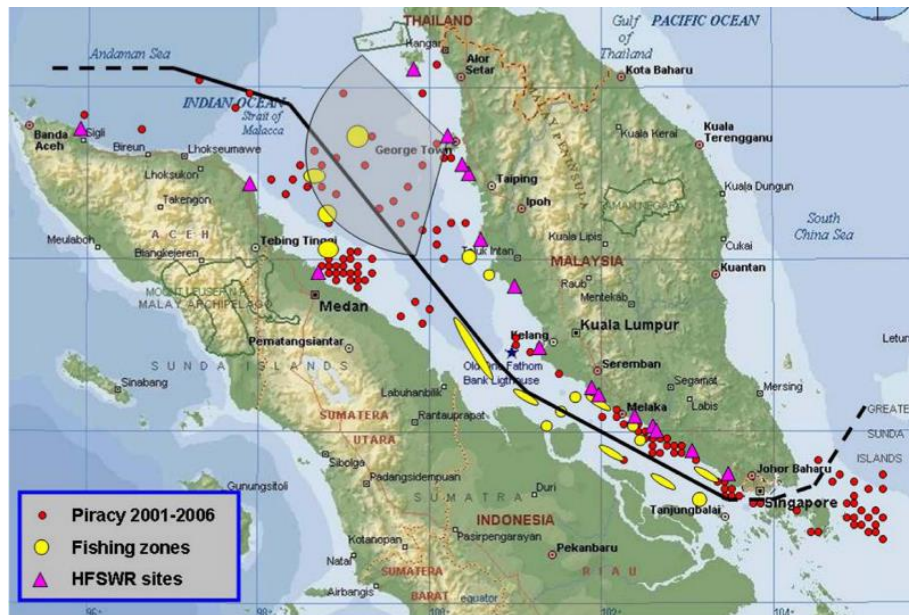


Fig 1-2. Candidate locations for radar sites surrounding the Strait of Malacca [18]

The types of radar employed within the strait span a large range of systems, which are suitable for land, sea, and air surveillance. Evidently, different types of radar are more suitable for certain applications, whether it is used for monitoring propagation conditions of a waterway or to detect and track targets of specific characteristics. The most common marine radar systems implemented along the coastal shoreline surrounding the strait are notably phased array systems and mechanical scanning radar systems employing slotted-waveguide or reflector antennas. Nonetheless, the type of surveillance radar and the chosen parameters of each system are optimized to obtain the data required within the designated area covered by the vessel traffic service. Above all, the visibility, precipitation rates, sea states and propagation conditions relevant for the individual radar sites appointed must be considered carefully to enable the optimal system to be specified [17].

The International Maritime Organization's (IMO) has imposed a rule requiring international voyaging ships with Gross Tonnage (GT) of 300 or more tons, and all passenger ships regardless of size, to be fitted with Automatic Identification System (AIS) aboard the ship. The AIS is a common data source for the maritime navigation used worldwide. AIS is a short-range coastal tracking system used on ships and by VTS for identifying and locating vessels by continuously electronically exchanging data with other nearby ships and VTS stations in real-time. Because it is a cooperative system, the information provided by AIS can be connected and combined with real-time sensor data provided from the network of radars implemented along the strait to develop an automated solution for cooperative mapping of targets. In addition to the network of surveillance radars and television cameras for visual

surveillance, the introduction of the compulsory use of AIS on certain ships allows the VTS to play a more significant role in marine traffic management (i.e. continuously report new arriving vessels in the Malacca Strait), which helps in improving safety and efficiency of navigation. As cooperative targets could now be tracked and positioned with AIS, the key question remained on non-cooperative ones [19].

Ever since significant improvements on maintaining a more secure and casualty free environment were realized, with recent reports indicating that attacks have dropped to near-zero levels in recent years [19], the requirements for capable and reliable sensor systems have increased correspondingly to reduce any evident disruption of activities within the strait. Officials have consistently focused on the continuous advancements within the field and allocated budgets to invest on the latest radar technology to ensure that potential catastrophe arising from both human and natural causes can be effectively reduced by providing necessary precautions.

1.1.4 Proposed Alternatives to Existing Radar Systems

The several key requirements that have been identified along the major waterway of the Malacca Strait are often categorized from the security and weather perspective. As mentioned above, the main requirements prioritize on monitoring the movement and behavior of medium to larger sized vessels passing through the strait and to provide authorities with sufficient awareness towards harsh propagation conditions in the event of bad visibility and high sea states. In many coastal waters around the world, the implementation of electronically scanning phased array radar systems has proven to deliver high-end performance that fulfils the surveillance and monitoring requirements for the detection and tracking of targets that passes through the monitored sector of the strait. Hence, these radar systems were initially chosen to create a network of multistatic radars along the coasts surrounding the strait due to its capability in delivering the highest detection performance that can be expected from any surveillance radar systems available, and therefore they are preferred especially for applications that requires very high requirements. The advantages of phased array radars as compared to other mechanical scanning surveillance radar systems are discussed in Section 2.1.

However, despite the excellent performance of electronic scanning radars in fulfilling the surveillance requirements of the strait, during the several years of operation the phased array antennas deployed had required regular maintenance to be performed as a portion of the radiating elements within the array may have stopped functioning. When this happens, it prevents the radar from operating at its maximum capability, while going unnoticed, and therefore it was difficult to identify whether the radars were functioning optimally unless there

was a significant deterioration in radar performance. Moreover, in addition to the maintenance issues, the authorities have found it challenging and costly to provide regular maintenance of the radars due to the limited infrastructure and poor accessibility to most of the allocated radar sites along the coast. The lack of logistics and difficulty in transporting people in and out of the radar sites within a short period of time have been an inconvenience over the past decade. Hence, as a result the government had evaluated the conditions to be unsuitable for the continuous operation of the existing electronic scanning radar systems, especially for large antennas that requires large fixed radar sites and a continuous large supply of power. The excessive overhead costs and maintenance issues encountered with the existing network of radars was a big driver to go with a simpler antenna solution or method of fulfilling the surveillance requirements. Meanwhile, instead of resolving the issues encountered with the existing radar systems, the government had opted for conventional patrolling methods to provide for the surveillance and monitoring of the Indonesian territorial waters. This decision has led to the purchase of approximately 200 locally produced patrol boats a year across the governing maritime organizations, which have undoubtedly contributed to the steep growth within the shipbuilding industry in recent years.

From a technological standpoint, the implementation of mechanically scanning radar systems at the numerous pre-determined radar sites along the coastline surrounding the strait can be proposed to replace the existing electronic scanning radar systems since most of the targets of interest are primarily large ships that are either stationary or propagating at relatively low speed (<20 knots). Hence, the use of sophisticated phased array antennas may prove to be over performing and unnecessary, especially where cost is of a significant factor. The two most common types of mechanical scanning radar for coastal surveillance are magnetron-slotted waveguide antenna radars and solid state-reflector antenna radars of FMCW type. The latter has become the preferred choice since its introduction within coastal surveillance radars due to its anti-intrusion function with a couple of watts, higher instantaneous bandwidth and frequency agility. Well-designed reflector antennas are also capable of producing beams of significantly higher gain and narrower principal plane beamwidths, where required, that translates to a further maximum detectable range and a higher angular resolution which benefits through better discrimination of smaller targets from the background and an improved detection accuracy. These properties are critically important towards the requirements of a coastal surveillance application, especially when dealing with the detection of ground and flying objects over considerably long operating ranges, and, thus, it generally offers a higher level of performance. Moreover, the suitable radar parameters, which are determined according to the surveillance requirements of the strait, can be fulfilled more flexibly with space fed antennas. Hence, the use of reflector antennas in mechanical scanning coastal surveillance radars has become the

most popular choice over the last few decades for applications requiring lower performance capability than electronically scanned radar systems. Such radar systems have been implemented along many major coastlines around the world to create a network of bistatic, or more frequently, multistatic radars.



Fig 1-3. The Arthur satellite at Goonhilly Earth Station [20]

Although conventional reflector antenna systems are a popular choice for providing effective coastal surveillance and monitoring of common types of target observed along the coastal waters, many existing reflector antenna systems in operation also have limitations from the design, cost and weight perspective, especially those systems that exhibits very high-performance capabilities, from which there are room for possible improvements through new ideas. The project aims to exploit this, thereby placing the focus on addressing the limitations of existing conventional reflector antenna systems by proposing a new reflector antenna design, or particularly feed system, that is novel and unique to current mechanical radar systems employing reflector antennas used for similar applications, and an alternative method of manufacturing medium sized reflector.

1.2 Scope of Research

The primary aim of the research reported in this thesis has been to develop a new reflector antenna system that replaces the antenna subsystem of an existing FMCW scanning radar unit. The aim of the proposed radar system are to fulfil the surveillance requirements of this strait from the security perspective concerning the detection and tracking of larger vessels and low

flying objects travelling through the strait, while the antenna design places a priority on cost effectiveness, and therefore minimum RF hardware complexity, manufacturing of a light weight antenna system using a simpler alternative method of fabrication and, most importantly, one that would achieve an enhancement in angular resolution and accuracy for the detection and tracking of identified targets based on the antenna design and from the application of a novel signal processing technique that is proposed in this research. To do this, the following scope of this research, which are outlined in this section, have had to be met.

The thesis outlines the investigation of the limitations of existing radars, or more specifically antenna systems, employed along the coast overlooking the Strait of Malacca from various important aspects and the improvements on these limitations that can be achieved with an alternative antenna system and novel signal processing method proposed in this research project. The thesis contains two parts. The first half of the project focuses on the design and modelling of a mechanical scanning parabolic reflector antenna for coastal surveillance and the application of the proposed signal processing technique on an existing radar output. The second half is focused on the manufacturing and construction of the antenna system designed, which is followed by the measurement and optimization of the antenna performance.

The project has utilized a CEM tool called CST and a CAD tool called SolidWorks to model three antenna systems (i.e. E-plane sectoral horn antenna, reflector antenna and monopulse antenna) and their respective antenna supports. The results of a number of CST simulations corresponding to each antenna model were validated by the far-field measurements of the prototypes of the respective antennas at the later stage of the project.

To demonstrate the signal processing technique proposed in this project, the algorithm that implements the technique on a simulated radar waveform, or output of a radar system, have been developed using MATLAB based codes (Appendix B). These would allow the benefit of the technique on several common types of antennas pattern to be evaluated, and the enhanced resolution performance of the radar antenna to be realized from the technique.

1.3 Thesis Layout

The opening chapter provides an overview to the importance of the Strait of Malacca from several perspectives and the challenges and many requirements of the Strait. It further states the objectives and scope of this research.

Chapter 2 begins by providing the background to the existing coastal surveillance radars that have been implemented along the coast of the Strait of Malacca and the limitations, or rather unsuitability, of the radars that is assessed from the performance, cost and operational

perspectives. It then places its focus on the use of mechanical scanning reflector antenna systems and the existing angle tracking methods available to improve the performance of such radar systems. This is followed by a brief proposal of designing a new reflector antenna system with its own angle tracking method and novel signal processing method that can potentially replace some of the existing radars on site.

Chapter 3 extensively describes the important principles and parameters of a radar antenna system. It is followed by the principles of RF devices and components, several space fed antennas and radar systems, and popular angle measurement techniques for reflector antenna systems.

Chapter 4 begins with choosing the most suitable radar parameters according to the requirements of the radar performance. This is followed by the modelling and design a center-fed reflector antenna system on CST, which is divided into two parts, that is, the modelling of a E-plane sectoral horn antenna that achieves maximum directivity and the design of a reflector according to the radiation pattern of the feed. A cross-validation between the simulation and theoretical results of the reflector antenna performance is presented at the end of the chapter.

Chapter 5 is relevant to the scanning and tracking strategy adopted for the proposed antenna system. The chapter contains two parts, that is, applying an angle measurement technique and a novel signal processing method. It begins with describing the underlying method used to implement amplitude-comparison monopulse on the horizontal plane of the reflector antenna that was designed in Chapter 4. The simulated performance of the monopulse antenna on CST allows the modelling to be verified. This is followed by providing the principles of the signal processing technique proposed and its application, and benefits, on the performance of the monopulse reflector antenna and other surveillance radar systems.

Chapter 6 is dedicated to the experimental measurements of the different types of antenna that was modelled for this project. This chapter includes the construction process and method used for the individual components of the reflector antenna. This is followed by measurements of the RF performance and the far-field radiation pattern of the various antennas. Hence, the measurement results obtained serves as a proof and validation of the simulated performance and, therefore, model of the proposed monopulse reflector antenna system.

Chapter 7 is divided into three parts. The first part concludes the thesis by giving a summary of the achievements outlined in the previous chapters. The second part contains a general discussion of the work conducted. It provides the novel contributions to research and analyzes the overall approach taken towards the objectives of the project, the issues that have arisen and the reliability of the simulated and measurement results that may have been affected

by certain factors. The third part considers how the results obtained from the research conducted thus far could be progressed further as future work.

1.4 Contributions to the Research Field

The following points summarise the novel contributions of the work presented in this thesis and the contributions to areas within the field of research that has limited exposure:

1. *Applicability of proposed feed configuration in monopulse antennas employing truncated reflectors:* The dual-horn feed arrangement proposed in this project introduces a simple method of implementing amplitude-comparison monopulse in a single-coordinate of a reflector antenna employing a truncated reflector. The feed system modelled in CST allows the direction of the pair of off-axis beams radiated from the reflector to be controlled independently, and therefore this allows the sum and difference (monopulse) patterns to be optimized individually according to the requirements of the application in hand, that is, the detection sensitivity (on-axis sum gain) and/or angular accuracy (on-axis difference slope) of the monopulse antenna.
2. *3D printing technology for manufacturing large reflectors using non-metallic materials:* The parabolic reflector designed in this project was manufactured using a 3D printer with a build area that is considerably smaller than the size of the reflector aperture. The manufacturing process have shown that a large reflector can be fabricated in numerous individual parts, or panels, of equal size, before solvent welded together to form the final reflector. The panels are designed with a T-section joint, using a tool called SolidWorks, which ensures that the panels would connect accurately together. The use of widely available profile systems to create the suitable framework, which includes the feed and reflector supports, for a given antenna system, according to the f/D ratio and dimensions of the reflector was also demonstrated. The chosen manufacturing process of the reflector antenna has convincingly shown its capability to produce a significantly cost and weight effective system within a short turnover period, and most importantly without compromising the performance of the reflector antenna.
3. *MATLAB Based Codes for Application of Pattern Selective Differential Processing:* Unlike most signal processing techniques, the proposed pattern selective differential processing technique is designed to make near-optimum use of prior knowledge of the antenna response pattern (or pulse shape) of the echoes sought to sharpen the beamwidth

of the original target response that is identified within the received signals. Hence, in addition to effectively reducing the beamwidth of an original response, and therefore substantially increasing the angular resolution and clutter resilience of the radar system, the differential processing technique proposed tend to be more robust, less complex and less dependent on high SNR. Furthermore, the technique can be directly operated on the video signal between the radar output and display unit, and therefore it can be implemented on any type of new or existing radar without requiring any changes to the RF circuits within the radar.

4. *MATLAB Based Codes for Application of Sidelobe Reduction Technique*: In most cases of reflector antenna design that prioritizes achieving maximum antenna gain over the sidelobe levels, the sidelobes formed within the radiation pattern of the antenna may not be sufficiently small enough, and at times could be a serious issue on the radar performance. Sidelobe reduction technique is a post processing technique that have been introduced to suppress these sidelobes to large extents without affecting the antenna gain and shape of the antenna pattern. As demonstrated in this thesis, the technique effectively redistributes the energy within the largest sidelobe of a target response evenly across several number (n) of smaller sidelobes. Hence, lower sidelobes are formed to replace the original sidelobe, but in the expense of increased noise within the processed response.

1.5 Author's Publications

1. Basuki, J. E. and Brennan, P., "Large Parabolic Reflector Antenna Development using 3D Printing Technology," Submitted to *IEEE Transactions on Antennas and Propagation*, Nov. 2018.
2. Basuki, J. E., Brennan, P. and Benjamin, R., "Pattern Selective Differential Processing of a Scanning Surveillance Radar Signal," Submitted to *IEEE Transactions on Signal Processing*, Dec. 2018.

Chapter 2

Background and Literature Review

2.1 Coastal Surveillance Radars in Strait of Malacca

As briefly mentioned in Section 1.1.4, a vast majority of the coastal surveillance radars incorporated on the coastal shores of Sumatra, along the Strait of Malacca, mainly for the surveillance of a variety of ships are large electronically scanning phased-array radar systems. Most of these existing radars have been installed over the past decade by the Indonesian Maritime Security Agency, which is a government institution in-charge of maritime patrol and rescue on the territorial waters of Indonesia.

The principles of phased array antennas are elaborated in Section 3.5.1, but characteristics of the antenna are discussed here. A phased array antenna provides electronic beam steering capability that allows the radiated beam to move rapidly at any given direction, without moving the antenna, in either one or both principal planes within milliseconds using a linear (2D) or planar (3D) array configuration, respectively. The direction of the radiated beam is controlled by varying the phase slope applied across the radiating elements of the array, which allows the radiated beam to be pointed towards the desired direction almost instantly, whereas a high antenna gain is achieved by integrating a larger number of elements together within the array. Since the array must consist of many small antennas (sometimes thousands) to achieve high gain, some large phased array systems can range up to a hundred meters wide and consist of a very large number of elements. Hence, such systems can have very complex RF circuitry and, therefore, high manufacturing cost. Phased array antennas are therefore most required and suitable for the surveillance and tracking of fast and agile moving targets, such as a flying aircraft, which requires a high angular resolution and accuracy, a high antenna gain and an instantaneous update rate of the identified target or the area under surveillance.

Although phased array antennas offer the highest performance in terms of target detection and tracking of a wide range of target types, these electronic scanning systems are obtained at the expense of several limitations from other important perspectives. The main

limitations include the high costs of designing and manufacturing the antenna as compared to similar mechanical scanning surveillance radar systems due to the very complex RF circuitry of the array and the restricted scan angle. This is observed especially for units that were designed to fulfil high gain and angular resolution requirements, such as for large coastal surveillance radars, that generally consists of large numbers of radiating elements to produce a narrow and directive beam. Thus, increasing the performance of a phased array antenna would translate to a significant increase on the RF complexity and production cost, which is reflected on the price of high-end electronic scanning surveillance systems to be very expensive, that could reach up to hundreds of thousands of dollars. Complicated architectures of large phased array antennas are also less robust systems as compared to similar mechanical scanning surveillance radar systems, which translates to the requirement for more frequent maintenance in order to realize the maximum performance of the antenna. Although phased array antennas eliminate the wear and tear issue encountered with conventional mechanical scanning antennas due to the use of non-moving parts, which enables them to be a stationary system even while tracking a target, the scan angle of a typical phased array radar is generally limited to just ± 60 degrees with respect to the antenna boresight axis in both principal planes. The restriction on the radar's coverage to a limited sector may be insufficient for certain surveillance applications that requires a wide-angle coverage of the area under surveillance. On top of the limitations mentioned thus far, phased array antennas are also generally known to exhibit a lower frequency agility, which is an undesirable characteristic when subjected to severe atmospheric effects, mutual interference with friendly sources, and jamming from external sources.

In addition to the large initial investment required for the project, a major drawback of the network of multistatic phased array radars implemented along the Strait of Malacca was the high costs and challenges of maintaining the network of radars. Moreover, a recent analysis on the surveillance requirements of the strait have shown a gradual shift in focus towards the monitoring of low-speed patrol boats and container vessels with a RCS of approximately between 30 to 50 m² and between 2000 to 10000 m² respectively (Approximate RCS of various types of ships can be found in Table A-1 (Appendix A)), especially with uncooperative targets significantly reducing over the years. Since the involvement with fast and uncooperative targets has substantially reduced, many have considered replacing a large portion of the phased array systems with simpler alternative systems that are more affordable and robust, such as mechanical scanning radars, which can be considered and opted for instead in most of the radar sites. In addition, mechanical scanning radars are suitable to provide surveillance across a considerably wider angle coverage that extends beyond ± 60 degrees from the boresight axis of the antenna for monitoring of areas close to the shoreline, which is not feasible to achieve with a typical phased array antenna system.

The objective of this project is to propose a radar system that is more suitable towards the environmental conditions of the radar sites and to minimize the issues encountered with the existing network of phased array antennas implemented along the coastline, which were elaborated in Section 1.1.4. A prominent alternative to phased array systems that is considered in this project is a mechanically scanning parabolic reflector antenna. Reflector antennas that are appropriately designed are capable of radiating beams with very narrow beamwidths and very high gain. The performance of such systems can be comparable to electronic systems, and more significantly possesses adequate performance to fulfil the current surveillance requirements of the strait.



Fig 2-1. Surveillance radars using phased array and parabolic reflector antenna in Iran [21]

A large existing range of mechanical radar systems employing a reflector antenna have been used for similar surveillance applications around the world. Conventional mechanical radar systems used for long-range surveillance related applications achieve its directivity with just one high gain parabolic reflector antenna that scans continuously in one direction. The gain of a reflector antenna is highly dependent on the size of the reflector aperture when it is optimally illuminated by the feed antenna, and therefore, unlike phased array antennas, it is independent on the complexity of the RF circuitry. At a given operating frequency, the beamwidth of the beam produced from the reflector in a desired plane is controlled by the dimension of the reflector in that plane. This makes it very common for reflector antennas to use very large dishes when high gain and narrow beamwidths are required in either principal plane. Nonetheless, reflectors come in many different shapes and sizes, and the most suitable type of reflector is dependent on the environmental conditions and the surveillance requirement

of the application. For an imaging and tracking radar, the use of a circular parabolic reflector is the most common choice.

A conventional center-fed reflector antenna consists of a single feed and parabolic reflector, and therefore has very minimal RF hardware. Hence, the RF circuitry for all types of reflector antenna would be similar regardless of performance requirements, and therefore the complexity and manufacturing cost of a high-end reflector antenna is significantly lower as compared to a phased array antenna, assuming both antennas were designed to have the same performance. The minimal use of RF components in typical reflector antennas also explains the less frequent maintenance required for mechanical scanning radars. Moreover, the frequency agility and broadband characteristics of reflector antennas is more superior and flexible as to compared to that of phased array antennas, which allows the adjustment of the operating frequency of the radar, when required, to account for any possible external factors encountered. In addition, the continuous rotation of the antenna allows the radar to provide a complete coverage of the area under surveillance. Although mechanical scanning radars are generally incapable of providing an update rate that is as rapid as phased array systems, a faster antenna rotation speed can be chosen relative to the average speed of the vessels passing through the strait to provide a shorter update rate of the area under surveillance (few seconds), which is necessary to achieve a higher probability of target detection through the integration of a larger number of scans. Experimental measurements shown in [22] have also proven that increasing the antenna rotation speed would improve the detection performance of a target in moderate sea state when integrating a fixed number of scans, providing the fundamental limits of the permissible rotation speed has been considered, which is based on time of flight of the pulse within the antenna beamwidth.

Although both types of scanning radar have been used in many surveillance systems along major waterways around the globe, the system of choice is heavily dependent on the surveillance requirement of the strait (i.e. type of target dealt with) and the financial resources available (i.e. optimization of the project cost). The main characteristics and advantages of an electronic scanning phased array antenna and of a mechanical scanning reflector antenna are compared to one another and summarized in Table 2-1.

Phased Array Antenna	Reflector Antenna
Electronic Beam Steering that allows rapid beam pointing.	Wider bandwidth
Fast beam shaping by aperture control.	Higher frequency agility
Stationary antennas with no moving parts allows inertialess beam movement	360 degree scan angle
Offers the highest performance in terms of target detection and tracking.	Use of a single high gain antenna allows for significantly less RF components and complexity.
	Quick and cheap design cycle.
	Significantly cheaper antenna systems.

Table 2-1. Comparison of a phased array antenna and parabolic reflector antenna [23] [24]

2.2 Mechanical Scanning Reflector Antenna Systems

Surveillance radar systems employing center-fed reflector antennas achieve very high gain and cross-range resolution by incorporating large parabolic dishes. The size of the reflector aperture is dependent on the principal plane beamwidth and gain requirements of the designed antenna, which is chosen to fulfil the maximum operating range and resolution performance of the radar (at maximum range) required for the application in hand. Thus, the use of large sized reflector apertures is common in situations where high detection performance is required. At operating frequencies within the X-band spectrum, which is the frequency band of most radars implemented along the strait, the diameter of the reflector used are generally in the range of a few meters up to tens of meters. However, the use of a large reflector to produce a narrow beamwidth is unattractive and has frequently become an issue especially when deployed in rural areas with limited accessibility and space constraints. The immobility of large reflector antennas also makes it difficult to transport under harsh conditions, given that some of the chosen radar sites are situated on small islands that do not have basic infrastructures that is suitable for transporting large objects. In addition to the unattractive antenna size, the use of metallic materials causes the overall weight of the antenna to become heavy and expensive to manufacture, although it would still be considerably cheaper than a phased array radar of similar performance.

Inevitably, the surveillance requirements of the strait from certain radar sites can be provided by implementing well-designed mechanical scanning radar systems. The proposed mechanical surveillance radar utilizes a reflector antenna system that aims to provide continuous monitoring over a complete 360 degree coverage of mainly medium to large sized

ships and low-grazing targets above the sea surface over operating ranges of approximately 20 to 40 km, and to minimize the limitations encountered with existing center-fed reflector antenna systems. This can be achieved through the design of a reflector antenna, or more specifically the feed design, and a newly proposed signal processing technique that prioritizes on improving the detection performance of the antenna without increasing the size of the reflector antenna and at a significantly lower cost. Hence, the proposed design also places significant importance on minimizing the weight and manufacturing cost of the reflector antenna, which is also further achieved by manufacturing the antenna using alternative materials and newer methods of construction.

Prior to discussing the proposed reflector antenna design and the signal processing technique introduced in this paper, several popular existing angle measurement techniques employed by reflector antennas to provide accurate positional information of a stationary or moving target relative to the antenna boresight axis, in azimuth and elevation, are discussed. The techniques described are popular methods used to provide the angular information of a detected target with an accuracy that is significantly higher than that of a conventional center-fed reflector antenna system employing a circular parabolic reflector of the same size.

2.2.1 Angle Measurement Techniques for Reflector Antennas

In any coastal surveillance radar system, the successful detection of a ship depends on many factors such as clutter intensity, detection range and the radar system performance itself. Since the target signal is mixed with noise and sea clutter, radar signal detection is probabilistic in nature [22]. The ability to distinguish between the target echo signal from sea clutter and system noise defines the performance of a radar system, which is quantitatively defined by the probability of detection (i.e. probability of detecting a radar target against the background noise and clutter) and the probability of false alarm (i.e. probability that the reflected clutter or noise signal is mistaken as a target) [25]. These radar parameters are justified based on the threshold value chosen by the designer, which is dependent on the requirements of the application in hand, the type of target dealt with and considering the environmental factors encountered.

Clutter refers to the unwanted interfering echo signals that reach the radar, typically returned from ground or sea due to manmade or natural objects which act like pseudo targets [26]. When a coastal surveillance radar is operational, competition with the desirable radar returns from targets such as small to medium sized patrol boats, ships, tankers and their movements, are many sources of clutter. For coastal surveillance radars, backscatter of the transmitted signal by sources of clutter include sea returns, the weather, and birds, which often places severe limits on the detectability of returns from ships, and other targets that shares the

radar resolution cell with the sea surface [26]. Due to the presence of clutter within the radar echo footprint at all operating ranges, supposedly straightforward detection of targets with low RCS is likely to remain undetected (i.e. lower probability of detection), and therefore poses a significant problem across a wide range of applications, although some target detection schemes and signal processing techniques can achieve better detection performance of targets (i.e. higher probability of detection and lower false alarm rate). Evidently, the dominant source of clutter observed in coastal surveillance radars are known as sea clutter (i.e. clutter attributed from elements of the sea surface such as sea wave crests and turbulent rough ocean surfaces), which appears to be strongly influenced by environmental conditions. Nonetheless, radar system parameters and its configuration, such as viewing geometry, range resolution or cell size, polarization, transmission frequency and grazing angle at the sea surface also strongly influences the amount of sea clutter observed [25].

In heavy sea conditions (high sea states), surface events such as breaking waves and other surface effects contributes to the production of sea spikes, that is, spikier sea clutter that has considerably higher power due to huge radar reflections. In practice, when real radar returns are presented on an A-scope (signal amplitude versus range), spikier sea clutter is seen as a “sunburst” in the radar display screen and is likely to obscure a target that is present within the same range bin under test [25]. Similarly, as shown in Figure 2-2, the appearance of spikier sea clutter on a PPI display may either obscure a small target or be mistaken for a valid target.

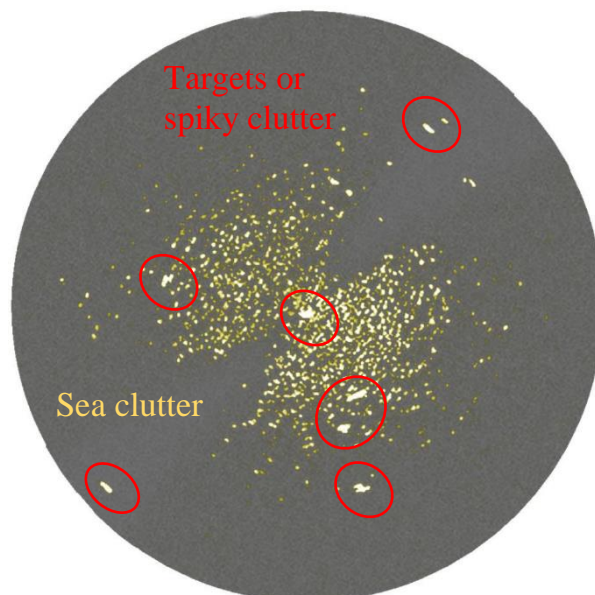


Fig 2-2. Sea clutter on a PPI-scope display [27]

For a 2D coastal surveillance radar, the appearance of sea clutter also depends strongly on the amount of radar echo footprint received, or the size of the resolution cell, which is determined by the range and angular resolution of the radar antenna. The azimuth beamwidth of the antenna pattern can be related to the importance of the radar resolution and the amount of clutter footprint within the radar echo received. It determines the width of the clutter patch or resolution cell on the surface of the sea [27], which is a measure of how wide a patch of sea is illuminated by the radar at a given distance. For large cells, clutter appears distributed in range and may be characterized by a surface-averaged cross section with relatively modest fluctuations about a mean value. As the size of the resolution cell is reduced, clutter increasingly appears to contain sequences of isolated target-like, or discrete, returns that vary in time. At even higher angular resolutions, the discrete target returns tend to stand well out of the background [25]. Hence, for optimum detection performance the resolution cell obtained should be made as small as possible to minimize sea clutter returns from a single sweep, and therefore a radar that radiates a beam with a narrow beamwidth is critical in increasing the interference immunity and clutter resilience of the radar. Nonetheless, achieving a narrow beamwidth is not feasible, and therefore a suitable antenna beamwidth is generally dependent on the angular resolution requirement of the system in both planes.

As mentioned, the -3 dB beamwidth of the beam produced determine the angular resolution of the antenna in the respective planes, which is defined as the angular separation at which two equal targets can be distinguished individually when at the same range from the antenna [25]. The relationship between the azimuth beamwidth, θ_a , of the radiated beam pattern and the angular resolution as a distance between the two targets, S_A , in the horizontal plane is given by (2-1) and described by Figure 3-19, since we are concerned with the resolution of the radar in the horizontal plane.

$$S_A \geq 2R \cdot \sin \frac{\theta_a}{2} \quad (2-1)$$

where R is the slant range of both targets from the radar.

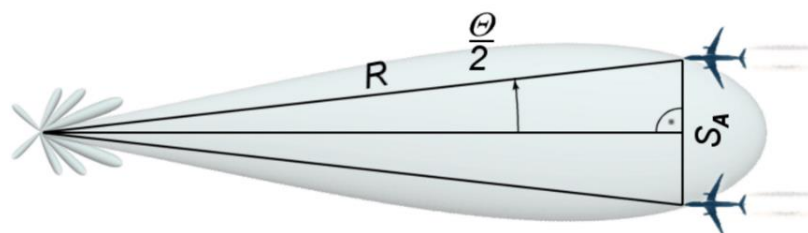


Fig 2-3. Illustration of angular separation or distance, S_A , between two targets [27]

Figure 2-4 provides an example of two separate targets that are located within the beamwidth of a main lobe (i.e. 17 degrees). In the given illustration, the wide beamwidth prevents the radar from distinguishing the two targets separately, but instead identifies them as a single target. In addition, a target echo received through a standard antenna pattern gives no information about the positional information of the target other than it is most likely within the main lobe of the beam. Hence, a wide beamwidth would correspond to a poor accuracy of the angular location of a target obtained.

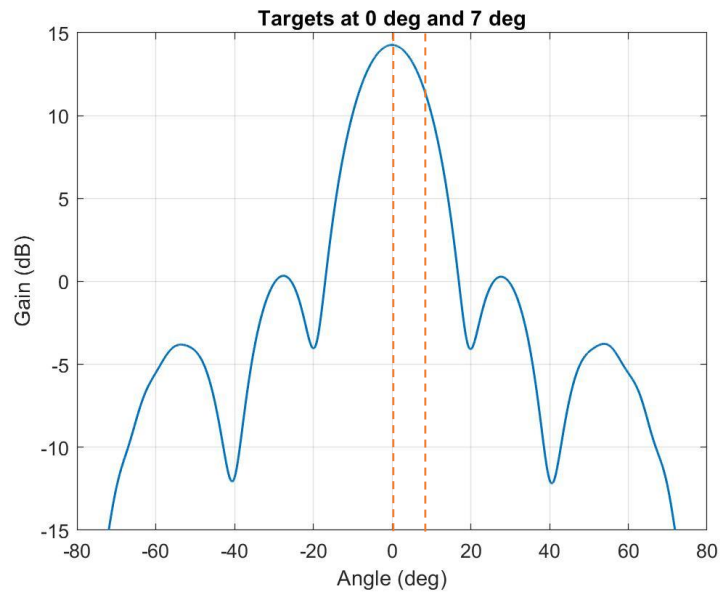


Fig 2-4. Two targets within a single beamwidth

The relationship between the angular resolution and beamwidth of the antenna shows that the resolution performance of an antenna worsens proportionately with increasing detection range, which can prove to be very critical at long ranges. In radar measurements, a higher direction determination or finding accuracy of the position of a detected target, which is assessed based on the difference between the measured value and true value of a target, is also received as a minor by product of a high angular resolution since the position of the target is within a smaller beam. Hence, a radar system with a narrow azimuth beamwidth is capable of providing accurate bearing information of a target and tend to produce radar systems with a higher clutter resilience and, therefore, a higher detection performance. Nonetheless, sources of measurement errors that can have a significant effect on both the accuracy and precision of the antenna measurements provided are due to a combination of many factors, including sources of target phenomenology, signal propagation characteristics, system measurement limitations, system uncertainties and most importantly, for a surveillance radar, due to sources of interference [29].

For a mechanically scanning radar operating at frequencies at VHF and above, the direction-finding capability of an ordinary radar can be improved to achieve a higher detection performance by mechanically rotating the entire antenna system in both principal planes until a maximum signal is observed. When a narrow beam is scanned through the direction of an incoming signal, the direction of the strongest signal allows the location of the maximum direction denoting the presence of a target to be determined. Nonetheless, the improvement in detection accuracy achieved through this method is only limited to within some fraction of the beamwidth, and therefore still provides unsatisfactory performance for applications requiring higher accuracies. This fraction can be made very small by implementing several angle measuring techniques on existing surveillance radar systems that have been devised to significantly enhance the accuracy of target imaging and tracking measurements, which is critical for applications requiring extremely high accuracy. The tracking methods allows an enhancement on the radar capability, each to a different extent, in more accurately locating targets that is within the same resolution cell.

The three most common tracking methods discussed in this section operates on certain common principles. The principle of these techniques involves comparing the signal strength of two or more radar returns, which measures the difference in echo signals received from two or more different positions, respectively, from which the angular position of the target in the plane of interest is determined. Hence, the radar uses the angular deviation of the target within the beam from the boresight, or tracking, axis of the radar to generate an error signal. This deviation is normally measured from the position of a target from the antenna tracking axis. The resultant error signal describes how much the target has deviated from the tracking axis of the antenna. If a target is positioned on the tracking axis, then the target angular position would be the same as that of the beam and a zero-error signal is produced, although in practice this is rarely the case [24].

To generate an error signal in any given plane, the techniques described below requires at least two or more stationary feed, or a single feed that is continuously shifted off-axis from the nominal beam direction by equal fractions of a beamwidth in both planes, to radiate two or more off-axis beams sequentially or simultaneously without moving the antenna as a whole. This beam shifting can be done either in rapid time sequence (sequential lobing) or by generating two beams at the same time (simultaneous lobing). The three methods described below are most popularly used in modern radar systems for angle of arrival (AOA) determination of a detected target. For any of the tracking methods employed by a tracking radar, in addition to providing the angular position of a detected target, the objective is for the tracking axis of the antenna to be continuously aligned to the position of the target in free space based on the error signals generated. Nonetheless, as will be described, modern tracking radar

systems that are used in many areas from civil, air traffic control, to various military applications tend to implement monopulse techniques [30] [31] as they provide the greatest enhancement in detection accuracy at the expense of higher cost.

2.2.1.1 Sequential Lobing

Sequential lobing is a popular technique used in earlier generation of radar systems employing reflector antenna systems to improve the angle measurement accuracy for target detection and tracking. The technique uses two consecutive dwells on the target from a single beam that is continuously switched between two pre-determined symmetrical positions around the antenna's boresight, or tracking axis to refine each angle measurement. A comparison of the amplitude of the target echo received from the two positions identifies the position of the target to be closer to the angle of the measurement with the larger amplitude. The first measurement is taken with the boresight of the antenna pointing slightly to one side of the predicted target position, while the second consecutive measurement is taken with the boresight of the antenna pointing slightly to the other side of the predicted position [29].

In a sequential lobing system this shift may be made by mechanically moving a single feed off-axis in one direction, then in the opposite direction, at a rapid rate. Another method is to use two separate feeds of a pre-determined position, each displaced a small amount from the optical axis, in opposite directions, and the receiver is continuously switched between the lobes [24]. If two fixed feeds are used, the radiation properties of the pair of beams must be identical to one another in order to obtain more accurate results. The type of beam used in a sequential lobing system must have a radiation pattern that is symmetrical in both principal planes, such that the principal plane beamwidths of the beam is identical. This type of beam is also known as a pencil beam.

For both feed systems described, switching the beam between the two pre-determined positions in a given plane allows the technique to provide the approximated angular position of the detected target relative to the tracking axis by comparing the amplitude of the received signals measured by the radar. The difference of the two measured signal levels is used to create an angular error voltage signal. For example, an on-axis target produces zero error signal as the strength of the pair of signals received are equal (Figure 2-5(a)). Thus, no difference voltage signal is created. The accuracy of the predicted target angle is improved when the power measured from the two positions are of equal strength. However, for an off-axis target a nonzero error signal is produced as the strength of the pair of signals received are not the same (Figure 2-5(b)). Thus, a difference voltage is created, which is used to drive the servo-control system that redirects the reflector antenna towards the target. The polarity of the voltage difference

determines the direction in which the antenna must be moved. The objective of the technique is to align the pair of beams such that the voltage difference signal is equal to zero.

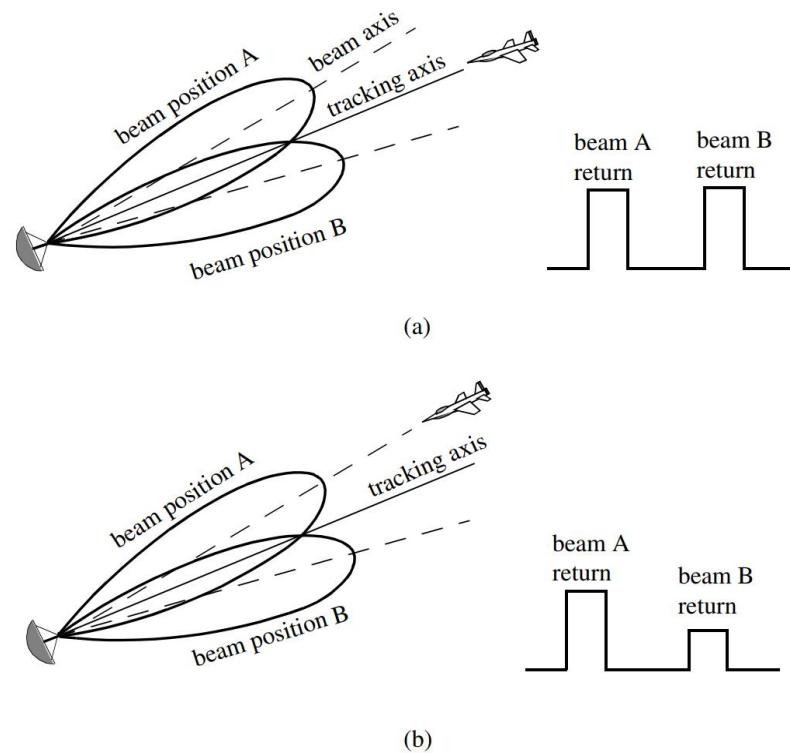


Fig 2-5. Sequential lobing (a) Target is located on track axis. (b) Target is off track axis [24]

The technique can be extended to obtain the angular error, or positional information of the target relative to the boresight axis, in the orthogonal coordinate (i.e. in azimuth and elevation). However, two more switching positions are required to implement sequential lobing in the second coordinate along with continuous lobe switching between azimuth and elevation, which requires another pair of feed. Tracking in two coordinates can be accomplished by using a cluster of four antennas (two for each coordinate) or by a cluster of five antennas. In the latter case, the middle antenna is used to transmit, while the other four are only used to receive [24]. The complexity of the RF circuitry is considerably increased when tracking in both principal planes are required.

The advantage of sequential lobing over other angle measurement techniques is its simple implementation. Radars employing sequential lobing only uses a single receiver since the pair of beams are switched consecutively between them in order for the amplitude of the received signal corresponding to each transmitted pulse to be compared. However, the angular accuracy of the positional information of a detected target provided by this technique is dependent on, and therefore limited by, the antenna beamwidth, and the continuous switching

of the beam makes the system very susceptible to pulse-to-pulse amplitude fluctuations of the target echoes due to scintillation in the RCS of the target. The accuracy is also affected by the noise caused by either mechanical or electronic switching mechanisms.

2.2.1.2 Conical Scan

The second angle measurement technique is known as conical scan. Conical scan is considered as an extension of sequential lobing due to same principles of the technique, except that conical scanning systems initiates for the detected target to always be on the tracking axis of the radar antenna. In a conical scanning system, the beam sweeps and outlines a shape of a cone about the boresight axis, from which the measured strength of the radar signals received from each individual position of the rotating feed is compared [29]. This is most commonly achieved by continuously changing the position of the antenna beam through moving a single feed in a circular motion around the boresight axis of the antenna, instead of switching between the pre-determined positions of the individual beams observed in sequential lobing [29]. Based on the received radar returns from the different positions, the method achieves angle tracking in both principal planes.

A typical conical scan beam is illustrated by Figure 2-6. The beam scan frequency, in radians per second, is denoted as ω_s , and the angle between the tracking axis of the antenna and the beam axis is the squint angle φ . The position of the radiated beam is continuously changed so that the tracking axis is always aligned to the position of the target based on the amplitude of the received signals at different positions [24].

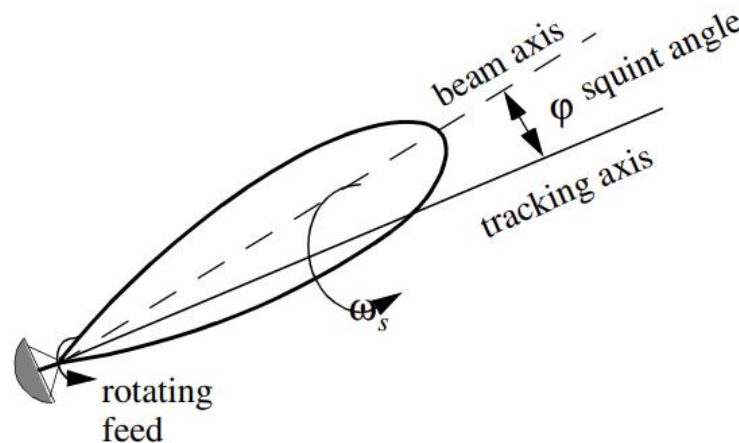


Fig 2-6. Conical scanning beam [24]

Figure 2-7 shows a simplified conical scan radar system. The envelope detector is used to extract the amplitude of the amplified received signal and the Automatic Gain Control (AGC)

generates the error voltage signal that continuously attempts to hold the receiver output to a constant value by realigning the position of the feed. It follows that the tracking error signals (azimuth and elevation) are functions of the target's RCS and of its angular position with the main beam axis [24].

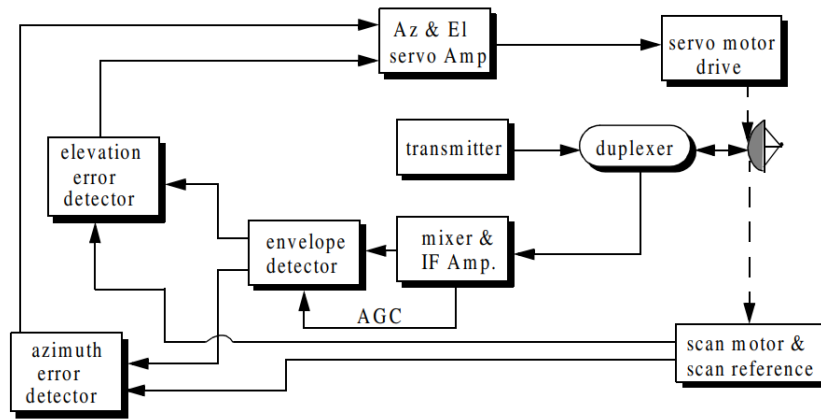


Fig 2-7. Simplified conical scan radar system [24]

There are two situations encountered in such systems while tracking a target. The first case, shown in Figure 2-8, occurs when the target is aligned with the tracking axis of the antenna system. In this case, as the antenna or radiated beam rotates around the tracking axis the strength of all the radar returns received from the different positions of the beam are the same. Hence, no error signal is produced, and the positional information of the target is obtained from the direction of the antenna tracking axis. At this instant no further action is required.

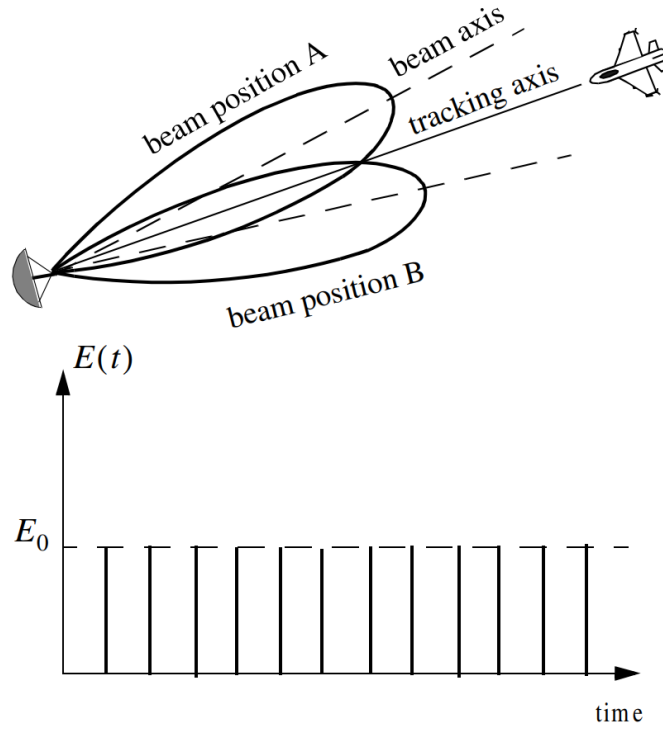


Fig 2-8. Received AM signal produced when target is on the boresight axis [24]

The second and most common case is illustrated in Figure 2-9. In this case, when the beam is at position B, the strength of the echo signal received from the target is the maximum. As the beam rotates and eventually is at position A, the strength of the echo signal received from the target is the minimum. Between these two positions, the strength of the target returns varies between the maximum value at position B, and the minimum value at position A. In other words, Amplitude Modulation (AM) is applied on the received return signal. This AM envelope corresponds to the relative position of the target with respect to the motion of the beam, which upon extraction of the envelope creates an error signal that the radar uses to drive a servo-control system that aligns the radar tracking axis on the position the target in both principal planes. It follows that the azimuth and elevation errors are in the form given by (2-2) and (2-3), respectively [24].

$$\varepsilon_a = \varepsilon \sin \varphi \quad (2-2)$$

$$\varepsilon_e = \varepsilon \cos \varphi \quad (2-3)$$

where the quantity ε defines the distance between the target location and the antenna's tracking axis and φ is the squint angle, that is, the angle between the beam axis and tracking axis.

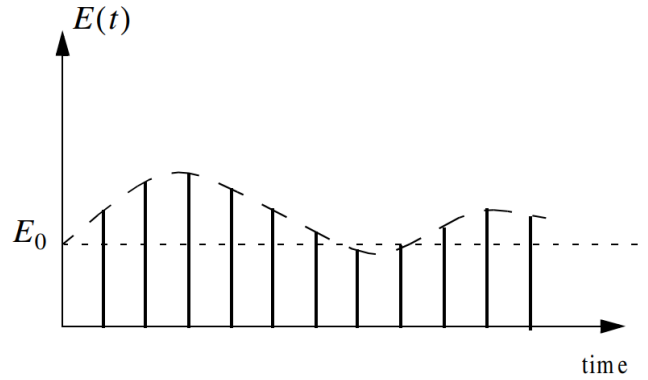
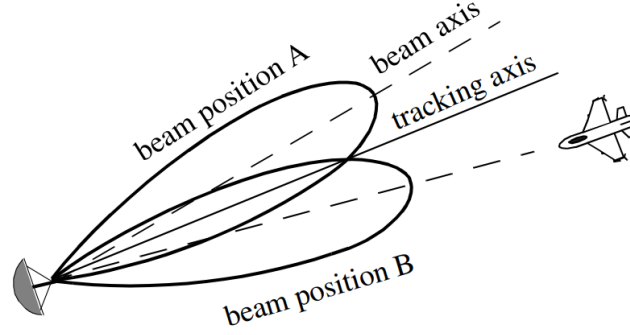


Fig 2-9. Received AM signal produced when target is off the boresight axis [24]

The received AM signal $E(t)$ can be written as

$$E(t) = E_0 \cos(\omega_s t - \varphi) = E_0 \varepsilon_e \cos \omega_s t + E_0 \varepsilon_a \sin \omega_s t \quad (2-4)$$

where E_0 is a constant called the error slope, ω_s is the scan frequency in radians per seconds, and φ is the defined squint angle.

The scan reference is the signal that the radar generates to keep track of the antenna's position around a complete path (scan). The elevation error signal $E_e(t)$ is obtained by mixing the signal $E(t)$ with $\cos \omega_s t$ (reference signal) followed by low pass filtering [24]. $E_e(t)$ is given by

$$E_e(t) = E_0 \cos(\omega_s t - \varphi) \cos \omega_s t = -\frac{1}{2} E_0 \cos \varphi + \frac{1}{2} \cos(2\omega_s t - \varphi) \quad (2-5)$$

and after low pass filtering the corresponding signal becomes

$$E_e(t) = -\frac{1}{2} E_0 \cos \varphi \quad (2-6)$$

The antenna beam is driven downward if the polarity of the elevation error is negative, and upward if positive. Similarly, the azimuth error signal is obtained by multiplying $E(t)$ by $\sin \omega_s t$ (reference signal) followed by low pass filtering [24]. $E_a(t)$ is given by

$$E_a(t) = \frac{1}{2} E_0 \sin \varphi \quad (2-7)$$

Although the accuracy of the angle measurement provided from a conical scan system is higher than a sequential lobing system, this method requires the radar to receive at least four target returns to determine the angular position of the detected target in azimuth and elevation coordinates (two returns per coordinate). Hence, the antenna scan rate is limited by the scanning mechanism of the radar (mechanical or electronic) since the theoretical maximum conical scan rate is equivalent to one fourth of the pulse repetition frequency (PRF) [29].

Furthermore, the squint angle of the rotating beam from the nominal tracking axis needs to be sufficiently large in order to measure a good error signal with a high SNR. However, continuously rotating the beam about the tracking axis of the antenna at a specific squint angle also causes the antenna gain to be less than maximum in the direction of the boresight axis. Hence, when a target is positioned on the tracking axis, the signal to noise ratio (SNR) is reduced by an amount equivalent to the drop in the antenna gain. This loss is known as the squint or crossover loss [24]. To reduce this loss the chosen squint angle is usually limited to a certain angle such that the two-way (transmit and receive) crossover loss is less than a few decibels.

When tracking of an identified target in both principal planes are required, the techniques mentioned thus far (sequential and conical scan) are both inefficient with respect to radar time and energy and are easily deceived or jammed by the projected target. Nonetheless, both methods are the most feasible with microwave reflector antennas that does not require very high accuracy since the required mechanical motion is not very great as well. The most frequently adopted angle measurement technique in current radar systems requiring very high angular accuracy is known as monopulse.

2.2.1.3 Monopulse Technique

Monopulse is a simultaneous lobing technique that was developed to overcome the limitations of sequential lobing and conical scan. It is the most accurate type of tracking method used to provide precise angular information in azimuth and elevation through error signal generating methods. Monopulse is mainly used for surveillance and tracking applications to fulfil the requirement of achieving very accurate target angle measurement for identifying the precise position of a target within the beamwidth. Monopulse radars can employ both reflector and

phased array antennas, but the discussion of both methods here are concentrated on reflector antennas only. There are two types of monopulse technique frequently implemented on existing reflector antenna systems, that is, amplitude and phase comparison monopulse. The principles and implementation of both types of monopulse technique are described here.

2.2.1.3.1 Amplitude-comparison Monopulse

Amplitude-comparison monopulse is a form of monopulse in which the angular deviation of the target from the antenna boresight axis in a single plane is measured as the amplitude ratio of the target as received by two antenna patterns [32]. The difference between monopulse and other angle tracking methods is that the beams are generated simultaneously rather than sequentially. For this purpose, a special antenna feed is utilized such that the beams are produced using a single pulse. In the most common form of amplitude monopulse reflector antenna employing multiple feeds, a pulse is transmitted directly at the predicted position of the target and the target echo is received with two separate feed horns, each corresponding to a squinted beam, in a single plane. The radar continuously compares the amplitudes and phases of the beam returns to sense the amount of target displacement off the tracking axis of the radar. Hence, the implementation of monopulse in both principal planes would require at least four feeds (four-horn feed system) to receive the echo signals of four separate squinted beams, where the amplitude of the echo signal received in each feed horn will differ from one another unless the position of the detected target is situated exactly on the tracking axis, from which the horns would receive an equal amount of energy. For the detection of an off-axis target, this unbalance of energy received at the respective feed horn provides the positional information of the target relative to boresight and is also used to generate a dc voltage that drives the servo-control system in each plane to redirect the position of the squinted beams.

There are several types of amplitude monopulse feed systems, which are described in Section 2.2.2, and for all feed systems the monopulse processing consist of the creation of a sum and two difference (azimuth and elevation) signals, which is typically the sum and differencing of the received signals from the feed outputs, respectively. The sum and difference signals are most commonly produced using sensitive passive RF devices such as microwave comparator circuitry, directional couplers or hybrid junctions. The signal received at the feed outputs are connected to the input of a receiver in the sum and difference channels through a hybrid junction for a one-coordinate monopulse antenna, or a comparator for a two-coordinate monopulse antenna, which performs the addition and subtraction of the received signals to produce a difference signal corresponding to each (single or dual) coordinate and a sum signal, before it is fed to the appropriate sum and difference channels (receiver) that is connected to the output of the device. Hence, it is critical that the sum and difference channels have a constant

phase relationship and are the same in both transmit and receive modes. Figure 2-10 shows a block diagram of a one-coordinate amplitude monopulse system.

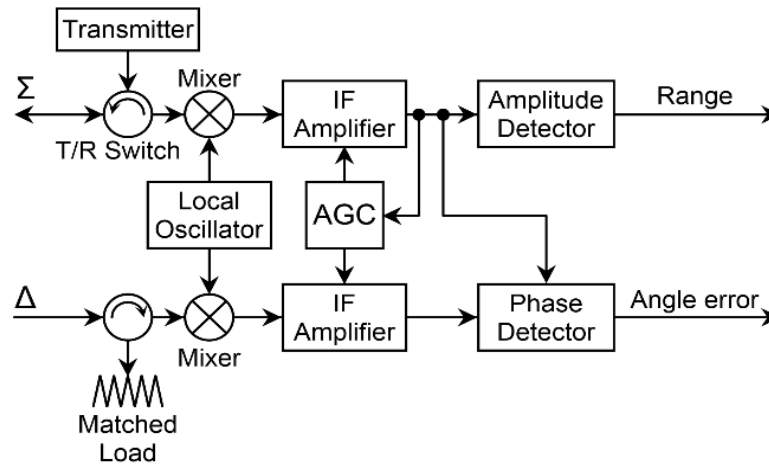


Fig 2-10. Amplitude monopulse radar block diagram [33]

The circuitry shown above for a 2D monopulse system consists of two separate receiver channels; one channel is fed with the difference signal (Δ) obtained from the difference of the pair of beams usually in the horizontal plane (azimuth angle difference channel), and a second channel that is fed with the sum signal (Σ) obtained from the sum of the feed outputs (sum channel). In a 3D monopulse system, a second difference channel is required to accommodate for the difference signal obtained from the difference of the pair of beams in the vertical plane (elevation angle difference channel). Hence, 3D monopulse radars are more complex systems with more complicated RF circuitry as it requires two difference channels, instead of one, and a sum channel. The important characteristics of a monopulse antenna are the sum pattern on-axis gain and beamwidth, the difference pattern on-axis slope, and the sidelobe profile of the two patterns [37]. Figures 2-11 illustrates the typical sum and difference monopulse patterns corresponding to either principal plane.

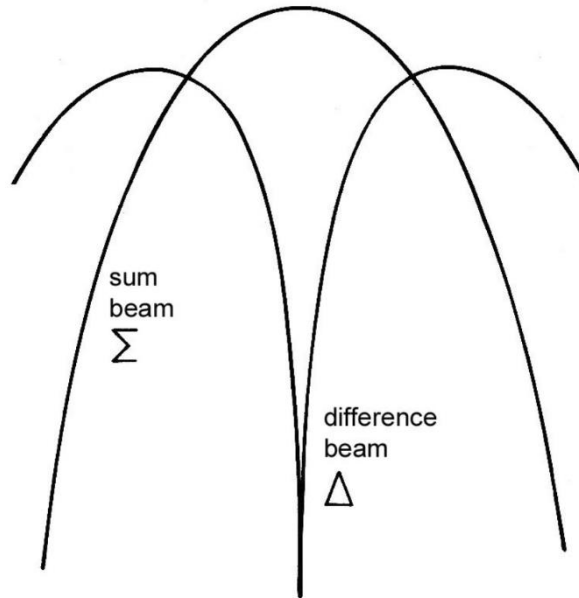


Fig 2-11. Monopulse antenna sum and difference beam

The sum channel produces a sum signal that corresponds to the sum of the signals at each feed. Hence, the shape of the sum beam pattern resembles closely to a cosine function with the highest gain at the antenna tracking axis. The sum signal exhibits a high SNR and, therefore, after amplitude detection, it is used for target detection and to provide range measurements of a target. However, the sum channel output does not provide the positional information of a target since the beamwidth of the sum pattern is usually several times wider than that of the individual beams. Hence, the sum channel is used in transmit and receive modes. The sum signal is also used to find the manipulation of the amplitude of the received pulse due to the target's RCS and range, which is explained below. The sum channel also provides a phase reference signal to the phase detectors of each difference channels, which is used to identify the direction sense of the target's position in both principle planes by realizing the polarity of the angle-error voltage measurement from the outputs of the respective difference channels.

The difference channel, on the other hand, produces a difference (error) signal that corresponds to the difference of the signals received from each feed when there is an unbalance in signal strength caused by an off-axis target. Passive RF devices mentioned in Section 3.6.1 are used to obtain the difference in signal strength of the output of the left pair of beam from the output of the right pair of beams to sense any unbalance in the azimuth direction, and the output of the top pair of beams from the output of the bottom pair of beams to sense any unbalance in the elevation direction, providing the operator with the target's position relative to the boresight axis of the antenna in both planes. Hence, each subtractor output is associated with the target's position in the respective principal plane, and any target movement along the

horizontal and vertical axis of the antenna would cause a rapid change in strength of the error signal produced. During operation, the antenna might have scanned across a fraction of a beamwidth and suddenly realize an absence of error signal in the difference channels when a target is positioned at the center of the antenna axis, or in the event of a target moving from left-to-right or right-to-left of the boresight axis, which corresponds to the null of the difference beam associated with both principal planes. Hence, the subtractor outputs zero signal when the target is on axis, and it is at this point where the angular position of a target is accurately located through the angle sensing information of the radar.

However, the estimated angle of arrival of the target obtained from the amplitude of the difference voltage signal obtained is not only a function of the target angular position, but also on the target's RCS and range. Hence, the error angle information of an off-axis target relative to the boresight axis of the antenna in both principle planes would not give a true indication of the target position. An error signal that is independent of the echo amplitude is required to achieve and maintain a constant angle-error sensitivity (volts per degree error), and therefore tracking sensitivity, for stable automatic angle tracking when implemented in a tracking radar. To achieve this, after the sum and difference signals obtained from the RF device are amplified by the receivers within each channel, the angle measurement dependency of the error signal on the target range and RCS is removed by estimating the angle of arrival of the target with the in-phase part (i.e. the real part) of the monopulse ratio. The monopulse ratio is obtained by normalizing the difference signal to the magnitude of the sum signal (reference signal), that is, the ratio of the difference to sum, so that the monopulse output is only a function of the target angle. This ratio can be obtained using an Automatic Gain Control (AGC) circuit that operates on the respective difference channels and is driven by the output of the sum channel, or by division after detection in a digital tracker [44]. The normalized monopulse output is linearly proportional to the angular deviation of the target from the boresight usually over a range of a few beamwidths, which allows the direction of arrival of the target to be accurately determined based on the error angle obtained.

The angle-error detector has an output [35]

$$|e| = \frac{\Delta}{|\Sigma|} \cos \theta \quad (2-8)$$

Where $|e|$ = magnitude of the angle-error-detector output voltage

$|\Sigma|$ = magnitude of sum signal

Δ = difference signal

θ = phase angle between sum and difference channels (0° or 180°)

The above error voltage that is proportional to the ratio of the difference signal divided by the sum signal is the desired angle-error-detector output, giving a constant angle error sensitivity.

Phase sensitive detectors within the difference channels associated with the principle planes are used to determine the sign of the error voltage signal produced, or to provide the sense (direction) of the error, through the comparison of the phases of the sum and difference signals in special receiver circuits [24]. Phase sensitive detectors demodulate the azimuth and elevation error signals using the sum channel IF signal as a reference to produce the two polarized error voltages [24]. Hence, the phases are adjusted to provide 0 or 180 degree on a point-source target depending on which side of the tracking axis the target position is on. The resultant is

$$|e| = \pm \frac{\Delta}{|\Sigma|} \quad (2-9)$$

The polarity of the difference signals, in both planes, will reverse as the signal direction changes from right-of-center to left-of-center in the horizontal plane, and from the top-of-center to bottom-of-center for the vertical plane, which correspond to a 180-degree change in phase from one side of center to the other. Thus, this enables the radar to obtain angular error signals in both planes that include both the amplitude and sign of the error relative to the boresight axis in both principal planes.

In tracking radar systems, the signed angle-error detector output voltage produced from the respective difference channels corresponding to the mutually perpendicular planes are used to drive the servosystem that accurately directs the antenna in both planes towards the position of the target. This would consistently position the target along the normal boresight axis of the antenna to achieve automatic angle tracking of a specific target. A zero-error signal is realized in both difference channels once the target is situated at the center of the boresight axis and the position of the tracked target is identified to a significantly higher precision and accuracy as compared to the performance of a conventional tracking radar employing a reflector antenna.

It is apparent that the difference pattern exhibits a very sharp null, rather than blunt like the shape of the peak of an original lobe, and therefore it is possible to achieve a very high accuracy that is much greater than by simply observing the maximum direction of a beam. The angular accuracy, or angle-error sensitivity, of an amplitude-comparison monopulse system is dependent on the on-axis slope of the difference pattern and the SNR of the system. If optimized, the accuracy of a monopulse radar can be as accurate as to a tenth of the beamwidth of the original system [36] in that plane, although a compromise between maximizing the angular accuracy (difference pattern) and detection sensitivity (sum pattern) of a radar frequently exist. Hence, the modelling of a suitable feed arrangement of the reflector antenna

is critical to ensure that the difference pattern obtained is optimized according to the requirement of the application in hand.

The advantage of monopulse is that it provides a refinement of the measurement accuracy of the angular position of a detected target with only a single pulse. Since the amplitudes of the squinted beams of a monopulse antenna are all obtained and compared to produce the error signals, on a single-pulse basis, the errors that degrades the tracking accuracy of the antenna due to amplitude fluctuations of target echoes observed in other radars employing other forms of tracking methods, which requires at least two successive pulses for its operation, are significantly reduced. Hence, monopulse tracking is more accurate and very efficient with respect to radar time and energy and is significantly less susceptible to lobing anomalies, such as AM jamming and gain inversion ECM, since the method relies on two or more simultaneous beams instead of a sequential approach. Monopulse systems are, therefore, more difficult to jam or deceive as compared to other similar angle tracking systems [29].

It is evident that a monopulse antenna is suitable for accurately locating and tracking targets in either one or both planes simultaneously, especially at long distances where angular resolution becomes a real issue, to a significantly higher accuracy as compared to conventional radar systems. The advantages of monopulse over other methods are particularly important for systems that are required to maintain simultaneous tracks on several targets. However, a noticeable disadvantage of monopulse that allows other angle measurement to be considered for less demanding applications is the higher cost of implementation and significantly more complex RF circuitry.

Main Advantages of Monopulse
Refinement of measurement accuracy with only a single pulse, and therefore less errors.
More accurate and very efficient with respect to radar time and energy.
Significantly less susceptible to lobing anomalies and jamming.
Offers the highest performance for target detection and tracking operations.

Table 2-2. Advantages of monopulse compared to other angle measuring techniques

An alternative approach to amplitude-comparison monopulse is phase-comparison monopulse. Both types of monopulse are essentially equivalent in theory and in its RF circuitry.

However, they differ in principles of operation, design and in practical performance since the former and latter relies on the amplitude difference and on the phase difference of two or more measured signals, respectively, to accurately determine the direction of arrival of a signal. Hence, the design and physical construction of a phase and amplitude monopulse radar employing a space fed antenna differs from one another.

2.2.1.3.2 Phase-comparison Monopulse

Phase-comparison monopulse employs receiving beams from separate aperture regions with different phase centers. It is often achieved by offsetting two or more individual antennas with their phase centers separated, usually side by side, or from separate portions of an array with radiating beams that are pointed in the same direction [27], from which the information on target displacement from the antenna boresight axis in one-coordinate appears as a relative phase between the signals received at the two phase centers [32]. Assuming the detection of an off-axis target with a phase monopulse system, the amplitude of the received signal arriving from an off-axis direction at the respective antenna outputs will be of equal strength but with a phase difference. The phase difference of the received signals is then used to generate an error signal in that plane that indicates the position of the target relative to the boresight axis in that plane.

Figure 2-12 illustrates a one-coordinate phase monopulse antenna employing two center-fed reflector antennas that are positioned side by side and joined together at their edges, with the respective phase centers separated by a distance, d . A baseline between the phase centers of the two antennas creates a path length difference ($d\sin\theta$) between the respective phase centers of each antenna and the detected target, which causes a phase difference ($\Delta\phi$) to be created between the signals received.

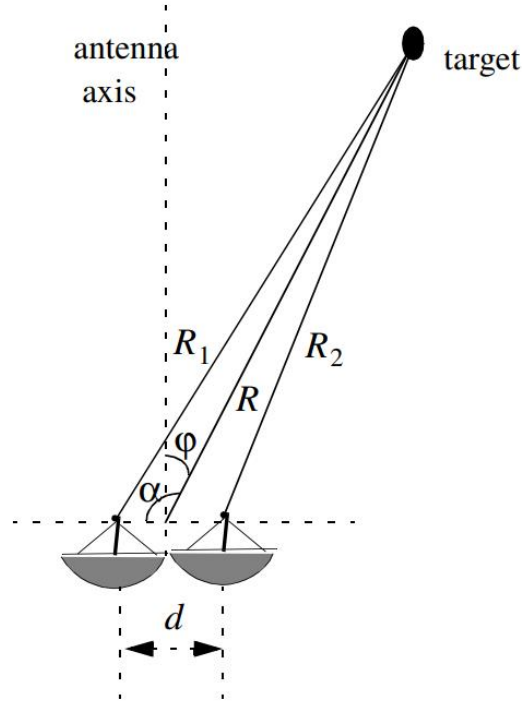


Fig 2-12. One-coordinate phase monopulse antenna [24]

Considering Figure 2-12, assuming a wavefront incident at an angle, φ , the angle α is equal to $\varphi + \pi/2$, it follows that

$$R_1^2 = R^2 + \left(\frac{d}{2}\right)^2 - 2\frac{d}{2}R \cos\left(\varphi + \frac{\pi}{2}\right) = R^2 + \frac{d^2}{4} - dR \sin \varphi \quad (2-10)$$

and since $d \ll R$ we can use the binomial series expansion to get

$$R_1 \approx R \left(1 + \frac{d}{2R} \sin \varphi\right) \quad (2-11)$$

$$R_2 \approx R \left(1 - \frac{d}{2R} \sin \varphi\right) \quad (2-12)$$

The phase difference between the two elements, or antennas, is then given by

$$\Delta\phi = \frac{2\pi}{\lambda}(R_1 - R_2) = \frac{2\pi}{\lambda}d \sin \varphi \quad (2-13)$$

Note that $\Delta\phi = 0$ corresponds to a target that is situated on the antenna tracking axis [24]. As shown in (2-14), the direction of arrival that provides the position of the target can be accurately calculated using the phase difference between the two received signals

$$\varphi = \sin^{-1}\left(\frac{\lambda\Delta\phi}{2\pi d}\right) \quad (2-14)$$

The issue with phase monopulse is the difficulty to maintain a stable measurement of the off-axis angle φ , which is likely to substantially reduce the radar detection performance. Similar to amplitude monopulse system, this can be prevented by obtaining the ratio of the difference to sum signal, Δ/Σ , that is, the modulus of the phase error signal.

Both types of monopulse technique are compared with the optimum monopulse antenna characteristics derived in 1952 by Kirkpatrick [28], defined as one that would produce the highest possible accuracy in an environment where thermal noise was the only factor interfering with target measurement, with respect to the on-axis gain of the sum pattern, on-axis slope of the difference pattern, and respective sidelobe levels. The comparison of both monopulse techniques provides reasons as to why the amplitude-comparison monopulse approach for space fed antennas has predominated in tracking radar. Both monopulse techniques can also be compared from the design and performance perspective, and this is summarized in Table 2-3.

In terms of the radar performance using both monopulse approaches, it is easier for a phase monopulse system to achieve a higher measurement accuracy than a amplitude monopulse system because the sharpness of the difference pattern, or error response, is not determined by the size of the antenna beamwidths, but rather by the separation of the phase centers of each individual antenna [27]. Nonetheless, although phase monopulse systems can provide slightly more accurate results as compared to an amplitude monopulse system with similar radar parameters, results of frequency variations for both monopulse receivers over the same range of frequency favors the amplitude monopulse system with a smaller maximum error and over a wider bandwidth as compared to that of a phase monopulse system [37]. In addition, for phase monopulse system employing reflector antennas, an undesirable characteristic of the sum illumination function is also the formation of a null at the center of the function, which results in a sum pattern with higher sidelobe levels. This is caused by the use of separate portions of the aperture to create widely spaced phase centers [38]. The sidelobes of the difference pattern are relatively small and comparable to those of the cosine tapered amplitude-comparison monopulse antenna. Moreover, an important limitation with the use of phase monopulse for angle measurement is that, excessively increasing the separation between the antennas also causes the interference pattern between the two radiated beams to become multilobed. Hence, ambiguity can exist if the individual beamwidths are appreciably greater than the lobe widths [27]. To prevent ambiguity in the estimated direction of an identified target, the target angle and antenna baseline separation must be given by [38]

$$|\sin \theta| < \frac{\lambda}{8d} \quad (2-15)$$

This infers the phase center of each antenna should be spaced apart by approximately half a wavelength or less. Nonetheless, in monopulse antennas employing compact phased array systems this may result in significant mutual coupling between the elements, which in return will cause the phase measurement of each array antenna to be corrupted by the other.

Both types of monopulse antenna employing reflector antennas differ in terms of the individual performance and systematic design. Inevitably, each antenna system presents its pros and cons, and the preferred choice is dependent on the application in hand. From the design perspective, the implementation of amplitude monopulse on a mechanically scanning reflector antenna is more common as such systems are more compact, cost-effective and simpler to construct. Since it can be operated using a single antenna they are also more readily steerable as a unit as compared to phase monopulse systems. Considering the accessibility of the radar site and the limited space available, employing the most compact radar system with the least RF circuitry is highly valued. This explains for the frequent implementation of amplitude monopulse in mechanical scanning radars. A comparison on the performance and design of both types of monopulse method on reflector antennas are summarized in Table 2-3.

Amplitude Monopulses	Phase Monopulse
Single phase center and therefore prevents mutual coupling and multilobing.	Can provide higher measurement accuracy.
Single antenna allows for a more compact, less complex and cost-effective system.	Higher measurement consistency of monopulse pattern with changes in input power.
Measurement accuracy is slightly less dependent on SNR.	
Smaller maximum error and wider bandwidth.	

Table 2-3. Comparison of amplitude and phase monopulse [37]

The improvement in angular accuracy of an amplitude-comparison monopulse antenna is largely dependent on the monopulse feed design, which is modelled to optimize the performance of the radar accordingly to meet the requirements of the application in hand. Two of the most common type of feed design is the use of a cluster of multiple horn antennas in the focal plane of the reflector (multiple feed system) or a multi-mode waveguide propagation feed system. A brief comparison on the performance of monopulse reflector antennas using either of the feed arrangement mentioned are provided, and the more suitable choice is evaluated based on the antenna requirements.

2.2.2 Monopulse Feed Systems

The underlying principle of the use of multiple feed horns was briefly described earlier for the implementation of monopulse in a single plane. This can be extended to a four-horn feed system to implement monopulse in both principal planes of the tracking axis. A four-horn monopulse system comprises of a parabolic reflector antenna that is fed by a cluster of four feed horns situated around the focal point of the reflector, and with each feed laterally offset symmetrically about the boresight axis. A typical illustration of the appearance of the aperture of a four-feed system is shown in Figure 2-13. The four horns each produce a squinted beam, where A, B, C, and D corresponds to the individual squinted beams, and all four beams intersects one another at a common point along the boresight axis of the antenna.

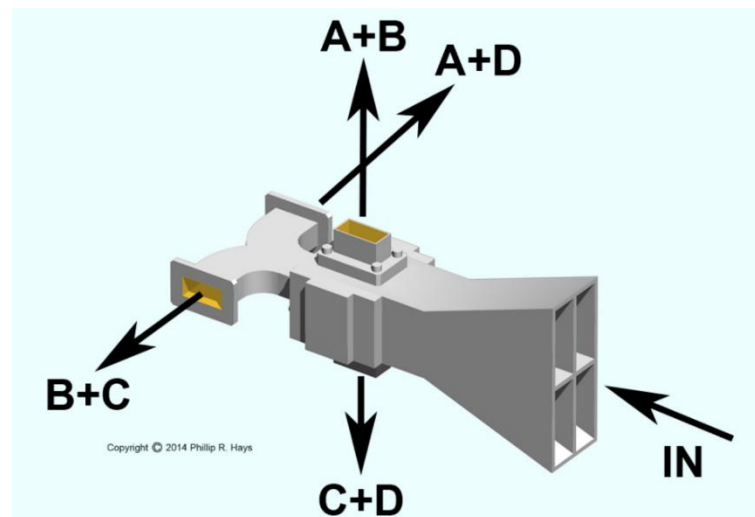


Fig 2-13. Four-horn feed system of monopulse antenna [39]

In a conventional four-horn feed, the horns are paired so that for each coordinate (principal plane) they act as two separate horns. In azimuth, the difference of the left lobe, given by 'A + C', and right lobe, given by 'B + D', provides an error signal that contains the angle error information of the target from the boresight axis. Likewise, the difference of the top lobe, given by 'A + B', and bottom lobe, given by 'C + D', provides an error signal that contains the angle error information of the target from the boresight axis in elevation. In similar feed systems using individual feed horns, laterally shifting the position of each feed horn from the focal line, or the direction of each squinted beam, causes the echo corresponding to an off-axis target to be received by each feed from slightly different positions at varying power. Thus, when a target moves off-axis the amplitude of the signal received at the output of each horn will vary depending on the new location of the target. In such case, if the output of each feed horn is connected to four separate identical receivers of equal phase, their responses to an incident

plane wave would all be in the same phase but would differ in amplitude in accordance with the beam patterns and the direction of arrival of the wave that is reflected from a detected target. From the ratios of the amplitudes of the pair of beams the angular components of the target position in both coordinates relative to the tracking axis can be directly determined. On the other hand, for the detection of an on-axis target, the amplitude of the signal received at the output of the four-horn feed will be the same and no difference (error) signal will be created in both coordinates.

Another popular type of feed system for a monopulse reflector antenna is the use of a multi-mode horn antenna. Waveguide theory (Section 3.3) states that at certain operating frequencies electromagnetic wave propagates in a rectangular waveguide along with multiple higher order modes, such as transverse electric field TE_{mn} and transverse magnetic field TM_{mn} . A multimode feed horn utilizes the higher order waveguide modes (multi-mode fields) to receive echo signals from a target. As described below, for a monopulse system using a multi-mode feed horn the corresponding sum signal of the antenna is composed of even modes, whereas the difference signal in each coordinate is composed of modes that are odd in that coordinate and even in the other [38]. To produce optimum sum and difference patterns in both planes a common radiating aperture is designed to ensure that the amplitude and phase relationships of the various propagating modes are in proper order. This type of feed is theoretically capable of closely approaching simultaneous optimization of the monopulse patterns [38]. Two types of horn antennas most commonly used for multimode feed systems are rectangular and sectoral horn antennas.

The design of a multi-mode feed for a monopulse reflector antenna using a dielectric loaded E-plane sectoral horn antenna is discussed here. The sectoral horn antenna is extended by a custom designed waveguide that allows for the propagation of the desired higher order waveguide modes [$TE_{01}, TE_{10}, TE_{20}, TM_{11}, TE_{11}$]. The waveguide dimensions (WR90) and the dielectric constant of the partially filling dielectric material are chosen to prevent any higher order modes from propagating along the guide [40]. Mode synthesizing in a E-plane sectoral horn antenna allows the feed aperture illumination to be shaped flexibly despite the fixed dimensions of the antenna aperture. The higher propagating modes associated with the three channels (sum, azimuth difference and elevation difference) of a multi-mode E-plane sectoral horn feed system is shown in Figure 2-14. The E-field distribution corresponding to the propagating mode(s) for each channel are also presented.

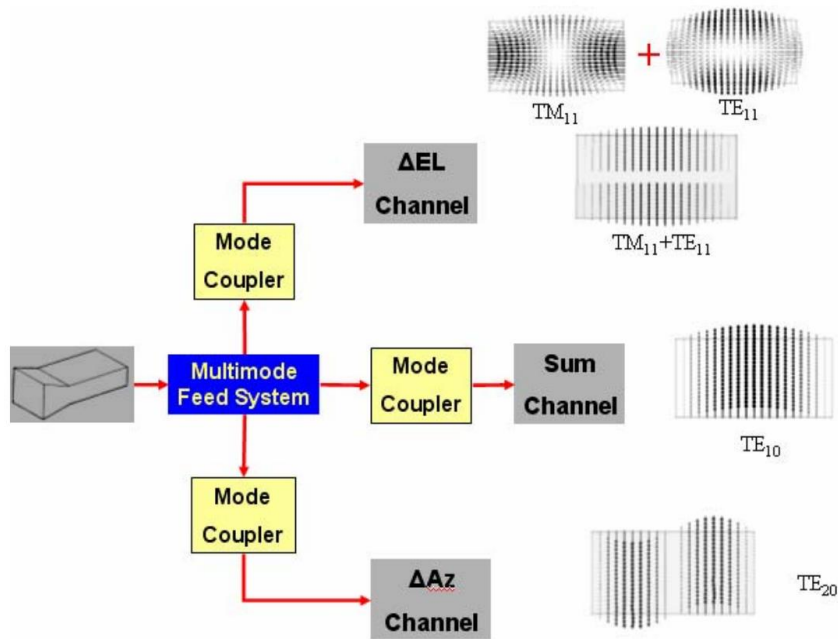


Fig 2-14. Multi-mode monopulse feed system with the associated propagating modes [41]

When the echo signal received arrives from an on-axis direction this causes the feed to be symmetrically excited. In this case, the field distribution on the horn aperture is even for both E-plane and H-planes, and only the TE_{10} mode is transmitted by the horn. If the direction of the signal received is offset from the tracking axis in azimuth, the diffraction pattern is shifted along the horizontal plane of the horn aperture (Figure 2-15). This causes the excitation of the feed to become asymmetrical and allows higher order modes to propagate. The filtering action of the horn only allows the propagation of TE_{10} and TE_{20} modes [41]. Similarly, if the direction of the signal received is offset from the tracking axis in elevation, the diffraction pattern is shifted along the vertical plane of the horn aperture (Figure 2-16). The asymmetrical excitation of the feed horn produces modes TE_{10} , TM_{11} , and TE_{11} . These two higher order modes (TM_{11} and TE_{11}) are generated together due to the offset in incident waveforms, from which they are combined together to form the field distribution shown in Figure 2-16.

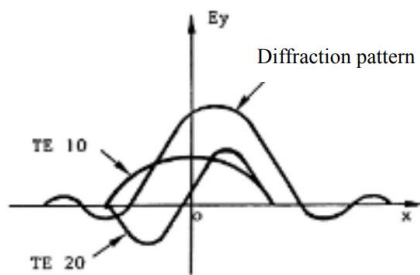


Fig 2-15. Diffraction pattern in azimuth

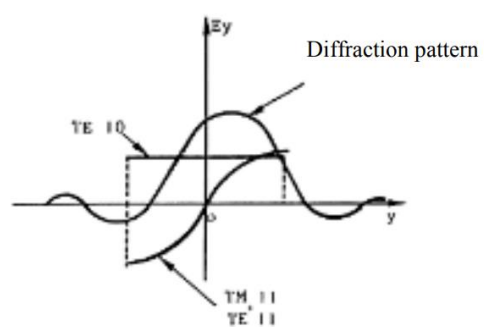


Fig 2-16. Diffraction pattern in elevation

In all cases of target detection, the TE_{10} mode is used to provide for the sum channel of the monopulse antenna. Any movement of the diffraction pattern on the horn aperture will correspond to a variation in the amplitude of the TE_{10} mode to occur. Hence, the sum channel will always produce an output regardless of whether it is for the detection of an on or off-axis target. On the other hand, the amplitudes of the higher order modes mentioned (TE_{20} , TM_{11} , and TE_{11}) only varies considerably in response to a certain movement of the diffraction pattern, that is, the amplitude of the TE_{20} mode and the combination of the TM_{11} , and TE_{11} modes are sensitive only to azimuth and elevation errors, respectively. Hence, the use of multiple modes are able to provide angular discrimination information of a detected target from the direction of the tracking axis through the generation of error signals in both principal planes. The results of the simulation performed in [40] has verified the modal analysis results, that is, the sum channel is formed by the TE_{10} mode, while the azimuth and elevation difference channels are formed through the generation of signals in the TE_{20} mode and by the combination of TE_{11} and TM_{11} modes, respectively.

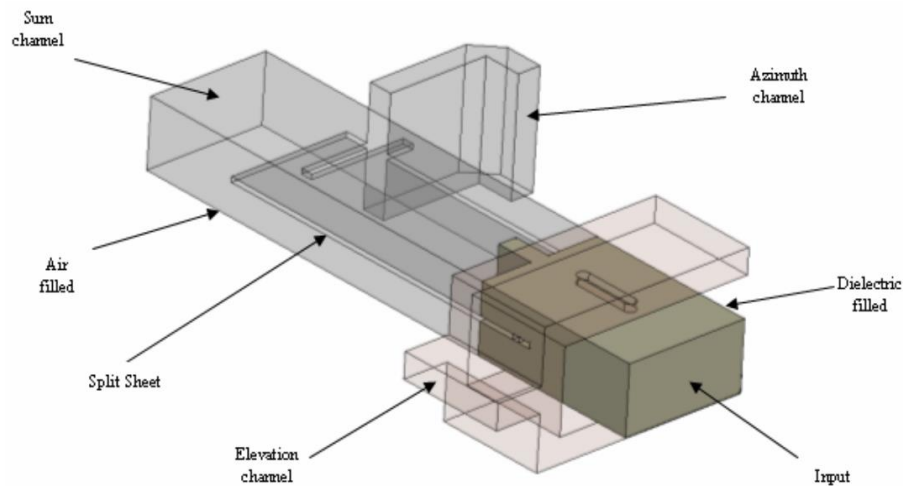


Fig 2-17. 3D model of proposed multi-mode monopulse antenna feed [40]

The monopulse antennas employing either feed systems possesses similar performances. For both feed systems, only an output voltage signal from the sum channel is produced when a detected target is positioned along the boresight axis of the antenna, from which the presence and range of the target is identified. Whereas for a target located at any off-axis position, in addition to the sum channel output, an output voltage signal from the azimuth and/or elevation difference channel corresponds to the position of an off-axis target, which indicates the position of the target relative to the boresight axis in both principal planes.

As compared to other monopulse feed systems available, the multi-mode feed horn is found to be better in terms of size, design and accuracy [42]. In a multi-mode monopulse

antenna the use of a single feed to produce a sum and difference pattern in both principal planes makes it the most compact feed system available. In addition, a multi-mode feed allows the sum and difference patterns to be controlled independently, and therefore it is possible to produce near-optimum sum and difference patterns simultaneously. In terms of performance, monopulse antennas employing multi-mode feed tend to have a slightly higher accuracy and provide a higher return and insertion loss as compared to employing multiple feed systems. However, multi-mode feed systems also present several disadvantages. The dielectric material of the multi-mode horn has some loss, usually in the order of a tenth of a decibel. Although the loss is small, this loss may cause excessive heating of the dielectric if it is not monitored [39]. The bandwidth for a rectangular waveguide emerging from a rectangular slot is also substantially narrower (approximately 10 percent bandwidth) as compared to a four-horn comparator. Moreover, despite its simpler appearance and ability to optimize the monopulse patterns, the control of various higher-order modes over a broad frequency band also makes it a difficult design problem [38]. Hence, the use of a multi-mode feed is less suitable for wide-bandwidth applications.

On the other hand, the use of a four-horn feed system is also widely accepted as it is considerably easier to design as compared to a dielectric filled multi-mode feed system, and yet it is able to achieve accurate results. Moreover, the feed system only propagates EM waves in a single mode, that is the dominant mode, and therefore, unlike multi-mode feed systems, higher-order modes of propagation are not required which prevents the possibility of signal coupling between the modes used in a multi-mode feed system. Although it is simpler to achieve the modelling of a multiple feed system according to the requirements of the monopulse antenna, implementing this horn arrangement to achieve simultaneous lobing in two orthogonal planes generally does not allow the sum and difference patterns to be optimized independently, and therefore a compromise must often be reached based on the importance of the application in hand. Table 2-4 summarizes the comparison of the two types of feed systems that has been discussed from the design and performance perspective [40].

Characteristics	Four-horn Feed System	Multimode Feed System
Extraction of sum and difference patterns	Collectively.	Separate controls allows both patterns to be extracted and processed individually.
Structure	Quite bulky.	Compact.
Gain	Considerably higher.	Comparatively less.
Bandwidth	Wide band.	Narrow band.
RSME (root mean square error) estimation	Better only if theta is half of 3 dB beamwidth.	Better.

Table 2-4. Comparison of a four-horn and multi-mode feed system [39]

Both feed systems described above are popular choices with pros and cons. For either feed system implemented, it is a common practice for the designer to seek some modification in either of the design. The more suitable feed is heavily dependent on the requirements and the type of application for which it is to be used for and, therefore, the preferred feed system is clearly a subjective choice. For the application in hand, out of the two monopulse feed systems evaluated the multiple feed horn antenna design would be the preferable choice since it can provide a larger radar bandwidth and higher gain, which are important properties of a surveillance radar. The much simpler design, modelling and construction of a multiple feed system also makes it highly favourable. In addition, the performance of multiple feed system is less sensitive to environmental factors and does not easily deteriorate when subjected to long and continuous operation. Hence, for the mechanical scanning reflector antenna that will be constructed in this project, a multiple feed system will be designed to fulfil the requirements of the surveillance radar.

Given the objective of the surveillance radar is to provide detection, imaging and tracking of targets in azimuth while the radar scans continuously along the plane that is perpendicular to the antenna boresight axis, a narrow azimuth beamwidth is required to achieve a high angular resolution and accuracy. On the other hand, the elevation beamwidth of the radiated beam must be broad enough to provide elevation monitoring capability, that is, providing sufficiently wide-angle coverage of the sea from the coastline that extends to the maximum operating range of the radar without having to rotate or displace the antenna vertically. Hence, the use of a vertically truncated parabolic reflector is an ideal choice over the more conventional circular parabolic reflector to produce a fan-shaped beam with the desired principal plane beamwidths and antenna gain. In addition, the use of a truncated reflector would effectively reduce the size and weight of the radar by a considerable amount.



Fig 2-18. Vertically truncated parabolic reflector - EA3462 X-band radar [43]

In a typical reflector antenna system employing a vertically truncated reflector, the feed pattern chosen must match the aperture outline, or shape, of the reflector in order to illuminate the reflector aperture optimally, which in return allows the maximum gain of the reflector antenna to be realized. As described in Section 4.3, a feed that radiates a beam with the widest possible azimuth beamwidth and a significantly narrower elevation beamwidth is a E-plane sectoral horn antenna. Hence, designing a sectoral feed horn antenna based on the reflector properties is necessary for optimal illumination of the dish.

Following the initial design of a center-fed reflector antenna that prioritizes on achieving maximum gain, this thesis describes the proposed monopulse feed design that is suitable for the implementation of amplitude monopulse on the existing reflector antenna employing the same truncated reflector. The direction of the beam produced from a parabolic reflector can be offset to a certain extent by laterally displacing the position of the feed along the focal plane and illuminating the reflector about the vertex. The beam produced from the reflector will move off axis on the side opposite the feed in proportion to the feed tilt applied, which is related to the known proportionality factor, or beam deviation factor (BDF), of the parabolic reflector (Figure 5-5). Figure 2-19 provides an illustration of a parabolic reflector that is illuminated about the vertex using an off-axis feed.

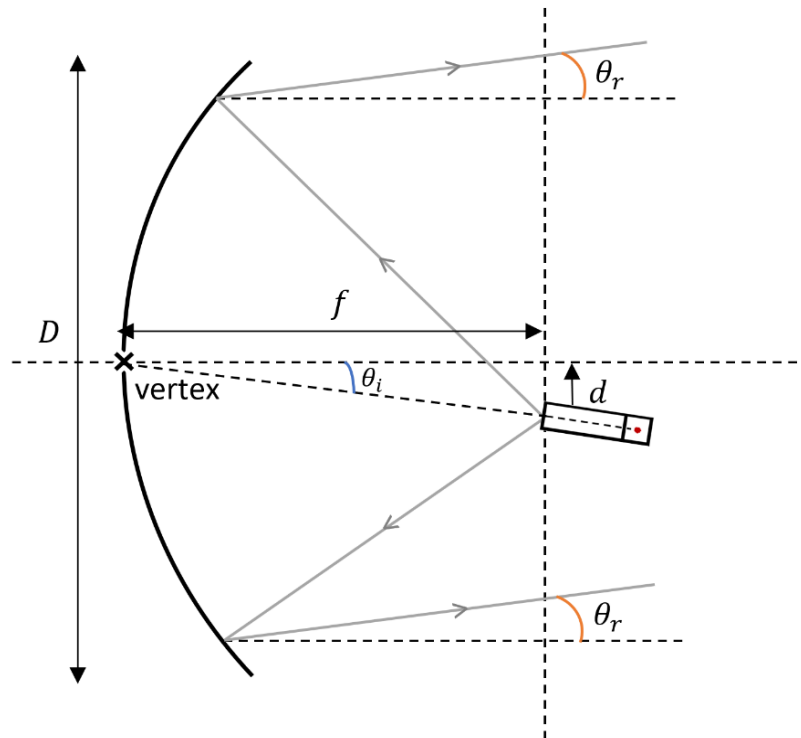


Fig 2-19. Reflector illumination about the vertex

Using this method of illumination, a pair of off-axis beams required for the implementation of amplitude monopulse in a single plane can be produced by slightly displacing a pair of feed laterally, in opposite directions, along the focal plane of the reflector, that is, perpendicularly to the boresight axis, and rotating the feed about the vertex of the reflector, such that the main lobe of the beam radiated from the feed intersect one another at the center, or vertex, of the dish. This feed arrangement allows the direction of the pair of off-axis beams produced to be easily controlled and determined beforehand. Since monopulse is only required in the horizontal plane of the antenna, the monopulse feed system comprises of two horns that is positioned symmetrically to one another about the focal point of the reflector in the horizontal plane.

With the proposed monopulse feed design, the direction, or deflection angle, of the pair of squinted beams produced from the reflector can be varied at very small intervals by applying the suitable angular displacement on the pair of feed. Given that the radiation properties of the pair of lobes produced can be approximated, producing the pair of lobes in this manner allows the crossover point of the squinted beams along the boresight axis to be varied. Hence, as shown in the monopulse feed modelling in Section 5.1.3, the corresponding monopulse sum and difference beam produced can be controlled independently, such that if the detection sensitivity of the radar is prioritized then the optimum feed tilt that optimizes the sum pattern is chosen. Likewise, if the angular accuracy of the radar is prioritized then the optimum feed tilt that

optimizes the difference pattern is chosen. The modelling of a dual-horn feed arrangement according to the requirements of the application in hand is therefore very simple to implement and achieve. However, this feed design only permits the feed to be laterally displaced from the focal point to a certain extent, otherwise, the ray of beams produced from the reflector would eventually become uncollimated and, therefore, will deteriorate exponentially with increasing feed tilt applied. At some point, the beam produced would exhibit undesirable radiation properties that makes it deemed unusable. Hence, the extent of beam steering that can be achieved in this manner is generally only limited to a couple of beamwidths.

The implementation of amplitude comparison monopulse technique has demonstrated tremendous improvement in the angular accuracy of the radar, which is critical especially for accurate target imaging and tracking. Nonetheless, applying monopulse actually degrades the angular resolution and increases the clutter footprint within the echo signal received due to the broadening of the sum beam pattern. Moreover, an extra antenna and receiver for it to be successfully implemented in a single plane. Thus, the implementation of monopulse in azimuth and elevation (i.e. 3D monopulse radar) is likely to significantly increase the complexity and cost of the RF circuitry and feed arrangement of the reflector antenna. The improvements realized from the implementation of amplitude monopulse on existing mechanical surveillance and tracking radars, however, still significantly outweighs the minor drawbacks mentioned.

2.3 Signal Processing Methods

The enhancement in detection performance of an existing coastal surveillance radar can also be achieved through various signal processing techniques instead of proposing more sophisticated antenna feed design and/or RF circuitry. For instance, signal processing techniques that combines multiple samples together to provide some integration against noise is a common and popular approach in more accurately estimating the target measurement in bearing and range. However, the enhancement in measurement accuracy using such techniques that implements this would be largely dependent on the number of samples combined and does not improve the resolution performance. Other simpler and cost-effective processing methods such as sharpening edges and enhancing contrast in video pictures are able to boost the high-frequency part of the spatial 2D frequency spectrum, which allows clutter and noise to be more clearly discriminated from valid targets. However, the benefits of such techniques are minimal and may be useful for only a narrow range of applications as it does not make use of the prior knowledge on the nature of the features sought within the data received from the antenna output.

The following technique that is widely used to provide higher gains in range resolution, or accuracy of a target range, is known as a split-gate tracker. To track the range of a target

more accurately, a split-gate tracker is frequently used to constantly adjust the range tracker to keep the target locked in range. In a split-gate tracker the range gate interval is split into two equal portions (early and late gate intervals), normally by half the antenna beamwidth, and the echo amplitude in each waveform is compared to one another to determine the position of the tracked target to a higher accuracy than conventional methods. Hence, split-gate tracking requires the assumption of symmetry and an approximation of the antenna beamwidth. The technique is considered as a time-domain analogue of monopulse as it is used to continuously estimate the range of a moving target by comparing the power within the early and late gate intervals. Alike monopulse systems, split-gate trackers are also subject to the same limitations regarding the enhancement in resolution and clutter resilience [44].

The split-gate tracker passes a two-part window, that is the early and late gates, across the received data. The early and late gates each pass across a portion of the target echo pulse. The early gate opens at the anticipated starting time of the received echo signal and lasts for half its duration, whereas the late gate opens at the center and closes at the end of the signal. For this purpose, good estimates of the echo duration and the pulse centertime must also be reported to the range tracker so that the early and late gates can be placed properly at the start and center times of the expected echo. This reporting process is widely known as the “designation process” [24]. One way of implementing the split-gate tracker is to convolve the noisy received radar output with the impulse response $h[l]$. This is shown in Figure 2-20 as the solid black line overlaid on the noisy data [29].

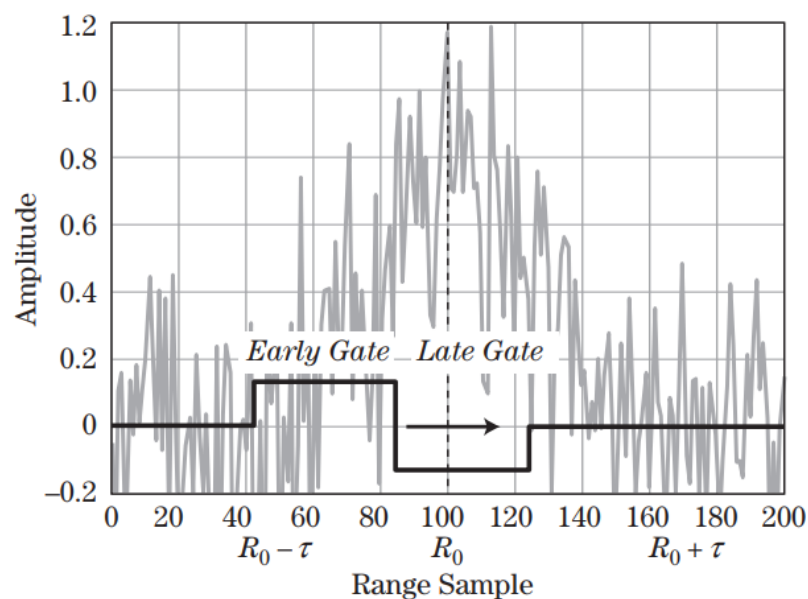


Fig 2-20. Implementation of split-gate tracker on radar output [29]

The early and late-gate produces a positive and negative voltage output, respectively. The error signal obtained from the difference of the early and late gate outputs is fed into an integrator that integrates the error signal obtained in time to determine its mean value over the range gate interval, which is used to either decrease or increase the range gate distance, or advance or delay the range gate interval, so that the range gate interval is realigned as perfectly as possible with the echo pulse corresponding to a tracked-target. The true difference between the range gate distance and the tracked target is provided from the magnitude of the mean value of the error signal, whereas the polarity of the signal, which is dependent on the position of the gate interval relative to the echo pulse, indicates if the range gate distance is to be increased or decreased accordingly. Trackers using split-gate system allows the antenna to continuously lock onto the centroid of the tracked target [44].

Simple timing diagrams are also used to illustrate the implementation of the technique on a simulated radar output. Figure 2-21 is a timing diagram of the early and late-gate signals produced when both gates are approximately centred on the peak signal of the simulated tracked-target echo pulse. In this case, the corresponding shape and amplitude in each gate are very similar to one another. Thus, the mean value of the error signal is equal to zero since there is no difference between the two signals, and, in return, the range gate distance, which is equivalent to the range of the target, is unchanged.

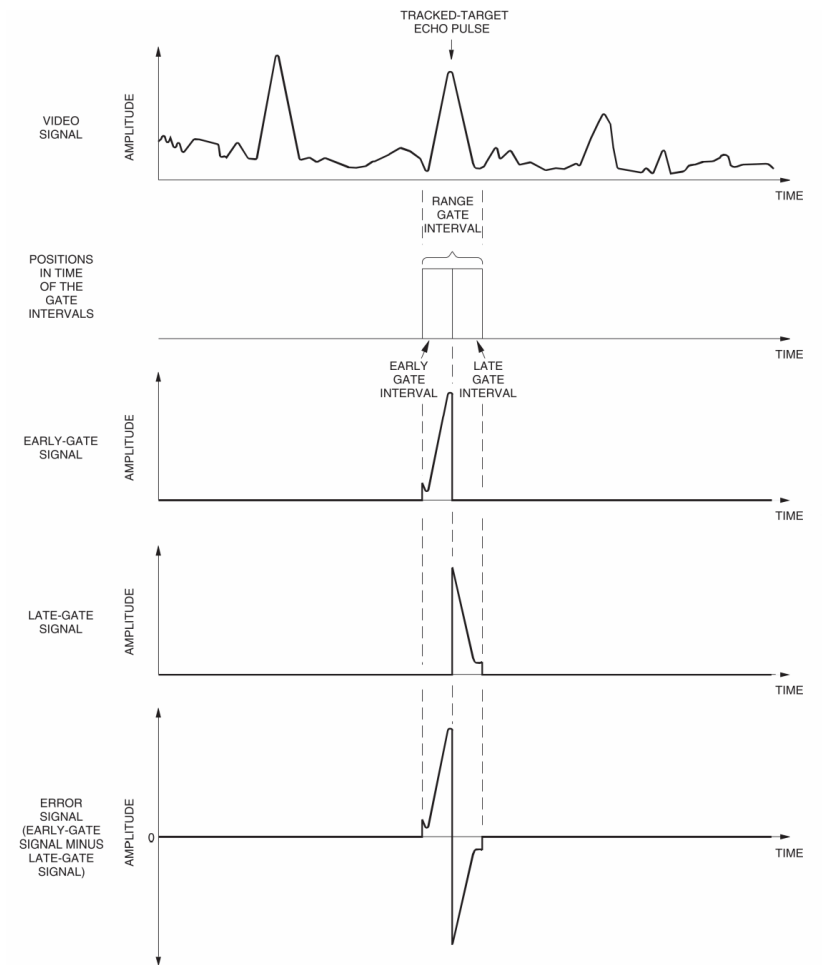


Fig 2-21. Range gate interval is aligned with the tracked-target echo pulse [44]

Alternatively, when the gates are not aligned with the tracked-target echo pulse, or not timed properly, the corresponding early and late-gate signals obtained will exhibit different shapes and amplitudes. A non-zero mean value of the error signal is produced from the integrator output due to the difference between the early and late gate voltage signals. The range gate distance is continuously realigned to the range of the echo pulse based on the magnitude and polarity of the error signal obtained. In the illustration shown in Figure 2-22, the mean value of the error signal is a negative value since the late-gate signal is larger. Hence, in this case the range-gate interval will be advanced accordingly, which corresponds to an increase in the range gate distance.

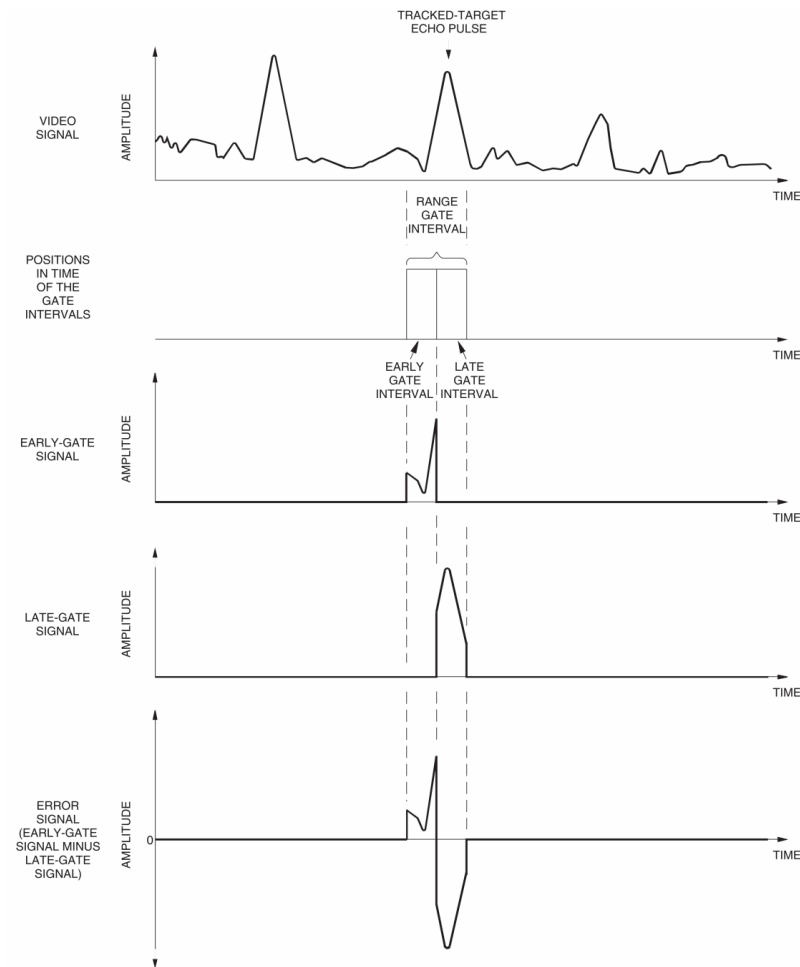


Fig 2-22. Range gate interval is not aligned with the tracked-target echo pulse [44]

In a conventional radar system, the received data is sampled at intervals that is approximately equivalent to a resolution cell, which is used to estimate the range of a detected target. On the other hand, the precision of a split-gate tracker is highly dependent on, and therefore limited to, the sampling density of the received signal to which it is applied. Hence, if there are many samples per resolution cell of the data received (highly oversampled), the precision of the radar system may be substantially higher than conventional systems as this allows the technique to benefit from averaging over a much larger number of samples. There are other newly proposed and yet more sophisticated super-resolution algorithms that may achieve even higher gains in accuracy, but these are generally less conventional techniques that have not been widely implemented in practice.

A novel signal processing technique is proposed in this thesis that is aimed to enhance the resolution performance of an existing radar by scaling down the echo footprint and/or beamwidth of the detected response corresponding to an identified target in both the time and/or angular-domain. This is achieved by the proposed processing technique that will be referred to

as pattern selective differential processing (PSDP). The technique simulates beam sharpening on the detected output of any new or existing radar system purely through a one-dimensional and non-coherent signal processing method. The underlying principles and method of implementation of the differential technique in the angular domain is briefly discussed here, and a detailed description is provided in Section 5.2.1.

In signal processing, it is vital to be able to recognize and identify the desired signal within the received radar returns. Knowing the amplitude gradient of the detected point-target response allows the radar resolution, or ability to discriminate closely-spaced targets, to be optimized to its maximum potential. To identify the amplitude gradient of the detected point-target response, it is most accurately extracted by matching the gradient profile of the detected target response to that of the known TX/RX antenna response. Likewise, the detection of the presence of a useful signal from a detected target within the received signal is based on its amplitude, which is best detected through correlation of the amplitude profile of the received signal waveform with the known amplitude profile of the antenna response using a correlator. Hence, the technique places huge importance on prior knowledge of the beam pattern of the echoes sought within the received radar returns, which is significant in achieving the above. The algorithm used to apply the proposed signal processing technique implements this and, in Figure 5-26 to 5-28, the technique is demonstrated on a simulated radar output signal, or point target-response, that is assumed to have the same function as the antenna response pattern in the absence of noise and clutter. Figure 2-23 presents the original point-target response received within the radar output, which is given by a sinc squared function and is assumed to have the same pattern as the antenna response in the absence of noise and clutter, and the sharpened point-target response obtained from the correlator output after pattern selective differential processing was applied on the original response.

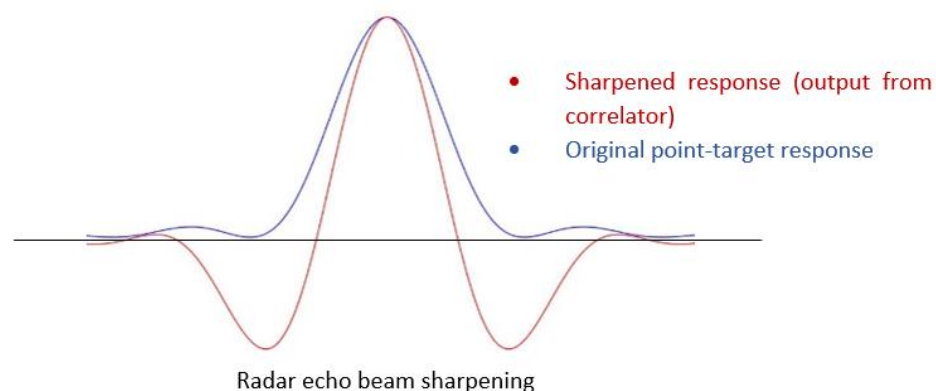


Fig 2-23. Original and sharpened point-target response

Applying the signal processing technique would effectively sharpen the blunt top of the original point-target response and, thus, enhance the resolution performance of the antenna considerably. The reduction in beamwidth of the sharpened response is also proportional to the reduction in echo footprint, and therefore clutter, within the target response. Therefore, applying the signal processing technique also corresponds to an increase in the maximum clutter-limited detection range of the radar, which translates to a substantial improvement in clutter resilience. Upon applying the technique on at least one beamwidth worth of information of the signal received at the radar output, the operator can analyze these data from a single pulse as a line of constant bearing and effectively discriminate the presence of a valid target against weaker echoes that do not conform to the shape of the antenna response pattern. Hence, based on prior knowledge of the pattern of the echoes sought, the radar performance would benefit by significantly reducing false detections due to antenna sidelobes or background clutter.

As shown in Section 5.2.1.6, the enhancement in resolution performance offered by the differential processing technique on the corresponding point-target response obtained is substantially dependent on the characteristics of the antenna pattern. Nonetheless, the simulation results have also shown that the technique offers a modest improvement of at least 20 percent or more, and by as much as 60 percent depending on the characteristics of the antenna pattern, on both the resolution and clutter-limited detection range of a new or existing radar system. An enhancement in angular accuracy is also observed as a minor-by-product of the enhanced angular resolution of the radar system.

In practice, the processing technique can be implemented in a form of a simple hardware, such as a digital processing box, that is connected between the radar output and pixels per inch (PPI) display unit. Hence, although the improvement in performance is considerably less as compared to a monopulse system, the significantly low cost and simple implementation of the proposed technique on any existing radar system will make it a largely attractive one. In addition to the minimal RF components required, the optimum use of the foreknowledge of the shape of signal sought allows the technique to be more robust and/or less complex and/or less dependent on the high SNR of a radar system. Above all, most other existing signal processing techniques do not scale down the clutter footprint of the signal received and, thus, do not provide significant improvements in the resolution performance and clutter resilience of a radar system as compared to the differential processing technique proposed.

Chapter 3

Radar Principles

This chapter provides the underlying theory for components (i.e. waveguide and antenna systems) of a surveillance radar system. It discusses the fundamental radar and other antenna concepts relevant to surveillance radars employing different types of antenna. In addition, it outlines several of the angle refinement measurement techniques that tracking radars most commonly use, with specific emphasis on present monopulse techniques, which have been assessed as part of this project to produce a novel feed system.

3.1 Friis and Radar Equation

The Friis and Radar equations (one way and two way RF propagation equations) can be used to determine how much transmitted free space RF energy from a transmitting antenna can be captured by a receiving antenna, provided that the direction of the gains for both the transmit and receive antennas are aligned and their polarizations are matched [45], and how the integrity of a received signal can be affected by the strength of the cumulative noise in a receiver. Utilization of these equation may allow prediction of free space antenna interactions.

3.1.1 Friis Equation

The Friis equation was first proposed by Harald Friis of Bell Laboratories in 1946. It is the one way free space transmission equation which can be used to show the power received by a receive antenna at a distance r in the far-field of a transmit antenna [46]. The power received by a receiving antenna is heavily determined by the effective capture area of the receive antenna and the power density of the transmitted signal at the receive antenna.

The effective capture area of the receive antenna A_e represents a smaller, uniformly illuminated aperture having the same gain as that of the actual, non-uniformly illuminated aperture [46]. It is given by

$$A_e = \frac{G_r \lambda^2}{4\pi} \quad (3-1)$$

where G_r is the gain of the receive antenna and λ is the wavelength of the EM wave.

The power density at the receive antenna Φ located at a distance r from the transmit antenna with an antenna gain of G_t is the power density from an isotropic antenna multiplied by the antenna gain

$$\Phi = \frac{P_t G_t}{4\pi r^2} \quad (3-2)$$

where P_t is the peak transmit power of the transmit antenna.

Only a small fraction of the power transmitted from the transmitting antenna is accepted by the receiving antenna. The one-way transmission propagation equation which can be used to calculate the peak power accepted as an input to the receiving antenna due to a transmitting antenna in free space is given by

$$P_{peak} = \Phi A_e = \frac{P_t G_t G_r \lambda^2}{(4\pi r)^2} \quad (3-3)$$

The Friis equation is subject to the inverse square law which means that the captured peak power decreases significantly with square of the distance of the receiver from the transmitter.

3.1.2 Radar Equation

The radar equation provides a relationship between the echo power accepted by the receiving antenna P_r and the specified radar and target parameters. The radar equation in free space is given by [35]

$$P_r = \frac{P_t G_t G_r \lambda^2 \sigma}{(4\pi)^3 r^4} \quad (3-4)$$

Where P_t is the transmitted power (watts)

G_t is the transmit antenna gain

G_r is the receive antenna gain

λ is the wavelength of the transmitted signal (meters)

σ is the radar cross section area of the target (meters²)

r is the range of the target from the sensor (meters)

For a monostatic radar, where the transmit and receive antenna gain are identical to one another ($G = G_t = G_r$), (3-4) is deduced to

$$P_r = \frac{P_t G^2 \lambda^2 \sigma}{(4\pi)^3 r^4} \quad (3-5)$$

The receiver noise power P_n is the measured noise power (watts) at the receiver. It is given by

$$P_n = k T_0 B F_n L \quad (3-6)$$

where k is Boltzmann's constant = 1.38×10^{-23} W/K/Hz

T_0 is the noise reference temperature, 290K

B is the receiver's bandwidth (Hz)

F_n is the receiver's noise figure.

L is a loss term accounting for other propagation losses ($L \leq 1$).

A detected target SNR for a single pulse of radar, which is the ratio of the received power to the amount of noise power observed at the radar receiver, usually expressed in decibels, is predicted by

$$SNR = \frac{P_r}{P_n} = \frac{P_t G^2 \lambda^2 \sigma}{(4\pi)^3 r^4 k T_0 B F_n L} \quad (3-7)$$

SNR is of fundamental importance and the basis for radar system analysis and design as it provides an estimate of the radar performance given a specific set of known radar and target parameters. It is also frequently used as an accurate estimate in defining the suitable radar parameters, which are required for the detection of different types of targets, to fulfil the anticipated performance of the radar.

SNR can be used to determine the ability of a radar to detect its desired signal against inherent noise. Furthermore, it is the basis for conceptual radar system design [25]. It is observed that the parameters in the radar equation strongly influences the way the radar interact with present targets. The criterion for accurate detection of a target that is located at a distance away from the radar generally requires the SNR to be above some threshold value. The SNR is greater at shorter ranges as a larger amount of power is returned to the receiver from a target that is located nearer to the radar. Hence, the SNR is often used as a measure of defining the general probability of a radar to successfully detect a target of a certain RCS area and at a specified range.

3.2 Antenna Parameters

An antenna is an electrical device capable of radiating and/or receiving radio waves [47]. Different types of antennas have different properties and performance, but they share certain characteristics which can significantly affect the way they interact with each other. An understanding of the general properties of antennas enables radar designers to choose the appropriate type of antenna and its properties according to the requirements of the application in hand. The general characteristics of antennas are outline below.

3.2.1 Field Regions

The surrounding space of an antenna is generally classified into three field regions: the reactive near-field region, the radiating near-field (Fresnel) region and the far-field (Fraunhofer) region. The beam characteristics of an antenna differs in each of the three field regions. Each field region surrounding an antenna is outlined below.

3.2.1.1 The Reactive Near-field Region

The first field region that immediately surrounds the antenna is the reactive near-field region, and in this region the reactive fields are dominant [48]. Fields in this region mostly contain reactive energy (field components mostly oscillate towards the antenna) that are stored and not dissipated in this region [49]. Furthermore, the electric field (E-field) and magnetic field (H-field) are 90° out of phase.

The boundary of an antenna's reactive near-field region can be defined by the following equation as [45]

$$r < 0.62 \sqrt{\frac{D^3}{\lambda}} \quad (3-8)$$

where D is the largest dimension of an antenna element.

3.2.1.2 The Radiating Near-field (Fresnel) Region

The radiating near-field region is the second field region that is located between the reactive near-field and far-field regions of an antenna. The boundary of an antenna's radiating near-field region can be defined by the following equation as [45]

$$0.62 \sqrt{\frac{D^3}{\lambda}} < r < \frac{2D^2}{\lambda} \quad (3-9)$$

where the limiting term on the right side of the equation is the far-field region of the antenna.

In this region the radiating fields begin to emerge and, therefore, it is no longer dominated by the reactive field energy [45]. The radiating fields becomes increasingly more prominent as compared to the reactive fields as the distance from the antenna is gradually increased from $0.62\sqrt{\frac{D^3}{\lambda}}$ to $\frac{2D^2}{\lambda}$.

3.2.1.3 The Radiating Far-field (Fraunhofer) Region

The third and furthest region surrounding the antenna, known as the far-field region, is present at distances larger than the minimum far-field range of the antenna. The boundary of an antenna's radiating far-field region can be defined by the following equation as [45]

$$r \geq \frac{2D^2}{\lambda} \quad (3-10)$$

Unlike in the near-field regions, the far-field region of an antenna is dominated by radiative fields. This causes the EM waves to behave like plane waves and, therefore, the radiation pattern of the antenna is unchanged for all distances greater than the minimum far-field range of the antenna. The E-field and H-field are orthogonal to each other and to the direction of propagation in the far-field region. Hence, the radiation pattern of an antenna is different in the near-field and far-field regions. The radiation pattern of an antenna in the near-field region, as compared to it in the far-field region, has a notably broader antenna beamwidth and larger near-in sidelobes, which accounts for the degradation of the radar performance at short range.

The measurement of an antenna's radiation pattern, and the power radiated from it, must be made in the far-field region since all surveillance antennas are operated in the far-field region. Moreover, the radiation pattern of an antenna is always referred to as the pattern in the far-field region, unless specified otherwise. An illustration of the three field regions surrounding a transmitting antenna are summarised in Figure 3-1.

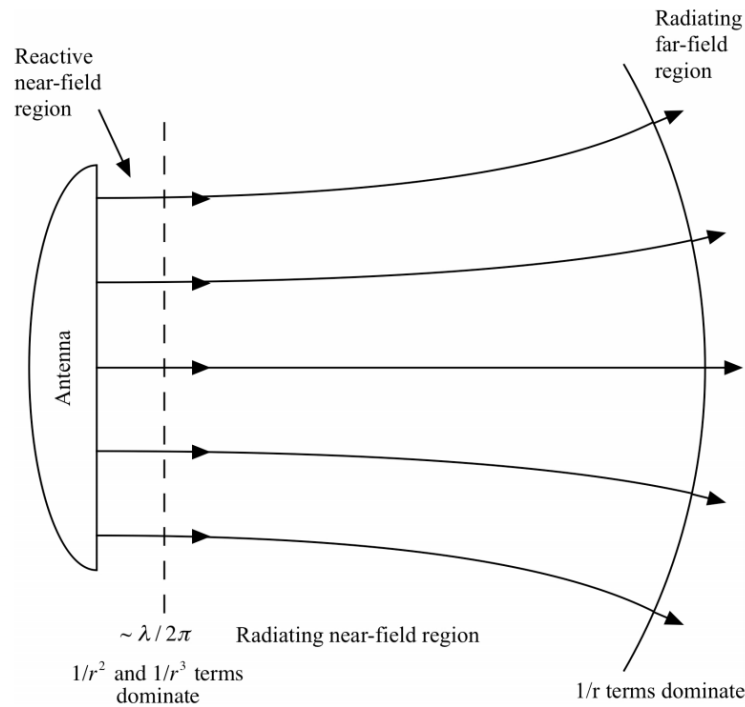


Fig 3-1. Illustration of the three regions surrounding a radiating antenna [50]

For a reflector antenna employing a truncated parabolic reflector that has a dimension of 1.2 meter by 0.3 meter, and an operating frequency of 9.2 GHz ($\lambda = 0.0326$), the calculated minimum far-field range is approximately 89 meters. Nonetheless, for considerably larger antennas with a large far-field range, it is possible to use reflector shaping techniques on the antenna for it to radiate similar beam patterns at both near and far-field regions.

3.2.2 Radiation Pattern

An antenna which is being used as a transmitter does not radiate uniformly in all directions, or conversely, an antenna being used as a receiver does not detect energy uniformly from all directions. This directional selectivity of an antenna is characterised in terms of its radiation pattern that is mostly determined in the far-field region of the antenna, which is a plot of the relative strength of radiated field as a function of the angular parameters θ and ϕ , for a constant radius r [51].

The radiation pattern provides a visualization of the EM energy distributed in free space, along with the beam properties, as it is produced from the antenna. It represents either electric or magnetic field strength or power intensity as a function of space coordinates [45]. The radiation pattern of a directional antenna is commonly displayed in either of the two forms; polar plot or rectangular plot.

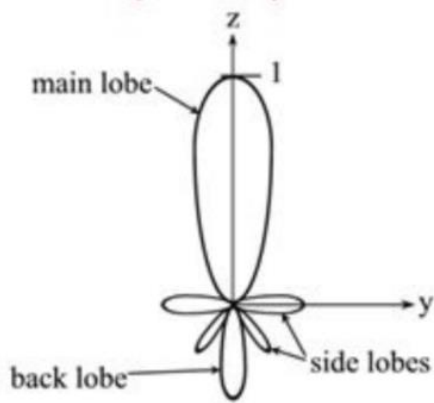


Fig 3-2. Polar plot [52]

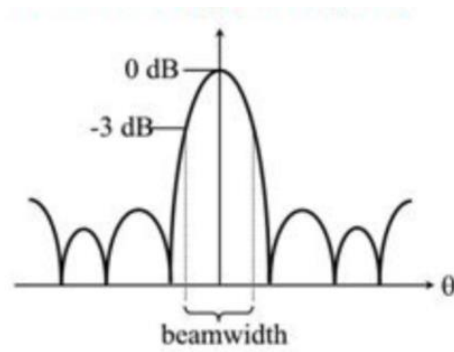


Fig 3-3. Rectangular plot [52]

The beamwidth of a radiated beam is defined as the points where the power falls to half of the maximum at the center of the beam in either principal-planes. Thus, the term is referred to as the -3 dB beamwidth of the beam. The azimuth and elevation beamwidth determine the angular resolution of the antenna in the respective planes, which is the angular separation at which two equal targets can be distinguished separately when at the same range. The principal plane beamwidths of an antenna also determines the antenna gain. A narrower principal plane beamwidth corresponds to a higher antenna gain, which is useful in differentiating the desired radar return against an unwanted signal that is either at or on nearly the same frequency.

The sidelobes are the lobes of the far-field radiation pattern that are not the main lobe. Sidelobes divert the power away from the main lobe and increase the vulnerability of a radar to jamming and interference. Therefore, it is important to keep them as low as possible [53]. In Figure 3-2, there are zeros or nulls in the pattern, indicating no radiation in those directions.

3.2.3 Radiated Power

In the far-field region, the radiated field resembles plane waves propagating at a certain direction, say y . The harmonic equation of the orthogonal fields can be written as [54]

$$E = Z_0 y \times H \quad (3-11)$$

$$H = \frac{1}{Z_0} y \times E \quad (3-12)$$

where E is the electric field of the propagated signal, H is the magnetic field of the propagated signal and Z_0 is the intrinsic impedance of free space (120π ohms).

Poynting's theorem [54] can be used to determine the time-averaged power density vector of the wave.

$$P(r, \theta, \phi) = \frac{1}{2} \text{Re}[E \times H^*] \quad (3-13)$$

where H^* is the complex conjugate of the magnetic field.

The total power radiated by the antenna P_{tot} is found by integrating $P(r, \theta, \phi)$ over a closed spherical surface [54].

$$P_{tot} = \oint P(r, \theta, \phi) \cdot dS = \iint P(r, \theta, \phi) r^2 \sin\theta \, d\theta d\phi \quad (3-14)$$

3.2.4 Impedance and Total Efficiency

For efficient transfer of EM energy, the impedance of the transmission line and the antenna being fed must match one another. Antenna impedance relates the voltage to the current at the antenna input and is given by [45]

$$Z_A = R_A + jX_A \quad (3-15)$$

where Z_A , R_A and X_A represents the antenna impedance, resistance and reactance, respectively. The resistance of an antenna can be expressed as

$$R_A = R_{rad} + R_L \quad (3-16)$$

where R_{rad} is the radiation resistance and R_L is the resistive losses of the antenna.

Assuming that the antenna is attached to a generating power source with an internal impedance of

$$Z_g = R_g + jX_g \quad (3-17)$$

where R_g is the resistance of the generator and X_g is the reactance of the generator. The magnitude of the current in the generator can be written as [45]

$$|I_g| = \frac{|V_g|}{|Z_t|} = \frac{|V_g|}{|Z_A + Z_g|} = \frac{|V_g|}{\left[(R_{rad} + R_L + R_g)^2 + (X_A + X_g)^2 \right]^{\frac{1}{2}}} \quad (3-18)$$

where V_g is the peak generator voltage. The power delivered to the antenna for radiation purpose is [45]

$$P_{rad} = \frac{1}{2} |I_g|^2 R_{rad} = \frac{|V_g|^2}{2} \left[\frac{R_{rad}}{(R_{rad} + R_L + R_g)^2 + (X_A + X_g)^2} \right] \quad (3-19)$$

The power dissipated as heat due to the resistive losses of the antenna is [45]

$$P_L = \frac{1}{2} |I_g|^2 R_L = \frac{|V_g|^2}{2} \left[\frac{R_L}{(R_{rad} + R_L + R_g)^2 + (X_A + X_g)^2} \right] \quad (3-20)$$

and the power dissipated as heat in the internal resistance of the generator, which makes up for the remaining transmitted power, is given by [45]

$$P_g = \frac{|V_g|^2}{2} \left[\frac{R_g}{(R_{rad} + R_L + R_g)^2 + (X_A + X_g)^2} \right] \quad (3-21)$$

The maximum amount of power is delivered to the antenna from the generator power source when there is conjugate matching. That is achieved when [45]

$$R_{rad} + R_L = R_g \quad (3-22)$$

$$X_A = -X_g \quad (3-23)$$

Similarly, an impedance mismatch between an antenna and a coaxial transmission line would also cause a degradation in antenna performance due to the reflected power between the two mediums. The reflection coefficient for the reflected power at the input terminals of an antenna is given by the S_{11} , which is derived as

$$S_{11} = \frac{Z_A - Z_0}{Z_A + Z_0} \quad (3-24)$$

where Z_A is antenna impedance

Z_0 is characteristic impedance of the transmission line

The return loss, which is often specified as a performance parameter in microwave applications, is given by the following equation in decibels [51]. It can be thought of as a measure of how close the actual input impedance of the network is to the nominal impedance value.

$$\text{return loss} = 20 \log_{10} |S_{11}| \quad (3-25)$$

Return losses of -15 dB are typical for many antennas but values of the order of -30 dB or more may be demanded for a high performance satellite communications ground station [51].

The S_{11} is also a parameter of the scattering matrix of a n-port network. The scattering matrix which contains the S-parameters ($S_{11}, S_{12}, S_{21}, S_{22} \dots$) is based on propagating waves

that enters and leaves a n-port network. The scattering matrix equation for a two-port network can be expressed as [55]

$$\begin{bmatrix} b_1 \\ b_2 \end{bmatrix} = \begin{bmatrix} S_{11} & S_{12} \\ S_{21} & S_{22} \end{bmatrix} \begin{bmatrix} a_1 \\ a_2 \end{bmatrix} \quad (3-26)$$

where a_1 and a_2 represents the incident waves

b_1 and b_2 represents the output of the network

S_{11} is input reflection coefficient

S_{21} is forward transmission coefficient

S_{12} is reverse transmission coefficient

S_{22} is output reflection coefficient.

Given the condition of two interacting antennas, the S-parameters are used to determine the operating frequencies of the respective antennas (S_{11} and S_{22}) and the interference between them (S_{12} and S_{21}) when one of the antenna is transmitting.

Both incident and reflected propagating waves within a transmission line creates a standing wave. The ratio of the standing wave, also known as the Voltage Standing Wave Ratio (VSWR), is given by (3-27) in terms of the reflection coefficient [56]

$$VSWR = \frac{V_{max}}{V_{min}} = \frac{1 + |S_{11}|}{1 - |S_{11}|} \quad (3-27)$$

The VSWR is a measure of the ratio of the maximum and minimum voltages set up on the transmission line [51]. It therefore relates to the magnitude of the voltage reflection coefficient and hence to the magnitude of S_{11} for the input port. It is always positive and has a minimum value of 1, which indicates the ideal situation where all the transmit waves are transmitted, or zero power is reflected back down the line.

The total efficiency of an antenna is the ratio of power radiated from the antenna relative to the power delivered to it when it is connected to a transmission line. A high efficiency antenna radiates most of the power present at the antenna's input into free space. Whereas in a low efficiency antenna, most of the input power is either absorbed within the antenna as losses or being reflected away due to impedance mismatch. The antenna's total efficiency can be expressed as

$$\eta = \frac{P_{rad}}{P_{in}} = \eta_i \eta_r \quad (3-28)$$

where η is the total efficiency of the antenna

η_i is the reflection efficiency accounting for impedance mismatch ($1 - |S_{11}|^2$)

η_r is the radiation efficiency of the antenna

and

$$\eta_r = 1 - \eta_c \eta_d \quad (3-29)$$

where η_c is the conduction efficiency of the antenna

η_d is the dielectric efficiency of the antenna

The reflection efficiency of an antenna is always less than unity due to impedance mismatch losses, which causes power to be reflected back down the transmission line. The remainder of the power delivered to the antenna is either radiated or absorbed as losses within the antenna. Hence, the radiation efficiency of the antenna is always less than its reflection efficiency due to losses within an antenna, although the majority of the power delivered is usually radiated as EM waves into free space since antennas are typically designed to be low loss. The S_{11} and VSWR is typically measured using a Vector Network Analyzer (VNA), which can plot them for direct interpretation of the properties.

3.2.5 Gain, Directivity and Radiation Efficiency

The power gain and directivity are quantities which define the ability of an antenna to concentrate energy in a particular direction. This quantity is an inherent property of the antenna and does not include losses which may arise from mismatch of impedance between the antenna and power source or mismatch of polarization of the receiving antenna [51]. The gain of an antenna, however, includes the ohmic or dissipative losses arising from the conductivity of metal and dielectric loss, while the directivity of an antenna does not.

The directivity of an antenna can be defined as a ratio of normalized power in a particular direction to the average normalized power in all directions [57]

$$D_i(\theta, \phi) = \frac{P_{norm}(\theta, \phi)}{P_{norm}(\theta, \phi)_{ave}} \quad (3-30)$$

The maximum directivity of the antenna, which mostly refers to the main lobe of the antenna radiation pattern, is as expressed as [45]

$$D_i(\theta, \phi)_{max} = \frac{P_{norm}(\theta, \phi)_{max}}{P_{norm}(\theta, \phi)_{ave}} \quad (3-31)$$

The ratio of power gain to directivity is termed the radiation efficiency η_r of the antenna [51].

$$\eta_r = \frac{\text{power gain in direction } \theta, \phi}{\text{directivity in direction } \theta, \phi} \quad (3-32)$$

or

$$\eta_r = \frac{G(\theta, \phi)}{D_i(\theta, \phi)} \quad (3-33)$$

Hence, the antenna gain is simply the product of its radiation efficiency and antenna directivity [58]. The directivity of an antenna only accounts for the directional properties of the antenna. The antenna gain, on the other hand, also considers the losses due to the conversion of electrical energy into EM energy, which are only associated to the losses from the internal circuitry within an antenna. Hence, the antenna gain considers the antenna electrical efficiency as well as its directional properties, and for a lossless antenna ($\eta_r = 1$) the antenna gain G equals its directivity D .

$$\text{Gain} = D_i \times \eta_r \quad (3-34)$$

For instance, the directivity and gain of a typical circular parabolic reflector antenna is almost the same since the efficiency of such antennas are close to unity. The numerical method of calculating the gain of a parabolic reflector antenna including the factors affecting it is elaborated in Section 3.5.2.2.

3.2.6 Polarization

The polarization of an electromagnetic wave is effectively the plane in which the electric field propagates in [59]. This is a significant property in antenna design because all antenna systems are sensitive to polarization, and their performance heavily relies on it. There are three main types of polarization, namely linear, circular and elliptical. Each of them is outlined below.

Most standard antennas only receive or transmit a signal with a particularly defined polarization. In simple horn antennas radio waves are usually transmitted and received in one common linear polarization, that is, either in vertical or horizontal polarization. In linear polarized antenna the E-field orientates in a single line and it is orthogonal to the direction of the H-field, as well as to the direction of propagation of EM waves. If an antenna has its E-field component horizontal to the ground, it is said to be horizontally polarised. Likewise, if the antenna has its E-field vertical to the ground, it is said to be vertically polarised. Antennas that are used to transmit and/or receive with the same polarization are said to be co-polarized. However, reflections from objects encountered within the propagation path can change the polarization of the transmitted signal. As the received signal is the sum of the direct signal plus a number of reflected signals, the overall polarization of the returning signal may be slightly changed upon propagating through the two-way journey. When this happens in a linearly

polarized system, the antenna polarization does not match the polarization of the returning signal at reception, and this results in a substantial reduction in the level of useful signal accepted by the antenna, which is given by a factor of cosine of the angle between the polarization of the antenna and that of the received signal [59]. The remaining signal that is not accepted is rejected or simply wasted. If the polarization were at right angles to one another then in theory absolutely no signal would be received. This term is known as cross-polarization and is undesirable due to the degradation in antenna performance.

To overcome the effects of cross-polarization in a single linear polarized antenna system, the antenna can be designed to transmit and receive signals in more than one polarization. This type on antennas are known to employ dual polarization. On transmission, electromagnetic waves of different polarizations can be transmitted subsequently (Horizontal (H) and vertical (V) parts), using a switch to direct energy to the different parts of the antenna in sequence, or even simultaneously (circular polarization). Likewise, on reception, waves of different polarizations can also be received separately. When horizontal and vertical polarization of radio waves of equal amplitude are used together by feeding the H and V parts of the antenna simultaneously, this results in a circular polarized signal. In circular polarization, the tip of the E-field of an antenna rotates in a circle [60] [61]. The two types of circular polarization are the Right Hand Circular Polarization (RHCP) and Left Hand Circular Polarization (LHCP). Circular polarization is sometimes used for satellite radio communications as there are some advantages in terms of propagation and in overcoming the fading caused if the satellite is changing its orientation [62]. One of the main advantages of using circularly polarised antennas is its ability to reject multipath interference. However, the complexity of designing an antenna system with circular polarization is high, it is more expensive and is not entirely necessary for certain applications.

Elliptical polarization is formed when the vertical or horizontal components of an E-field are not equal. The analogy used to describe RHC and LHC polarizations can be employed to describe Right Hand Elliptically (RHE) and Left Hand Elliptically (LHE) polarizations of an antenna. The three polarization states of an EM wave are illustrated in Figure 3-4. In the illustration provided, the EM waves travel in the direction that the arrow is pointing towards.

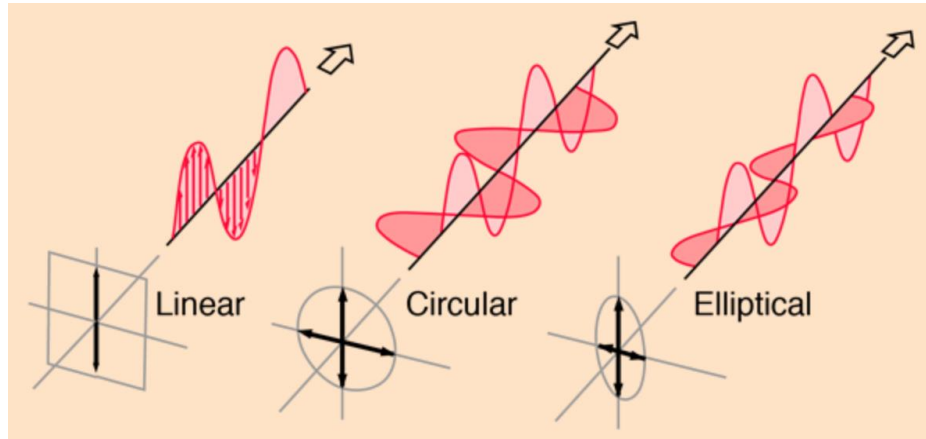


Fig 3-4. Polarization states of an EM wave [49]

3.2.7 Bandwidth

The term bandwidth is used to describe the frequency range over which the antenna will operate satisfactorily. There is no unique definition for satisfactory performance and this will differ from application to application [51]. The bandwidth is a range of frequencies on either sides of the centre frequency where the general properties of an antenna, such as the efficiency, beamwidth, radiation pattern, gain, sidelobe levels and polarization, are within the acceptable values of those at the centre frequency [45] that fulfils the performance requirements of the application in hand. The radar bandwidth also determines the range resolution of the radar. Range resolution is the ability of a system to distinguish two targets located at the same angle with respect to the radar axis but at different range from the system. The following equation that calculates the range resolution, ΔR , of a radar system is given by

$$\Delta R = \frac{C}{2B} \quad (3-35)$$

where C is the speed of light in free space and B is the bandwidth of the radar system.

A large receiver bandwidth is preferable to achieve a higher range resolution. However, a radar system with a very wide bandwidth introduces a higher receiver noise, which reduces the target SNR. Hence, from this viewpoint, the receiver bandwidth used should only be sufficient to fulfil the range resolution requirements of the application in hand, due to the persistent trade-off between the receiver noise and resolution performance.

The expression used to describe antenna bandwidth depends if the antenna is a wideband or narrowband antenna. Bandwidth is expressed either as an absolute frequency range in hertz, or as a percentage of the centre frequency. A wideband antenna could imply anything from several octaves down to perhaps a 40% band, although in some applications a 15% band

would be considered broadband operation. On the other hand, a narrowband antenna may have a bandwidth of only just a few percent or less [51].

3.2.8 Noise Floor

The noise floor in a receiver is the sum of the noise from the environment and the noise added from the receiver itself.

$$P_n = kT_0B + kT_sB \quad (3-36)$$

where P_n is noise power

k is Boltzmann's Constant

T_0 is Noise Reference Temperature

T_s is Receiver Noise Temperature

B is Signal Bandwidth

The Noise Figure, which measured in decibels, is defined as [35]

$$F = \frac{\text{Input SNR}}{\text{Output SNR}} = \frac{\frac{P_s}{kT_0B}}{\frac{P_s}{kT_0B + kT_sB}} = 1 + \frac{T_s}{T_0} \quad (3-37)$$

Substituting the above expression in (3-36) gives the noise floor in terms of the noise figure

$$P_n = kT_0B \left(1 + \frac{T_s}{T_0}\right) = kT_0BF \quad (3-38)$$

3.3 Waveguide Theory

A transmission line is known as a linear passive two-port that is used to convey electrical power or signals between two points that are appreciably separated in distance. There are many types of transmission lines and each is suitable for a certain type of application. Waveguides are used to transmit RF power at operating frequencies that are too high for successful operation of conventional transmission lines. The dimensions of the cross section are such that an EM wave can propagate in the interior of the guide. Confining the electric and magnetic fields within the waveguide prevents the field from spreading spherically as it would in free space. Hence, therefore there is no inverse-square-law decrease of the power density and no power is lost to radiation. However, there is some attenuation due to currents in the walls of the guide which results in some power lost in the form of heat, given by IR^2 , although this loss is usually very small and less than in a coaxial line of comparable size. Moreover, since the guides are normally

filled with air, dielectric losses are negligible. There is also virtually no “leakage” loss and less tendency to flashover at high voltages since no insulating supports are required [27].

Experimental results have shown that waveguides behave like transmission lines apart from some significant differences in properties. [27] presents the differences and the important properties of a waveguide, which is outlined in this section. Understanding waveguide properties is essential to approximate its performance accurately.

A waveguide can take any form of shape depending on the requirement of the application, although its most common form is a hollow pipe with either a circular, rectangular or ridged cross section. Nonetheless, this section will only refer to rectangular waveguides since it will be used to feed a sectoral horn antenna, as will be shown in the later parts of the project.

3.3.1 Phase Velocity of EM Waves in a Waveguide

Unlike the velocity of EM waves in conventional transmission lines, the wave (*phase*) velocity V_{ph} in a waveguide varies with the frequency of the EM waves. The phase velocity in a given waveguide can be calculated using the following equation [27]

$$V_{ph} = f\lambda_g \quad (3-39)$$

where f is the operating frequency and λ_g is a measurement of the wavelength in the waveguide λ_g , which can be done by setting up a standing wave and measuring the separation of two minima.

The phase velocity of EM waves in waveguide is always greater than or equal to the velocity in free space ($c = 3 \times 10^8$ m/s), and therefore the wavelength of the wave at a given frequency is also always greater in the guide than in free space [27]. The relationship between the wavelength in the guide and the wavelength in free space λ_o is given by

$$\lambda_g = \lambda_o \left(\frac{V_{ph}}{c} \right) \quad (3-40)$$

The differentiation between the wavelength in free space and of the waveguide is an important principle of waveguide theory.

3.3.2 Cut-off Frequency

Rectangular waveguides are commonly used for power transmission at microwave frequencies. Waveguides are characterized by the cut-off frequency which is an absolutely limiting frequency whereby frequencies below this value will not be propagated in the guide. The

following waveguide property presents its importance in ensuring that a waveguide used for a specific application is suitable for the operating frequency, otherwise the RF performance of the guide could be extremely poor.

At a particular operating frequency, the relationship between the guide-wavelength and the cut-off frequency f_c of the waveguide given by [27]

$$\lambda_g = \frac{c}{\sqrt{f^2 - f_c^2}} \quad (3-41)$$

which can also be expressed as

$$\lambda_g = \frac{\lambda_o}{\sqrt{1 - (f_c/f)^2}} \quad (3-42)$$

Hence, the phase velocity of an EM wave propagating within a vacuum-filled waveguide can be expressed in terms of the cut-off frequency as

$$V_{ph} = c \left(\frac{\lambda_g}{\lambda_o} \right) = \frac{c}{\sqrt{1 - (f_c/f)^2}} \quad (3-43)$$

It is evident that the phase velocity of the EM waves within the guide will become imaginary if the operating frequency is lower than the cut off frequency of the waveguide, which implies that the EM wave will not be propagated through the waveguide.

The cut-off frequency is determined by the cross-sectional dimensions of the guide in relation to the wavelength [27]. Hence, the physical dimensions of a waveguide are regulated by the frequency of the signal being transmitted. The most common form of waveguide has a rectangular cross section with dimensions a and b , as illustrated in Figure 3-5.

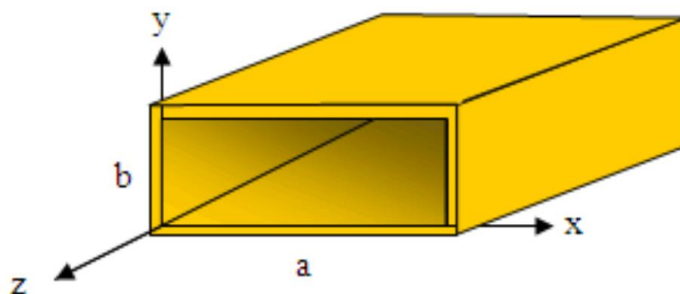


Fig 3-5. Cross section of the opening of a rectangular waveguide

A section of a rectangular waveguide, also known as an adapter, is most commonly used to construct horn antennas. The longer dimension a determines the cut-off frequency of the adapter according to the relation [27]

$$f_c = \frac{c}{2a} \quad (3-44)$$

or

$$\lambda_c = 2a \quad (3-45)$$

where λ_c is the cut-off wavelength.

This relation states that the cut-off occurs at the frequency for which the largest transverse dimension of the waveguide, a , is exactly a half of the cut-off wavelength [27]. For instance, the cut-off frequency of a WR-90 adapter ($a = 22.86$ mm, $b = 10.16$ mm), which is designed to accommodate frequencies within the X-band spectrum, is 6.56 GHz.

3.3.3 Modes of Propagation in Rectangular Waveguides

It is possible to propagate several modes of electromagnetic waves within a waveguide. The physical dimensions of a waveguide determine the cut-off frequency for each propagating mode. If the frequency of the signal is above the cut-off frequency of a given mode, the EM energy can be transmitted through the guide for that particular mode with minimal attenuation. Otherwise, the EM energy with a frequency below cut-off for that particular mode will be attenuated to a negligible value in a relatively short distance [27].

The dominant mode in a particular waveguide is the mode having the lowest cut-off frequency. For rectangular waveguide this is the TE_{10} mode. The configuration of the EM field of a wave propagating through the waveguide at frequencies slightly above the cut-off frequency (TE_{10} mode) is schematically represented in Figure 3-6.

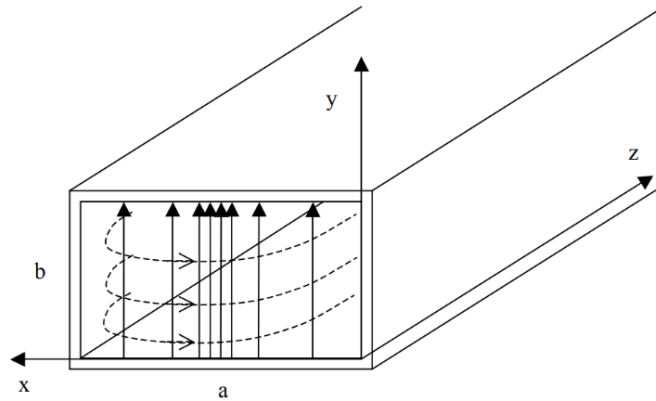


Fig 3-6. Configuration of the EM field in TE_{10} mode [63]

As shown in Figure 3-6, the electric field (\mathbf{E}) vectors are parallel and are perpendicular to the wide face of the guide. Their amplitude is the greatest midway between the narrow walls and decreases to zero at these walls, in a cosinusoidal fashion, because the fields are confined in the transverse directions. The magnetic field (\mathbf{H}) vectors, shown dashed, are also parallel to each other and perpendicular to the electric vectors. The magnetic intensity is constant in the vertical direction across the guide section. The wave is propagating in the longitudinal direction of the guide and is perpendicular to the \mathbf{E} and \mathbf{H} vectors [27]. This particular field arrangement is the only possible one at operating frequencies that is just above the cut-off frequency of the waveguide. This mode of propagation is called the TE_{10} mode. The TE (transverse electric) signifies that all electric fields are transverse to the direction of propagation (perpendicular to the guide walls) and that no longitudinal electric field is present. The magnetic field lines are also transverse; but this is not true for all views. Transverse-magnetic (TM) modes and transverse-electric-magnetic (TEM) modes may also be propagated under certain conditions [27], although less commonly encountered.

At operating frequencies that are well above the cut-off frequency of the guide, higher-order TE modes of propagation are possible. For rectangular guides of low aspect ratio, the TE_{20} mode is the next higher order mode and is harmonically related to the cut-off frequency of the TE_{10} mode. Figure 3-7 shows a graphical depiction of the \mathbf{E} field variation in a waveguide for the TE_{10} , TE_{20} , and TE_{30} modes. As can be seen, the first index indicates the number of half-sinusoid cycles in the transverse electric field pattern parallel to the width (a) and height (b) of the guide, respectively [63].

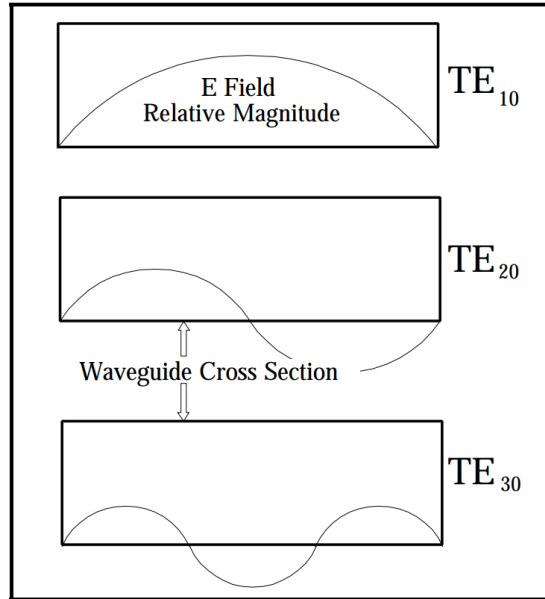


Fig 3-7. E-field variation in a waveguide for various TE modes [63]

Allowing EM waves to propagate at higher modes is undesirable because they will not be properly coupled to the load, and therefore would result in losses and signal issues due to reflections and the formation of standing waves. Thus, it is undesirable to operate a guide at frequencies which allows these higher modes of propagation, and for this reason, rectangular guides are usually operated at frequencies that lies between the frequency range of f_c and $2f_c$. When the free-space wavelength is equal to a , that is, at just twice the cut-off frequency, the next higher mode can be sustained by the guide. Hence, it is advisable to choose the dimensions of a guide in such a way that, for a given input signal, only the energy of the dominant mode can be transmitted through the guide. Rectangular waveguides with an aspect ratio b/a of approximately 0.5 is commonly used to preclude generation of field variations with height and their attendant unwanted modes. [27]

3.3.4 Impedance in Rectangular Waveguides

The characteristic wave impedance of a waveguide Z_c is defined similarly to the concept of wave impedance in free space (377 ohms). The characteristic impedance of a rectangular guide at a given operating frequency is given by

$$Z_c = \frac{377}{\sqrt{1 - (f_c/f)^2}} = 377 \left(\frac{\lambda_g}{\lambda_o} \right) \text{ ohms} \quad (3-46)$$

Unlike in conventional transmission lines, the wave impedance in a waveguide is dependent on its operating frequency. In general, Z_c is greater than the wave impedance in free space (377 Ω).

At the cut-off frequency it becomes infinite, and at twice the cut-off frequency it has a value of 435Ω [27]. A waveguide does not permit the propagation of EM waves at operating frequencies below the cut-off value, which automatically prevents the waveguide from functioning. For instance, based on (3-46) the characteristic impedance of a WR-90 waveguide used at an operating frequency of 9.2 GHz is 478Ω .

3.4 Horn Antennas

A horn antenna is essentially formed when the walls of a waveguide is flared outwards. When it is properly flared, it allows for a gradual transition from a wave propagating in a transmission line (i.e. waveguide), also known as a waveguide mode, to a wave propagating in free space, also known as free-space mode. The field that is illuminating the aperture of the horn is essentially a spatially expanded version of the waveguide field. The wave impedance of the flared waveguide (the horn) gradually approaches the intrinsic impedance of free space as the width of the horn aperture increases. Not only does it result in a matched impedance (low VSWR) over a wide bandwidth, but it also produces a desirably concentrated radiation pattern, that is, narrower beamwidth and higher directivity. Hence, at an operating frequency, the beamwidth and gain of a horn antenna would vary with the flare angle itself, and it can be imagined that for a given horn length the radiation properties of the antenna is optimized at a specific flare angle. The gain of a horn antenna can usually be calculated very accurately from their physical dimensions. Horn antennas are simple to manufacture and are frequently used as feeds for reflector antennas due to its desirable radiation properties, and for standard-gain devices in antenna measurements [50].

There are various possible flaring arrangements that each would result in different types of horns. There are notably two types of horn antennas, that is, horns with a rectangular or circular aperture. A rectangular guide may be flared on the narrow walls, the wide walls, or all four walls. A pyramidal horn is formed when all four walls are appropriately flared. A sectoral horn, on the other hand, is formed when the walls is only flared in one dimension. Hence, there are two types of rectangular horns that are ideally suited for rectangular waveguide feeds, which tend to have either horizontal or vertical polarization. Likewise, a conical horn is formed by uniform flaring of the walls of a circular waveguide, and this type of horn tend to have circular polarization.

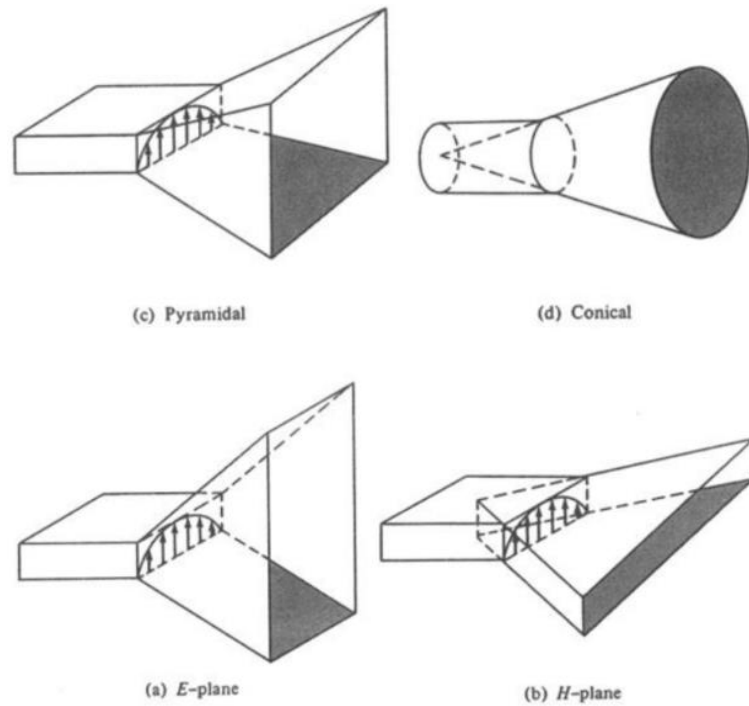


Fig 3-8. Main types of horn antennas [27]

Since rectangular horn antennas with either vertical or horizontal polarization are most frequently used as the feed of a mechanical scanning surveillance radar system, only rectangular horn antennas will be described in this section. The two basic types of conventional rectangular horns are the pyramidal and sectoral horn antennas.

3.4.1 Sectoral Horns

As mentioned, a sectoral horn is formed when the walls of a rectangular waveguide are flared in only one dimension. Sectoral horns consist of two parallel sides and two flared sides that forms an angle, ϕ_o , called the flare angle. There are two types of sectoral horn antennas, that is, the *E*-plane and *H*-plane type. An *E*-plane sectoral horn is formed when only the broad walls of the guide are flared with the TE_{10} mode, or in the direction of the electric vector (vertical direction). On the other hand, a *H*-plane sectoral horn is formed when only the narrow walls are flared in the horizontal direction. As presented in the following chapters, this project involves designing a reflector antenna system that utilizes a *E*-plane sectoral horn antenna as the feed to a vertically truncated parabolic reflector. Hence, only the design requirements and properties of the *E*-plane sectoral horn that achieves maximum directivity will be discussed in this section.

The dimensions of the aperture of a E -plane sectoral horn is significantly larger in the vertical plane than in the horizontal plane, which has the same dimension as the width of the guide since it is unflared in this direction. This type of horn antenna is used when a fan-shaped beam with a beamwidth that is significantly larger in azimuth than in elevation is required. The flaring of the horn antenna in the vertical plane, however, causes the aperture field to be affected by a phase error in the E -plane, which reduces the antenna gain.

The waves travel down the horn as spherical wavefronts from the horn apex (phase center), and because the wavefronts are spherical, the phase increases smoothly from the edges of the aperture plane towards the center due to the difference in path lengths of the center and edge points from the apex point [64]. As a result, the complication in the analysis arises from the fact that the waves arriving at the horn aperture are not in phase, and this phase difference is called the phase error. Since the horn aperture is not flared in the x -plane, the phase is uniform along this plane and no phase error is introduced. Nonetheless, the phase error introduced in the E -plane, which increases with the flare angle, reduces the gain, increases the beamwidth, and elevates the sidelobe level that causes it to fill the null between adjacent side lobes.

The geometry and each of the parameters shown in the Figure 3-9 will be used in the subsequent analysis to identify the design requirements, that is, identifying the optimum flare angle of the E -plane sectoral horn that provides the maximum gain for a given horn length, or vice versa. The derivation provided is adopted from [64].

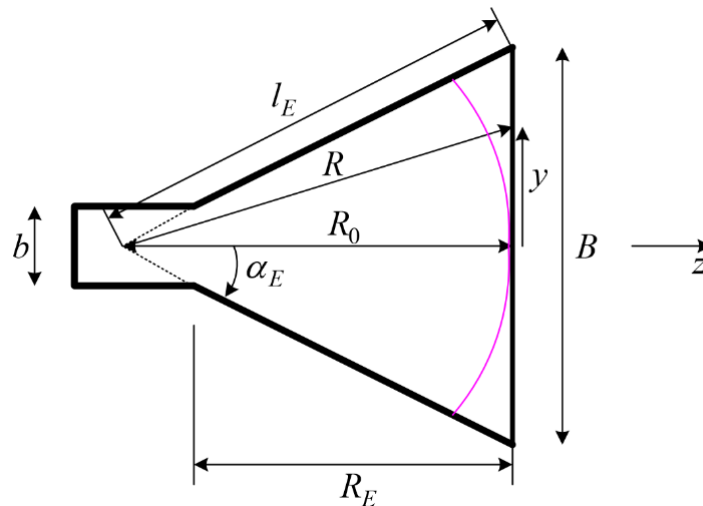


Fig 3-9. E-plane (y - z) cut of an E-plane sectoral horn [64]

$$l_E^2 = R_0^2 + \left(\frac{B}{2}\right)^2 \quad (3-47)$$

$$\alpha_E = \arctan\left(\frac{B}{2R_0}\right) \quad (3-48)$$

$$R_E = (B - b) \sqrt{\left(\frac{l_E}{B}\right) - \frac{1}{4}} \quad (3-49)$$

The two required dimensions for the construction of the horn are B and R_E

The tangential field arriving at the input of the horn is composed of the transverse field components of the waveguide dominant mode TE_{10}

$$E_y = E_0 \cos\left(\frac{\pi}{a}x\right) e^{-j\beta_g z} \quad (3-50)$$

$$H_x = -E_y(x)/Z_g \quad (3-51)$$

where Z_g is the wave impedance and β_g is the propagation constant of the TE_{10} mode.

Due to the walls of the guide being flared in the vertical direction, the complication arises from the fact that the waves arriving at the horn aperture are not in phase due to the different path lengths from the horn apex. The aperture phase variation in the flared plane of the E -plane sectoral horn is given by

$$e^{-j\beta(R-R_0)} \quad (3-52)$$

Since the aperture is not flared in the x -direction, the phase is uniform along this plane. We first approximate the path of the wave in the horn along the y -plane:

$$R = \sqrt{R_0^2 + y^2} = R_0 \sqrt{1 + \left(\frac{y}{R_0}\right)^2} \approx R_0 \left[1 + \frac{1}{2} \left(\frac{y}{R_0}\right)^2\right] \quad (3-53)$$

and if $x \ll R_0$, or $A/2 \ll R_0$, we can assume that

$$R - R_0 \approx \frac{1}{2} \frac{y^2}{R_0} \quad (3-54)$$

Substituting (3-52) and (3-54) into (3-50), the field at the aperture that is affected by a phase error in the E -plane is approximated as

$$E_{a_y} = E_0 \cos\left(\frac{\pi}{a}x\right) e^{-j\frac{\beta}{2R_0}y^2} \quad (3-55)$$

The radiation far-field at the aperture is obtained as

$$E = j\beta E_0 \frac{4a}{\pi} \sqrt{\frac{\pi R_0}{\beta}} \frac{e^{-j\beta r}}{4\pi r} e^{j\left(\frac{\beta R_0}{2}\right)\left(\frac{\beta B}{2} \sin \theta \sin \varphi\right)^2} \cdot (\hat{\theta} \sin \varphi + \hat{\phi} \cos \varphi) \times \frac{(1 + \cos \theta) \cos\left(\frac{\beta a}{2} \sin \theta \cos \varphi\right)}{2 \left[1 - \left(\frac{\beta a}{2} \sin \theta \cos \varphi\right)^2\right]} [C(r_2) - jS(r_2) - C(r_1) + jS(r_1)] \quad (3-56)$$

The arguments of the Fresnel integrals used in (3-56) are

$$r_1 = \sqrt{\frac{\beta}{\pi R_0}} \left(-\frac{B}{2} - R_0 \frac{\beta B}{2} \sin \theta \sin \varphi\right) \quad (3-57)$$

$$r_2 = \sqrt{\frac{\beta}{\pi R_0}} \left(+\frac{B}{2} - R_0 \frac{\beta B}{2} \sin \theta \sin \varphi\right) \quad (3-58)$$

Using (3-56) we can identify the normalized far-field principle-plane radiation patterns.

The normalized H -plane pattern is found by substituting $\varphi = 0^\circ$ into (3-56)

$$\bar{H}(\theta) = \left(\frac{1 + \cos \theta}{2}\right) \times \frac{\cos\left(\frac{\beta a}{2} \sin \theta\right)}{1 - \left(\frac{\beta a}{2} \sin \theta\right)^2} \quad (3-59)$$

The second factor in (3-59) is the pattern of a uniform-phase cosine-amplitude tapered line source.

The normalized E -plane pattern is found by substituting $\varphi = 90^\circ$ into (3-56)

$$\bar{E}(\theta) = \left(\frac{1 + \cos \theta}{2}\right) |f_E(\theta)| \quad (3-60)$$

$$\bar{E}(\theta) = \frac{(1 + \cos \theta)}{2} \sqrt{\frac{[C(r_2) - C(r_1)]^2 + [S(r_2) - S(r_1)]^2}{4[C^2(r_{\theta=0}) + S^2(r_{\theta=0})]}} \quad (3-61)$$

Here, the arguments of the Fresnel integrals are calculated for $\varphi = 90^\circ$

$$r_1 = \sqrt{\frac{\beta}{\pi R_0}} \left(-\frac{B}{2} - R_0 \frac{\beta B}{2} \sin \theta\right) \quad (3-62)$$

$$r_2 = \sqrt{\frac{\beta}{\pi R_0}} \left(+\frac{B}{2} - R_0 \frac{\beta B}{2} \sin \theta\right) \quad (3-63)$$

and

$$r_{\theta=0} = r_2(\theta = 0) = \frac{B}{2} \sqrt{\frac{\beta}{\pi R_0}} \quad (3-64)$$

The E-plane pattern calculated is only an approximation due to the approximation of the phase distribution made, as shown in (3-54). Accurate value of $\bar{E}(\theta)$ is obtained if the accurate value of the function $f_E(\theta)$ is calculated by numerical integration of the aperture field distribution, given by

$$f_E(\theta) \propto \int_{-B/2}^{B/2} e^{-j\beta\sqrt{R_0^2+y'^2}} e^{j\beta y' \sin \theta} dy' \quad (3-65)$$

The directivity of the E-plane sectoral horn is calculated using a general directivity expression for specified apertures

$$D_0 = \frac{4\pi}{\lambda^2} \cdot \frac{\left| \iint_{S_B} \mathbf{E}_b ds' \right|^2}{\iint_{S_B} |\mathbf{E}_b|^2 ds'} \quad (3-66)$$

The integral in the denominator is proportional to the total radiated power. Hence, the directivity of the E-plane sectoral horn, D_E , is obtained by integrating the power at the aperture. In the solution of the integral in the numerator of equation (3-66), the field is substituted with its phase approximated as in (3-55). The final result is

$$D_E = \frac{a}{\lambda} \frac{32}{\pi} \left(\frac{B}{\lambda} \right) \varepsilon_{ph}^E = \frac{4\pi}{\lambda^2} \varepsilon_t \varepsilon_{ph}^E aB \quad (3-67)$$

where

$$\begin{aligned} \varepsilon_t &= \frac{8}{\pi^2}, \\ \varepsilon_{ph}^E &= \frac{C^2(q) + S^2(q)}{q^2}, \\ q &= \frac{B}{\sqrt{2\lambda R_0}} \end{aligned}$$

The factor ε_t explicitly shows the aperture efficiency associated with the aperture cosine taper. The factor ε_{ph}^E is the aperture efficiency associated with the aperture phase distribution in the E-plane.

A family of universal directivity curves, $\lambda D_E / a$ vs. B / λ , for different horn apex length, R_0 , of a E-plane sectoral horn is presented in Figure 3-10. The graph was generated by aperture theory and have been validated, generally, by measurements [65].

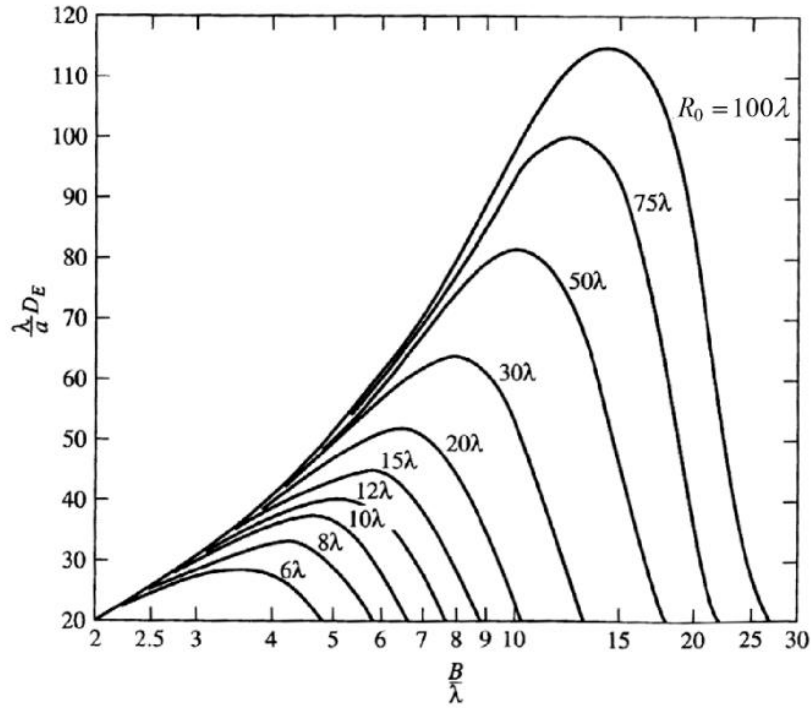


Fig 3-10. A family of universal directivity curves, $\lambda D_E / a$ vs. B / λ [65]

For every value of R_0 , there is an optimum aperture height, B , that gives maximum directivity. Based on the family of universal directivity curves for a E -plane sectoral horn antenna, an optimal relation between the flared height B and the horn apex length R_0 that produces a E -plane sectoral horn with maximum possible gain is given by [64]

$$B = \sqrt{2\lambda R_0} \quad (3-68)$$

3.4.2 Pyramidal Horn

As mentioned, in a pyramidal horn the feeding waveguide is flared in both directions, the E -plane and the H -plane. All results are combinations of the E -plane sectoral horn and the H -plane sectoral horn analysis. The field distribution at the aperture is approximated as [64]

$$E_{a_y} \approx E_0 \cos\left(\frac{\pi}{A}x\right) e^{-j\frac{\beta}{2}\left(\frac{x^2}{R_0^{E^2}} + \frac{y^2}{R_0^{H^2}}\right)} \quad (3-69)$$

The E -plane principal pattern of the pyramidal horn is the same as the E -plane principal pattern of the E -plane sectoral horn. The same holds for the H -plane patterns of the pyramidal horn and the H -plane sectoral horn. The directivity of the pyramidal horn can be found by

introducing the phase efficiency factors of both planes and the taper efficiency factor of the H-plane [64]

$$D_P = \frac{4\pi}{\lambda^2} \varepsilon_t \varepsilon_{ph}^E \varepsilon_{ph}^H (AB) \quad (3-70)$$

where

$$\begin{aligned} \varepsilon_t &= \frac{8}{\pi^2}; \\ \varepsilon_{ph}^H &= \{[C(p_1) - C(p_2)]^2 + [S(p_1) - S(p_2)]^2\}; \\ p_1 &= 2\sqrt{t} \left[1 + \frac{1}{8t}\right], \quad p_2 = 2\sqrt{t} \left[-1 + \frac{1}{8t}\right], \quad t = \frac{1}{8} \left(\frac{A}{\lambda}\right)^2 \frac{1}{R_0^H/\lambda}; \\ \varepsilon_{ph}^E &= \frac{C^2(q) + S^2(q)}{q^2}, \quad q = \frac{B}{\sqrt{2\lambda R_0}} \end{aligned}$$

The gain of a horn is usually very close to its directivity because the radiation efficiency is very high (low losses). The expression of the antenna gain provided is a physical optics approximation, and it does not take into account only multiple diffractions, and the diffraction at the edges of the horn arising from reflections from the horn interior [64]. These phenomena which are unaccounted for, however, lead to only very minor fluctuations of the measured results from the approximated value. For this reason, horn antennas are often used as gain standards in antenna measurements. The best accuracy of the antenna gain calculation can be achieved if ε_{ph}^H and ε_{ph}^E are calculated numerically without using the second-order phase approximations.

The optimal directivity of an E -plane horn is achieved at $q = 1$ [see also (3-68)], $\varepsilon_{ph}^E = 0.8$. The optimal directivity of an H -plane horn is achieved at $t = 3/8$ [64], $\varepsilon_{ph}^H = 0.79$. Thus, the optimal horn has a phase aperture efficiency of

$$\varepsilon_{ph}^P = \varepsilon_{ph}^H \varepsilon_{ph}^E = 0.632 \quad (3-71)$$

The total aperture efficiency includes the taper factor, too:

$$\varepsilon_{ph}^P = \varepsilon_t \varepsilon_{ph}^H \varepsilon_{ph}^E = 0.81 \cdot 0.632 = 0.51 \quad (3-72)$$

Therefore, the best achievable directivity for a rectangular waveguide horn is about half that of a uniform rectangular aperture.

3.5 Coastal Surveillance Radars

Modern coastal surveillance radars employ two predominant types of antennas, that is, either phased array antennas or parabolic reflector antennas. As mentioned in Section 2.1, each system exhibits advantages over one another from several perspectives. This section outlines the theoretical principles of both types of antennas and their individual properties.

3.5.1 Phased Array Antenna

A phased array antenna is a computer-controlled array of radiating elements that creates a beam of radio waves that can be electronically steered individually to point in any different directions within microseconds, without moving the radiating elements or antenna. In a linear or phased array antenna, the direction of the radiated beam produced from the array is perpendicular to the line or plane of the elements when all the radiating elements are in phase (broadside). On the other hand, if the phases of the elements of a linear array progressively change by an amount that is equal, in radians, to $2\pi d/\lambda$, where d is the element spacing and λ is the operating wavelength, the beam direction will be parallel to the line joining the elements (endfire) [27]. This suggest that progressively changing the phase of each element along the array between the broadside and endfire values is likely to radiate a beam that is directed at a certain angle. Phased array antennas are suitable for operation at the high frequency end of the radio spectrum, in the UHF and microwave bands, in which the radiating elements used can be conveniently small, since the array must consist of hundreds to thousands of radiating elements in order to produce a narrow directive beam that achieves a high gain and narrow beamwidth.

The directional beam produced from a phased array antenna is steered in direction and shape by shifting the phase of the radiated signal from each radiating element, such that the EM waves from each element add together in-phase at the wavefront to increase the radiation in a desired direction, while cancelling to suppress radiation in undesired directions (to provide constructive/destructive interference so as to steer the beams in any direction). In modern phased array antennas, the phasing of each radiating element is most commonly achieved by using variable phase or time delay compensation at the array elements [27]. Nonetheless, both approaches present its pros and cons. Ultimately, the more suitable approach of successfully scanning the beam direction towards a designated angle in space is dependent on the performance requirement of the phased array antenna.

3.5.1.1 Beam Shaping and Steering Techniques

Beam shaping and steering in a linear phased array system can be achieved using a set of linearly increasing phase shifts or time delays. Figure 3-11 compares two phased array

arrangements that are similar except for the use of phase or time delay compensation to steer the direction of the beam produced from the array and provide agile beam-pointing capabilities [50]. Both methods are described in this section.

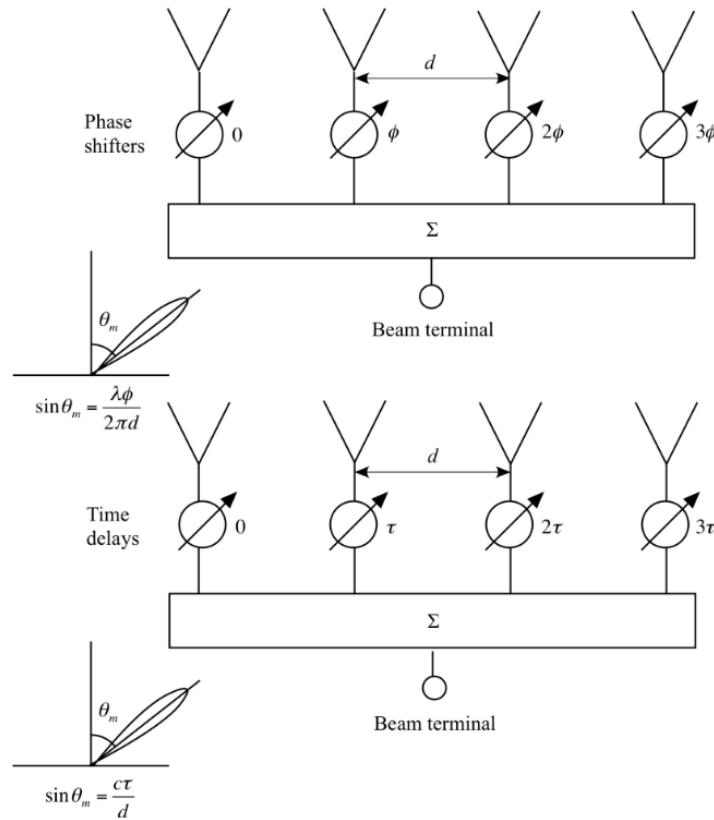


Fig 3-11. Comparison of phase and time delay compensated arrays [50]

In the case of phase compensation method, phase shifters, or phasers, are inserted in the feed of each array element to provide a linearly increasing phase shift across the array elements. Thus, the power from the transmitter that is fed to the individual elements, each through a phase shifter, can alter the phase of each radiated beam electronically, which, as mentioned above, allows the beam of radio waves to be focused and steered towards a certain direction, providing the wave phases arriving at the wavefront from the respective elements are equal. For narrow bandwidth operation, the required range of phase shift is between zero and 2π , that is, 0 and 360 degrees. The implementation of a linearly increasing phase shift from one element to the other, in intervals of ϕ , is illustrated in Figure 3-12.

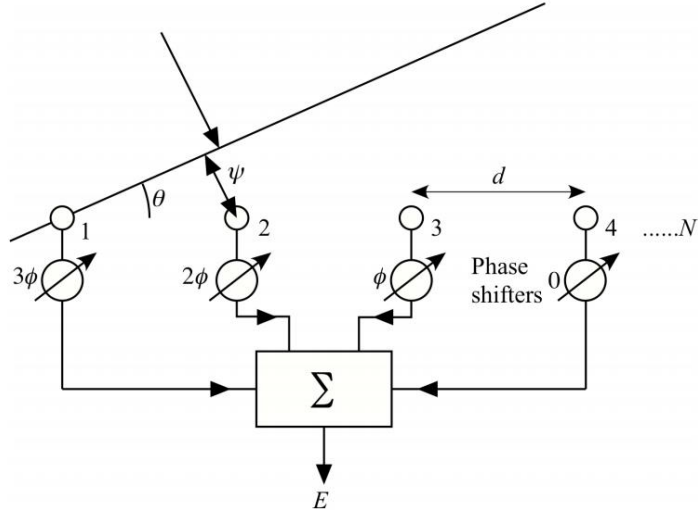


Fig 3-12. An electrically scannable phased array system [50]

For perfect phasing of an array, the phase of each radiating element must change accordingly for each change in either scan angle or operating frequency. Hence, for focusing to be achieved the required phase shift for each element is different, and all of the phases must change with a change in either scan angle θ_m or frequency. This shows that there must be a progressive decrease, from left to right, in phase delay between elements, with an element spacing d [50], that is given by

$$\phi = \left(\frac{2\pi d}{\lambda} \right) \sin \theta_m \quad (3-73)$$

It will be assumed that the phase shifters provide a phase lag equal to (3-73) for each radiating element. The array output signal is therefore

$$E = E_o \exp(j\omega t) \sum_{n=0}^{N-1} \exp(-jn(\psi - \phi)) \quad (3-74)$$

And the pointing direction of the main beam is given by $\psi = \phi$, or

$$\theta_m = \sin^{-1} \left(\frac{\phi \lambda}{2\pi d} \right) \quad (3-75)$$

The radiation pattern of the phased array is therefore

$$D(\theta) = \frac{\sin \left[\frac{\pi N d}{\lambda} (\sin \theta - \sin \theta_m) \right]}{N \sin \left[\frac{\pi d}{\lambda} (\sin \theta - \sin \theta_m) \right]} \quad (3-76)$$

The gain of a phased array antenna is a function of both the gain of the individual radiating elements and on the total number of elements used. In practice, although the antenna gain is significant, maximizing the scan volume of the antenna is usually prioritized. Therefore, using large numbers of low gain elements is preferred instead of using high gain elements but of a considerably less number (due to the increasing size). This is to prevent the antenna gain from rapidly reducing as the antenna is steered from broadside direction due to the element pattern. Most radiators used in phased arrays provide about 6 dB gain [50].

The disadvantage of the use of phase shifters is that the beam pointing direction is a function of the operating wavelength, or signal frequency, which implies a bandwidth limitation. This means that the array is compensated precisely for only a single operating frequency. In practice, a bandwidth limitation is imminent if the overall length of the array is significant as compared to a wavelength corresponding to the signal bandwidth. The limitation of a phase delay compensation can be overcome by using another method to achieve phasing of an array, known as time delay compensation. Both methods are similar in principle.

As mentioned, for a focused beam pointing at any given direction, the wave phases from the elements on arriving perpendicular to the wavefront must be equal to one another. In the case of an array using time delay compensation method to achieve focusing, the beam can be steered from one angle to another by changing the relative time delay between elements by adding a time delayer at the input of each element such that the overall time delay from each element input to the wavefront, which is given by the delay time of the time delayer plus the propagation time from element, is equal to one another. In principle, this delay can be obtained by adding a transmission line for each array element [27].

The pointing direction of the main beam produced from a phased array antenna that achieves beam steering using time delay compensation method is given by

$$\theta_m = \sin^{-1} \left(\frac{c\tau}{d} \right) \quad (3-77)$$

The beam pointing direction is now independent of frequency, and this means that the phased array is compensated over a larger bandwidth, although in practice, the bandwidth will still be limited by the performance of the antenna elements and/or RF components.

Time delay compensation method also presents several drawbacks. The limitation of the use of transmission lines is that the length of the transmission line would be different for each scan angle realized, and the lengths for each array element required would also be different in order to introduce the appropriate phase variation. This becomes a larger issue when the method is used for an array with several hundreds or thousands of elements; and the capability

to change to a different length of transmission line at each element for every scan angle desired. Although time delayers permit an array to be focused over a wide bandwidth, time delayers are bulky, heavy, and expensive. Therefore, time delayers are used only when very broad-band performance is required.

3.5.1.2 Grating Lobes

For broadside arrays, periodically occurring major lobes, also known as grating lobes, exist when the spacing between uniformly spaced elements, d_{\max} , is λ or greater. A grating lobe is any lobe other than the major lobe that occurs when the radiation from all elements add in-phase [27]. If the beam produced from an array is focused to point in a direction other than broadside, grating lobes occur when the array is widely steered from broadside and this causes the main beam to reappear in another direction. In such systems, a grating lobe tend to be produced at larger element spacing, and therefore it is critical to choose a sufficiently small separation.

For an Electronically Scanned Array (ESA), such as the one illustrated in Figure 3-12, the element spacing must be less than λ to avoid grating lobes. In particular, for arrays that are designed to continuously change the beam pointing direction, the maximum acceptable element spacing d_{\max} that would prevent the formation of grating lobes when the main lobe is pointed in directions other than broadside is given by [27]

$$d_{\max} \leq \frac{\lambda}{1 + \sin|\Delta\theta|} \quad (3-78)$$

where λ is the operating wavelength and $\Delta\theta$ is the maximum look angle, or the largest angle to be scanned away from broadside.

The designs of ESAs typically limit the scan angle of the antenna to a maximum of 60 degrees off-broadside due to the loss in effective aperture due to pointing off of broadside [27]. Hence, to fully avoid the possibility of creating part or all of a full grating lobe, the element spacings opted for is usually about less than or equal to $\lambda/2$.

3.5.2 Parabolic Reflector Antenna

The symmetrical, prime-focus-fed (center-fed) paraboloid is the most commonly used reflector for medium and high-gain, pencil-beam applications. This reflector is relatively straightforward to analyse, design and fabricate [51]. Depending on the reflector size (with respect to the operating wavelength of the radar) and reflector illumination by the feed, parabolic reflector antennas are known for producing beam patterns with very high gain and narrow principal plane

beamwidths on either principal plane while also possessing substantially low side lobe level. Such antennas are therefore commonly used for long range detection applications as it is most suitable to accommodate the low angular resolution and high gain requirements.

Typical beam patterns of parabolic reflector antennas have a high gain (30 to 35 dB is common) with relatively low sidelobe level (-20 to -30 dB) and low cross polarization, although these properties are solely dependent on the feed and reflector design. However, there are certain applications that require a reflector antenna system to produce beam patterns with either very low sidelobes (-50 dB) or very high gain (>50 dB), which are two notably desirable characteristics of reflector antenna systems that can be individually achieved through specific design techniques.

3.5.2.1 Focusing and Collimation

Reflector antennas enables a beam of parallel rays that is incident on the reflector to be brought to focus at a point, f . Similarly, placing a source of radiation at this point allows the rays emanating from the radiator to be reflected off the reflector in such a way that the reflected beams emerge as a parallel beam, which are said to be collimated, and are focused at infinity. Hence, the directions of all ray lines are reversed. It can be shown that this collimation only occurs when the shape of the reflector is a parabolic [27].

The source of radiation, which is placed at the reflector focus, used to illuminate the reflector is known as a primary radiator, or more simply as a feed, and its pattern is either called the *primary pattern* or *feed pattern*. The pattern of the entire antenna, or the beam produced from the reflector, is called the *secondary pattern*. When the term *antenna pattern* is used, the secondary pattern is meant [27]. These terms will be used frequently in the thesis.

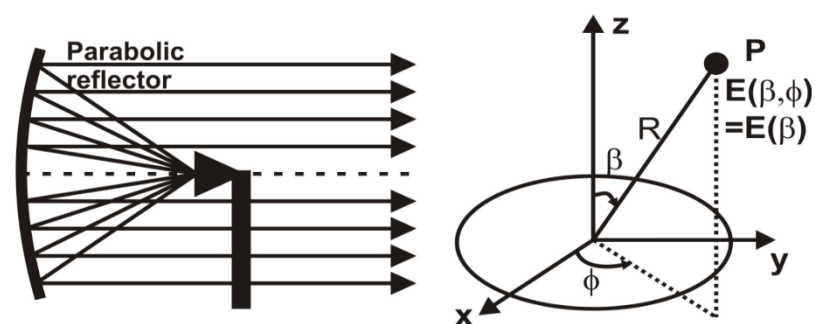


Fig 3-13. Collimation of a beam using a parabolic surface [23]

The underlying principles of the focusing action of the parabolic reflector is based on the laws of reflection. With a suitable reflector antenna design, this allows reflector antennas to

produce directional beams that exhibits very high gains and narrow beamwidths as compared to other types of antennas.

3.5.2.1.1 Focusing by a Parabolic Reflector

The geometry of a parabola can be expressed in terms of the coordinate system of Figure 3-14. The horizontal axis of the parabola, denoted by z , is the line of symmetry. This axis is also referred to as the boresight or parabolic axis. The point at which this axis intersects the parabolic curve is called the vertex, which is located at the center of the parabola. The x and y -coordinate axis (x -axis not shown) also passes through the vertex. The mouth of the parabola is called the aperture. For a circular parabola, the dimension of the aperture is the same in both principal planes, and is labelled D .

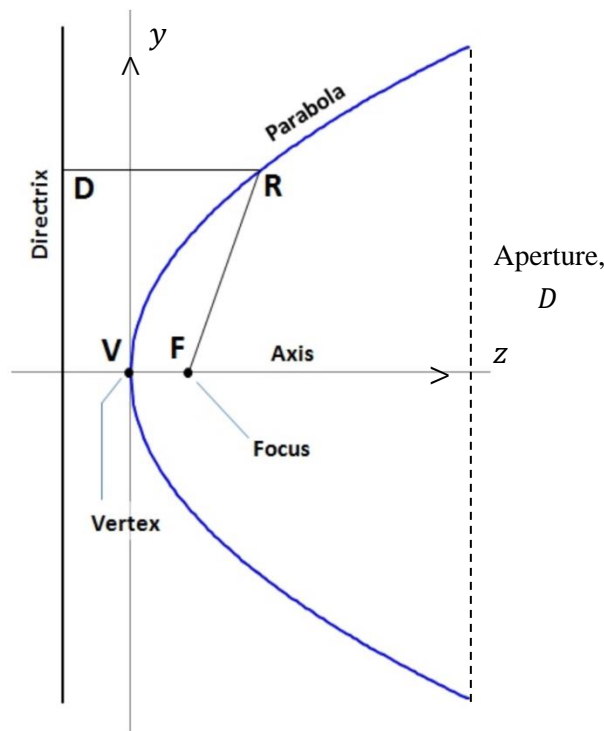


Fig 3-14. Geometry of a parabolic reflector

At a certain distance f from the vertex, that lies along the parabolic axis, is a point labelled focus. The focal point, or focus, is the point at which incoming collimated rays will converge upon reflecting the parabola, or from which the diverging rays of a point source will be collimated upon reflecting the parabola. The equation of the parabolic curve, in terms of the coordinates shown in Figure 3-14 and the parameter f is given by [27]

$$x^2 = 4fz \quad (3-79)$$

The ratio of the focal length to the aperture size, f/D , is an important characteristic of a parabolic reflector. The f/D ratio of a reflector is determined by the depth of the parabola in relation to the focal length f . As elaborated in Section 3.5.2.1.2, the f/D ratio greatly influences the properties of the beam produced from the reflector.

An analysis of the parabolic curve shows that as a ray leaves the focal point at a specific angle with respect to the parabolic axis and encounters the parabolic curve at a point A, the incident ray will be reflected in such a direction that the incident and reflected rays make equal angles with the line that is tangential to the curve at point A. This causes the direction of the reflected ray to be parallel to the parabolic axis. By the principle of reciprocity, incoming parallel rays will be reflected from the parabola in the same path so that they converge to focus at the focal point of the parabola.

The result can also be shown in another way by considering the total distance that a ray travels, which is, starting from the source (focal point) to the reflection point (A) and from the reflection point to the aperture plane. It can be shown based on simple geometric analysis that the length of this path is always equivalent to $f + z_{ap}$, for all values of the angle α . This means that the phases of all EM waves that arrives at the aperture plane are always the same and, thus, a wavefront (a surface of constant phase) is formed. The rays that are reflected from the parabolic surface are all parallel to the parabolic axis since the rays that propagates through this path are always perpendicular to the wavefront.

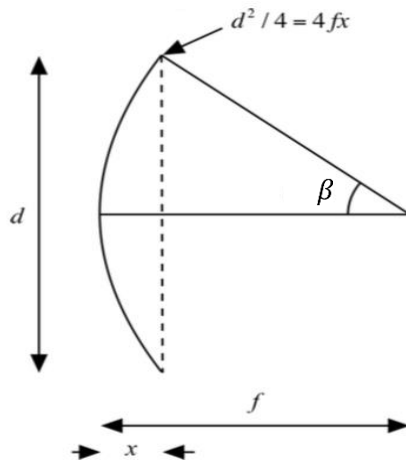
3.5.2.1.2 f/D Ratio

The ratio of the focal length, or distance between the reflector vertex and the focal point, to the diameter of a parabolic reflector is known as the f/D ratio of the reflector. The f/D ratio is a very important characteristic of the reflector as it determines the curvature, or shape, of the dish. A reflector with a small f/D ratio implies a deep dish, whereas a large f/D ratio implies a shallow dish. Assuming two separate reflector antennas employing a reflector with the same diameter but different f/D ratio, the properties of the beam produced from each antenna would have different properties and their own pros and cons. Hence, choosing a reflector design with a suitable f/D ratio is dependent on the requirements of the application in hand.

The angle subtended between the phase center of the feed and the edges of the reflector, β , varies with the f/D ratio of a reflector. Through geometric analysis of a parabolic reflector, the value of β may be expressed in terms of its f/D ratio [27] given by

$$\cot \beta = \frac{2f}{D} - \frac{1}{8(f/D)} \quad (3-80)$$

The values of β for reflectors of several shapes are presented in Table 3-1.



f/D	Total Angle Subtended (deg)
0.1	273
0.25	180
0.5	106
1	56

Table 3-1. Angle subtended by the aperture, 2β , for various f/D ratios [27]

Fig 3-15. Relationship between f/D ratio and β

As described in Section 3.5.2.3, designing a reflector antenna that produces a secondary beam pattern of desirable radiation properties heavily relies on the feed radiation pattern and the reflector curvature. The reflector curvature causes power to drop off at the reflector edges. When optimally illuminated, a circular parabolic reflector with a low f/D ratio provides a greater rejection of unwanted signals and forms lower sidelobes in the radiation pattern of the beam produced from the reflector. However, such reflectors tend to have a lower aperture efficiency as compared to a shallower dish and, therefore, antenna gain, which may be less favourable for long range detection capabilities of targets. Consequently, a reflector with a large f/D ratio is less sensitive to cross-polarization of the radiated fields as compared to a deep dish. However, the disadvantage of a shallow dish is that it increases the reaction of the reflector on the feed that causes impedance mismatch and reduces the spillover efficiency.

Moreover, the inherent taper imposed due to the redistribution of power density across the reflector aperture caused by the reflector curvature is larger for reflectors with a low f/D ratio. Thus, for deep reflectors, assuming a -10 dB illumination taper is to be applied across the reflector edges the taper imposed by the radiation pattern of the feed must be sufficiently small, and to achieve this a considerably narrow feed pattern is required. This in turn means a larger feed aperture is necessary, which corresponds to an increase in feed blockage and, thus, a reduction in antenna gain. On the other hand, for very shallow reflectors, since the inherent taper imposed is less, the tapering effect due to the radiation pattern of the feed must be sufficiently larger in order to maintain a -10 dB aperture illumination taper. Nonetheless, designing a feed that has a sufficiently wide radiation pattern with a uniform phase and low cross-polarization is also difficult to achieve. Hence, it is uncommon for reflectors to be

designed with a f/D ratio that is seldom smaller than 0.25 or larger than 0.75. In general, most reflectors tend to have a f/D ratio that is between 0.4 and 0.6 [50], from which a suitable f/D ratio is chosen based on the objectives of the application in hand.

3.5.2.2 Reflector Antenna Properties

This section describes the theoretical approximation of the antenna beamwidth and gain of a circular parabolic reflector antenna using well defined general equations. The beamwidth of the beam produced from the reflector is approximated based on the reflector diameter, shape and operating wavelength. The corresponding gain can be approximated using two methods. The first method is approximating the gain based on the principal plane beamwidths and shape of the cross-sectional area of the beam produced from the antenna. The second method is based on the physical area of the reflector, reflector aperture efficiency and operating wavelength.

3.5.2.2.1 Parabolic Reflector Antenna Beamwidth

The beamwidth of a beam produced from a reflector antenna in either principle planes can be estimated quite accurately by the following formula [27]

$$BW = \frac{57.3\lambda}{\alpha D_a} = k_1 \frac{\lambda}{D_a} \quad (3-81)$$

where λ is the operating wavelength, D_a is the aperture width or diameter of the reflector and α is a factor representing overall degradation loss effects in reflector antenna due to various causes. The value of α is 1 for an ideal uniform illumination of the parabolic reflector aperture. Generally, k_1 is approximately 70 for a circular parabolic reflector antenna and 60 for a non-circular parabolic reflector antenna. Hence, k_1 is of the order of 60 to 70 when the beamwidth (BW) is expressed in degrees.

For a parabolic reflector of non-circular aperture, D_a is the dimension, or diameter, of the reflector in the plane in which the principle plane beamwidth of the reflector antenna is to be calculated. Hence, the beamwidth of the beam produced will have different values in both planes if the height and width of the aperture is different.

3.5.2.2.2 Parabolic Reflector Antenna Gain and Directivity

Antenna gain is determined by comparing the radiation intensity of an isotrope and the actual test antenna that are both provided with the same input power. As briefly described in Section 3.2.5, the isotrope is assumed to radiate all its input power, whereas some of the power delivered to the test antenna is dissipated in ohmic resistance (i.e. converted to heat) [27]. The ratio of the power radiated by the test antenna to the total input power is known as the radiation or electrical

efficiency factor, η_r , which provides the relationship between the antenna gain G and directivity D , given by (3-33). For a lossless antenna, or an isotrope, $\eta_r = 1$. Otherwise, $0 \leq \eta_r \leq 1$ for an antenna that has dissipative losses. Hence, this factor only accounts for the losses due to the resistive or Ohmic losses within the antenna.

Nonetheless, it is common for the reflector antenna gain to be accurately approximated by its directivity since the electrical efficiency of a parabolic reflector antenna is high and often close to unity. Therefore, the radiation efficiency does not have a major effect on the parabolic reflector antenna gain and is normally ignored. Hence, in evaluating the factors that determines only the directional properties of the antenna, or antenna directivity, we will assume that the antenna gain is equal to its directivity.

The gain of a parabolic reflector antenna can be approximated using two methods. It can be approximated based on the principle plane beamwidths of the beam produced from the reflector, or, more commonly based on the effective aperture area of the reflector. Both methods of approximating the reflector antenna gain are discussed.

3.5.2.2.3 Antenna Gain Based on Principal Plane Beamwidth of Radiated Beam

The parabolic antenna gain can be calculated solely based on the principle plane beamwidth of the secondary beam produced if the beamwidths are small.

$$G = \frac{\pi^2 k_2^2}{\theta_a \theta_e} \quad (3-82)$$

where k_2 is the antenna factor whose value is dependent on whether the energy is radiated into a pyramid or a conic cross-sectional area of the beam produced [66].

If the energy of the beam produced is radiated into a pyramidal section, such as for reflector antennas using a elliptical reflector, the gain is given by

$$G = \frac{4\pi}{\theta_a \theta_e} = \frac{12.57}{\theta_a \theta_e} \quad (3-83)$$

Whereas if the energy of the beam produced is radiated into a conical section, such as reflector antennas using a circular reflector, the gain is given by

$$G = \frac{\pi^2}{\theta_a \theta_e} = \frac{9.89}{\theta_a \theta_e} \quad (3-84)$$

The common similarity of both antenna gain formulas is that they are both of the same form and that the gain is inversely proportional to the product of the beamwidths of the beam produced from the reflector [66].

3.5.2.2.4 Antenna Gain Based on the Aperture Efficiency of Reflector

At a given operating frequency, very high reflector antenna gain is commonly achieved by increasing the electrical size of the dish, or the physical collecting area of the reflector. However, for a given reflector antenna of a specified diameter or size, the antenna gain is dependent on the aperture efficiency of the reflector antenna, where if maximized the highest possible antenna gain is achieved.

The aperture efficiency of the reflector antenna ε_{ap} is the ratio of the effective aperture to physical aperture of the reflector. The relationship between the effective and physical aperture area of the reflector, denoted by A_e and A , respectively, is given by [67]

$$A_e = \varepsilon_{ap}A \quad (3-85)$$

The aperture efficiency indicates the percentage of the theoretical power incident upon the reflector that is available at the feedpoint. Depending on the shape of the aperture and the characteristics of the source of the radiation used, the aperture efficiency of a reflector antenna is typically in the range of 0.5 and 0.7 [67], or between 50% and 70%. Among other factors, which will be elaborated, the aperture efficiency is dependent mainly on the illumination profile of the feed and feed blockage effects.

The gain of a reflector antenna in terms of the effective aperture area of the reflector, A_e , and operating wavelength of the radar, λ , is given by

$$G = \frac{4\pi A_e}{\lambda^2} \quad (3-86)$$

The first factor determining the antenna gain is the physical aperture area of the antenna. For a typical circular parabolic reflector, the physical aperture of the reflecting surface is given by

$$A = \pi r^2 \quad (3-87)$$

where r is the radius of the reflector surface.

The diameter of the reflecting surface determines the physical area of the reflector. The gain of the parabolic reflector is therefore higher when the diameter is increased as this corresponds to a higher effective aperture. Hence, it is common for reflector antennas to employ very large dishes for certain applications requiring very high antenna gain, especially for systems operating at lower frequency bands (larger operating wavelengths).

The second factor that has significant effect on the reflector antenna gain is the aperture efficiency of the antenna itself. As mentioned, typical aperture efficiency of a reflector antenna

lies in between 0.5 and 0.7. For instance, an aperture efficiency of 60% would imply 60% of the radiated power illuminating the reflector is available at the feedpoint, while the remaining 40% is lost due to several factors. Hence, the gain of a reflector antenna employing a reflector of a specific size and operating at a fixed frequency is maximized by optimizing its aperture efficiency. The reflector antenna aperture efficiency consists of several individual factors of efficiencies, which is obtained by multiplying these factors together. The reflector antenna aperture efficiency is given by [67]

$$\varepsilon_{ap} = \varepsilon_r \cdot \varepsilon_t \cdot \varepsilon_s \cdot \varepsilon_m \quad (3-88)$$

- **Radiation Efficiency (ε_r):** Since metallic parabolic reflectors exhibit a very high conductivity and horn antennas, which are often used as feeds, have very little loss, this efficiency is typically close to one and often neglected.
- **Aperture Taper Efficiency (ε_t):** It is a measure of how uniform the E-field is across the reflector aperture. To realize the maximum gain of a reflector antenna the field distribution across the reflector aperture must be uniform in amplitude and phase ($\varepsilon_t = 1$). However, in practice the tapering imposed on the feed pattern and the shape of the reflector itself causes some parts of the reflector aperture to be under illuminated by the feed, which results in an aperture field that diminishes away from the main axis of the reflector and, thus, causing the antenna gain to be reduced. In practice, the highest achievable gain of the reflector antenna is generally achieved when the power illuminated at the edges of the reflector is approximately -10 dB less than that at the center.
- **Spillover Efficiency (ε_s):** Any energy that spills over the edge of the reflector surface are not being reflected and, therefore, will reduce the efficiency and the corresponding antenna gain. In the ideal case, the reflector surface needs to be illuminated optimally without any spillover of energy outside the reflector aperture. However, in practice this is not viable. This efficiency can be improved by moving the feed closer to the reflector, or by increasing the size of the reflector.
- **Various Miscellaneous Efficiency Elements (ε_m):** The term ε_m is used to denote the various miscellaneous efficiency elements that are often more difficult to determine. These include those due to surface error, cross polarization, aperture blockage, and the non-single point feed.
 - **Surface Error (Reflector surface deviation):** In order to provide the highest levels of parabolic reflector antenna gain, the surface must follow the parabolic contour as accurately as possible. Deviations from this will result in poor reflection accuracy. The tolerable surface accuracy is dependent on the requirement of the application.

- **Cross-Polarization:** As with any antenna employing linear polarization, the polarization of the transmitted and received signals must match otherwise there is a loss equal to the sine of the angle between the polarizations.
- **Aperture Blockage:** The physical structure of the feed and other elements of the antenna often mask part of the reflector. This naturally reduces the efficiency and, therefore, the antenna gain especially for reflector antennas employing a reflector with a small aperture and a relatively large feed. Significantly reducing, or eliminating, the aperture blockage caused by the feed structure, with their supporting struts, can be achieved using an offset-reflector configuration, which is described in Section 3.5.2.4.
- **Non-Single Feed Phase Center (Defocusing):** The focal point of the reflector is a single point and the parabolic dish has desirable properties relative to the focal point. However, since the feed antenna is not a point source, there will be some loss due to a non-perfect phase center for a horn antenna. The larger the radiating element with respect to the reflecting surface, the more of a problem this is and the larger impact it has on the antenna gain.

3.5.2.3 Reflector Illumination

The variation of the intensity of the feed radiation pattern across the aperture is called the aperture field distribution, whereas the radiation from the feed is called the illumination of the dish [50]. The properties of the beam produced from a reflector is significantly dependent on the total illumination taper of the reflector antenna, which is defined as the ratio of the edge illumination to the center illumination of the reflector aperture in decibels. This section discusses the factors that contributes to the total illumination taper of the antenna, and it also provides an analysis on the effect of the aperture taper on the performance of a reflector antenna.

The total illumination taper imposed on the reflector aperture is contributed by the sum of three factors, that is the tapering effect due to the geometry of the surface and curvature of the reflector that relies on the f/D ratio of the reflector (τ_1), by the properties of the feed radiation pattern (τ_2) and by the shape of the aperture outline of the reflector (τ_3) [27].

The first factor contributing to the aperture illumination taper is the natural tapering effect imposed by the reflector on the feed pattern due to the way in which the curvature of the reflector redistributes the power density across the aperture as compared to its original distribution in the primary radiation from the feed [27]. This tapering effect is also known as the inherent taper, which occurs even if the primary pattern within the solid angle subtended by the reflector has a uniform radiation intensity. This is due to the fact that the difference in distance between the center and edge of the dish from the reflector focus is larger for reflectors

with a small f/D ratio. It has been experimentally proven that the inherent taper for the parabolic reflector can be calculated based on the power density on the aperture edge, p_β , to that at the center of the reflector, p_o , which can be expressed in terms of the angle subtended from the focal point to any edge of the reflector, β , assuming that is illuminated by a feed of uniform-intensity throughout the solid angle of the feed.

As derived in [50], the ratio of the power density at an angle α to that at the center of a parabolic reflector, for a primary pattern of uniform-intensity, is given by

$$\frac{p_\alpha}{p_o} = \left(\frac{1 + \cos \alpha}{2} \right)^2 = \cos^4 \left(\frac{\alpha}{2} \right) \quad (3-89)$$

Since $\alpha = \beta$ at the aperture edges of the reflector, as shown in Figure 3-15, the inherent taper of a circular paraboloid reflector, in decibels, is given by

$$\tau_1 = 40 \log \cos \left(\frac{\beta}{2} \right) \quad (3-90)$$

The inherent taper imposed on the feed pattern due to the reflector curvature is larger for a reflector with a small f/D ratio, as deep reflectors tend to relate to larger values of β . The relationship between the amplitude taper imposed and the f/D ratio of the reflector for a primary pattern of uniform intensity is provided in Figure 3-16.

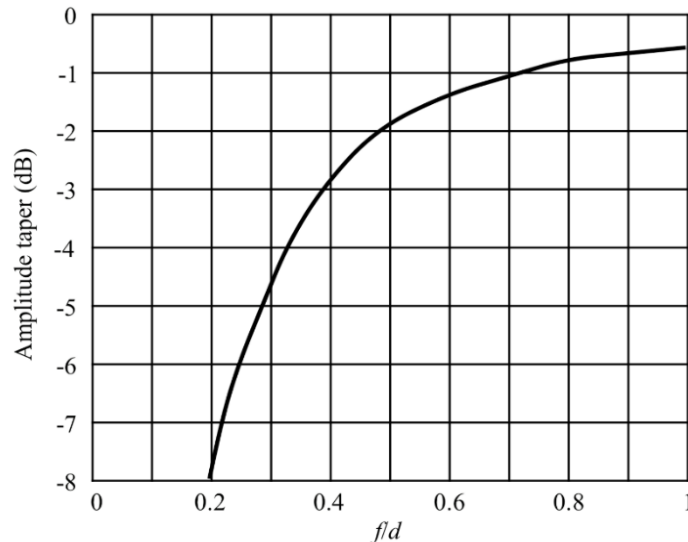


Fig 3-16. Amplitude taper vs reflector shape - primary pattern of uniform intensity [50]

The second factor contributing to the illumination taper of the reflector is the tapering effect due to the non-uniform radiation pattern of the feed. This tapering effect, expressed in decibels, is approximately given by

$$\tau_2 = -12 \left(\frac{\beta}{BW} \right)^2 \quad (3-91)$$

where BW is the beamwidth of the feed pattern.

For a given reflector with a specified f/D ratio, the beamwidth of the feed pattern used to illuminate the reflector determines the tapering imposed. Assuming several reflectors of different f/D ratios are being illuminated by the same feed pattern, (3-91) shows that the tapering imposed due to the feed pattern is also larger on reflectors with a small f/D ratio.

The final factor contributing to the total illumination taper is the tapering effect that occurs on reflectors with a non-rectangular aperture outline (i.e. hexagonal or circular aperture outline). An example would be to consider an approximately hexagonal aperture with height h_c at the center and h_e at the edge, as illustrated in Figure 3-17.

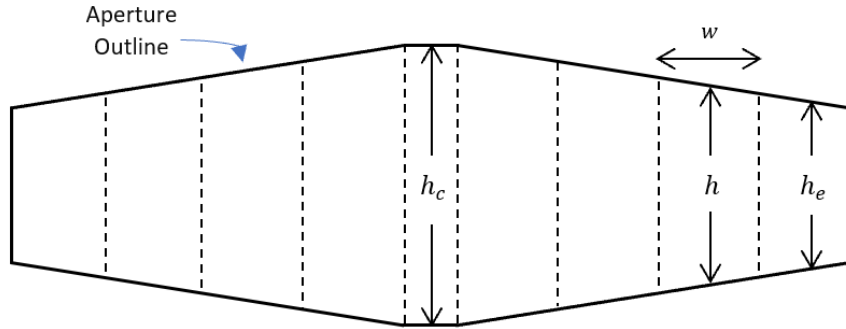


Fig 3-17. Tapering effect imposed on reflectors with a non-rectangular aperture outline

The reflector shown above is divided into several vertical strips, of width w and height h , to analyse the tapering effect due to a non-rectangular aperture outline of the reflector. Assuming the aperture illumination is uniform, the total power radiated from a given strip is proportional to its area, hw . Hence, the ratio of the power radiated from the center strip to that from the edge strip is h_c/h_e . This is equivalent to a horizontal illumination taper (in the direction perpendicular to the strips), in decibels, that is given by [50]

$$\tau_3 = -10 \log \frac{h_c}{h_e} \quad (3-92)$$

The tapering effect due to this factor can be large if, for instance, the vertical dimension of the dish is significantly larger at the center than it is at the edge of the reflector. The tapering effect due to this factor is usually very similar for aperture outlines that are different but have similar outlines, such as for circular and elliptical apertures. The taper contributed due to this factor is insignificant and often ignored for reflectors with near rectangular aperture outlines.

Table 3-2 is a result of a published study by Adams and Kelleher [68] for a reflector with an elliptical aperture, which presents the relationship between the aperture illumination taper imposed on the horizontal plane of the reflector, due to τ_1 and τ_2 , and the corresponding sidelobe level of the of the beam produced by the reflector antenna.

Aperture Illumination Taper (dB)	Sidelobe Level (dB)
-6	-20
-11	-25
-14.5	-30
-17.5	-35

Table 3-2. Relationship between tapering and formation of sidelobes [68]

Since the amount of tapering applied approximates the sidelobe level of the beam produced by the antenna, the illumination taper required to achieve a certain sidelobe level can be identified. Hence, it is common for the feed and reflector to be designed in an accurate and systematic manner that allows the appropriate aperture illumination taper required to be imposed, especially in cases where it is critical for a reflector antenna system to produce a beam pattern that fulfils the low side lobe level requirement of the application in hand.

Designing a reflector antenna with an excessive amount of taper causes a loss of gain and widening of the radiated beam due to inefficient use of the reflector aperture, but achieves very low sidelobe levels. This would result in a larger-than-necessary value of k_1 and a smaller-than-necessary value of ε_{ap} in (3-81) and (3-85), respectively. On the other hand, too little taper would also result in a loss of gain due to excessive amount of radiation from the feed that falls outside the reflector edges, or defined as the term “spillover”, which causes the formation of larger-than-necessary side lobes and back lobes but achieves a narrower beamwidth. When the nature of typical patterns is considered, it is evident that a persistent trade-off exists between achieving maximum antenna gain and minimum sidelobe level of the beam produced from the reflector, and therefore both desirable characteristics cannot be achieved simultaneously.

A suitable amount of illumination taper to be employed in a given case depends on the relative importance of achieving maximum gain and reducing side lobes and back lobes to the minimum practical level. Thus, for a given reflector, it is inevitable that the properties of the corresponding beam pattern produced by the reflector antenna is largely determined by the aperture illumination taper applied, which also affects the aperture efficiency. Nonetheless,

conventional reflector antenna designs are known to produce beam patterns with considerably low sidelobes (< -20 dB) and high gain (> 30 dB).

3.5.2.4 Offset Parabolic Reflector Antenna

As mentioned in Section 3.5.2.2.4, the issue with employing conventional center-fed parabolic reflector antenna for 2D surveillance radars is that some of the reflected radiation from the reflector is blocked by the feed. The effect of aperture blockage by a feed, with their supporting struts, is considerable especially when the size of the feed is considerably large relative to the size of the reflector, such as in 2D surveillance radar systems. The amount of aperture blockage is further increased due to the feed support that holds the feed in place, which is most severe for reflector antennas that requires the direction of the beam produced to be steerable in any direction, or over a large range of angles, as this means that the feed support must be directly attached to the edges of the reflector by a rigid structure, rather than to the base of the radar, as is the case in stationary reflector antenna systems.

Depending on the reflector antenna design, the feed and, to some extent, the feed support causes the beam pattern produced from the reflector to be adversely affected in two ways. The principal reasons for the undesirable effects of feed blockage is that it leads to scattered radiation due to some power being reflected into directions other than the forward direction, which contributes to a lower aperture efficiency of the antenna and, thus, results in a reduction of antenna gain on one hand and a general degradation in the suppression of sidelobe and cross-polarised radiation on the other [51]. If the feed is a horn antenna, a portion of the radiation of the secondary beam that is blocked by the feed will be reabsorbed, as it enters the horn aperture, and propagate back down the guide. This in effect may cause a reflection mismatch and, thus, the standing wave ratio would deteriorate on the line to the antenna, even though the horn radiating into empty space would properly match the guide. This effect can, however, be compensated for by impedance-matching devices in the expense of reducing the bandwidth or range resolution of the antenna [27].

The aperture blockage caused by the feed and/or feed support can be eliminated by using an offset-reflector configuration, in which the feed horn is placed at the focus of the parabolic reflector but the direction of the primary beam is inclined at a certain angle to illuminate only a small section of the reflector, while the remainder of the lower half of the reflector is redundant and therefore removed [50]. As illustrated in Figure 3-18, alike a center-fed parabolic reflector, collimated light that is incident on an offset dish is focused to the focal point of the reflector. However, it can be observed that the position of an offset feed is generally closer to one edge of the dish than the other within the vertical plane. This infers the bottom

edge, or rim, of the reflector to be illuminated with a higher radiation intensity than the top rim as the former is closer to the position of the feed. Nonetheless, experimental results in [51] have shown that small variations in the direction of the primary beam have minimal effect on the antenna performance, and thus, illuminating towards the center of the offset reflector is the most ideal approximation and design choice.

The angular displacement applied on the horn antenna is dependent on the size of the feed, such that a larger inclination is generally required for a large feed in order to significantly reduce or prevent the feed structure out from obstructing the beam path. Most common offset-fed reflectors are usually illuminated by a feed that is rotated along the phase center, or reflector focus, by 15° to 20° . Hence, in an offset feed arrangement it is possible to minimize, if not prevent, any pattern deterioration due to aperture blocking (i.e. achieve a higher aperture efficiency). The section of the parabolic reflector used is shown by the solid curve, while the full symmetrical parabolic section is shown dotted.

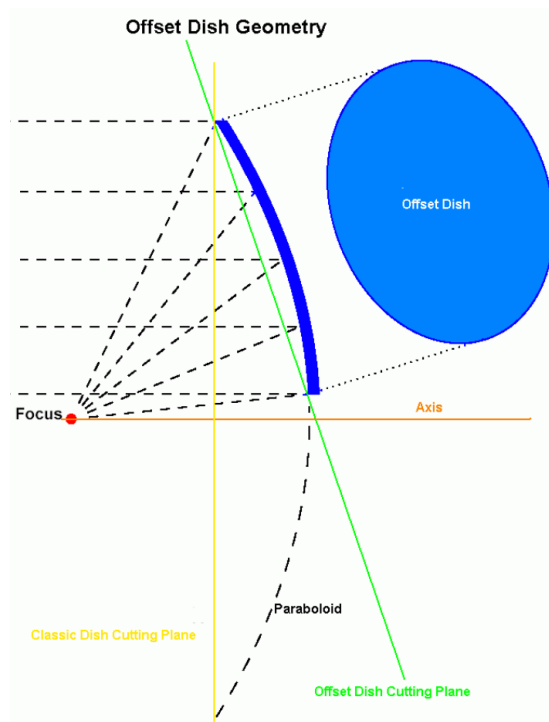


Fig 3-18. Offset Parabola Geometry [69]

Since the offset-parabolic reflector is a somewhat more complicated structure to deal with both structurally and analytically [51], it will be as well to briefly review its principal advantages and disadvantages as an antenna and as compared to the more conventional center-fed reflector antenna. This is also summarized in Table 3-3. As already mentioned, a very significant and clear advantage of the offset-reflector antenna over its axisymmetric

counterparts is that the former system may considerably reduce aperture-blocking effects [51] and, therefore, be capable of achieving a higher aperture efficiency (i.e. antenna gain), as compared to a full parabolic dish with the same dimensions. The design of an offset-reflector antenna also ensures that the high transmit power of the feed is not reflected directly back to itself [27] and therefore, the reaction of the reflector upon the feed is reduced to a very low order. The excellent isolation between reflector and primary-feed implies that the primary-feed VSWR is essentially independent of the reflector, and when multiple-element or dual-polarised primary-feeds are to be employed, the mutual coupling occurring between feed elements via the reflector can be reduced to an insignificant level [51].

The offset-reflector configuration also has its disadvantages. A major drawback of such systems as compared to its axisymmetric counterpart is the asymmetrical structure of the offset reflector, that is, it is significantly more complicated and, therefore, more difficult to fabricate the dish and correctly position the feed with the appropriate feed rotation along the focus to ensure that a collimated secondary beam is produced. Moreover, although this feed arrangement avoids aperture blockage, it somewhat complicates the feed design in providing the desired primary pattern required [27]. Due to the higher complexity of the offset-reflector configuration, it is evident that the offset geometry is more difficult to deal with and generally more expensive to implement as compared to conventional parabolic dishes [51]. For these reasons its use is generally restricted to applications where electrical performance specifications is critical (i.e. for applications involving terrestrial microwave communications). When illuminated by a conventional linearly polarised primary-feed, the elimination of one of the planes of symmetry by the offset feeding technique destroys the symmetry of the cross-polarization components of the aperture field, generating a cross-polarised component in the antenna radiation field that results in cross-polarization (i.e. the presence of an orthogonal component of polarization in the radiated field) [50]. When circular polarisation is employed the reflector does not depolarise the radiated field, however, the antenna beam is squinted from the electrical boresight. For small offset reflectors this squinting effect has also been observed with linear polarisation [51].

Advantages	Disadvantages
<p>Reduce aperture blocking effects and, therefore, increases antenna gain and reduces sidelobe level of the antenna pattern.</p> <p>The high transmit power of the feed is not directly reflected back and, therefore, the reaction of the reflector upon the feed is reduced to a very low order.</p> <p>The excellent isolation between reflector and primary-feed implies that the primary-feed VSWR is essentially independent of the reflector.</p>	<p>Significantly more complicated and, therefore, more difficult to fabricate the dish and correctly position the feed with the appropriate feed rotation along the focus.</p> <p>The desired radiation pattern of the feed is often difficult to achieve.</p> <p>Offset geometry is more difficult to deal with and generally more expensive to implement.</p> <p>Destroys the symmetry of the cross-polarization components of the aperture field.</p> <p>Only effective for antennas employing a reflector with a small aperture or a relatively large feed.</p>

Table 3-3. Pros and cons of offset-reflector antenna [25]

Although we have shown that implementing an offset reflector design can increase the aperture efficiency of a reflector antenna, this type of reflector design is only likely to make a realizable improvement in antenna performance for reflector antennas employing small parabolic reflectors and/or large feed systems that would otherwise block a significant portion of the transmit and receive signal, where it is likely to minimize or eliminate blocking effects and, therefore, provide a higher antenna gain than a center-fed reflector antenna employing a reflector of the same aperture size. Hence, employing an offset reflector in smaller reflector antenna systems is a very popular choice. However, for 2D surveillance radars employing a truncated reflector that is significantly wider (~20 to 30 times) than the size, or width, of the feed blocking the aperture plane, the difference in antenna performance realized between an offset reflector design and a conventional reflector antenna is very minimal (i.e. ~0.3 dB improvement with offset-reflector antennas) since the feed blockage is insignificant as compared to the size of the reflector. In such systems, such as the 1.2 meter wide vertically truncated reflector designed in this project (Section 4.4.2) that is illuminated using a E-plane sectoral horn feed (i.e. imposing an aperture blockage of only 25.4 mm for one feed), the effect of aperture blockage on the aperture efficiency of the antenna is insignificant and will often be ignored, and the benefits of an offset-reflector antenna are usually not considered to be worth the extra complexity and higher cost of implementation.

3.6 Monopulse Processing and Circuitry of 2D Monopulse Systems

The principles of monopulse reflector antenna systems employing phase or amplitude-comparison monopulse techniques were extensively described in Chapter 2. This section

focuses on discussing the monopulse processing methods used in modern monopulse radar systems for forming the sum and difference patterns and the subsequent RF circuits used to form a sum signal and a normalized difference signal in a one-coordinate monopulse system, since a 2D monopulse antenna is of interest in this project. The most common passive RF devices used for monopulse processing and the RF circuitry of the sum and difference channels in a one-coordinate monopulse system are discussed in Section 3.6.1 and 3.6.2, respectively.

3.6.1 Devices for Forming Sum and Difference Signal

The received echo signal at each feed horn could be directly connected to individual receivers for frequency conversion, filtering, and amplification before amplitude or phase measurements could be made followed by monopulse processing (adding and subtracting the received signals accordingly) in RF or using digital networks to create the sum and difference signals in both principal planes. However, in practice, even if the receivers were adjusted initially for equal gain and phase, the receivers would likely vary unequally as a function of time, signal level, radio frequency, and environmental conditions. In such cases, the result would be large mismatches or drifts in the gains or phase shifts of the individual receiver channels, which would cause significant errors in the boresight axis and in the measurement accuracy of off-axis target angles [38].

The usual method in both amplitude and phase comparison monopulse, therefore, is to form the sum and difference signals, or rather linear combination of the feed outputs, at RF using stable passive microwave devices, before any active devices acted on the signals [38]. These devices used for monopulse processing, to create the sum and difference signals, usually have two input ports and two output ports (four-port devices). The voltage signal obtained from each output port is a linear combination of the two input voltages, that is, usually the addition and subtraction of the two inputs. Two major categories of such devices are hybrid junctions and directional couplers, with the former being the more commonly used device in a one-coordinate monopulse antenna (2D radar) [38].

In a 3D amplitude monopulse radar employing a reflector antenna, for instance, several hybrids in tandem and in parallel are required to produce a sum and two difference signals (one for each coordinate). The assemblage of hybrids that converts the signal from the output of the individual feed into a single sum and two difference signals is better known as a comparator [38]. The comparator has much less drift than the active circuits of receivers due to it being electrically and mechanically more compact and rigid, which makes the null axis, or point of intersection of the beams, to remain much more stable in the boresight direction than if the differencing were done after the receivers [38]. Moreover, the comparator is generally placed

as close as possible to the feed horns in a single and compact assembly in order to minimize variations or distortions due to long transmission lines. For an off-axis target, the sum and difference signals produced from the comparator are connected to the receivers within the sum and appropriate difference channels, respectively, where it is converted into a dc error voltage. The error voltage created from both difference channels are proportional to the target deviation from the tracking axis in both planes, which is used to steer the direction of the beams towards the position of the target in both coordinates so that the tracking axis will always be kept aligned to the position of the target. Since a one-coordinate monopulse antenna system will be designed in this project, the principal forms of a hybrid junction that is used in such systems will be described and illustrated. Hence, this section will solely focus on hybrid junctions only since a one-coordinate monopulse antenna will be designed and manufactured.

3.6.1.1 Hybrid Junction

In a one-coordinate monopulse system, a hybrid junction is responsible for simultaneously producing a sum signal and a difference signal in one plane through the coherent addition and subtraction of the output signals of both antennas. This section describes the principles of a common type of hybrid junction, that is, a π -hybrid. Figure 3-19 illustrates a π -hybrid, where only two inputs are required to produce a sum and difference signal in a single plane.

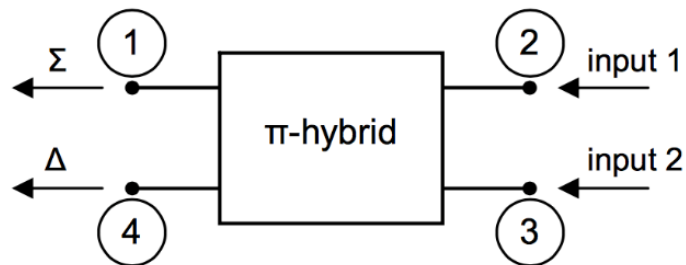


Fig 3-19. Symbol of the π -hybrid [33]

The inputs to the π -hybrid, input 1 and 2, are the outputs from the two feed horn antennas that are connected to ports 2 and 3 by a pair of phased match cables. The diode detectors of the scalar network analyzer are connected to the sum and difference outputs of the hybrid (ports 1 and 4) that contain the sum and difference voltage signal, respectively, whereas the other end of the network analyzer is connected to the respective inputs of the sum and difference channel [33]. Theoretically, the behaviour of this device is not frequency sensitive; therefore, it can work over a wide frequency band.

If v_1 and v_2 are the input voltages at ports 2 and 3, the output voltages at ports 1 and 4, v_3 and v_4 , are given by

$$v_3 = \frac{1}{\sqrt{2}}(v_1 + v_2) \quad (3-93)$$

and

$$v_4 = \frac{1}{\sqrt{2}}(v_1 - v_2) \quad (3-94)$$

The equations for v_3 and v_4 may have to be interchanged, depending on the polarity convention of the inputs, but in either case one output is proportional to the sum and the other to the difference [38]. The reason for the factor $1/\sqrt{2}$ is that the total power out must equal the total power in, that is, ignoring a small loss in the device.

The π -hybrid is also often called a Σ - Δ hybrid when used for adding and subtracting two signals. Its symbol, with port numbering, is shown in Figure 3-19. Following the convention of port numbering, the π -hybrid is described by its scattering matrix [70]:

$$[S] = \frac{1}{\sqrt{2}} \begin{bmatrix} 0 & 1 & 1 & 0 \\ 1 & 0 & 0 & -1 \\ 1 & 0 & 0 & 1 \\ 0 & -1 & 1 & 0 \end{bmatrix}$$

This matrix can be obtained by various technical realizations like magic-T or ring hybrid [30] [70]. The overall cost and complexity of a π -hybrid can be reduced by manufacturing it in the form of ring hybrid in microstrip technology.

3.6.1.2 Digital Signal Processing

An alternative approach of obtaining the sum and difference patterns of a monopulse antenna is to process the feed output signals of each feed horn directly using digital networks, or signal processing, without using any passive RF devices. This method of monopulse processing can be useful and convenient when obtaining, or performing, antenna measurements of the monopulse patterns, that is, the sum and difference voltage patterns, from only a single antenna rotation (for a mechanically scanning radar) under ideal conditions. For instance, upon designing or calibration of a monopulse antenna, the operator could seek to obtain the radiation patterns of the monopulse antenna from only a single measurement.

With this processing method, the measured output voltage signal (in amplitude and phase) from each feed horn is added and subtracted accordingly to obtain the sum and difference patterns. The sum and difference patterns, in terms of gain in decibels (dBi) and relative to power, is given by

$$\text{Sum gain} = 20 \log \left(\sqrt{(AM1 + AM2)^2 + (PH1 + PH2)^2} \right) \quad (3-95)$$

$$\text{Difference gain} = 20 \log \left(\sqrt{(AM1 - AM2)^2 + (PH1 - PH2)^2} \right) \quad (3-96)$$

where $AM1$ and $AM2$ is the amplitude and $PH1$ and $PH2$ is the phase of the received signal from the left horn (Horn 1) and right horn (Horn 2), respectively. In this case, the measurements were recorded for the combined measurements in voltage real and imaginary pairs. Hence, (3-95) and (3-96) are used to obtain the measurements in terms of power in a dBi scale.

However, during practical operation of the radar, it would be computationally intensive to sample the output signals of the pair of feed horns and then perform the sum and differencing to obtain the monopulse patterns. Hence, in practice, the use of passive RF devices for direct monopulse processing is the most ideal and preferred method as it is a much more efficient and simpler approach.

3.6.2 Sum and Difference Channel of a One-coordinate System

A one-dimensional monopulse radar system uses one sum channel to transmit and receive radar signals and one difference channel that is only used during reception. In transmission, only the sum channel transmits a signal that is used to detect the presence of a target. In reception, the sum and difference channels are used to accommodate the sum and difference signal, respectively, from which, Channel 1 is fed with the sum of the two horn antenna signal returns and Channel 2 is fed with the difference of the signal received by the two horn antennas. In a one-dimensional monopulse system, the difference channel is usually dedicated to providing angle error information related to a target in the horizontal plane based on the signal strength at the feed output. With this implementation, presented by a simple illustration in Figure 3-20 the target range and angular position relative to the tracking axis are provided simultaneously based on the sum and difference signals obtained.

Although the formation of sum and difference signals before the receivers greatly reduces boresight shift, the mismatch or drifts in the receiver of both channels will still cause errors on off-axis angle measurements. Hence, for a one-dimensional monopulse system to accurately transmit on the sum channel (Channel 1) and receive on both the sum and difference channels (Channels 1 and 2) simultaneously, the RF circuitry of the monopulse system must be equipped with two well isolated channels that is equal in both gain and phase of the receivers to ensure that constant tracking-loop gain or accurate off-axis target measurements is achieved and maintained, in order to provide target information that is of a high degree of accuracy.

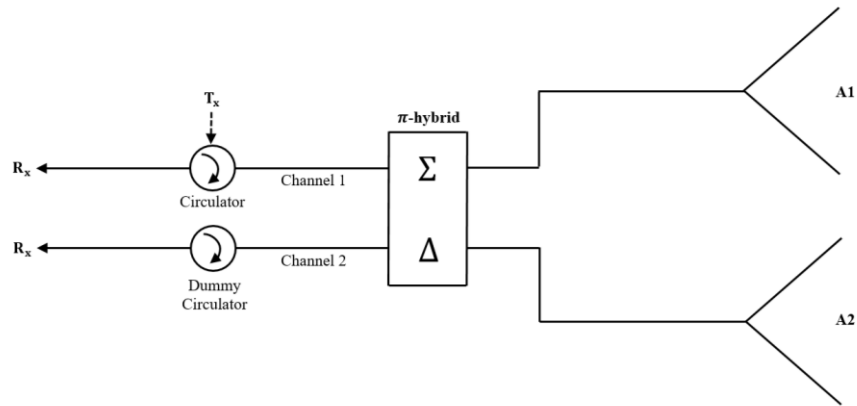


Fig 3-20. Two-channel monopulse system

For the sum channel to transmit and receive radar signals simultaneously, the transmitter and receiver within this channel must be isolated to prevent any transmit signal from leaking into the receiver when the channel is in transmit mode. The isolation between the transmitter and receiver is achieved by connecting a T/R switch (circulator) between them. Consequently, no transmit signal is coupled into the difference channel since this channel is dedicated to receiving the error signal of a target in either principle planes. For that reason, coupling a transmitter within the difference channel it is not required and therefore, in theory, a circulator is not required to provide isolation here. However, a T/R switch is frequently included as a dummy circulator to ensure that both sum and difference channels are perfectly matched to one another with an equal phase relationship, which, as mentioned above, is critical in achieving a very high performance. The T/R switch in the difference channel is denoted by a ‘Matched Load’, as shown in Figure 3-20.

3.7 Summary

This chapter has provided a theoretical grounding for radar and other antenna systems. It has summarized the key properties of antennas and the design principles of several types of electronic and mechanical scanning antennas that are commonly used in a surveillance radar, which have shown to provide significant knowledge on the modelling of the different types of antenna in this project. Finally, this chapter has outlined the common monopulse processing methods used in modern monopulse radar systems for forming the monopulse patterns and the RF circuitry of a one-coordinate monopulse radar system. The material presented in the subsequent chapters rely heavily on understanding of the antenna characteristics and principles provided in this chapter.

Chapter 4

Modelling and Simulation of Reflector Antenna System

This chapter consists of five sub-sections. Section 4.1 evaluates several significant radar parameters suitable for a coastal surveillance radar. The options available for each radar parameter are evaluated before the most suitable choice for each parameter is justified. The remaining of the chapter focuses on the design of the center-fed reflector antenna system. All the modelling and corresponding simulations of the antenna performance provided in this project were performed on a CEM tool called CST MICROWAVE® STUDIO (CST MWS). CST MWS is a powerful tool for the 3D electromagnetic simulation of high frequency components. It provides accurate and efficient 3D electromagnetic EDA computational solutions for the numerical solution to Maxwell's Equations which are used to calculate the field strengths, surface currents and coupling between the modelled antennas, for applications at frequencies ranging from statics up to optics, and from the nanoscale to the electrically very large structures [71].

Section 4.2 presents the modelling of a WR90 adapter, or rather an optimization of the length of the transition probe extending into the adapter, that achieves optimum RF performance at the chosen operating frequency of the radar system (9.2 GHz). In Section 4.3, the rectangular aperture of the adapter is extended to produce a E-plane sectoral horn antenna that will be used as the feed of the reflector antenna. The dimensions of the horn antenna are chosen based on the optimal relationship between the horn apex length and the vertical dimension of the antenna aperture, as described in Section 3.4.1, to produce a E-plane sectoral horn that achieves maximum directivity at a specified operating frequency.

Following the design of the E-plane sectoral horn antenna in Section 4.3, Section 4.4 has outlined the design of a vertically truncated reflector according to the radiation properties of the feed horn. The objective of the reflector design is to produce a reflector antenna that

prioritizes gain over the sidelobe levels of the radiated beam. The modelling of the reflector shown achieves this by identifying the optimum illumination taper to be applied across the reflector aperture as it is illuminated by the known radiation pattern of the feed.

Section 4.5 provides a comparison between the simulated radiation properties of the reflector antenna design obtained in Section 4.4 and its calculated theoretical counterpart. An analysis on both sets of results would serve as a cross-validation of one another, and also provide the expected radiation properties of the beam produced from the physical reflector antenna.

4.1 Radar Parameters

This section discusses several significant radar parameters and how it determines the performance of the radar. The parameters discussed are the chosen radar waveform, frequency band, bandwidth, principal plane beamwidths, transmit power, polarization and sweep time (modulation period).

The chosen parameters of the coastal surveillance radar that will be implemented along the coast of the Strait of Malacca are summarized in Table 4-1. The reasoning for the chosen properties of the radar corresponding to each of the parameter mentioned above are briefly discussed in this section.

Radar Parameters	
Radar Waveform	FMCW
Frequency Band	X-Band (9.2 GHz)
Bandwidth	60 MHz
Principal Plane BW	1 by 6 - 8 deg
Transmit Power	2 W
Polarization	Vertical
Sweep Time	2.5 ms

Table 4-1. Summary of radar parameters

- **Radar Waveform: Frequency Modulated Continuous Wave**

Frequency Modulated Continuous Wave (FMCW) radar is an ideal and popular choice for coastal surveillance radar applications due its low power requirement and high range resolution

capabilities. FMCW radar systems transmits a continuous wave signal that is frequency modulated over a certain bandwidth. The system uses a broad band of frequency to interrogate a target. The bandwidth of this signal determines the range resolution, whereby a larger bandwidth corresponds to a higher range resolution. This type of radar compares changes in frequency between the transmitted and received signals to calculate the range of a target, instead of the conventional pulsed radar system of timing the interval between outgoing and returning signals [72]. The illustration comparing the differences in FMCW radars with conventional pulsed radar is shown in Figure 4-1.

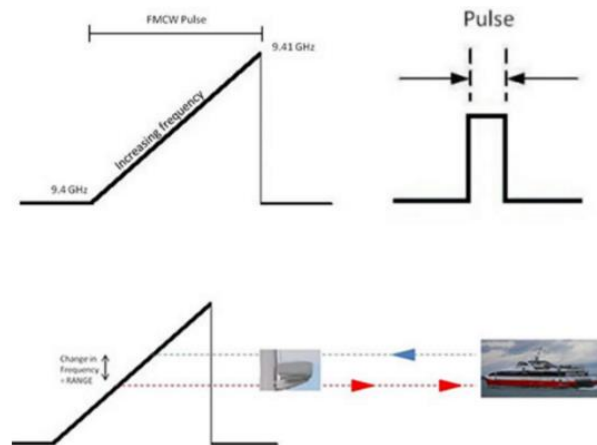


Fig 4-1. FMCW waveform [72]

At low power, FMCW radar sends out a long pulse that typically last for about a few milliseconds. Conventional pulsed radar, on the other hand, sends out a very short pulse but at very high power. The longer FMCW pulse increases its frequency at a constant chirp rate and the range of the target is identified by obtaining the difference between the frequencies of the returning signal and the transmit signal at that instant. This frequency difference, which is proportional to the range of a target, is known as the beat frequency. Figure 4-2 provides a simple block diagram of the RF circuitry of a FMCW radar that generates a beat signal.

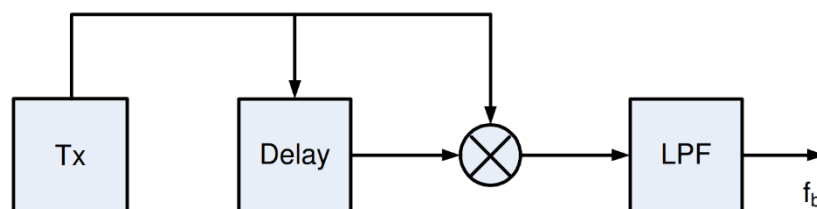


Fig 4-2. Beat signal generation [73]

When a transmit signal is radiated it propagates through the medium and hits the target, from which the target reflects a fraction of the pulse back to the radar receiver at the same frequency at which it was sent, while the transmitting frequency have increased steadily. The received signal is an attenuated version of the transmit signal that is delayed by a time t_o [73]. The received signal in the time domain can be expressed as

$$S_{Rx}(t) = \cos(2\pi f_o(t - t_o) + \pi k(t - t_o)^2) \quad (4-1)$$

The received radar signal is mixed (multiplied) with a sample of the transmit signal in the receiver. This multiplication gives the sum and difference terms. The difference between the frequency of the current transmitting and received signals is called the beat frequency and is proportional to the range between the antenna and the target. Since the required information is contained in the difference term, the output signal from the mixer is fed to a low-pass filter to filter out the higher order terms [73]. The difference term, which is known as the beat signal, is given by

$$S_{Beat}(t) = \cos(2\pi f_o t_o + 2\pi k t_o t - \pi k t_o^2) \quad (4-2)$$

The frequency of the beat signal can be obtained by differentiating the phase of the signal, and it is given by

$$f_{Beat} = \frac{1}{2\pi} \frac{d\phi}{dt} = k t_o = \frac{BW}{T} t_o \quad (4-3)$$

where k is the chirp rate of the transmit signal and the delay t_o is the two-way travel time that can be mapped to range of the target using the equation

$$t_o = \frac{2R\sqrt{\epsilon_r}}{c} \quad (4-4)$$

By taking the FFT of the time-domain beat signal, a peak at the beat frequency is observed in the spectrum. This frequency can be transformed to the range of the target using (4-3) and (4-4) [73].

Due to the low power pulse used the low power output from FMCW radar allows it to receive and transmit simultaneously, which makes it highly responsive to receiving radar signals that constantly changes in frequency. Conventional pulsed radar, on the other hand, uses an input power that is significantly larger than that of a FMCW radar, and therefore must constantly switch between transmit and receive.

FMCW radar is a major break though in marine radar. It has many notable advantages over pulsed radar systems and only a few disadvantages, which are mainly due to cost and the

lower peak power of the transmit signal and, therefore, the received signal. The advantages and disadvantages are summarized in Table 4-2.

Advantages	Disadvantages
No warm up - instant on	Lower operating range
No minimum detection range	More expensive and computing power
Quick measurement update	Susceptible to interference from nearby radio systems
Good sensitivity and stability	Not suitable for fast-moving targets
Low power consumption	
Better safety	

Table 4-2. Properties of FMCW radar

- **Frequency Band: X-Band (9.2 GHz)**

Radar systems that require fine target detection capabilities and yet cannot tolerate the atmospheric attenuation of higher-frequency bands are typically X-band. Since the small size and light-weight antenna provides good performance, the X- and Ku-bands are relatively popular radar frequency bands that are suitable for long range operation and are often used for military applications such as surveillance and airborne radars, which are applications that involves situations where space and weight is of limited resource. This frequency band is also widely used in maritime civil and military navigational radars [74]. Moreover, in the X-band frequency range (8.2 – 12.4 GHz) the relationship between the operating wavelength and antenna size is considerably better than in lower-frequency bands, which allows for electrically large antenna systems to be manufactured with desirable antenna radiation properties.

The operating frequency allocated by the Indonesian government for marine and coastal surveillance radars is between 9.2 and 9.4 GHz. Hence, the chosen operating frequency of the radar is 9.2 GHz, which is equivalent to an operating wavelength of 3.26 cm.

- **Bandwidth: 60 MHz (> 50 MHz)**

As mentioned in Section 3.2.7, the bandwidth of a radar system is highly associated with the range resolution performance of the radar. The receiver bandwidth used is, therefore, greatly influenced by the range resolution requirement of the system, which can easily be one to several meters. Moreover, due to pulse compression in FMCW radar systems, the maximum non-ambiguous range, or maximum detection range, is dependent on the duration of the transmitted pulse, or sweep time, and the power of the transmit signal, and is independent on the bandwidth since the inverse relationship between the bandwidth and duration of transmitted pulse does not

exist. Hence, unlike conventional pulsed radars, employing a rather large bandwidth is acceptable since the duration of the transmitted pulse is not reduced.

For the application in hand, the radar requires the detection of targets ranging from 20 to 200 meters in length and usually 3 to 10 meters wide. These targets are generally vessels of various types. To increase the signal to clutter ratio (SCR) a range resolution equivalent to the size of the ship may be selected so that the entire ship's return lies within a single range bin. Based on the types of target mentioned, a suitable range resolution required would be within a range of several meters that is comparable to the width of the target size. Using (3-35), the radar bandwidth required to achieve a range resolution of at least 3 meters is 50 MHz. Therefore, a suitable operating bandwidth of the radar would be in excess of 50 MHz. The legal licensable bandwidth available within the frequency spectrum (X-band) in Indonesia is limited to 60 MHz, and this could be the optimum choice.

- **Azimuth and Elevation Beamwidth: 1 and 6 - 8 degrees**

The surveillance radar is designed mainly for the detection of medium to large sized ships along the Strait of Malacca that ranges from tens of meters to a few hundred meters long. The chosen maximum detection range of the radar is 20 km, or distances approximately half the minimum width of the strait (40 km). Generally, operators are concerned with the detection of smaller sized vessels that travels close to the shoreline, and much larger vessels that travels in the center of the strait.

At the maximum detection range capability of the radar, the azimuth beamwidth of the radar required to successfully distinguish two large sized vessels (i.e. 300 meter tanker) of the same or similar size located at the same distance but at different bearing must not be larger than approximately 1 degree, as calculated using (2-1). The diameter of the circular parabolic reflector required to produce a beam that achieves this beamwidth must at least be 2.4 meters wide (3-81), which is a rather large dish. Nonetheless, as shown in Section 4.4, the reflector antenna designed in this project will utilize a reflector that is 1.2 meter-wide to produce a secondary beam of approximately 2 degrees beamwidth. The targetted angular resolution of the antenna, which is achieved with a beam that is 1 degree wide, will be achieved through the implementation of angle measuring and signal processing techniques instead of increasing the reflector size. In this way, the objective of using a compact reflector antenna while achieving a high resolution performance can be fulfilled.

The elevation beamwidth of a radiated beam is primarily dependent on whether the radar is required to provide surveillance and tracking of flying objects. Similar to the azimuth beamwidth, a narrow elevation beamwidth is essential to provide surveillance and tracking of

flying objects. Applications that requires a pencil beam (i.e. very narrow principal plane beamwidths) are mainly for air surveillance monitoring, which are provided by 3D radars capable of accurate positioning and tracking of flying targets.

The objective of the radar is to provide surveillance and tracking of targets on the surface of the ocean (horizontal plane). Since the application does not require beam scanning in the vertical plane, unlike the azimuth beamwidth of the radiated beam, the elevation beamwidth is significantly less critical. In fact, a rather broad elevation beamwidth is required to provide elevation monitoring capability, that is, providing sufficiently wide-angle coverage of the sea from the coastline, or at the minimum far field range of radar, extending until the maximum operating range of the radar without having to rotate or displace the antenna vertically. Given that the mechanical scanning radar is remotely operated from a stationary high ground, a suitable elevation beamwidth of the radiated beam would be between 6 to 8 degrees. If the radar is mounted on-board the top deck of the ship, the elevation beamwidth must also be wide enough, that is, comparable to the maximum roll angle of the ship in order to overcome the ships naturally occurring pitch and roll. Otherwise, at times during the scan only some part of the beam will remain directed at the horizon and this presents the risk of leaving targets that are not within the area covered by the radiated beam to be undetected. However, this can be partly overcome through methods of stabilizing the beam, such as using a stabilizer.

For a reflector that is expected to radiate a beam with a principal plane beamwidth of 2 degrees by 6 to 8 degrees, the reflector height to width ratio would approximately be 1:4. This is a common ratio observed in many vertically truncated reflectors employed in surveillance radar using reflector antennas.

- **Transmit Power: ~ 2 W**

The transmit power is a variable radar dependent parameter selected to ensure that sufficient amount of power is received at the radar receiver when a radar, with known radar and target parameters and a specified SNR threshold, is used to operate at the required maximum detected range. The required peak transmit power of the radar transmitter, P_t , can be calculated using (3-7), or rearranged to be in terms of P_t as

$$P_t = \frac{P_r(4\pi)^3 R^4}{G^2 \lambda^2 \sigma} \quad (4-5)$$

Assuming a monostatic radar operating at a specified frequency has an antenna gain of G , and the target of interest has a known RCS of σ , the maximum detectable range of a radar system R is largely dependent on the transmit power of the radar system. Hence, a high peak

transmit power is generally desirable to achieve a further maximum detection range, when it is required. However, if the radar is used for continuous transmission and reception of signals, such as in a FMCW radar, the transmit power must be sufficiently small to prevent the transmit signals from leaking into the receiver. Moreover, solid-state transmitters used in FMCW radar systems are not capable of producing such high-power pulses due to their limited dielectric strength and operational temperature. The transmit power of FMCW radars are generally varied between 0.1 to 5 Watts. However, the pulse compression ratio, or time-bandwidth product, which is given by the product of the effective receiver bandwidth and coherent processing interval of the transmitted pulse ($t_o B$), achieves the effect of a much higher transmit power in pulse compressed (FMCW) systems by a factor of the pulse compression ratio. Thus, in FMCW radars or other pulse compressed systems, the advantages of employing long pulses (i.e. increased maximum detection range and higher SNR or energy) and very short pulses (i.e. increased signal bandwidth) observed in pulsed radar systems can be achieved simultaneously.

Given that the application in hand is particularly interested with the detection of small patrol boats ranging between 10 to 15 meters long ($\sigma = 30 \text{ m}^2$) and mostly at a detection range of approximately 20 km, and assuming the threshold of the desired SNR of the received signal is chosen to be 25 dB, based on the assumption of the radar and target parameters presented in Table A-2 (Appendix A) the transmit power required to achieve a SNR of 25 dB is 2 Watts. With the same radar parameters, a transmit power budget analysis is also produced using the radar equation to identify the smallest target RCS that is able to generate radar returns with a SNR of 25 dB at several chosen operating ranges ($10 \text{ km} < R < 50 \text{ km}$) when a transmit power of 3 Watts is used. The power budget analysis is presented in Table A-3 (Appendix A).

- **Polarization: Linear (Vertical)**

Although the probability of detection of a target depends on various factors such as the detection range, intensity of clutter and scan-to-scan processing (scan averaging), the capability of a radar system to discriminate between a certain target and clutter signals is also influenced by the polarization of the antenna especially for long range detection application involving high sea states. The presence of scatterers from sea clutter due to high sea states can change the polarization of the reflected signals to be different from the polarization of the incident wave [75]. Under these situations, the problem arises when the presence of sea clutter buries small stationary or fast-moving targets, therefore mistaking targets for clutter. Hence, to optimize the radar's target detection capability it is important to match the polarization of the antenna to that of the incoming signal so that the maximum signal can be obtained by the receiving antenna. The use of polarization diversity is an antenna characteristic that is considered to be a clutter reduction technique.

In FMCW coastal surveillance radars, the effect of sea clutter on the processed radar returns will be different on radar systems employing different forms of polarization. For linear polarization, although the sea clutter reflectivity, σ^0 , for H-polarization is about 3-5 dB less than for V-polarization ($\sigma_{HH}^0 < \sigma_{VV}^0$), the high-resolution requirements makes the sea clutter echoes spikier for H-polarization than V-polarization [75]. Due to the statistical advantage of V-polarization over H-polarization, this increases the false alarm rate for H-polarization as compared to V-polarization for a high-resolution radar. Hence, the use of V-polarization is more advantageous as compared to a H-polarized radar under Constant false alarm rate (CFAR) detection due to the fact that less SNR is required, and therefore a higher probability of detection is achieved for a fixed threshold detection below a critical radar height [75]. For the detection of small targets in low sea states and at relatively close range (10 km), it has been experimentally proven by [22] that given a set of radar parameters the performance of radar systems with either linear vertical or horizontal polarization is very close, or equally effective.

Radar systems with circular polarization is more effective in minimizing the undesirable effects of clutter on the data extracted from received signals, particularly for the detection of small vessels within a sector of the sea with high sea states due bad weather conditions. Nonetheless, circular polarized antennas are more complex systems that are commonly used for applications with detailed imaging requirements (i.e. land mapping). Applications requiring circular polarization are frequent within the field of astronomy.

The polarization of the transmitted EM waves is chosen to be vertically polarized as it conforms with the aperture shape of the E-plane sectoral horn antenna. The field illuminating the horn aperture is essentially a spatially expanded version of the waveguide field. In reception, the radar can be designed to simultaneously receive both polarization components of the EM wave, which will be useful for discriminating clutter signals and targets of interest in longer range detection application.

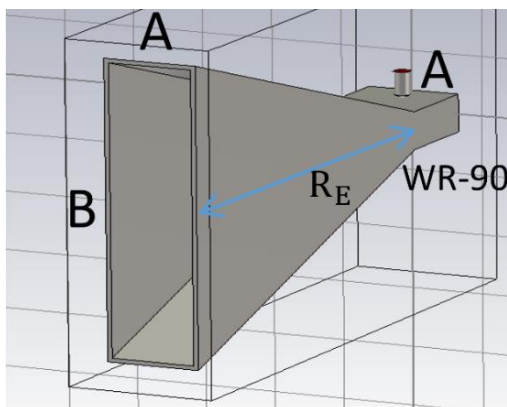


Fig 4-3. E-plane sectoral horn dimensions

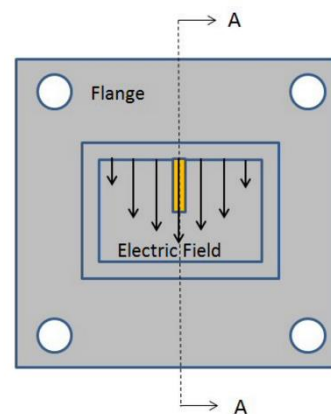


Fig 4-4. View looking into the waveguide

- **Sweep Time (Modulation Period): 2.5 ms**

In FMCW radars, the minimum sweep time (pulse length) chosen is greatly dependent on the maximum detection range requirement of the radar system, while the range resolution of the system depends on the modulation of the transmitted signal over a range of frequency, or the signal bandwidth. As a rule of thumb, the duration of the transmitted signal should be substantially larger than the required two-way propagation or receiving time that is used to measure the range of a detected target.

Two factors must be considered in choosing a suitable modulation period of the FMCW waveform [76]. The first factor is relevant especially for the detection of fast-moving targets. During target detection, it is critical that a target must only occupy one range bin, or resolution cell, for at least the entire modulation period, t_m . Otherwise, this causes the radar to produce a smeared image of the target at the radar output and the corresponding signal-to-clutter ratio to decrease. The consideration is given by

$$t_m < \frac{\Delta R}{V_t} \quad (4-6)$$

where V_t is the maximum closing velocity of the target.

This condition requires that the modulation period must be chosen according to the range resolution of the antenna and the velocity of the target dealt with.

The second factor is that t_m should be at least approximately 10 times the maximum round trip delay, t_d , of the target's return signal. Firstly, this is necessary in order to have enough samples of the detected target that applies not only for close range but also from the range near the maximum allowed range, since the required number of samples per sweep is larger for radars operating at increased detection range [77]. This is also required in order to minimize the loss in effective transmit bandwidth and power due to the partial overlap between the transmit and receive signals [76]. As shown in Figure 4-5, the partial overlap between the transmit and receive waveforms reduces the effective bandwidth of the radar, B' .

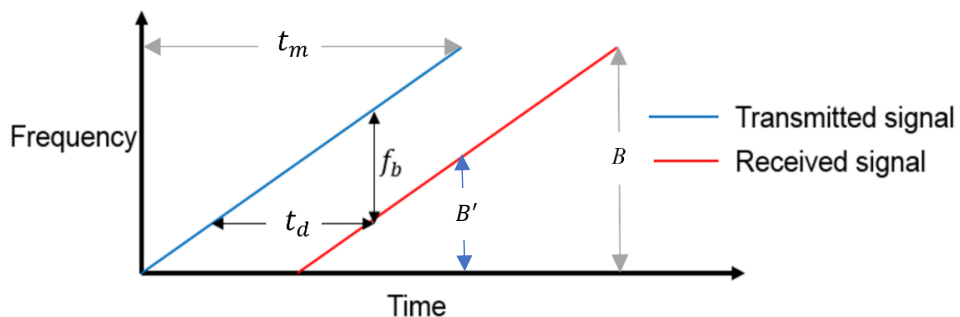


Fig 4-5. FMCW transmit and receive pulses

The effective bandwidth of the radar is given by

$$B' = B \left(1 - \frac{t_d}{t_m}\right) \quad (4-7)$$

The processed bandwidth becomes considerably less when the overlap between the transmit and receive signals is reduced. In return, the range resolution of the radar corresponding to the effective bandwidth is slightly reduced from (3-35) to (4-8). Hence, a longer t_m is preferable and necessary especially for long range radars to achieve a larger overlap and, therefore, an effective bandwidth that is only reduced by a slight amount from the original bandwidth.

$$\Delta R' = \frac{c}{2\Delta B'} = \frac{c}{2\Delta B \left(1 - \frac{t_d}{t_m}\right)} \quad (4-8)$$

Secondly, a longer pulse duration is also required to provide a high velocity resolution. The velocity resolution of a radar system, or first blind speed, Δv , is the speed at which the Doppler goes through one complete cycle from one sweep to the next [76]. It is also at this speed where the target will not be visible to the radar.

The maximum round trip delay of a target's return signal is denoted by t_d , and the coherent processing interval, t_o , for the detection of a target at a specified range is given by

$$t_o = t_m - t_d \quad (4-9)$$

The reciprocal of t_o is the spectral width of the beat frequency, Δw , and the corresponding velocity resolution or first blind speed is determined according to this parameter, given by

$$\Delta v = \frac{\lambda \Delta w}{2} \quad (4-10)$$

For the application in hand, the radar system is only required to detect slow moving large sized vessels. Hence, this factor will not be greatly considered since the movement of a large vessel across a range bin within the chosen modulation period is unlikely to happen.

Unlike conventional pulsed radar and moving target indicator (MTI) systems, the pulse duration of the transmitted signal does not determine the radar range resolution. Hence, providing the target remains within the resolution cell for at least the entire modulation period, t_m , employing a relatively long pulse duration is acceptable as it does not correspond to a poor range resolution. In most monostatic FMCW radar systems, the value of t_m is chosen such that a single transmit and corresponding receive pulse would overlap one another by at least 90 percent. For the application in hand, the sweep time is chosen to accommodate for a maximum detectable range of 30 km. Since it takes approximately 0.225 ms for the two-way propagation

of the transmitted pulse for the detection of a target located 30 km away from the radar, a suitable pulse duration would be 2.5 ms in order for the transmitted and received pulse to overlap by 91%.

4.2 Optimization of Adapter (WR90) RF Performance

For all types of horn antenna, the supply of transmit signals from the radar transmitter into the horn antenna followed by the transmission of power between the horn antenna and free space are critical in providing a suitable transition region in which the changeover from the coaxial line to the guided propagation to free-space propagation takes place. The transition between the respective modes of propagation involves a significant change of phase velocity and the wave's characteristic impedance. The RF performance of an antenna is optimized when the low impedance of the coaxial line, typically 50Ω , matches the much higher characteristic impedance of the antenna, which is typically greater than the impedance of free space (377Ω). Hence, to provide the transmitted signal with a low loss of power as it propagates in between the respective mediums the characteristic impedance of the coaxial line, the waveguide and free space must be as closely matched as possible to one another. A poorly matched antenna impedance would result in an undesirably poor antenna performance due to the significant loss of power. It is common for such antennas to produce a distorted radiation beam pattern of considerably low gain.

For the horn antenna that will be constructed in this project, the section of the waveguide used has a rectangular cross section. Rectangular horn antennas are typically fed by a section of a rectangular waveguide that has a rectangular cross section of height a and width b , with itself often fed by a short dipole. The efficient transition of radar signals between the coaxial cable, which is connected to the transmitter of the radar, and a rectangular waveguide fed antenna is achieved using a waveguide to coax adapter, or also known as a waveguide-to-coax transition, which allows radar signals to be transmitted out of the antenna as electromagnetic radiation with almost no loss of power. There are two types of transitions, either right-angle transitions or in-line transitions. In general, in-line transitions have a higher VSWR and loss across the designated frequency band, and so they do not perform as well as right-angle transition designs. However, they exhibit higher power handling as the coax is tied to ground which offers a good heat path [78]. The 'right-angle' transition is the preferred choice given that the RF performance of an adapter is prioritized and low power is used. The principles of modelling a waveguide-to-coax right-angle type of transition with optimized RF performance at a specified operating frequency will be discussed in this section. An illustration of a both types of transition are presented in Figure 4-6.

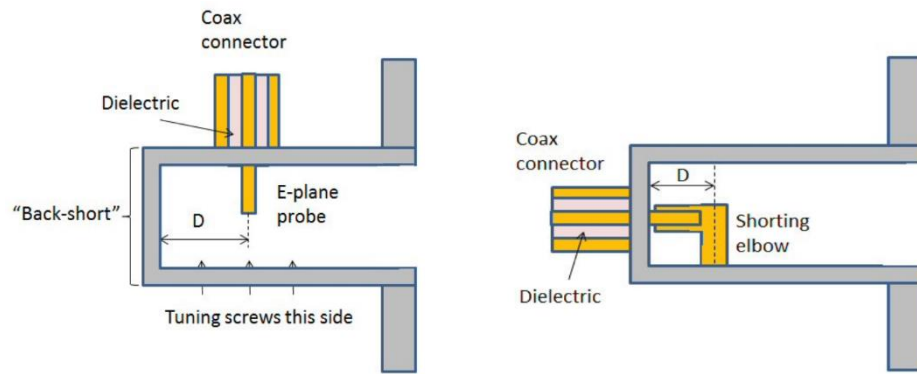


Fig 4-6. 'Right-angle' and 'In-line' transitions [78]

As mentioned in Section 3.3.2, the waveguide dimensions is significant in allowing EM waves to propagate in the interior of the guide at the appropriate frequency band with a high RF performance (i.e. low return loss (S_{11}) and voltage standing wave ratio (VSWR)). Table 4-3 presents a range of standardized adapters that are specially designed to operate at every frequency band. An industrial adapter typically has a VSWR smaller than 1.3 and a S_{11} of at least -15 dB across the frequency band. While the dimensions of each adapter ensure acceptable RF performance across the frequency band, the positioning of the transition probe on the broad surface of the adapter (right-angle transition) are optimized for superior RF performance at the operating frequency of the radar. An adapter with an optimized transition design offers a VSWR less than 1.1 and a S_{11} in excess of -20 dB across a narrow range of frequencies close to the centre frequency of the antenna.

The range of adapters shown in Table 4-3 are manufactured for instrumentation grade quality by various RF component manufacturers. Commercial adapters are manufactured with various types of flange attached to the adapter, which is used to provide a connecting mount between the adapter and, for instance, the flared walls of a horn antenna. Nonetheless, the RF performance of an adapter would remain the same regardless of whether a flange is attached to it or if it is directly extended to an antenna (i.e. horn antenna).

Waveguide Size	JAN WG Desig	MIL-W-85 Dash #	Material	Freq Range (GHz)	Freq Cutoff (GHz)	Power (at 1 Atm)		Insertion Loss (dB/100ft)	Dimensions (Inches)	
						CW	Peak		Outside	Wall Thickness
WR284	RG48/U RG75/U	1-039 1-042	Copper Aluminum	2.60 - 3.95	2.08	45 36	7650	.742-.508 1.116-.764	3.000x1.500	0.08
WR229	RG340/U RG341/U	1-045 1-048	Copper Aluminum	3.30 - 4.90	2.577	30 24	5480	.946-.671 1.422-1.009	2.418x1.273	0.064
WR187	RG49/U RG95/U	1-051 1-054	Copper Aluminum	3.95 - 5.85	3.156	18 14.5	3300	1.395-.967 2.097-1.454	1.000x1.000	0.064
WR159	RG343/U RG344/U	1-057 1-060	Copper Aluminum	4.90 - 7.05	3.705	15 12	2790	1.533-1.160 2.334-1.744	1.718x0.923	0.064
WR137	RG50/U RG106/U	1-063 1-066	Copper Aluminum	5.85 - 8.20	4.285	10 8	1980	1.987-1.562 2.955-2.348	1.500x0.750	0.064
WR112	RG51/U RG68/U	1-069 1-072	Copper Aluminum	7.05 - 10.0	5.26	6 4.8	1280	2.776-2.154 4.173-3.238	1.250x0.625	0.064
WR90	RG52/U RG67/U	1-075 1-078	Copper Aluminum	8.2 - 12.4	6.56	3 2.4	760	4.238-2.995 6.506-4.502	1.000x0.500	0.05
WR75	RG346/U RG347/U	1-081 1-084	Copper Aluminum	10.0 - 15.0	7.847	2.8 2.2	620	5.121-3.577 7.698-5.377	0.850x0.475	0.05
WR62	RG91/U RG349/U	1-087 1-091	Copper Aluminum	12.4 - 18.0	9.49	1.8 1.4	460	6.451-4.743 9.700-7.131	0.702x0.391	0.04
WR51	RG352/U RG351/U	1-094 1-098	Copper Aluminum	15.0 - 22.0	11.54	1.2 1	310	8.812-6.384 13.250-9.598	0.590x0.335	0.04
WR42	RG53/U	1-100	Copper	18.0 - 26.5	14.08	0.8	170	13.80-10.13	0.500x0.250	0.04
WR34	RG354/U	1-107	Copper	2.0 - 33.0	17.28	0.6	140	16.86-11.73	0.420x0.250	0.04
WR28	RG271/U	3-007	Copper	26.5 - 40.0	21.1	0.5	100	23.02-15.77	0.360x0.220	0.04

Table 4-3. Rectangular waveguide adapter models [78]

For the application in hand, a mechanical scanning radar employing a reflector antenna operating at a frequency of 9.2 GHz will be designed and manufactured. The feed to the reflector is a certain type of horn antenna that is chosen to fulfil the desired characteristics of the radiated beam. To successfully manufacture a horn antenna with high RF performance at 9.2 GHz, a suitable transition adapter used to feed the horn antenna would be the WR90 right-angle adapter; a X-band waveguide to SMA coaxial adapter that cover the frequency range of 8.2 to 12.4 GHz. Figure 4-7 is a modelled illustration of a WR90 adapter with a square flange attached to it.

Adapter Model	Frequency (GHz)	Inner Dimensions (mm)
WR-90	8.2 - 12.4	10.16 x 22.86 x 34.73

Table 4-4. Standard dimensions of a WR90 adapter

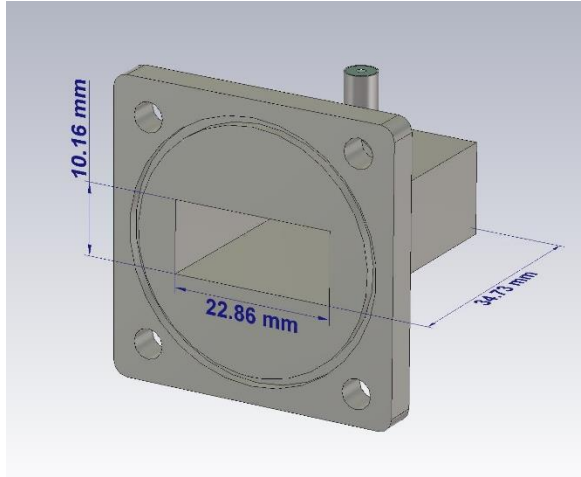


Fig 4-7. WR90 adapter with square flange attached

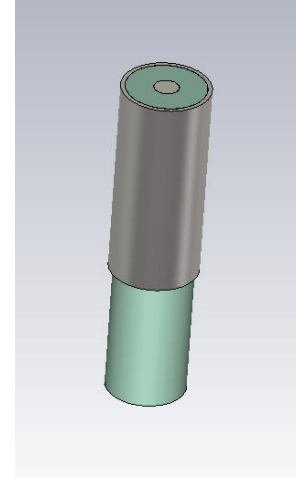


Fig 4-8. Coax to adapter transition

A typical coaxial line to adapter transition consists of a SMA connector positioned on the broad surface of the adapter with the inner conductor extended as a probe, and the short end of the adapter ending in a short circuit. For vertical polarization, the adapter is interfaced with a coaxial cable by using a simple antenna probe reaching into the top wall of the waveguide to excite only the preferred dominant TE_{10} mode [78]. The maximum electric field is at the centre of the wide dimension of the adapter, as illustrated in Figure 4-4, where the probe is positioned. This type of transition is also known as E-plane transitions, or orthogonal transitions. An illustration of the coaxial transmission line to adapter transition probe is shown in Figure 4-8.

The transition probe acts as an impedance transformer from the low impedance of the coaxial line to the much higher impedance of the WR90 adapter. Since there is no loop for current to flow in and create a magnetic field, the probe must be an electric field transformer [79]. The material surrounding the full length of the probe is a cylinder of teflon dielectric layer that concentrates the electric field near the probe and increases the coupling. Thus, surrounding the probe with a dielectric would require a shorter probe to match the impedance of the adapter as compared to using a bare probe. The cylinder of teflon dielectric layer is typically 4.06 mm in diameter, with an inner diameter of 1.27 mm, which is also the optimum diameter of the SMA inner conductor suitable for X-band transitions [79].

A comparison between the RF performance of a WR90 adapter operating at the same frequency using two different transition designs, one with the full length of the probe surrounded by the dielectric material, and the other with a bare probe extending into the guide, is demonstrated in [79]. As expected, the experiment performed proves that the former transition design would require a shorter probe length to match the impedance of the coaxial line to the characteristic impedance of the adapter at the chosen frequency of interest due to the

coupling effect of the dielectric around the probe. The only difference in terms of performance between the two transition designs (with and without the dielectric) is that the transition with the teflon dielectric extending into the adapter provides slightly better bandwidth than a transition with a bare probe, although the improvement is not a significant one. Nonetheless, despite the fact that all adapters have been designed and manufactured for full frequency band operation, performance degradation of the waveguide varies across the range of frequencies within the frequency band especially at the higher end of the frequency range due to the performance limitation of certain coax connector types.

For a given adapter model the distance between the back-short wall and the centre of the probe, also known as the back-short distance, and the length of the probe extending into the adapter, also known as the probe length, determines the centre frequency of the adapter at which the RF performance of the adapter is optimized. In practice, the RF performance of the adapter would be optimized at the operating frequency of the antenna, at which the return loss and VSWR is the minimum across the frequency band of the adapter. Hence, the back-short distance and probe length extending into the adapter is modelled for the centre frequency of the adapter to be aligned to the operating frequency of the antenna.

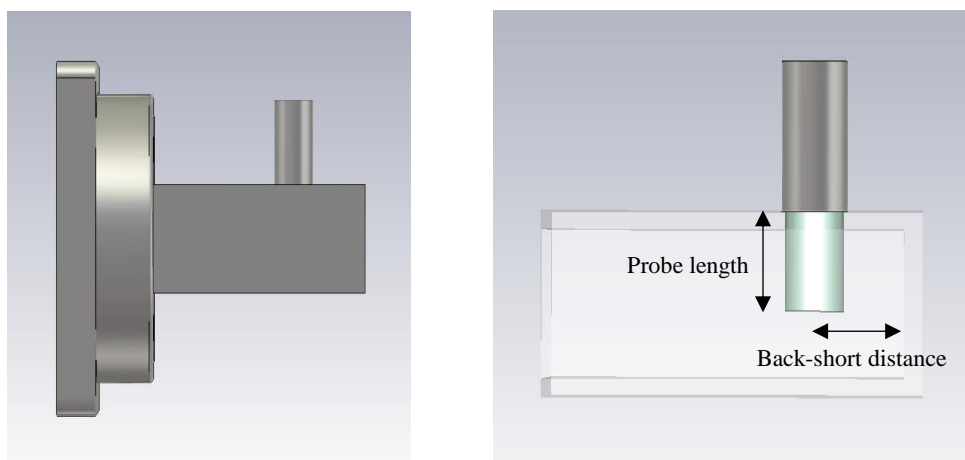


Fig 4-9. Critical dimension parameters of transition

The back-short wall of the adapter is at some distance away from the position of the probe. The back-short forms a section of shorted transmission line behind the probe, creating a reactance at the probe that varies with the length of the line to the back-short [79]. It reflects EM energy that was propagating the wrong way back towards the probe where it combines in-phase with the incident wave. Thus, the probe sets up a time-varying electric field, which is constrained to propagate down the guide [78]. An ideal probe does not introduce any inductance or capacitance of its own. If this assumption is applied, the back-short distance of all adapters

should be exactly $\lambda/4$ because a shorted quarter-wavelength of transmission line acts an open circuit, and at this distance no reactance will be added at the probe [79]. Thus, a back-short distance of $\lambda/4$ would only be suitable for an ideal probe. However, since the probe is a wire it must have some inductance that varies slightly with the length of the probe extending into the adapter, which introduces capacitance at the waveguide walls. Given an adapter with a constant back-short distance, by varying the probe length extending into the adapter at small intervals it comes to a point where the reactance of the probe is tuned out at the operating frequency, such that only the resistive component of the impedance remains. This occurs at the point where the reactance contributed at the probe, from the section of shorted transmission line behind the probe, equals the reactance of the probe but with a conjugate phase, which effectively cancels out the reactance of the probe. Therefore, in practice, a pure resistive impedance is often achieved when the back-short distance is slightly smaller than $\lambda/4$. Intuitively, it is realizable that the back-short distance required to tune out the reactance of the probe to obtain a purely resistive impedance also varies slightly with probe length.

For the application in hand, the RF performance of the WR90 adapter will be optimized by tuning the centre frequency of the adapter's return loss to occur at, or close to, 9.2 GHz. This is achieved by ensuring that the resistive impedance of the probe is matched to the characteristic impedance of the adapter at the desired operating frequency. Since the back-short distance of a commercially available WR90 adapter is fixed at 7 mm, the length of the probe extending into the adapter is the sole parameter that determines the resistive impedance of the probe, and therefore the centre frequency of the adapter's return loss.

The optimum probe length is defined as the probe length that matches the impedance of the probe to the characteristic impedance of the WR90 adapter at 9.2 GHz. The optimum probe length that achieves this is identified based on a set of impedance measurements for different probe lengths through an iterative approach. An optimization of the adapter's RF performance at 9.2 GHz is accurately achieved based on the S_{11} and VSWR measurements of the adapter upon varying the probe length. The measurements presented in this section are obtained from the simulated RF performance of the adapter on CST.

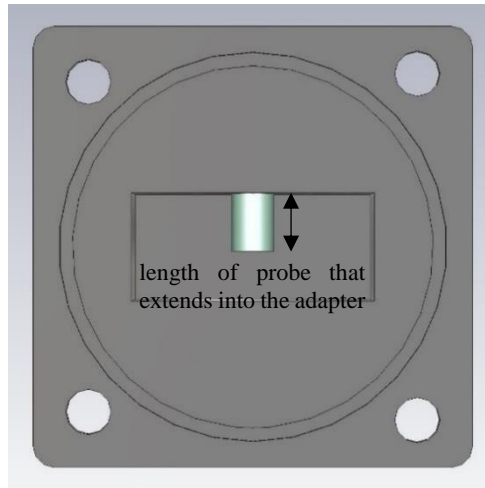


Fig 4-10. Front view of an adapter

The RF performance of the WR90 adapter is simulated for different probe lengths of the SMA connector connected to the adapter. The length of the probe is varied between 3 mm and 8 mm, in intervals of 0.5 mm, while a back-short distance of 7 mm is kept constant. Bearing in mind that the waveguide walls are 1.27 mm thick, the length of the probe extending into the adapter is 1.27 mm shorter than the stated probe length. The return loss and VSWR measurements of the adapter at 9.2 GHz for the different probe lengths of the SMA connector, with a constant back-short distance of 7 mm, are presented in Figure 4-11 and 4-12 respectively. The numerical values of the parameters are presented in Table 4-5.

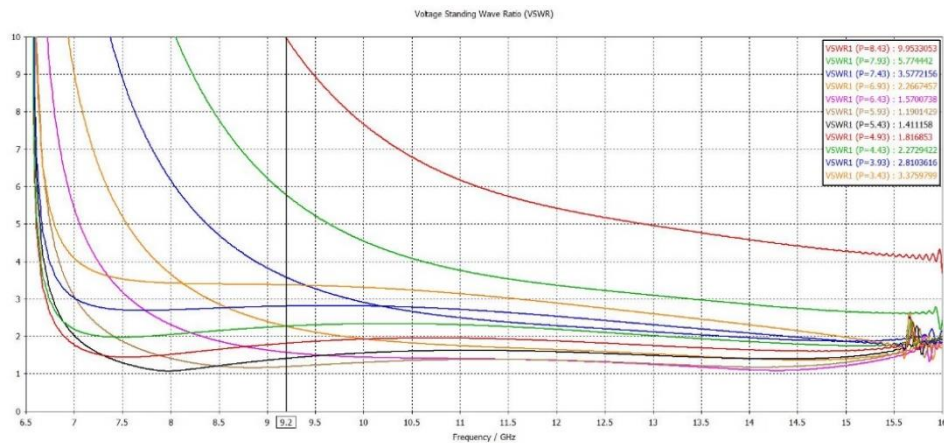


Fig 4-11. VSWR of WR90 for different probe lengths

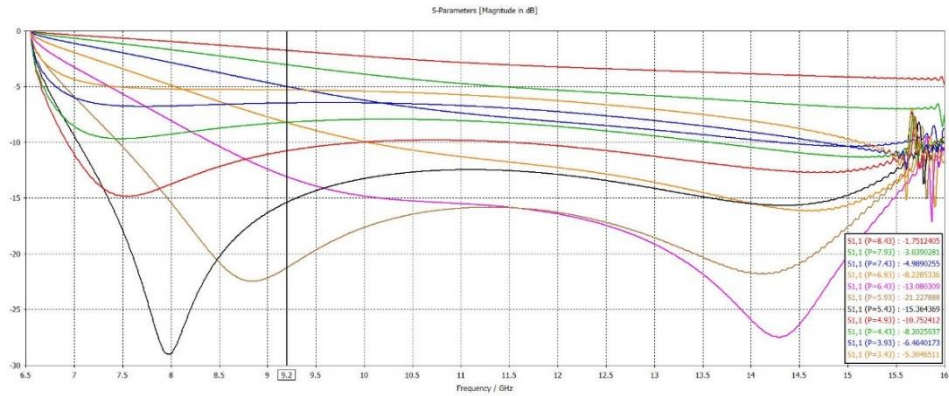


Fig 4-12. Return loss (S11) of WR90 adapter for different probe lengths

Probe Length (mm)	S11 (dB)	VSWR
3	-1.8	10
3.5	-3	5.8
4	-5	3.6
4.5	-8.2	2.3
5	-13.1	1.6
5.5	-21.2	1.2
6	-15.4	1.4
6.5	-10.8	1.8
7	-8.2	2.3
7.5	-6.5	2.8
8	-5.3	3.5

Table 4-5. Simulated RF performance of WR90 adapter for different probe lengths

Based on the simulation results, the iterations performed identifies the optimum probe length of the WR90 adapter to be 5.5 mm, at which the centre frequency of the S_{11} and VSWR of the adapter is the closest to the operating frequency of the antenna. The optimum probe achieves a S_{11} and VSWR of -21.2 dB and 1.19 respectively at 9.2 GHz, and a S_{11} and VSWR that is at most -15 dB and 1.35 respectively across the X-band frequency spectrum.

Predictably, a longer probe extending into the adapter intersects more of the electric field and thus couples more tightly to the low impedance in the coax. Therefore, a longer probe has a resistive impedance that is lower than Z_0 , whereas a short probe has a higher resistive impedance than Z_0 . The plots show that the S_{11} and VSWR of the adapter at a specific frequency of interest initially begins to decrease, and then starts to increase from the lowest point once the probe length is increased beyond the optimum length.

The simulation results indicate that the WR90 adapter with the optimised transition design is suitable to be used as part of the construction of a horn antenna with high RF performance, particularly at frequencies close to 9.2 GHz. The S-parameters of the adapter using the optimum transition design are presented in Figure 4-13.

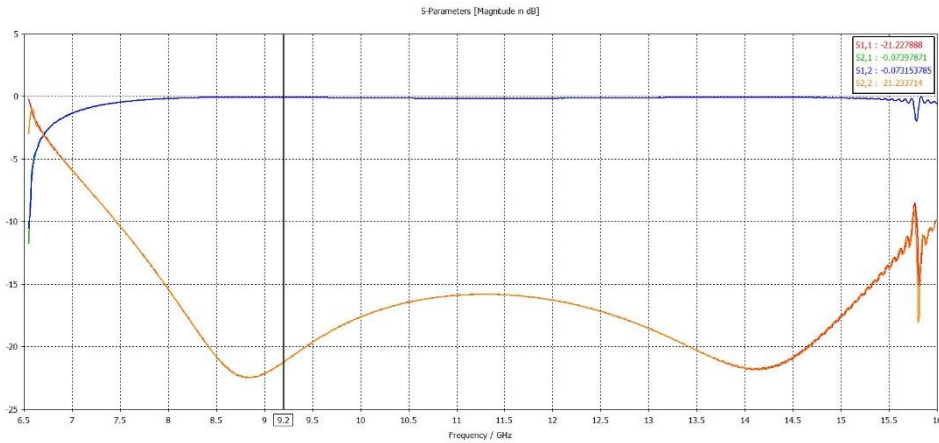


Fig 4-13. S-parameters of WR90 adapter with a probe length of 5.5 mm

The validation of the simulated RF performance of the WR90 adapter is performed through the same iterative method by measuring the RF performance of the antenna using a Vector Network Analyzer (VNA) for different probe lengths. The measurement of the RF performance will start with a long probe extending into the adapter and trimming the length of the probe at intervals of 0.5 mm after each successive measurement is made. The length of the probe extending into the adapter will be of the same values simulated in this section. The test equipment used to measure the antenna under test (AUT) and the measurements obtained are presented and discussed in Section 6.1.

To achieve very high RF performance (very low S_{11} and VSWR values), fine tuning the centre frequency of the adapter to occur at the operating frequency of the antenna can also be achieved using tuning screws. The tuning screws function by terminating either the adapter or the coax into a low VSWR load (1.05) and observing the VSWR looking into the other end while sweeping over the frequency band [78]. The screws are drilled into the adapter at the appropriate positions, which are always on the opposite side of the adapter from the probe, once the tuning is completed, as shown in Figure 4-14.

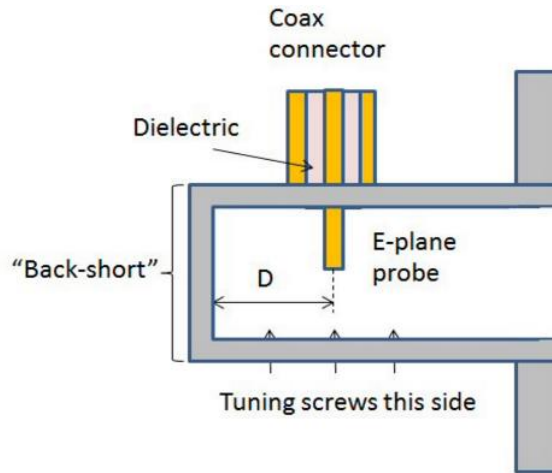


Fig 4-14. Tuning a waveguide using tuning screws [78]

Although it is a rather complicated approach of tuning the RF performance of an adapter, this method is capable of achieving VSWR as low as 1.05 if properly executed. However, utilizing good test equipment is required to easily locate the required positions of the screws accurately, otherwise this could cause the performance of the adapter to deteriorate instead. Hence, this approach of optimizing the RF performance of an adapter was not considered.

4.3 Modelling of E-plane Sectoral Horn Antenna

The reflector antenna is designed to produce a fan-shaped secondary beam with an azimuth beamwidth that is approximately 4 times narrower than the elevation beamwidth. Since the ratio of the reflector dimensions is approximately proportional to the ratio of the principal plane beamwidths of the beam, the ideal width of the vertically truncated reflector is expected to be approximately 4 times larger than its height. In return, to illuminate the reflector aperture optimally the radiation pattern of the feed must match the shape and collecting area of the dish. Therefore, a vertically truncated parabolic reflector would require a rather unusual feed with an azimuth and elevation beamwidth of approximately the same aspect ratio.

Horn antennas are known for their high gain characteristics (~ 14 dB) and is a popular choice for feeding reflector antennas that are used in long range detection applications (i.e. surveillance radars). Comparing all types of horn antenna available, the E-plane sectoral horn antenna would be the most suitable feed that has a radiation pattern with the required beam shape. The aperture of this type of horn antenna is only flared in the vertical plane, while unflared in the horizontal plane, and therefore it has the widest radiation pattern in azimuth as compared to other horn antennas available. Unlike the wide azimuth beamwidth of the antenna, which is similar to that of an open-ended waveguide (~ 70 degrees), the elevation beamwidth

is significantly narrower due to the wider vertical dimension of the horn aperture. The antenna gain is typically in excess of 14 dBi.

Nonetheless, commercially available E-plane sectoral horn antennas are always designed to achieve maximum directivity, which, as described in Section 3.4.1, is achieved by calculating the appropriate dimensions of the horn based on the optimal relation between the flared height and horn apex length. As derived in Section 3.4.1, this relation is given by

$$B = \sqrt{2\lambda R_E} \quad (4-11)$$

where B is the flared height of the horn antenna

R_E is the horn apex length

λ is the operating wavelength of the radar

A simplified illustration of the geometrical dimensions of a E-plane sectoral horn antenna is shown in Figure 4-15.

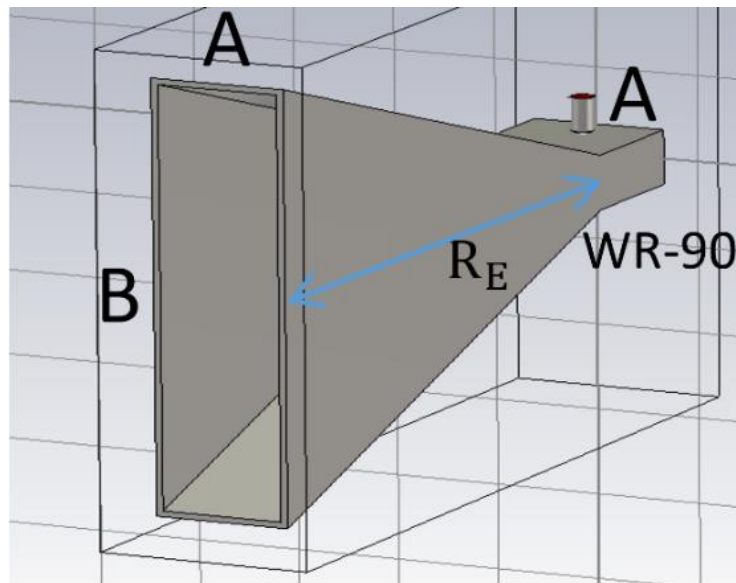


Fig 4-15. Dimensions of a E-plane sectoral horn antenna

An example of a E-plane sectoral horn with maximum directivity is commercially sold by *L3 Narda-ATM* for different frequency bands [80]. The dimensions of the sectoral horn antenna fulfils the relation in (4-11) to achieve maximum directivity when operating at the specified frequency band. For the horn designed to operate in the X-band spectrum (8.2 – 12.4 GHz), the dimensions of the horn aperture is 0.9 inch ($A = 10.2$ mm) by 3.82 inches ($B = 97$ mm). The width of the antenna aperture, A , equals the width of the waveguide model WR90 since the horn is unflared in the horizontal plane. Based on the horn aperture dimensions, a horn

apex length of 5.69 inches ($R_E = 144.4$ mm) or greater is required to achieve the maximum possible directivity when operating at a frequency of 9.2 GHz. Nonetheless, the overall length of the horn varies with the type of flange attached to it.

The commercial horn antenna from *Narda-ATM* is modelled on CST according to the provided dimensions. The horn, which is fed using a right-angle transition WR-90 adapter, has a linear vertical polarization. The simulated radiation pattern and properties of the E-plane sectoral horn antenna in azimuth and elevation are shown in Figure 4-16 and 4-17. The distribution of the radiated E-field is concentrated at the center of the aperture and at a direction perpendicular to the narrow walls of the horn (Figure 4-4).

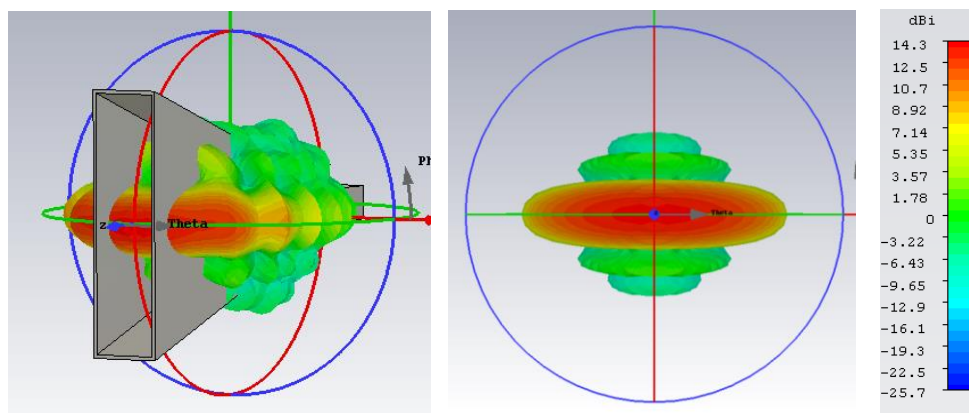


Fig 4-16. Radiation pattern of E-plane sectoral horn antenna

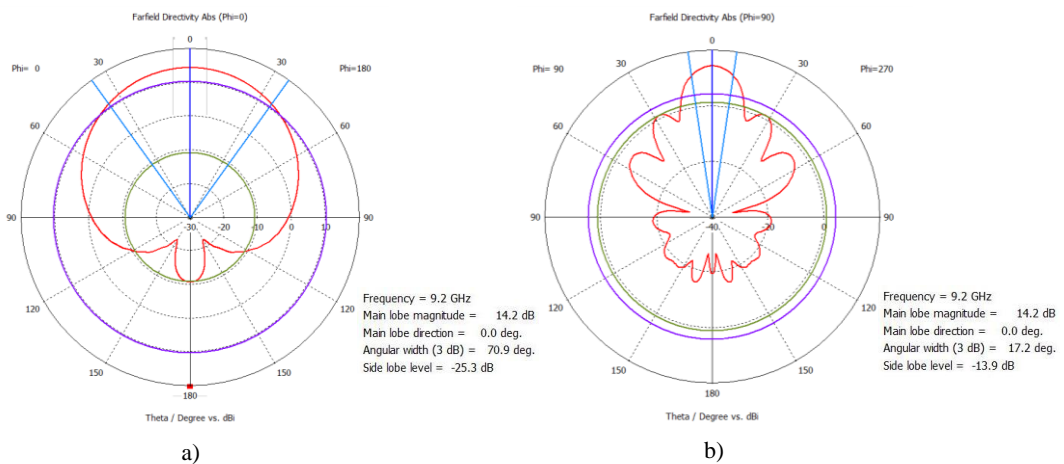


Fig 4-17. Radiation pattern (polar plot) in the a) H-plane and b) E-plane

The simulated -3 dB azimuth and elevation beamwidth of the horn antenna is 70.9 degrees and 17.2 degrees respectively, with an antenna gain of 14.2 dB and sidelobe levels of -25.3 dB and -13.9 dB in the respective planes.

In practice, the phase center of a horn is not easy to locate and at times can be inaccurately determined through geometrical calculations. As mentioned in Section 3.4, the location of the apparent phase center is most accurately determined through experimental trials or modelling. The method used to identify the apparent phase center of the horn antenna is described in Section 4.4.3, as it is used as a feed to illuminate a vertically truncated reflector.

4.4 Reflector Antenna Design

In designing a parabolic reflector, the pertaining issue lies with the inability of the feed to illuminate the reflector aperture perfectly although the feed pattern exactly matches the physical collecting area of the dish. Perfect reflector illumination is not achievable in practice due to the natural tapering effect from the reflector curvature and feed pattern, as discussed in Section 3.5.2. In theory, a 100 percent aperture efficiency is only achieved when the reflector aperture is uniformly illuminated with a constant field strength to its edges, which would require a feed with an ideal radiation pattern that has a constant field strength throughout the solid angle of the dish, dropping abruptly to zero at the edges [81].

The feed used to illuminate the reflector aperture produces a beam pattern of a certain beamwidth in both principal planes. The first step in designing a reflector is to ensure that the shape of the reflector aperture must first conform to the radiation pattern of the feed, or vice versa, to ensure that most of the signal radiated from the feed is reflected as much as possible with little or no energy radiated in directions that falls outside the collecting surface area. For instance, if a reflector with a rather small collecting area is illuminated by a feed with a wide radiation pattern, a substantial amount of radiated power will be wasted due to over illumination of the reflector aperture, or also known as spillover, and this causes the aperture efficiency to be substantially reduced. On the other end, under illuminating the reflector with a feed pattern that is too narrow would not make optimum use of the entire reflector aperture, and therefore the aperture efficiency of the reflector will be reduced as well. Hence, the maximum possible gain of the reflector antenna will not be achieved for both cases of under and over illuminating the reflector aperture, but instead it is achieved by identifying the best compromise between fully covering the surface of the reflector and not “spilling over” the aperture edges any more than necessary [27]. This is fulfilled by applying the optimum taper on the reflector aperture, which will be demonstrated in the reflector design.

4.4.1 Type of Reflector used and Approximated Reflector Width

The reflector antenna designed for the application in hand is required to produce a beam pattern that has a -3 dB azimuth and elevation beamwidth of approximately 2 degrees and between 6 to 8 degrees respectively, with a theoretical gain of approximately 35 dB and side lobe levels of -20 dB. The significantly narrower azimuth beamwidth is required to achieve a high angular resolution in azimuth for accurate detection of targets along the coastal water across several tens of km in range. On the other hand, radiating a beam with a sufficiently wide elevation beamwidth is required for a scanning radar to detect targets at close and far range in elevation without displacing the antenna along the vertical plane. In marine radars an acceptably wide elevation beamwidth is also required to compensate for the pitch and roll of the ship.

Conventional circular parabolic reflectors are used to create pencil beams that have the same beamwidth in both principal planes. A reflector antenna designed to radiate a secondary beam pattern with a azimuth beamwidth that is several times smaller than the elevation beamwidth can be achieved by appropriately illuminating a vertically truncated reflector, which is the central portion of a circular parabolic reflector that can be easily designed by removing the top and bottom portions of the reflector symmetrically (Figure 4-18). The reflected energy is focused into a narrow beam in azimuth while spreading out in the vertical plane. The secondary beam produced resembles a 'fan' shape that possesses the required beamwidths ratio of both planes. This type of reflector is therefore greatly considered as the aperture outline is the most suitable to achieve the requirement of the application in hand.

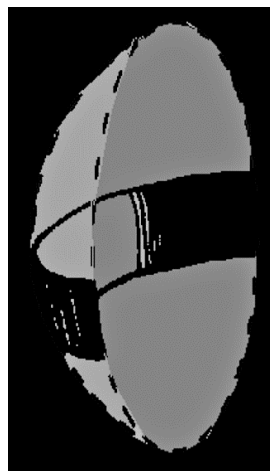


Fig 4-18. Illustration of a truncated reflector as a section of a complete parabolic reflector

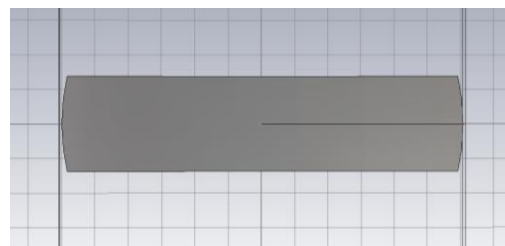


Fig 4-19. Vertically truncated reflector

The area projected onto the aperture plane of a typical parabolic reflector is the area containing the collimated radiation of the reflected feed pattern. As described in Section 3.5.2,

the feed pattern and shape of the reflector aperture are important characteristics of a reflector antenna as it determines the properties of the secondary beam produced. Nonetheless, assuming a uniformly illuminated reflector aperture and taking into account the contribution of overall degradation loss effects for shaped parabolic reflectors, an approximation of the relationship between the beamwidth of the beam produced and the diameter of a circular parabolic reflector, D , is given by

$$BW = 70\lambda/D \quad (4-12)$$

At an operating frequency of 9.2 GHz ($\lambda \approx 3.3$ cm) the reflector must be at least 1.2 meters wide to produce a secondary beam pattern with an azimuth beamwidth that is at most 2 degrees. Hence, a suitable approximation of the reflector width is 1.2 meters. The height of the reflector and reflector curvature (f/D ratio) is designed in Section 4.4.2 based on the radiation pattern of the feed horn and the chosen aperture taper to be applied.

4.4.2 Reflector Design per Specified Width and Feed Radiation Pattern

As described in Section 3.5.2, applying a small aperture taper results in an excessive spillover of radiated power from the main lobe of the primary pattern that will result in the reduction of antenna gain and an undesirable increase in side and back lobe level of the beam produced, which may lead to interference in receiving antennas or an increase in susceptibility to ground noise [81]. Consequently, under illumination of the reflector aperture is observed when a large aperture taper is applied. Although it considerably reduces the side lobe level, it also reduces the antenna gain and causes the widening of the radiated beam due to inefficient use of the available reflector area. This section discusses the design process of a vertically truncated reflector that is based on the known feed radiation pattern and aims to identify the optimum aperture taper to be applied that will achieve maximum reflector antenna gain.

The designer can opt to design the feed according to the properties of an existing reflector or to establish a new reflector design (f/D ratio and height of dish) based on the radiation pattern of the feed to produce a secondary beam that satisfies the antenna requirements. Using the former method would require the feed to be specially designed in order to radiate a beam that will apply the desired aperture taper on both planes of the existing reflector. Consequently, in the latter case of illuminating a reflector with a known feed pattern, the optimum taper applied across the reflector aperture would be solely dependent on the f/D ratio of the reflector instead. Nonetheless, as described in Section 3.5.2.3, the total aperture illumination taper applied is heavily dependent on both the feed pattern and the curvature (f/D ratio) of the reflector used. For the application in hand, modelling the reflector based on the

radiation properties of the feed horn is preferable since the feed horn used is a standard E-plane sectoral horn antenna that is known for producing the widest radiation pattern in azimuth.

As presented in Section 4.3, the E-plane sectoral feed horn was modelled on CST and the simulated radiation pattern in the horizontal and vertical plane is shown again in Figure 4-20. The feed pattern has a -3 dB beamwidth of 70.9 degrees and 17.2 degrees in azimuth and elevation, respectively, and a gain of 14.2 dB. A vertically truncated reflector with a horizontal dimension of 120 cm can be modelled optimally based on the properties of the feed pattern to produce a secondary beam pattern with a theoretical azimuth beamwidth of 2 degrees, maximum achievable antenna gain (~35 dB) and acceptable sidelobe level (~-20 dB).

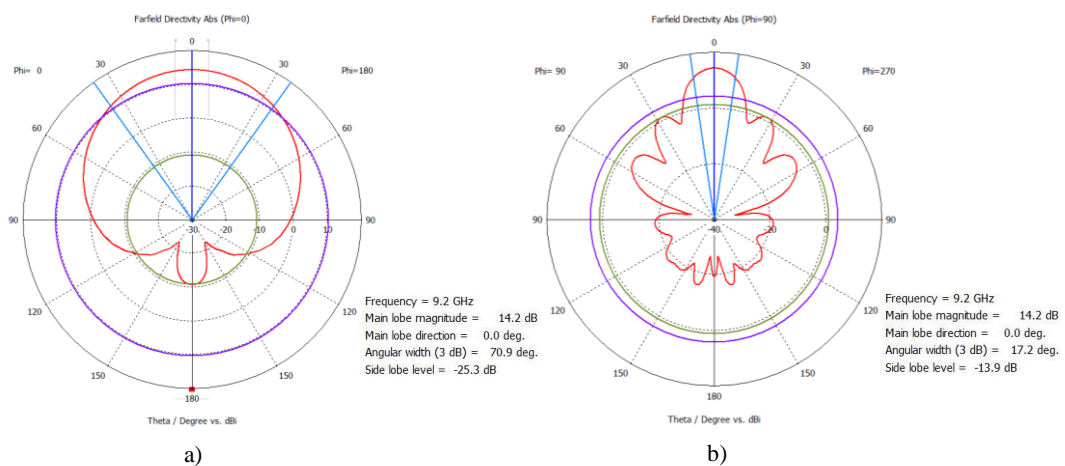


Fig 4-20. Radiation pattern of horn antenna (polar plot) in the a) H-plane and b) E-plane

The curvature (f/D ratio) and dimensions of the truncated reflector is designed according to the feed profile and the chosen aperture illumination taper that optimizes the performance of the antenna. As mentioned, the truncated reflector is essentially a rectangular section of the center of a circular paraboloid that is symmetrical about the vertex of the dish. The corners of the reflector are curved to reduce the effects of diffraction and lower the sidelobes of the beam produced. Unlike a circular parabolic reflector, the f/D ratio of a truncated reflector is different in both principal planes due to the non-circular aperture outline of the dish. Hence, the f/D ratio of the reflector in both principal planes must be individually calculated.

Since the reflector aperture has a rectangular outline, the tapering effect due to the outline of reflector aperture (τ_3) is very minimal and will be ignored. Hence, in this case the total aperture taper imposed on the reflector aperture is due to the contribution of two factors, that is; the inherent taper due to the surface curvature of the reflector, τ_1 , and the taper due to the feed pattern, τ_2 . τ_1 and τ_2 is calculated using (3-90) and (3-91), respectively.

As a rule of thumb for reflector antennas employing circular parabolic dishes, the optimum reflector illumination taper is often referred to as the aperture taper that maximizes the reflector antenna gain, and it is most commonly achieved when the power radiated by the feed horn is about 10 to 11 dB less at the edges of the dish than its maximum value at the center of the dish [81] (including the effects of space attenuation), or somewhat more if extremely low sidelobe levels are desired [82] [83]. Thus, as a first approximation in optimizing the reflector antenna performance, an aperture taper of -10 dB will be imposed across both principal planes of the reflector. To impose a taper of -10 dB across the reflector aperture the required angles subtending from the focus to the horizontal and vertical edges of the reflector, that is denoted by β_a and β_e respectively, is calculated using (4-14), and BW is the -3 dB beamwidth of the primary pattern in the desired plane.

$$\tau_1 + \tau_2 = -10 \text{ dB} \quad (4-13)$$

$$40 \log \cos\left(\frac{\beta}{2}\right) + -12\left(\frac{\beta}{BW}\right)^2 = -10 \text{ dB} \quad (4-14)$$

where $\beta = \beta_a$ in the horizontal plane and $\beta = \beta_e$ in the vertical plane

$BW = BW_a$ in the horizontal plane and $BW = BW_e$ in the vertical plane.

Given the azimuth and elevation beamwidth of the E-plane sectoral horn antenna is 70.9 degrees (BW_a) and 17.2 degrees (BW_e), respectively, (4-15) and (4-16) shows that a reflector with a β value of 57 degrees and 15.5 degrees is required in the horizontal and vertical plane, respectively, in order to successfully apply a taper of -10 dB across the principal plane of the reflector.

$$40 \log \cos\left(\frac{57}{2}\right) + -12\left(\frac{57}{70.9}\right)^2 = -10 \text{ dB} \quad (4-15)$$

$$40 \log \cos\left(\frac{15.5}{2}\right) + -12\left(\frac{15.5}{17.2}\right)^2 = -10 \text{ dB} \quad (4-16)$$

The angle subtending between the focus and the reflector outline in the horizontal and vertical plane is 114 degrees ($2\beta_a$) and 31 degrees ($2\beta_e$), respectively, which, based on the principal plane plots of the feed horn simulated, is equivalent to the -7.2 dB and -11.5 dB beamwidth of the feed radiation pattern in the azimuthal and elevation planes, respectively.

With the calculated values of β in the horizontal and vertical plane of the reflector, the relationship between β and the f/D ratio of a parabolic reflector, as shown in (4-18), allows the

appropriate f/D ratio in both principal planes of the reflector to be identified. The values of β for typical f/D ratios are shown in Table 3-1.

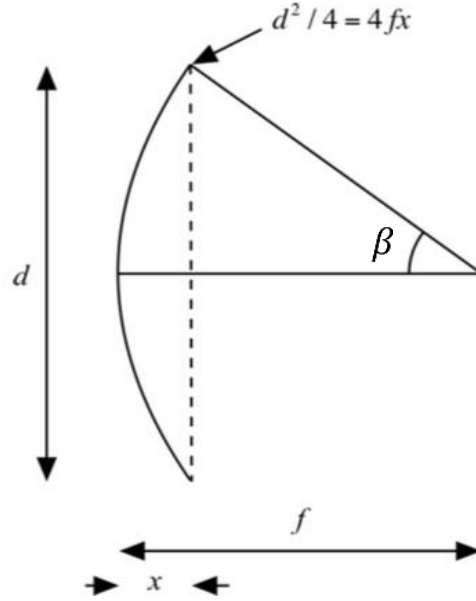


Fig 4-21. Relationship between f/D ratio of reflector and β

$$\beta = \tan^{-1} \left[\frac{d}{2(f-x)} \right] = \tan^{-1} \left[\frac{d}{2 \left[f - \frac{d^2}{16f} \right]} \right] \quad (4-17)$$

$$\tan(\beta) = \frac{8(f/d)}{16(f/d)^2 - 1} \quad (4-18)$$

A suitable f/D ratio required to apply an aperture taper of -10 dB across the reflector as it is illuminated by sectoral horn antenna is identified in the horizontal plane first, followed by the same in the vertical plane.

The angle subtending from the focal point to either horizontal edges of the reflector is denoted by β_a ($\beta = \beta_a$). The corresponding f/D ratio of the reflector in the horizontal plane is given by

$$\tan(\beta_a) = \frac{8(f/d_a)}{16(f/d_a)^2 - 1} \quad (4-19)$$

$$\tan(\beta_a) = \tan(57^\circ) = \frac{8(f/d_a)}{16(f/d_a)^2 - 1} \quad (4-20)$$

$$\frac{f}{d_a} = 0.46 \quad (4-21)$$

The f/D ratio of the reflector required to apply an illumination taper of -10 dB on the horizontal plane is 0.46. The reflector is of a very common shape as neither is it too shallow nor too deep.

The focal length f of the reflector is given by

$$f = 0.46 \times 120 \text{ cm} = 55.2 \text{ cm} \quad (4-22)$$

Similarly, the required angle subtending from the focal point to either vertical edges of the reflector to apply an aperture taper of -10 dB in this plane is denoted by β_e ($\beta = \beta_e$). The corresponding f/D ratio of the reflector in the vertical plane is given by

$$\tan(\beta_e) = \tan(15.5^\circ) = \frac{8(f/d_e)}{16(f/d_e)^2 - 1} \quad (4-23)$$

$$\frac{f}{d_e} = 1.84 \quad (4-24)$$

The f/D ratio in the vertical plane of the reflector is 1.84. The vertical dimension of the reflector, d_e , is given by

$$d_e = \frac{55.2}{1.84} = 30.1 \text{ cm} \quad (4-25)$$

In theory, the dimensions of the reflector for it to be optimally illuminated by the E-plane sectoral horn antenna must be 120 cm wide by 30 cm high. The designed reflector is essentially a portion of the center of a circular paraboloid with a width to height ratio of 4 to 1. Hence, the reflector antenna is expected to produce a secondary beam pattern with an azimuth beamwidth that is approximately four times narrower than its elevation beamwidth. An illustration of the designed reflector is shown in Figure 4-22.

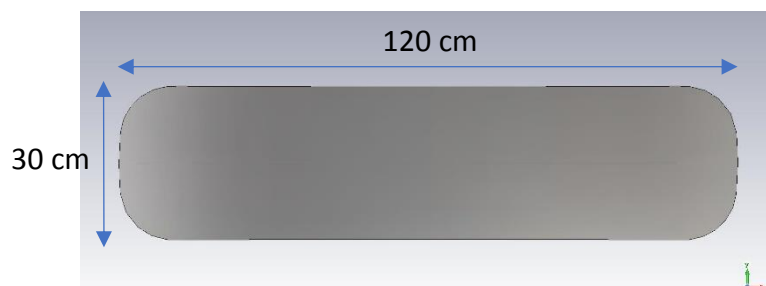


Fig 4-22. Vertically truncated parabolic reflector with calculated dimensions

The illustration shown in Figure 4-21 also provides the geometrical relationship between the depth of the reflector, x , and the diameter, D , and focal length, f , of the reflector [50], for parabolic reflectors of all f/D ratios. The depth of the reflector x is given by

$$x = \frac{D^2}{16f} \quad (4-26)$$

The reflector depth is approximately 16.3 cm in the horizontal plane and 1 cm in the vertical plane. Hence, the distance between the aperture plane of the reflector and the focal plane of the reflector, $f - x$, is 38.9 cm and 54.2 cm in the horizontal and vertical plane, respectively. The reflector depth is considerably deeper in the horizontal plane as compared to the vertical plane due to the significantly smaller f/D ratio.

Since the amount of space occupied by the reflector antenna (~ 85 cm) exceeds beyond the diameter of the existing radar platform (47 cm), the design of the feed and reflector support within the limited space available is critical in ensuring that the weight of the large antenna is evenly distributed across the radar base. This is necessary to prevent the mechanical limits of the radar from being tested during operation and to produce a balanced system, otherwise the rotating lifetime of the radar platform may be reduced, or even cause the system to be placed off balance under harsh conditions. In Section 6.2, the design of the feed and reflector support frames are based on an analysis of the weight distribution of the reflector antenna in order to successfully mount the antenna on the radar platform provided by Guidance.

4.4.3 Feed Positioning Relative to the Focus of Reflector

If the feed of a reflector antenna is shifted from the focal point in any direction along the boresight axis, the radiation pattern of the beam produced will be broadened, and the properties will deteriorate, since the rays do not collimate in free space (parallel). It is therefore important for the feed to be correctly positioned along the focal line of the reflector to optimise the properties of the beam produced from the reflector design established in Section 4.4.2. This is achieved by positioning the apparent phase center of the feed at the focus of the reflector with the main lobe of the primary beam directed towards the vertex of the reflector. However, the phase center of a feed horn is not an obvious place, and calculating the phase center location of a horn antenna may be a complex problem. Unless the feed antenna is an isotropic radiator, there is not just one absolute phase center for all enclosing angles of the antenna. Hence, only an apparent phase center of the feed can be identified. The position of the apparent phase center of the feed horn depends on the plane for which the designer wants the radiation pattern to be close to that of an isotropic radiator. Therefore, there are multiple points that can be identified

as the phase center of the feed horn, which makes it not an obvious place to position the feed horn relative to the reflector.

The far-field radiation pattern of the E-plane sectoral horn antenna is significantly narrower in elevation than in azimuth, which is due to the horn being flared in just the vertical direction. Hence, unlike pyramidal horn antennas, the phase center is situated around the aperture plane of the horn. Nevertheless, the apparent phase center of the feed is identified as the point situated along the focal line that coincides with the reflector focus, at which the secondary beam produced possesses the most favourable radiation properties. Ultimately, the designer must optimize the feed position relative to the reflector. This can be experimentally achieved by varying the feed position along the focal line of the reflector, or the distance between the center of the feed horn aperture and the focus, until the beam produced from the reflector antenna realizes the most desirable radiation properties, which in this case would be a secondary beam that exhibits the narrowest beam and the highest antenna gain.

Based on the modelling that adjusts the position of the horn aperture along the focal line of the reflector, the properties of the secondary beam produced for each value of x enables the optimum position of the feed aperture to be identified. An illustration showing the position of the horn aperture plane relative to the reflector focus is shown in Figure 4-23, where the distance between the two points is denoted by x . For instance, x is zero when the mid-point of the feed aperture plane is placed at the focus. The chosen values of x ranges from -30 mm to +30 mm in intervals of 10 mm.

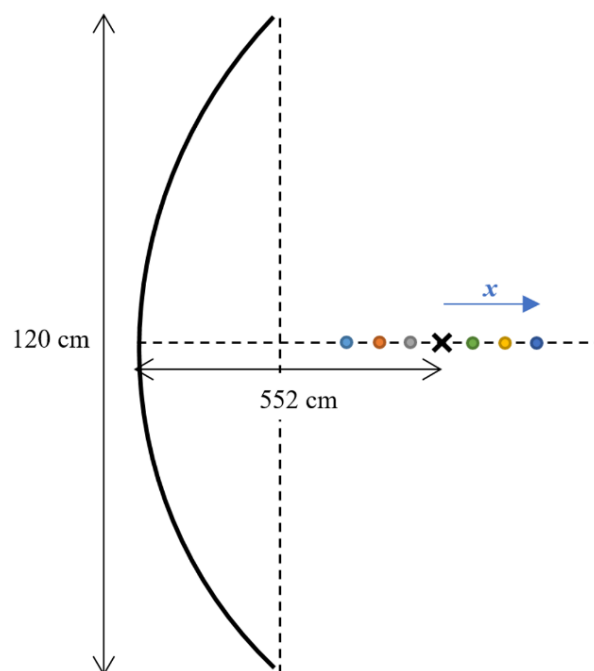


Fig 4-23. Identifying the position of the feed aperture relative to the focus of reflector

As shown in Figure 4-24, the reflector antenna employing the designed vertically truncated reflector and a feed horn that is positioned according to the illustration shown in Figure 4-23, for $x = 0$, is modelled in CST.

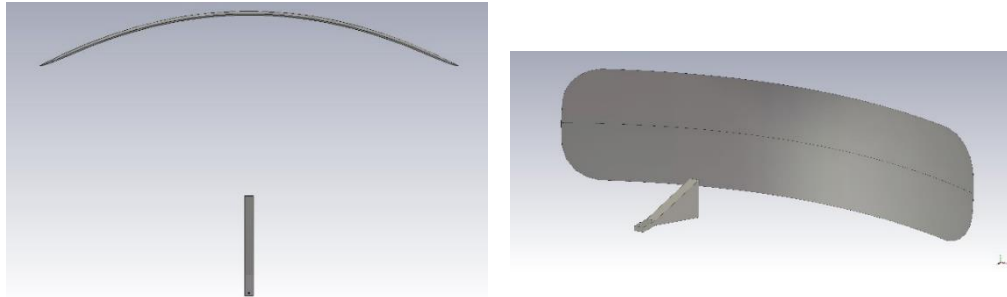


Fig 4-24. Reflector antenna arrangement ($x = 0$)

The simulated properties of the beam produced from the reflector antenna, for each value of x , is provided in Table 4-6.

x (mm)	Horizontal plane		Vertical plane		Both plane
	Azimuth -3 dB BW (deg)	Sidelobe level (dB)	Elevation -3 dB BW (deg)	Sidelobe level (dB)	
-30	2.1	-23.4	6.1	-24.3	32.3
-20	1.8	-21.2	6.1	-23.8	33.4
-10	1.6	-16.2	6.1	-23.1	34.1
0	1.6	-18.9	6.1	-22.7	34.4
10	1.6	-15	6.2	-22	34
20	1.8	-17.6	6.2	-20.9	32.9
30	2.3	-14.7	6.2	-19.8	32

Table 4-6. Optimizing the position of the feed aperture relative to the focus

The set of results obtained infers that positioning the aperture of the feed horn at the focus of the reflector ($x = 0$) optimizes the reflector antenna gain regardless of the illumination taper applied on the reflector aperture, to within an accuracy of ± 5 mm. With this arrangement, the secondary beam has an azimuth and elevation beamwidth of 1.6 degrees and 6.1 degrees respectively, with a sidelobe level of -18.9 dB and -22.7 dB and an antenna gain of 34.4 dB. As observed, shifting the position of the horn aperture in either direction along the focal line of the reflector reduces the antenna gain, at first by a small amount, and then deteriorates substantially at increasing distances away from the focus. This is caused due to defocusing of the apparent phase center of the feed from the focus, which disrupts the collimation of EM waves at the focal plane of the reflector. Hence, it is important to position the feed along the focal line of the reflector appropriately in order to optimize the properties of the beam produced. If the sidelobe

level of the secondary beam produced is prioritized instead of maximizing antenna gain, applying a larger aperture taper would be the preferable choice at the expense of a slightly reduced antenna gain.

A perspective view of the modelled reflector antenna and the simulated secondary beam pattern produced is presented in Figure 4-25. Figure 4-26 and 4-27 presents the polar plots of the secondary beam in the horizontal and vertical planes, respectively. Figure 4-28 presents the antenna far-field pattern in both principal planes.

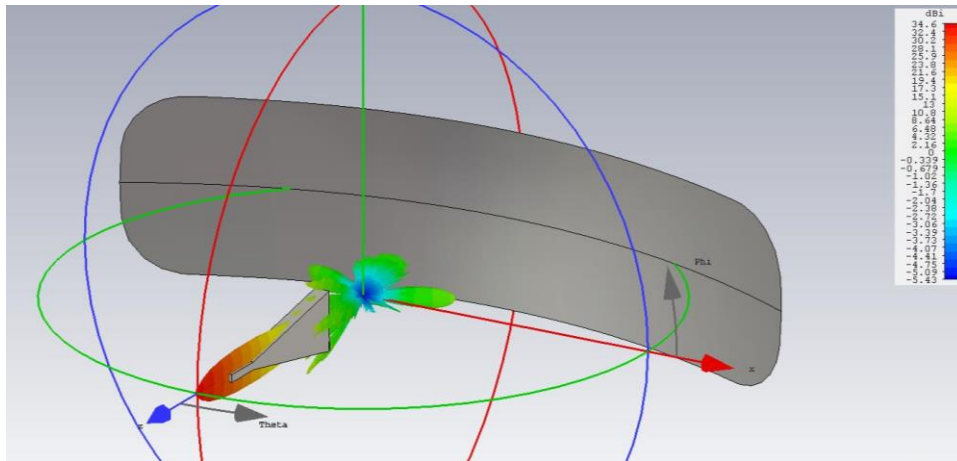


Fig 4-25. Radiation pattern of reflector antenna ($f/D = 0.46$)

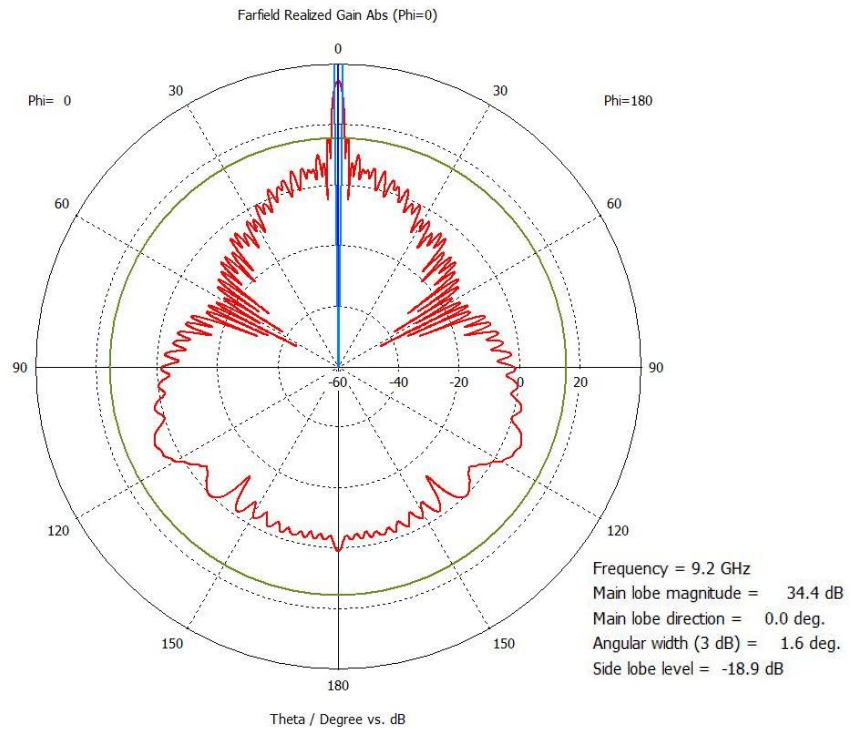


Fig 4-26. Radiation pattern of reflector antenna in horizontal plane (polar plot)

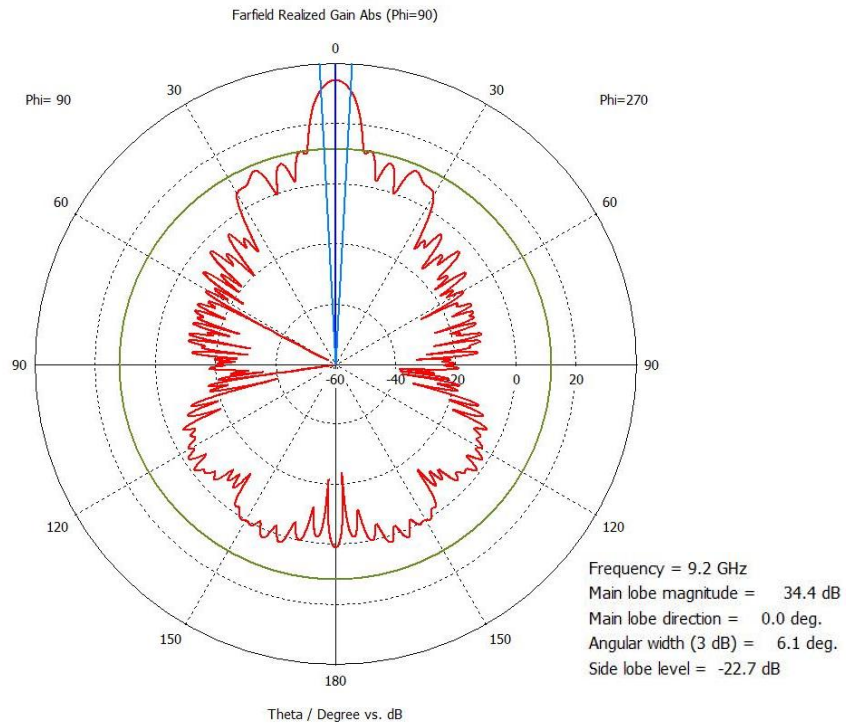


Fig 4-27. Radiation pattern of reflector antenna in vertical plane (polar plot)

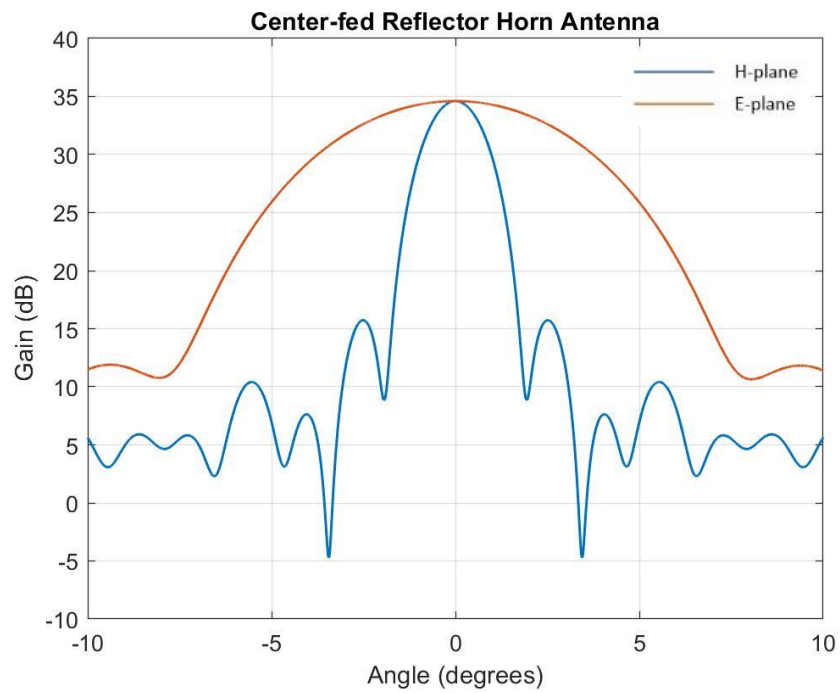


Fig 4-28. Radiation pattern of reflector antenna in both principal plane (rectangular plot)

4.4.4 Optimization of Illumination Taper to Maximize Antenna Gain

This section analyses the performance of the reflector antenna, which is based on the principal plane beamwidths, sidelobe level and gain of the secondary beam pattern, for a range of different aperture illumination taper applied on the reflector while using the same E-plane sectoral horn antenna as the feed. The aim of performing a further set of simulations is to identify an optimum illumination taper on both planes of the reflector that maximizes the antenna gain.

Since the reflector width and radiation pattern of the feed illuminating the truncated reflector is unchanged, the range of aperture taper applied on both planes of the reflector is achieved by varying the f/D ratio of the reflector. The range of aperture taper applied on both planes of the reflector is between -4 to -13 dB. The angle β_a and β_e and the corresponding principal plane f/D ratio of the reflector required to apply each of the following aperture taper τ , due to τ_1 and τ_2 , in both principal planes are calculated individually using (4-18) and presented in Table 4-7. For each value of τ , the corresponding focal length f and height of the reflector d_e is provided under the column ‘Reflector properties’.

Total Illumination Taper (dB)	Angle of subtention, β (deg)		Principal plane f/D ratio		Reflector properties	
	Horizontal	Vertical	Horizontal	Vertical	Focal Point (mm)	D.e (mm)
-4	36.5	9.8	0.677	2.916	923	317
-5	40.5	10.95	0.678	2.608	814	312
-6	44.5	12	0.611	2.379	733	308
-7	48	12.95	0.562	2.203	674	306
-8	51	13.85	0.524	2.058	629	306
-9	54	14.7	0.491	1.938	589	304
-10	57	15.5	0.46	1.837	552	301
-11	60	16.25	0.433	1.751	520	297
-12	62.5	16.95	0.412	1.678	494	295
-13	65	17.65	0.392	1.61	470	292

Table 4-7. Reflector modelling for various illumination taper

The calculated values of $2\beta_a$ and $2\beta_e$ corresponding to each value of illumination taper applied on the principal planes of the reflector aperture is presented in Table 4-8. The corresponding X dB azimuth and elevation beamwidth of the feed pattern that matches the values of $2\beta_a$ and $2\beta_e$, respectively, corresponding to each aperture taper applied is presented in Table 4-8.

Total Illumination Taper (dB)	Horizontal 2β (deg)	Azimuth BW (X dB)	Vertical 2β (deg)	Vertical BW (X dB)
-4	73	-3.2	19.6	-4
-5	81	-3.9	21.9	-5.1
-6	89	-4.6	24	-6.3
-7	96	-5.3	25.9	-7.5
-8	102	-5.9	27.7	-8.8
-9	108	-6.6	29.4	-10
-10	114	-7.2	31	-11.5
-11	120	-7.9	32.5	-12.9
-12	125	-8.5	33.9	-14.3
-13	130	-9	35.3	-15.7

Table 4-8. X dB principal plane beamwidths subtending to the reflector edges

The properties of the beam produced from the reflector antenna is simulated and presented in Table 4-9 across the range of aperture taper applied, from which the reflector design (f/D ratio), or the optimum aperture taper applied across the reflector, that achieves the highest antenna gain is identified.

Total Illumination Taper (dB)	Horizontal plane		Vertical plane		Both plane Gain (dB)
	Azimuth -3 dB BW (deg)	Sidelobe level (dB)	Elevation -3 dB BW (deg)	Sidelobe level (dB)	
-4	1.4	-15.1	5.1	-17.5	33.9
-5	1.5	-15.1	5.3	-18.5	34.1
-6	1.5	-15.8	5.5	-19.4	34.2
-7	1.5	-16.8	5.7	-20.3	34.4
-8	1.5	-17.8	5.8	-21.3	34.5
-9	1.5	-16.9	6	-21.7	34.2
-10	1.6	-18.9	6.1	-22.7	34.4
-11	1.6	-20	6.4	-23.5	34.3
-12	1.6	-18.6	6.5	-24	33.8
-13	1.7	-22.4	6.7	-25.2	34

Table 4-9. Simulated radiation properties of reflector antenna for various f/D ratios

The simulated results infers that applying an excessively small or large aperture taper causes the antenna gain to be substantially reduced, whereas the sidelobe level continuously decreases as the aperture taper applied is increased from -4 dB to -13 dB. The results verify an aperture taper of -10 dB to be the optimum value that maximizes the antenna gain. The reflector antenna produces a secondary beam with a -3 dB beamwidth of 1.6 degrees and 6.1 degrees in azimuth and elevation, respectively, and an antenna gain of 34.4 dB. The f/D ratio of the reflector suitable to impose an aperture taper of -10 dB across the reflector aperture is 0.46 and 1.84 in the horizontal and vertical plane, respectively. With this reflector antenna design the angle subtended between the focus and the edges of the reflector in the horizontal and vertical

planes matches the -7.2 dB and -11.5 dB beamwidths of the feed pattern in the azimuthal and elevation planes, respectively.

4.5 Theoretical and Simulation Results of the Antenna Radiation Properties

The reflector antenna design established in Section 4.4 was simulated on CST to realize the radiation properties of the reflector antenna. The simulated radiation characteristics of the beam produced is an accurate representation of the actual performance of the reflector antenna under ideal conditions. In addition to the simulated properties, the theoretical radiation properties of the beam produced are provided and assessed in this section to closely approximate the expected performance of the reflector antenna. This section progresses with a comparison between the calculated theoretical and simulation results of the antenna radiation. The radiation properties analysed are the principal plane beamwidth and the effective gain of the antenna.

4.5.1 Theoretical Results

The beamwidth of the beam produced from a parabolic reflector antenna is approximated by

$$BW \approx k_1 \frac{\lambda}{D} \quad (4-27)$$

For a paraboloid reflector of a non-circular aperture, such as a vertically truncated reflector, a suitable approximation for the value of k_1 is 60. The reflector dimension in the plane in which the radiation properties of the beam produced is to be calculated is denoted by D . Reflector apertures with a different horizontal and vertical dimension will radiate a beam with different beamwidths in these directions.

Given the width of the reflector to be 120 cm, at an operating frequency of 9.2 GHz ($\lambda = 3.26$ cm) the theoretical azimuth beamwidth is 1.6 degrees, as approximated by

$$BW_{az} \approx \frac{60\lambda}{D_a} \quad (4-28)$$

Subsequently, given the vertical dimension of the reflector to be 30 cm, the theoretical elevation beamwidth is 6.5 degrees, as approximated by

$$BW_{el} \approx \frac{60\lambda}{D_e} \quad (4-29)$$

In relation to the principal plane beamwidth of the radiated beam is the approximate reflector antenna gain. Since the reflector has a rather elliptical aperture outline and the beamwidth of the radiated beam is several times narrower in azimuth than in elevation, the cross-sectional area of the energy of the beam produced from the antenna can be approximated by a pyramidal section. The gain of such reflector antennas can be approximated by (4-30), where the beamwidths are expressed in radians.

$$G = \frac{4\pi}{BW_{az}BW_{el}} = \frac{12.57}{BW_{az}BW_{el}} \quad (4-30)$$

The theoretical gain of the reflector antenna that produces a secondary beam with a principal plane beamwidths of 1.6 degrees and 6.5 degrees is approximately 3883 or 35.9 dB.

A more accurate method of approximating the reflector antenna gain is based on the effective aperture area of the reflector. For reflector antennas employing parabolic reflectors that are designed to optimize antenna gain, a directive beam that has a fan-shaped pattern generally causes the gain to be reduced by a factor of 0.7 or 1.5 dB [84], or an aperture efficiency of 70 percent. Reflector antennas that produce other special beam shapes also tend to have a lower aperture efficiency, which, for a given reflector area, corresponds to a lower antenna gain. The relationship between the physical collecting area of the reflector surface, which in this case is approximated by the product of the vertical and horizontal dimensions of the reflector due to its approximately rectangular aperture outline, and the gain of the parabolic reflector antenna is approximated by

$$G = \varepsilon_{ap} \frac{4\pi A}{\lambda^2} \quad (4-31)$$

Given that the reflector dimensions are 120 cm by 30 cm ($A = D_e D_a = 0.36 \text{ m}^2$) and assuming an aperture efficiency of 70 percent ($\varepsilon_{ap} = 0.7$), the theoretical reflector antenna gain is approximately 2980 or 34.7 dB when operational at 9.2 GHz ($\lambda = 0.0326 \text{ m}$).

4.5.2 Comparison of Theoretical and Simulation Results

This section provides a comparison between the calculated theoretical and simulation results of the reflector antenna performance. The two separate sets of results obtained are presented in Table 4-10. The principal plane beamwidths and effective gain of the beam produced by the reflector antenna are analysed since these are the underlying properties that were optimized in designing the antenna to satisfy the requirements of the application.

Radiation Properties	Theoretical	CST Simulation
Azimuth Beamwidth (deg)	1.6	1.6
Elevation Beamwidth (deg)	6.5	6.1
Antenna Gain (dB)	34.7	34.4

Table 4-10. Theoretical and simulation results of reflector antenna radiation properties

The simulated secondary beam pattern has an azimuth and elevation beamwidth of 1.6 degrees and 6.1 degrees, respectively, with a gain of 34.4 dB, whereas the calculated theoretical azimuth and elevation beamwidth of the beam produced by the same reflector antenna is 1.6 degrees and 6.5 degrees, respectively, with a gain of 34.7 dB. The radiation properties of the secondary beam obtained from the two sets of results satisfies one another with a deviation that is less than 0.3 dB, or 6 percent in both planes. The agreement makes the results obtained reliable and convincing representation of the performance of the physical reflector antenna. Moreover, the agreement in simulation and theoretical results shows that an appropriate value of k_1 in (4-27) for a parabolic reflector of this type is approximately 60, while the results also suggests that the aperture efficiency of the reflector antenna employing a truncated reflector is approximately 0.7, which validates [84].

4.6 Summary

This chapter outlines the modelling and design of a center-fed reflector antenna system that produces a secondary beam with the required radiation properties that is suitable for the application in hand. Following the chosen radar parameters of the proposed reflector antenna system that was provided in Section 4.1, the remaining of Chapter 4 focuses on the feed horn and reflector design of the reflector antenna system.

Section 4.2 provides the modelling of the WR90 adapter that achieves optimum RF performance at the chosen operating frequency of the radar. The adapter is used to feed the horn antenna, which in turn will be used as the feed to the reflector antenna. Given the back-short distance of the WR90 adapter to be fixed at 7 mm, the probe length of the WR90 adapter was modelled to achieve optimum RF performance at 9.2 GHz. The optimization of the adapter's transition probe has shown the center frequency of the return loss to be closest to 9.2 GHz when the probe length of the adapter is 5.5 mm (to an accuracy within 0.5 mm), from which the S_{11} and VSWR is -21.2 dB and 1.19 respectively, and at most -15 dB and 1.35 respectively across the X-band frequency spectrum.

Section 4.3 provides the modelling of a E-plane sectoral horn antenna that achieves maximum gain, which was based on the optimal relation between the horn apex length and vertical dimension of the horn aperture. The horn antenna design is extended from the WR90 adapter that was designed in Section 4.2. The simulated principal plane beamwidths of the horn antenna is 70.9 degrees and 17.2 degrees respectively, with an antenna gain of 14.3 dB and sidelobe levels of -25.3 dB and -13.9 dB in the respective planes.

Section 4.4 has outlined the steps taken in the design of a reflector according to the radiation properties of the feed, which in this case is of the E-plane sectoral horn antenna designed in Section 4.3. The reflector modelling has shown an illumination taper of -10 dB across both planes of the reflector aperture to be the optimum taper that produces a reflector antenna with the highest possible gain. To achieve this amount of tapering applied as it is illuminated by the feed horn, the reflector with a pre-determined width of 120 cm and a calculated height of 30 cm must have a f/D ratio of 0.46 and 1.84 in the horizontal and vertical planes of the reflector, respectively. The simulated principal plane beamwidths of the beam produced from the reflector antenna is 1.6 degrees and 6.1 degrees respectively, with a corresponding sidelobe level of -18.9 dB and -22.7 dB and an antenna gain of 34.4 dB.

A comparison of the calculated theoretical and simulated performance of the reflector antenna provided in Section 4.5 has shown close agreement between the two sets of results. The deviation between the theoretical and simulated radiation properties of the antenna is less than 6 percent in both planes. The cross validation of results provides a convincing representation of the performance of the physical reflector antenna, which will be manufactured accordingly for this project based on the modelling of the antenna presented in this chapter.

Chapter 5

Radar Scanning and Imaging Strategy

This chapter consists of four sub-sections. Section 5.1 discusses the method introduced to achieve monopulse in the horizontal plane of a mechanical scanning radar, which employs a parabolic reflector antenna, through the creation of a pair of off-axis lobes that overlaps one another along the vertical boresight axis of the antenna. The approach taken to produce the pair of simultaneous off-axis lobes required for the implementation of amplitude monopulse on the reflector antenna is discussed, which includes the modelling of a well-defined dual-horn feed arrangement. The desired enhancement in angular accuracy, in azimuth, of an existing radar employing the center-fed parabolic reflector antenna that was designed in Section 4.4, is achieved through the formation of the monopulse difference pattern.

Section 5.2 introduces a novel signal processing technique that aims to provide a considerable enhancement in resolution performance of an existing radar without modifying the RF circuitry of the radar. It is a non-coherent post-processing technique that is applied on the received radar signal to produce a sharpened point-target response that, depending on the properties of the antenna radiation pattern, allows for a substantial reduction in beamwidth and therefore an increased clutter resilience to be observed. The processing technique can be incorporated by means of a simple digital processing box, which is interposed between the radar output and the video display. Section 5.2.3 discusses the application of the signal processing technique on typical coastal surveillance radars and/or navigational radar systems and the benefits that the technique provides, due to the enhancement in detection performance of the radar, on coastal surveillance and other similar navigational applications. This is followed by Section 5.2.4, which similarly demonstrates the technique on the sum pattern of a monopulse antenna that, without processing, exhibits poor resolution properties as compared to that of the original system. Both sections outline the benefits of the processing technique on each application.

5.1 Amplitude Monopulse Reflector Antenna

The reflector antenna system in Section 4.4 is designed to have an imaging capability of vessels at short and long detection range (tens of km) with relatively high angular resolution that is achieved through the narrow azimuthal beamwidth (1.6 degrees) of the beam produced. The reflector antenna uses a vertically truncated centre-fed parabolic reflector that is 120 cm wide and is illuminated by an E-plane sectoral horn antenna with an illumination taper of -10 dB applied across both principal planes. The angular resolution of the radar in azimuth is sufficient for close range operation; in the detection range of 10 km or so, but this may not be the case for significantly longer-range operation as the angular resolution deteriorates with increasing operating range. For instance, the angular resolution of the reflector antenna in azimuth is approximately 350 meters when operating at a detection range of 20 km. This angular resolution is considered quite poor under these circumstances and has become a likely cause for two or more targets to be detected within the same beamwidth at any point in time, especially given that typical carrier vessels are a few hundred meters in length and the presence of many other types of smaller vessels within the background. Moreover, this would also make the radar unsuitable for more accurate target tracking operations as the precise position of an identified target within the large resolution cell of the main lobe produced is unknown. Hence, in most conventional cases a poor angular resolution would relate to a radar system with a poor angular accuracy, which is vital for target tracking operations. In any reflector antenna system, producing a very narrow azimuth beamwidth is most commonly achieved by illuminating a significantly large reflector that could extend to several meters in diameter. This method is frequently opted for in many applications that requires both very high angular resolution and accuracy for effective target discrimination and tracking, respectively. However, employing a very large reflector often proves to be too costly to manufacture and would also be impractically large, immobile and visually unattractive when mounted on a surveillance radar.

Given an existing mechanical tracking scanning radar, instead of increasing the dimensions of a reflector to enhance the resolution and/or angular accuracy of the radar system, an alternative method of achieving the angular accuracy of a narrow beamwidth can be realized through the implementation of amplitude monopulse on either plane of an existing reflector antenna. This requires a monopulse feed to be implemented on the existing reflector to produce a pair of simultaneous lobes in the horizontal plane. In a 2D monopulse radar, a further enhancement in angular accuracy is achievable through the means of analysing the radar returns from a pair of slightly off-axis simultaneous lobes produced in the desired plane. On the other hand, a 3D monopulse radar is required for the detection and tracking of targets in both principal planes, instead of one. Hence, analysing the radar returns from a pair of slightly off-axis simultaneous beams produced in both principal planes are required to realize the enhancement

in angular accuracy in azimuth and elevation, which would require a more complex feed arrangement from the design perspective as two pairs of off-axis simultaneous lobes will be required to implement amplitude monopulse in both planes. The superior angular accuracy of a monopulse reflector antenna, as compared to its center-fed counterpart, is achieved from the improvement in angular accuracy due to the implementation of monopulse and from the natural accuracy of the original center-fed reflector antenna. Hence, it is significant that the pair of off-axis lobes has a narrow -3 dB beamwidth itself.

Since the antenna developed in this project is mainly intended to provide for coastal surveillance and monitoring of vessels and hovering targets above the sea over long distances, the angular resolution and accuracy of the reflector antenna in azimuth is particularly of interest, whereas the elevation beamwidth is not critical. Therefore, it is sufficient to retain a 2D radar system that can provide accurate monitoring and detection capabilities in azimuth only. The detection accuracy of the reflector antenna designed in Section 4.4 can be significantly improved through the implementation of amplitude monopulse on the horizontal plane of the existing antenna. While there are various monopulse feed designs for reflector antennas, a dual-horn feed arrangement is proposed to implement this.

5.1.1 Amplitude Monopulse in a Single Plane

Thus far, simultaneous lobing operation in two mutually perpendicular planes of a 3D radar system have been discussed in Section 2.2.1.3, whereas implementing monopulse technique in just the azimuthal plane is required for the application in hand. Simultaneous lobing in the horizontal plane of the radar can be achieved by splitting the transmit signal into two parts before it is radiated from the corresponding antennas to create two simultaneous off-axis beams from the reflector that overlaps one another along the boresight axis of the antenna, from which the sum and difference patterns is formed in the desired plane.

The implementation of amplitude-comparison monopulse in the horizontal plane of the reflector antenna designed in Section 4.4 is achieved by illuminating the vertically truncated parabolic reflector using a pair of off-axis E-plane sectoral horn antenna. The proposed dual-horn feed arrangement comprises of a pair of sectoral horn that are slightly displaced from the optical axis at opposite directions. The pair of feed horn then illuminates the truncated reflector about the vertex to generate the pair of off-axis beams required in a monopulse antenna (Figure 5-1). In a 2D monopulse radar only a pair of beams are radiated in the desired plane, that is the left and right lobe with respect to the nominal beam axis, and only one sum and difference signal is created in that plane. To ensure that the pair of secondary beams produced are identical to one another the radiation pattern of both feed horns used must be identical.

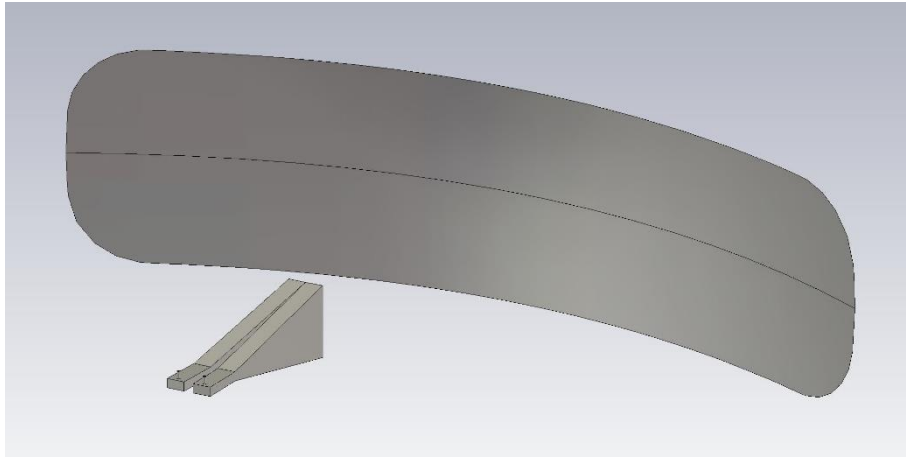


Fig 5-1. Reflector antenna with proposed monopulse feed

During transmission, the transmit signal is divided equally into two parts and fed to the pair of feeds to produce two signals of equal phase at slightly different directions. The position of the two feeds are symmetrical about the focal line of the reflector and tilted towards one another by a defined angle to radiate a pair of converging off-axis primary beams towards the center of a common reflector. The main lobe direction of the beams (beam 1 and beam 2, as shown in Figure 5-2) produced from the reflector is expected to peak at an angle off the center of the normal axis that is approximate and proportional to the feed tilt applied. Hence, the angular displacement applied on the pair of feed horn determine the properties of the off-axis lobes produced and the crossover point between them, which is used to create the sum and difference pattern of the monopulse antenna in the horizontal plane. The overlapping lobes superimpose naturally along the boresight without introducing any nonlinear effects, creating the sum transmit beam. In reception, the horn antenna outputs are connected to the monopulse comparator (coupler) to create the sum and difference signals before it is fed to the respective sum and difference channels. As mentioned, the output of these two receiver channels are responsible for providing the necessary information of the detected target in terms of target range and angular position relative to the boresight axis. Using this configuration, The detection performance of the monopulse antenna in azimuth is, therefore, dependent on the feed tilt applied about the reflector vertex. Nonetheless, implementing monopulse in just one plane would substantially reduce the manufacturing cost of the radar due to a simpler monopulse feed, and also a much simpler RF circuitry since only two channels are required, instead of three channels in a 3D monopulse radar.

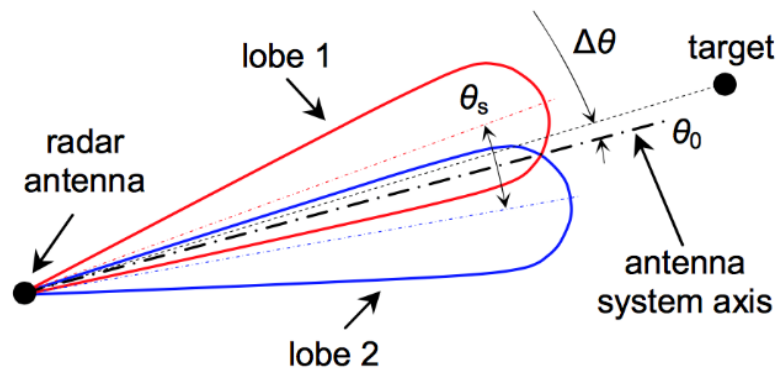


Fig 5-2. Pair of off-axis lobes for sum & difference monopulse [33]

When the parabolic reflector is illuminated about the vertex using a pair of offset feed, the pair of simultaneous off-axis lobes produced is directed away from the boresight axis, in opposite directions, at an angle that is proportional to the angular displacement applied on the respective feed with respect to the focal point of the reflector. The proportionality factor between the feed tilt applied, θ_i , and the deflection angle, θ_r , of the corresponding off-axis beam produced is known as the beam deviation factor (BDF), which is smaller than unity and varies with the curvature (f/D ratio) of the parabolic reflector. Considering the BDF of the parabolic reflector into account, the total squint angle formed, θ_s , between the two simultaneous off-axis lobes produced is similar, and proportional, to the sum of the angular displacement applied on each feed. The relationship between the angular displacement of the feed about the vertex of the reflector and the corresponding deflection angle of the main lobe of the beam produced from the reflector is elaborated in Section 5.1.2 for reflectors across a wide range of useful f/D ratios, and will be used to create the pair of off-axis beams that is suitable for the implementation of monopulse on the vertically truncated parabolic reflector.

5.1.2 Beam Deviation Factor for Parabolic Reflectors of Useful Shapes

Assuming an offset feed is used to illuminate a plane reflector from a certain angle, θ_i , the beam deflection angle of the secondary beam produced with respect to the normal axis, denoted by the vertical dotted lines, is equivalent to θ_i . The proportionality factor, or beam deviation factor, is unity for a plane reflector (Snell's Law) ($\theta_i = \theta_r$). Thus, the angle formed between the pair of lobes produced, or squint angle, is $2\theta_i$ for the case of illuminating a plane reflector with a pair of offset feed that is symmetrical along the normal axis.

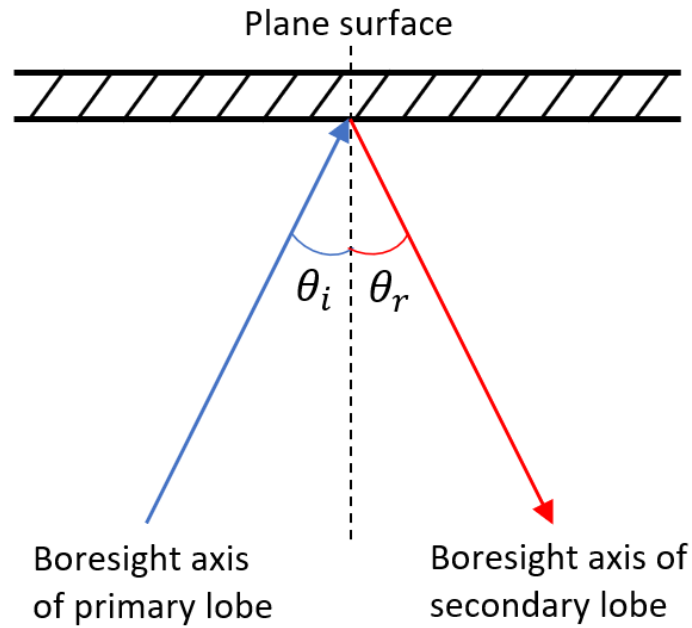


Fig 5-3. Illuminating a plane reflector surface

A plane wave incident upon a parabolic reflector is transformed into a converging field upon reflecting the parabolic reflector surface. Except for diffraction effects a wave or normal incidence is perfectly focused, but for the case of illuminating a parabolic reflector about its vertex with an offset feed horn that is laterally displaced from the focus of the reflector along the focal plane by a distance, d , there are several aberrations that distort the focal region fields. Apart from these aberrations, lateral displacement of the feed causes the secondary beam produced to be driven off-axis to the opposite side of the feed, which results in scanning the reflector beam to an angle θ_r , in proportion to the feed displacement applied. Thus, the angle between the focal line of the reflector and the secondary beam produced, or also known as the beam deflection angle, θ_r , is proportional to the feed tilt applied, θ_i , by the BDF of the reflector. An illustration of producing an off-axis beam from a parabolic reflector by illuminating the collecting surface about its vertex is shown in Figure 5-4.

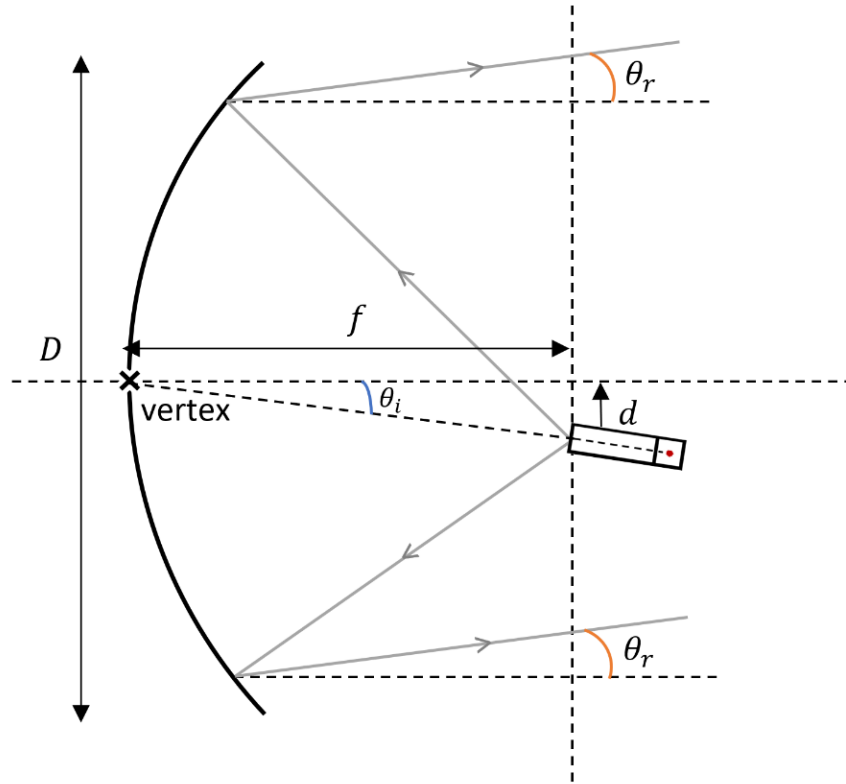


Fig 5-4. Illumination of reflector about its vertex to produce an off-axis beam

The relationship between θ_i and θ_r for a parabolic reflector of any given shape is described by the BDF, given by

$$\text{BDF} = \frac{\theta_r}{\tan^{-1}(d/f)} = \frac{\theta_r}{\theta_i} \quad (5-1)$$

which is effectively the ratio of θ_r to θ_i , both measured from the axis of the reflector with the vertex as origin [85]. The beam deflection angle is a factor of the feed tilt applied given by the BDF, which varies with the f/D ratio of the reflector. The BDF of a reflector can also be expressed in terms of the f/D ratio of the reflector. It is given by

$$\text{BDF} = \frac{\theta_r}{\tan^{-1}(d/f)} \quad (5-2)$$

$$\frac{d}{f} = \tan\left(\frac{\theta_r}{\text{BDF}}\right) \quad (5-3)$$

$$\frac{f}{d} = \cot\left(\frac{\theta_r}{\text{BDF}}\right) \quad (5-4)$$

$$\text{BDF} = \frac{\theta_r}{\cot^{-1}(f/d)} \quad (5-5)$$

Figure 5-5 illustrates the BDF of a parabolic reflector as a function of the reflector curvature.

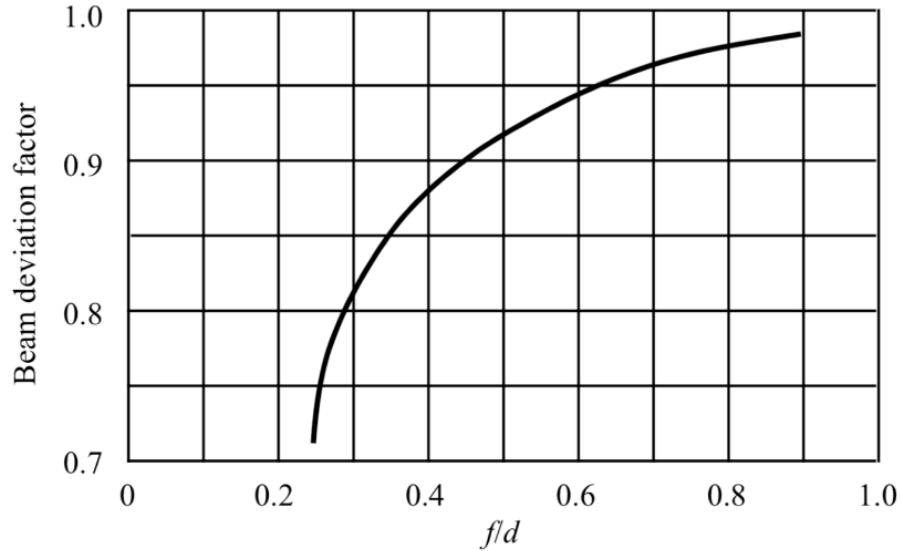


Fig 5-5. Beam deviation factor of parabolic reflector as a function of reflector curvature [50]

The beam deviation factor of a parabolic reflector increases with its f/D ratio. It is exponentially lower for deep parabolic reflectors (low f/D ratio) as compared to shallow dishes (high f/D ratio). For a parabolic surface, The relationship between the incident and reflected wave can be simply described as $\theta_r = k\theta_i$, where k is the beam deviation factor of a particular circular parabolic dish. The proportionality factor for parabolic reflectors in the useful range of shapes is generally between 0.85 and slightly less than unity ($0.4 < f/D < 0.7$).

Unlike a center-fed reflector antenna, the boresight axis of the feed is not along the focal line of the reflector. It is known in reflector antenna design that the phase center of the feed must be positioned on the focus of the reflector to produce a collimated secondary beam with the highest achievable gain. By tilting the laterally displaced feed from the focus about the vertex of the parabolic reflector, the properties of the off-axis beam deteriorates with increasing angular displacement of the feed. The affected properties of the secondary lobe includes a reduction in directivity, increase in principal plane beamwidth of the main lobe and a series of neighbouring side-lobes, known as coma lobes, to be formed along either side of the displaced beam. The extent of these undesirable effects on the properties of the radiated beam can be described in terms of the angular displacement of a directive feed from the focus as it illuminates towards the vertex of the reflector. In addition to these pattern changes an antenna initially matched in impedance with the feed on axis will undergo an impedance change as the

feed is tilted [27]. The variation of antenna gain, which is expressed as the ratio of the gain of the offset beam produced to the gain of the beam produced by a center-fed parabolic reflector employing the same feed and reflector, with feed tilt applied (in beamwidths) was experimentally measured and is presented in Figure 5-6 for reflectors of several f/D ratios.

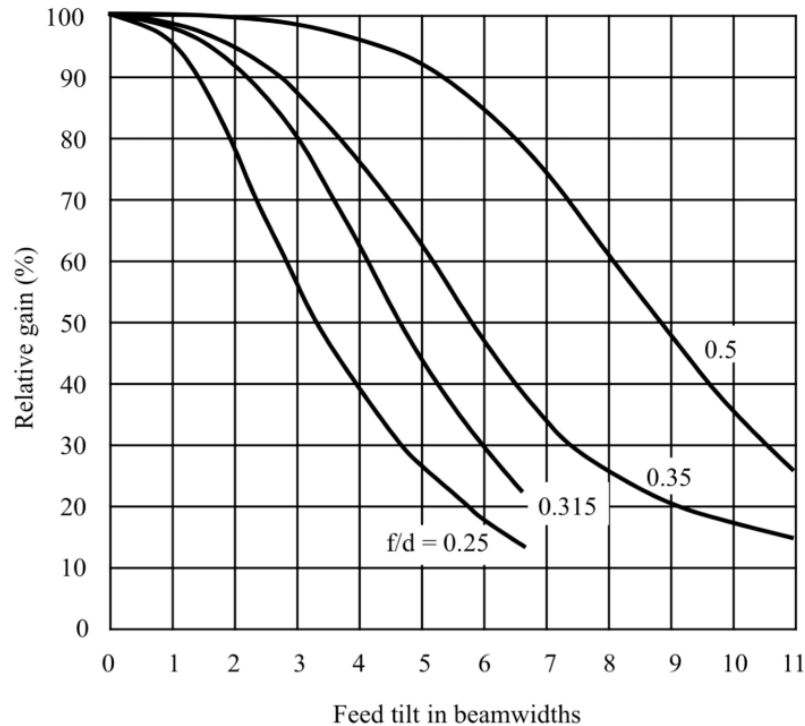


Fig 5-6. Dependence of antenna gain on feed tilt and reflector curvature [50]

When a small feed tilt is applied the properties and shape of the off-axis lobe produced deteriorates by only a small fraction as compared to the main lobe of the beam produced by a center-fed reflector. The offset lobe produced deteriorates a lot more rapidly, with increasing coma and astigmatism on the off-axis lobe produced, as the angle of tilt applied on the feed is increased beyond a certain extent. For a given angular displacement applied on the feed, the effect of feed tilt on the properties of the secondary beam produced is also dependent on the shape of the reflector - it is worst on parabolic reflector with a low f/D ratio. This method of producing an off-axis lobe is therefore more suitable on reflector antennas employing shallow reflectors (high f/D ratio) as the reduction in effective gain of the secondary beam produced with increasing feed tilt (in beamwidths) applied is significantly less pronounced. Nonetheless, regardless of the f/D ratio of the reflector, this method of producing an off-axis lobe is generally limited to only small deflection angles of a few beamwidths before the properties of the lobe produced deteriorates beyond an acceptable level. Though, a very small angular displacement of the feed in the range of a few degrees is usually sufficient in many applications where the required deflection angle of the off-axis lobe produced from the reflector is very small. In such

cases of producing minimally offset beams ($\theta_r < 2^\circ$), the undesirable effects of feed tilt on the properties of the secondary beam produced are very small, which has limited to no realizable influence on the performance of the radar antenna.

5.1.2.1 Producing Off-axis Beam through Lateral Displacement of the Feed

The vertically truncated reflector designed in Section 4.4.2 can be illuminated about the vertex to produce an off-axis beam with a range of beam deflection angle by applying a range of angular displacement, θ_i , on the E-plane sectoral horn antenna. For a center-fed parabolic reflector, $\theta_i = 0^\circ$. Figure 5-7 presents a simple illustration of the method of reflector illumination and Table 5-1 provides the lateral displacement of the phase center of the horn from the focus of the reflector along the focal plane, d , for different values of θ_i , ranging from 0 to 10 degrees and the simulated properties of the off-axis beam produced for θ_i .

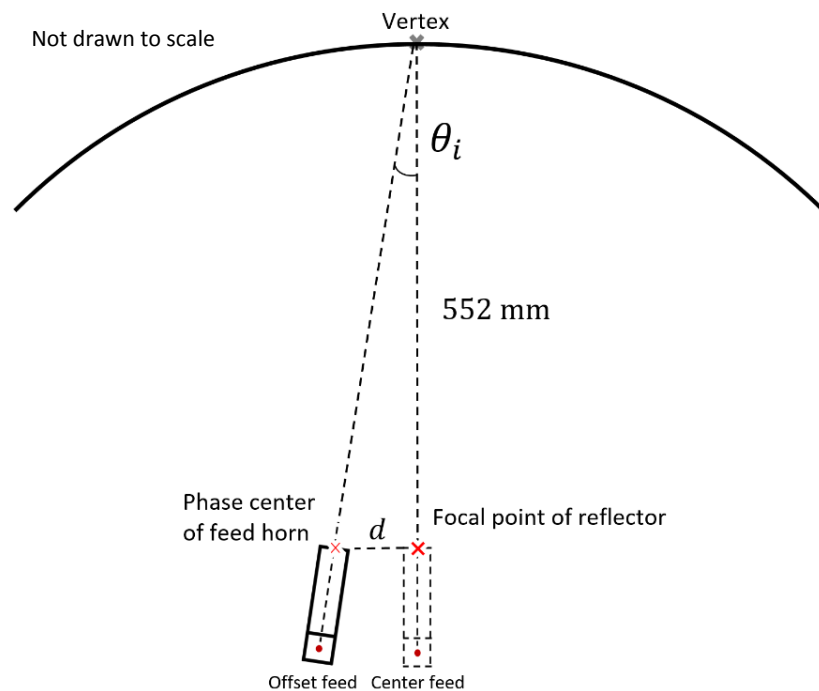


Fig 5-7. Illuminating the parabolic reflector about its vertex across a range of feed tilt, θ_i .

θ_i	d (mm)	θ_r	Azimuth -3 dB BW (deg)	Sidelobe level (dB)	Gain (dB)
0	0	0	1.6	-18.9	34.4
1	9.6	0.9	1.6	-16.1	34.4
2	19.3	1.7	1.6	-14.2	34.3
3	28.9	2.6	1.6	-12.5	34.2
4	38.6	3.4	1.6	-11.1	34.1
5	48.3	4.3	1.7	-10.1	33.9
6	58	5.2	1.7	-8.9	33.7
7	67.8	6.1	1.7	-8	33.4
8	77.6	6.9	1.7	-7.1	33.1
9	87.4	7.9	1.8	-6.4	32.7
10	97.3	8.8	1.9	-5.7	32.2
...
15	147.9	13.7	2.4	-3.8	30.9
...
20	200.9	18.9	2.6	-4.2	30

Table 5-1. Properties of radiated beam across the range of feed tilt applied

The plot presenting the dependence of antenna directivity (i.e. assuming 100% radiation efficiency) on the feed tilt applied about the reflector vertex is provided in Figure 5-8 for a vertically truncated parabolic reflector with a f/D ratio of 0.46.

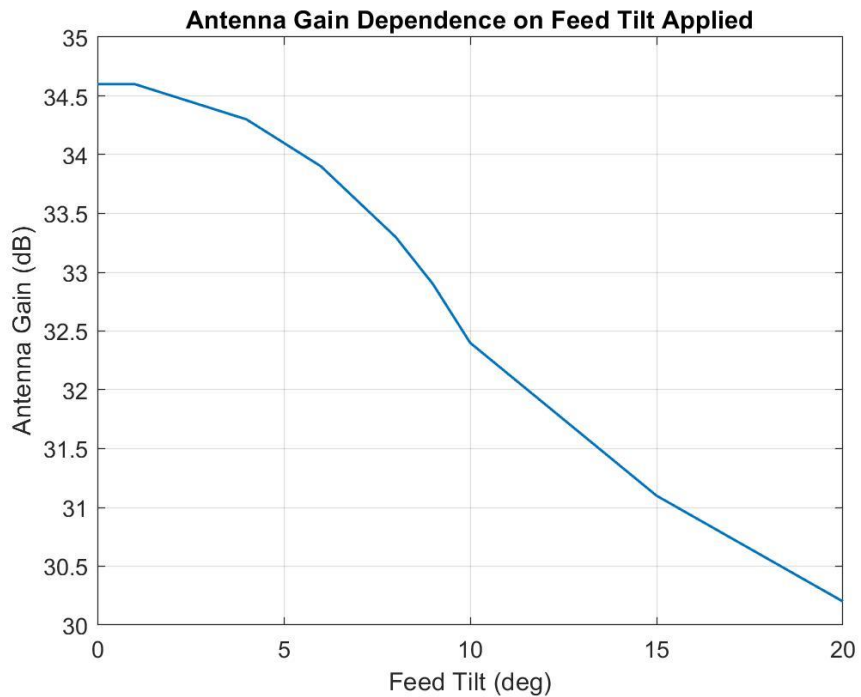


Fig 5-8. Dependence of antenna gain on feed tilt for $f/D = 0.46$

The simulation of the parabolic reflector antenna designed in Section 4.4, across the range of increasing feed tilt applied, shows that the sidelobe level and gain of the off-axis beam produced from the vertically truncated reflector ($f/D = 0.46$) at first deteriorates by a small amount as the feed tilt begins to increase, and worsens at higher values of θ_i . The deterioration in properties of the off-axis beam produced at small values of θ_i is insignificant as the displacement of the phase center from the focus is much smaller than the focal length of the dish. Hence, this method of producing an off-axis beam by applying an angular displacement on the feed about the vertex of the reflector is only suitable for producing an off-axis beam from a parabolic reflector with small deflection angles, in the range of a few beamwidths, and is useful in various applications where relatively small beam deflection angles are required and low sidelobe requirement is not critical. *Rush and Ludwig* has proven that a higher gain is achieved by pointing the displaced directional feed parallel to the boresight axis of the reflector instead of redirecting it toward the vertex, unless the f/D ratio of the reflector is very large or there is an excessive spillover of energy [27]. However, laterally displacing the feed without applying a feed tilt would limit the range of deflection angle that can be achieved and also prevent the beam direction from being controlled flexibly.

The plot of the deflection angle of the main lobe produced versus the feed tilt applied is presented in Figure 5-9, where the beam deviation factor of the parabolic reflector ($f/D = 0.46$) is given by the slope of the graph.

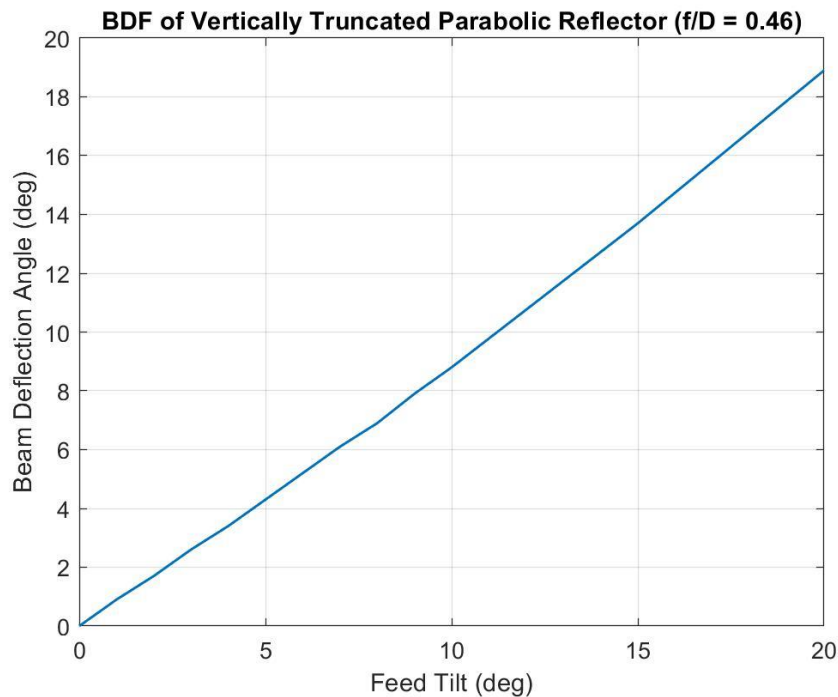


Fig 5-9. Reflected angle vs. incident angle for a vertically truncated reflector (f/D ratio = 0.46)

The calculated BDF of the vertically truncated reflector, given by the gradient of the simulated plot, is 0.87 when it is illuminated across a range of a few beamwidths, and this increases rather exponentially at larger incident angles of illumination. The BDF of the reflector designed in Section 4.4.2 highly conforms to the plot shown in Figure 5-5, where the BDF of a circular parabolic reflector with a f/D ratio of 0.46 is 0.9.

Opting for this method of illumination to achieve beam scanning on the vertically truncated reflector shows that the maximum deflection angle of the beam produced that can be scanned with a sidelobe in the order of -10 dB and at most 1 dB loss in gain is 4.3 degrees, or approximately 2.5 beamwidths, given that the beam produced by the center-fed reflector antenna has an azimuth beamwidth of 1.6 degrees and sidelobe level of -18.9 dB. The limitations of producing an off-axis beam using this method is therefore severely restricted to certain beam scanning applications. Nonetheless, this method can be implemented on the existing reflector antenna to produce the pair of simultaneous beams required for amplitude monopulse, since only a slight angular displacement of the feed is required to produce the suitable pair of off-axis lobes with a deflection angle that is expected to be within only a beamwidth of the main lobe.

The properties of the pair of off-axis beams produced from the reflector that optimizes the sum and difference patterns of the monopulse antenna is identified through the modelling of the proposed feed arrangement across a range of angular displacement applied on the pair of E-plane sectoral feed horns. The modelling of the monopulse reflector antenna employing the proposed dual feed arrangement, across a range of feed tilt applied about the reflector vertex, is presented in Section 5.1.3, and the properties of the pair of off-axis beams produced for each angular tilt applied along with the corresponding monopulse patterns obtained are evaluated to identify the feed tilt that optimizes the requirements of the antenna for the application in hand.

5.1.3 Modelling of Dual-horn Feed for a 2D Monopulse System

The proposed approach taken to produce a pair of simultaneous off-axis (squinted) beams in the horizontal plane of the antenna is based on illuminating the vertically truncated reflector about its vertex using a pair of laterally displaced E-plane sectoral horn that is symmetrical about the focal line of the dish. The pair of off-axis beams produced from the parabolic reflector, which radiates at slightly different directions away from the antenna boresight axis, is responsible for producing the corresponding sum and difference voltage signals.

The issue with most monopulse reflector antennas, such as the four-horn feed design, generally lies with the inability of optimizing both sum and difference patterns simultaneously [27], and therefore the spacing between the feed horns (feed design), or the corresponding

squint angle formed, is usually based on a compromise between maximizing the detection sensitivity and angular accuracy of an antenna for target detection. Consequently, the modelling of the proposed dual feed arrangement that optimizes the corresponding sum and difference patterns of the monopulse antenna according to the requirement, or prioritization, of the application in hand will be discussed and analysed. This involves identifying the optimum angular feed tilt to be applied on the pair of feed horns, which is directly dependent on the properties of the pair of beams produced and the crossover point between them along the boresight axis of the antenna.

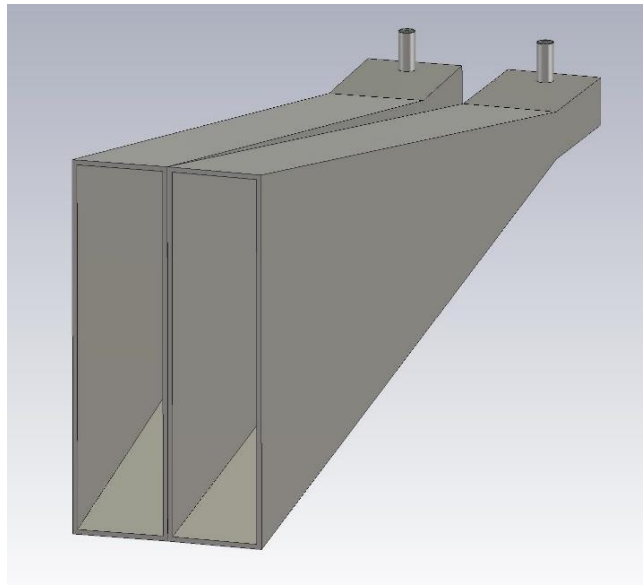


Fig 5-10. Dual-horn monopulse feed

As shown in Section 5.1.2, for a laterally displaced horn illuminating the reflector about the vertex, the off-axis beam produced from the reflector undergoes an angular shift and the properties of the lobe may differ significantly from one another as the feed tilt is varied across a large range of angles. However, at feed tilts that are similar, or within one degree, the variation between the properties of the respective off-axis lobes produced for each feed tilt applied is minimal. With the exception of the beam direction, if the properties of the off-axis lobes produced is the same for different feed tilts applied (i.e. produced from a phased array), the variable to be optimized would simply be the squint angle formed between the pair of off-axis lobes produced. However, since the properties of the individual off-axis lobe produced changes with increasing feed tilt applied, this causes the crossover point between the pair of lobes, corresponding to each feed tilt applied, to not be solely dependent on the deflection angle of the off-axis lobes but also on the properties of the individual lobes (i.e. -3 dB beamwidth). For instance, an off-axis secondary beam with a wider azimuth beamwidth would require a larger

beam deflection angle, or feed tilt applied, to allow the pair of beams to exhibit a lower crossover point. Hence, the variable to be optimized with this feed design is the crossover point along the boresight axis of the antenna instead of the squint angle formed between the pair of off-axis lobes, from which the most suitable sum and difference patterns can be identified.

Choosing the optimum angular feed tilt involves considering the detection sensitivity and angular accuracy of the radar, where the former and latter is defined by the characteristics of the sum and difference patterns obtained, respectively. The detection sensitivity of a monopulse antenna is notably determined by the gain (on-axis voltage) and beamwidth of the sum pattern, which varies with the squint angle formed between the pair of off-axis lobes produced. A narrow sum pattern beamwidth and high gain corresponds to a higher detection sensitivity of the antenna for target identification. Hence, if the detection sensitivity of targets is prioritized, the feed arrangement should be modelled to ensure that the sum pattern obtained exhibits a high gain and narrowest beamwidth possible, consistent with sidelobe requirements.

At least for targets that are located on or close to the boresight axis of the reflector antenna, the on-axis slope of the difference pattern indicates the sensitivity of the signal strength in response to a change in position of the detected target relative to the direction, or boresight axis, of the reflector antenna. For the detection of a target that is close to the boresight axis of the antenna, the angular error measurement obtained from the difference pattern is used to determine the positional information of a detected target relative to the boresight axis of the antenna, that is usually accurate to within a fraction of a beamwidth of an individual beam. A monopulse antenna with a high sensitivity, and therefore high angular accuracy, is realized when the on-axis slope of the difference pattern is large. The on-axis slope of the difference pattern is dependent on the squint angle and properties of the overlapping off-axis lobes along the boresight axis of the antenna, and therefore it differs from one pattern to another for each feed tilt applied. Thus, a pair of off-axis lobes with a narrow beamwidth would contribute significantly to the angular performance of a monopulse antenna by attaining a high degree of pointing accuracy within the beam that adds to the natural accuracy of the existing radar system. Since the accuracy of the angular error measurement provided is justified by the on-axis slope of the difference pattern, the on-axis slope of the difference pattern should be maximized, again consistent with sidelobe requirements, if optimizing the angular accuracy of the monopulse antenna is prioritized.

The angular displacement applied on the pair of feed as it illuminates the vertex of the reflector is critical to ensure that the pair of lobes overlap one another at the most suitable point. It is therefore vital to model and justify the optimum feed tilt, with respect to the properties and direction of the pair of off-axis lobes produced from the reflector. The optimum feed tilt can be

identified by varying it across a range of angles until the desired crossover point between the pair of lobes is achieved, from which the corresponding sum and difference pattern obtained is optimized accordingly to the requirement of the application in hand.

5.1.3.1 Optimization of Feed Tilt

The issue with the proposed dual feed-horn arrangement lies with the fact that there is a minimum angular displacement that must be applied on the pair of feed for both horns to illuminate the reflector about the vertex. To position the two horns side-by-side, in contact with one another, and symmetrical along the focal line of the reflector, the apparent phase centre of both horns must be laterally displaced from the focal point of the reflector by at least ± 12.7 mm, respectively, given that the horizontal dimension of the sectoral horn aperture is 25.4 mm (i.e. broad dimension of the WR90). The reflector antenna employing a pair of feed horn with no feed tilt applied is shown in Figure 5-11.

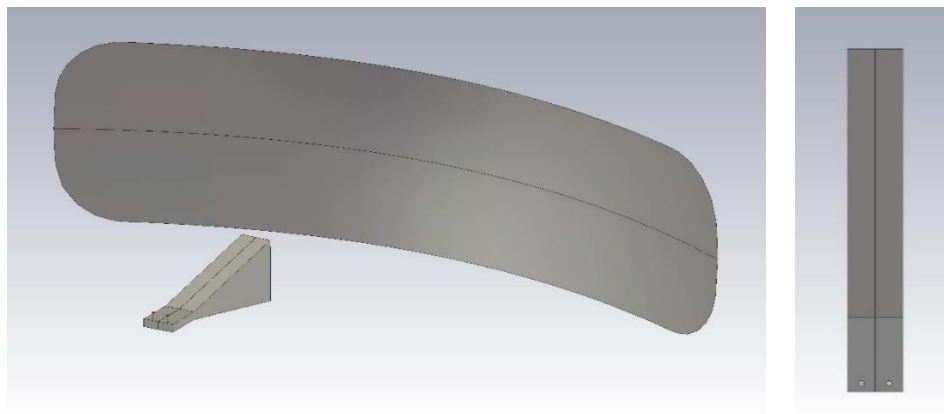


Fig 5-11. Dual-horn feed with zero feed tilt

The pair of feed horn shown in Figure 5-11 (zero feed tilt) prevents both feed from illuminating the parabolic reflector about the vertex. The main lobe of the primary beam radiated, which is parallel to the focal line of the reflector, illuminates the reflector about a point that is ± 12.7 mm from the vertex.

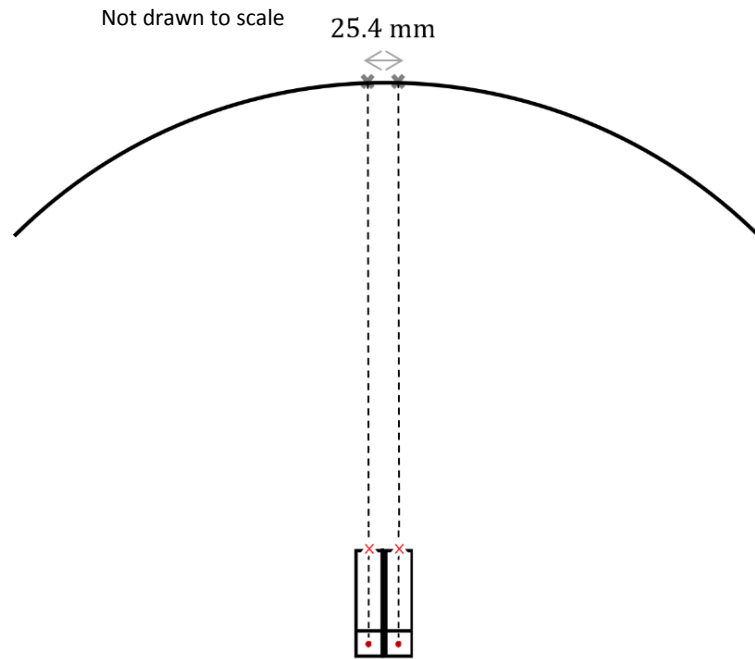


Fig 5-12. Dual-horn feed with no feed tilt applied - Point of illumination ± 12.7 mm

A trigonometric calculation illustrated by Figure 5-13 verifies a minimum feed tilt of 1.3 degrees must be applied on the pair of feed in order to illuminate the reflector about the vertex.

$$\theta_i = \tan^{-1}\left(\frac{12.7}{552}\right) \quad (5-6)$$

$$\theta_i = 1.3^\circ \quad (5-7)$$

Applying an angular displacement smaller than ± 1.3 degrees ($0^\circ \leq \theta_i < \pm 1.3^\circ$) on both feed will prevent the off-axis primary lobes from illuminating the reflector about its vertex, but instead about a point along the surface of the reflector that is within ± 12.7 mm from the vertex.

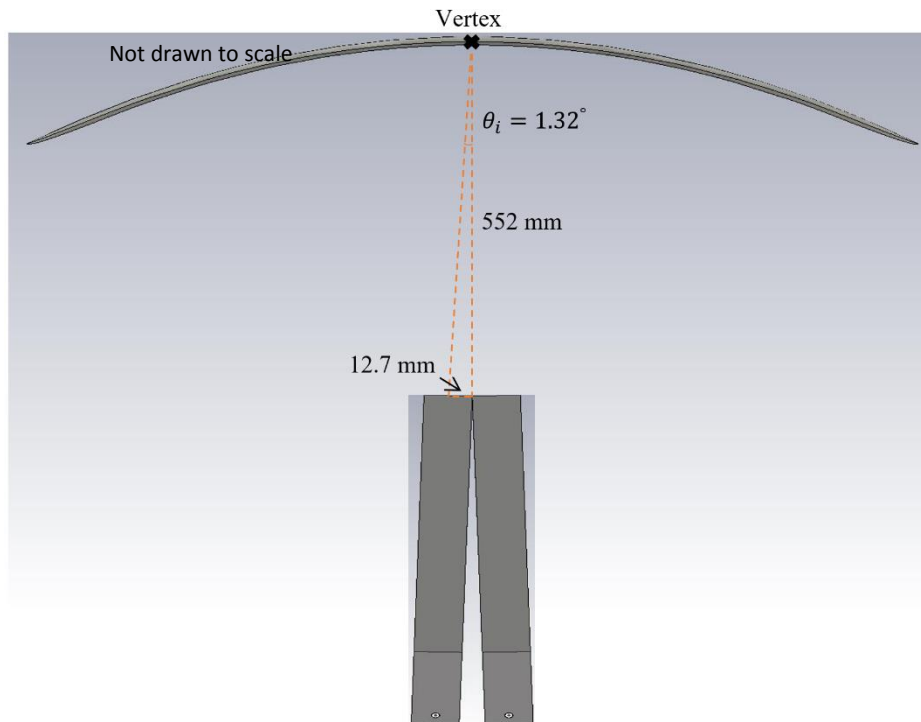


Fig 5-13. Identifying the minimum feed tilt required to illuminate the reflector about the vertex

Thus, for X-band radar systems, the proposed method of producing a pair of off-axis lobes is only possible when the feed tilt applied is larger than or equal to 1.3 degrees. Figure 5-14 illustrates the dual-horn feed arrangement across a range of increasing feed tilts applied, and in all cases the pair of feed horn is illuminating the reflector about the vertex.

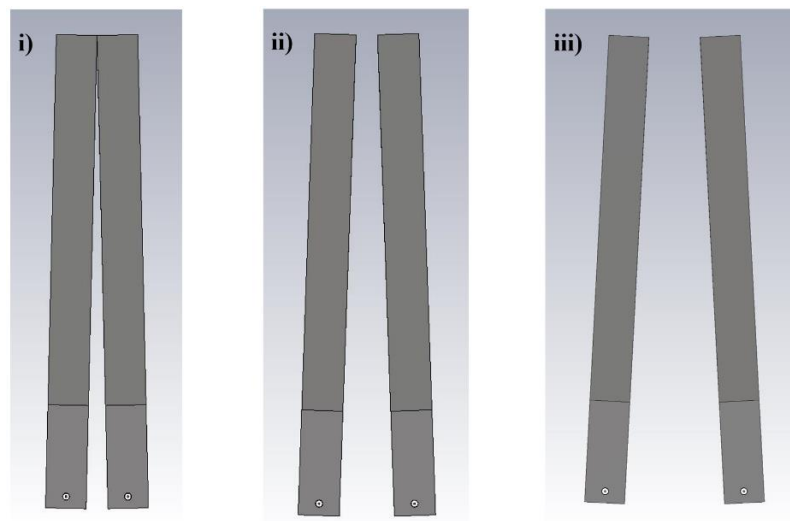


Fig 5-14. Feed tilt about the vertex of the reflector, for i) $\pm 1.3^\circ$, ii) $\pm 2.0^\circ$, iii) $\pm 3.0^\circ$.

The phase center of the respective feed drifts further away from the focus of the reflector, in opposite directions from the antenna boresight axis, as the feed tilt is increased beyond 1.3 degrees. Hence, at increasing feed tilts, the increasing separation between the phase center, or aperture, of both feeds from the focus of the reflector limits this method of producing the pair of off-axis beam to only small beam deflection angles of a beamwidth or two.

The reflector antenna employing the dual-horn feed arrangement proposed, with the minimum angular displacement of ± 1.3 degrees applied on the respective feed, that achieves simultaneous lobing is presented in Figure 5-15. The monopulse reflector antenna presented is simulated on CST.

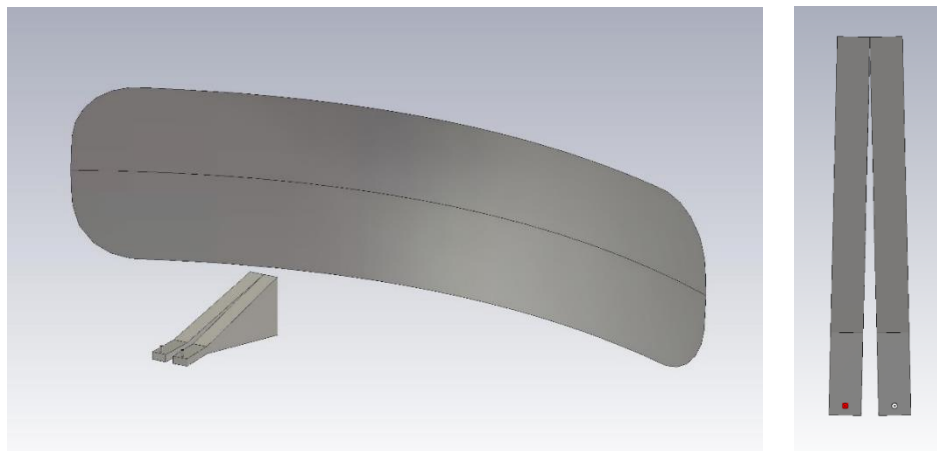


Fig 5-15. Reflector antenna employing a dual-horn feed with a feed tilt of $\pm 1.3^\circ$

The radiation pattern of the off-axis beams produced from the reflector in the horizontal plane is essentially a mirror image of one another that is symmetrical about the boresight axis of the antenna. Hence, simulating the radiation pattern of either one of the off-axis beams produced is possible to reduce the simulation time taken. This would require only one out of the two feeds to be fed with a transmit signal.

In the simulation performed only the feed positioned to the left of the focal line is fed with a transmit signal by a waveguide port, denoted by the red port in Figure 5-15, to produce the off-axis beam deflected to the opposite (right) side of the focal line. Since the radiation pattern of the second (right) off-axis beam is symmetrical about the boresight to that of the first (left) off-axis beam in azimuth, the radiation plot of the beams produced are theoretically an inversion of data to one another. Thus, the properties of the pair of beams produced from the truncated parabolic reflector are identical to one another apart from the polarity of the beam deflection angle. On the other hand, the radiation plot of both left and right lobes in elevation

are identical to one another. The simulated principal plane radiation pattern of the left beam produced from the reflector are shown in Figure 5-16, for a feed tilt of 1.3 degrees.

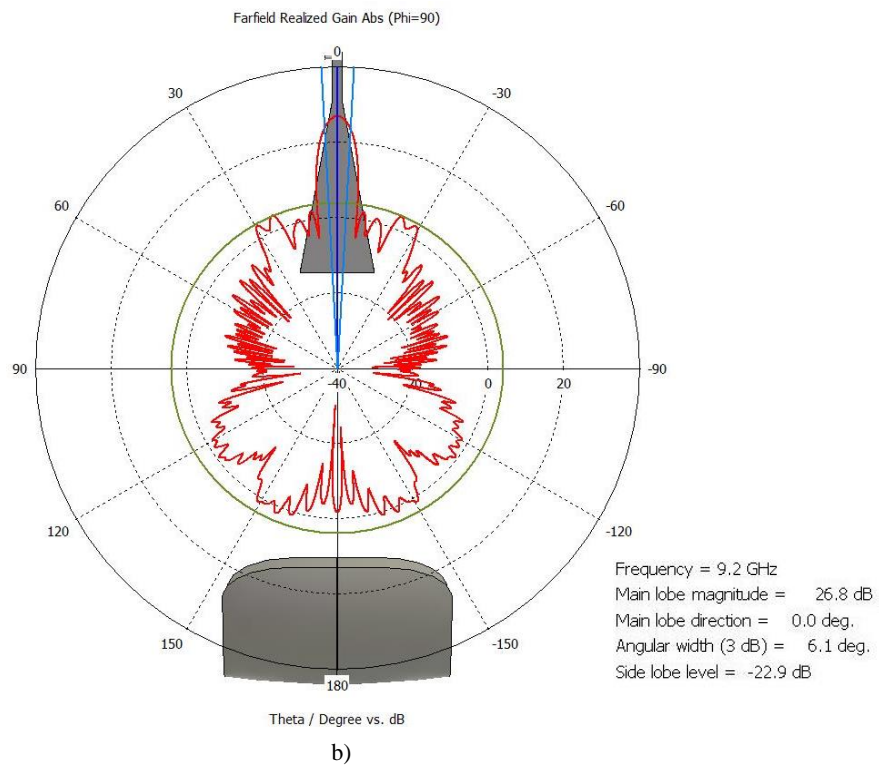
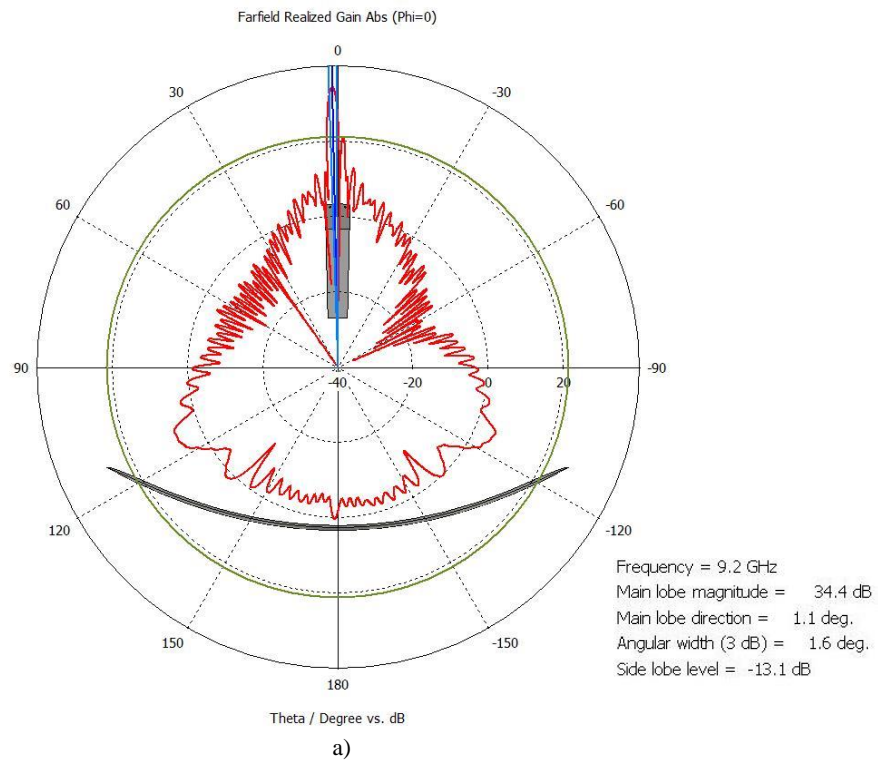


Fig 5-16. Radiation pattern of the left beam in the a) H-plane and b) E-plane

Illuminating the truncated parabolic reflector with the proposed dual-horn feed arrangement, with an angular displacement of ± 1.3 degrees applied on both feed, produces a pair of off-axis beams with an antenna gain of 34.4 dB and an azimuth and elevation beamwidth of 1.6 degrees and 6.1 degrees, respectively. In the horizontal plane, a single coma lobe, or a largest sidelobe level of -13.1 dB, flanks the main lobe of both left and right beams produced. Nonetheless, the presence of a coma lobe in the horizontal plane of the radiation pattern would overlap and interfere with the main lobe of the neighbouring off-axis lobe, and vice versa, which causes the on-axis gain of the sum pattern to be reduced by a few dB. In the vertical plane, the side lobe level is significantly lower at -22.9 dB. The main lobe direction of the right and left off-axis beam in azimuth is ± 1.14 degrees, respectively, with respect to the boresight axis of the antenna. The simulated patterns of the overlapping pair of off-axis beams produced in azimuth are plotted on a cartesian graph, shown in Figure 5-17, where the y-coordinates is the antenna gain on a dBi scale.

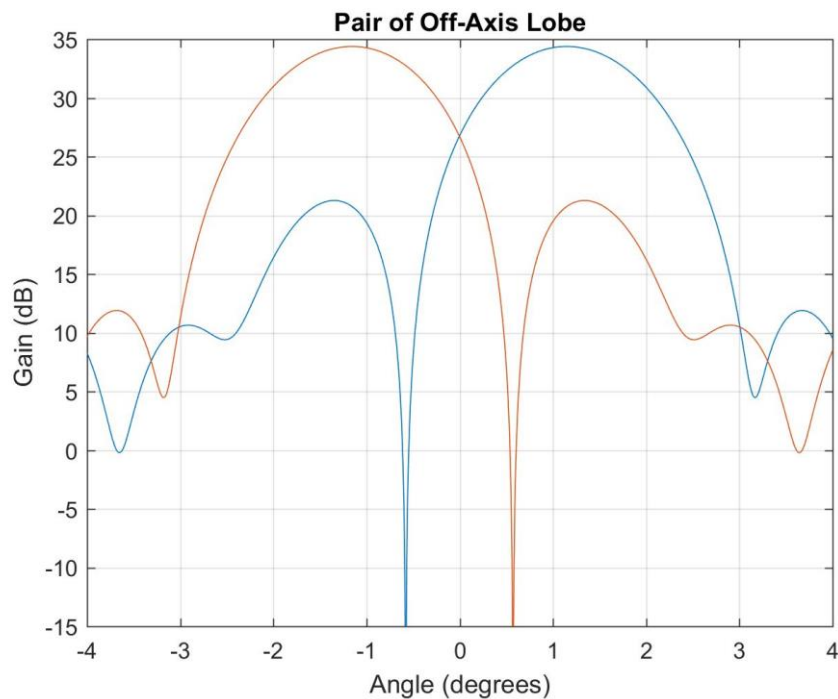


Fig 5-17. Simulated pair of off-axis lobes ($\theta_i = \pm 1.3^\circ$) (power gain scale)

It is apparent that the undesirable effects of feed tilt on the properties of the off-axis beams produced is minimal since the displacement of the phase centre of each feed from the focus of the reflector is insignificant to the focal length and horizontal dimension of the reflector. A squint angle of 2.28 degrees is formed between the secondary lobes produced, which corresponds to the ± 1.14 degrees beam deflection angle of each lobe. The crossover

point between the pair of overlapping lobes at the boresight axis of the antenna occurs at the – 7.6 dB point of the respective main lobes.

Assuming the absence of noise and clutter, let v_1 and v_2 be the output voltages from the pair of horns which produce the squinted beams (Figure 5-18), from which the sum and difference patterns in azimuth are formed. In all the plots provided, the x -coordinates is the target angle in degrees and the y -coordinates is the voltage gain which are normalized to the peaks of the individual off-axis beams. In all these plots the field strength of the echo wave arriving at the antenna is assumed constant in amplitude.

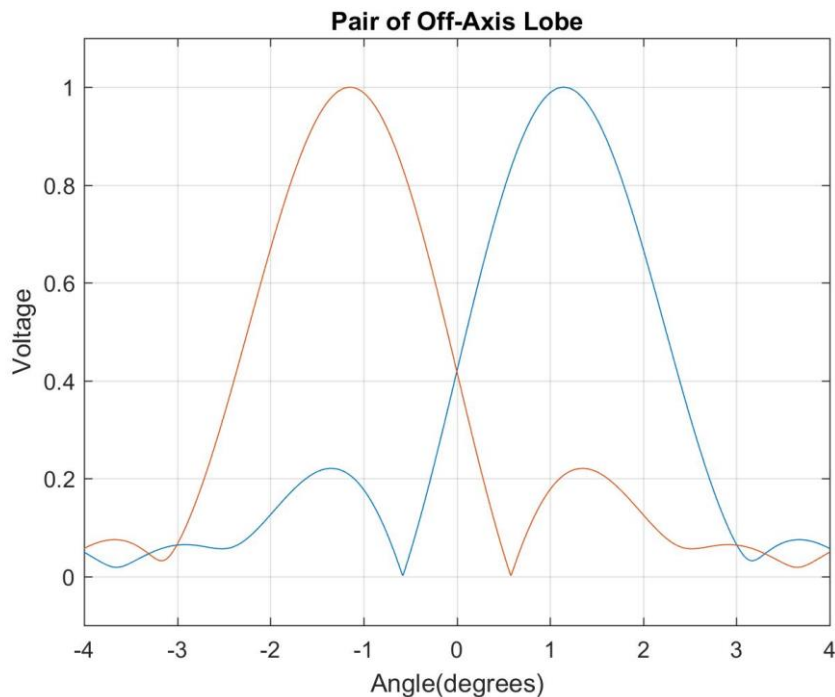


Fig 5-18. Simulated pair of off-axis beams ($\theta_i = \pm 1.3^\circ$) (voltage gain scale)

The sum and difference voltage patterns obtained through signal processing are given by

$$s = v_1 + v_2 \quad (5-8)$$

$$d = v_1 - v_2 \quad (5-9)$$

If the sum and difference pattern are obtained using a passive hybrid (assumed lossless, with all ports terminated in matched impedances), a $1/\sqrt{2}$ factor is introduced to the equations above. Ignoring a small loss in the device, the $1/\sqrt{2}$ factor arises from the fact that the total output power must equal the total input power [38].

In general, the voltages are phasors (i.e. complex quantities), but in pure amplitude comparison they have the same phase. Since absolute phase is arbitrary, they will be treated as real quantities for this example. In an actual radar the phases differ slightly because of the physical separation of the horns [86], but within the half-power beamwidth of the sum pattern this effect is negligible. The sum and difference voltage patterns obtained in the horizontal plane of the monopulse antenna that corresponds to the pair of off-axis beams produced in azimuth when a feed tilt of 1.3 degrees is applied is presented in Figure 5-19 and 5-20, respectively.

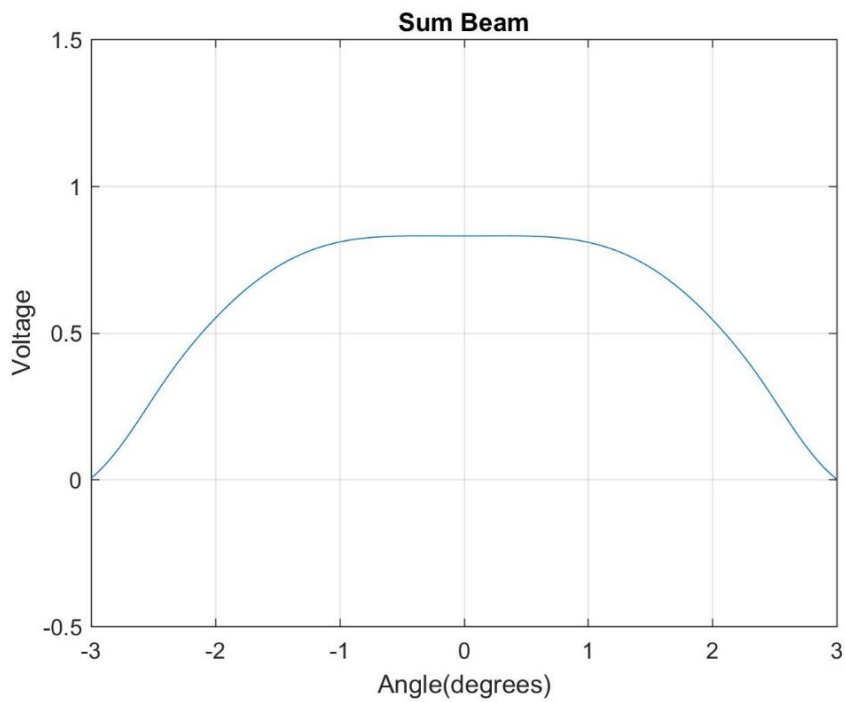


Fig 5-19. Sum pattern ($\theta_i = 1.3^\circ$)

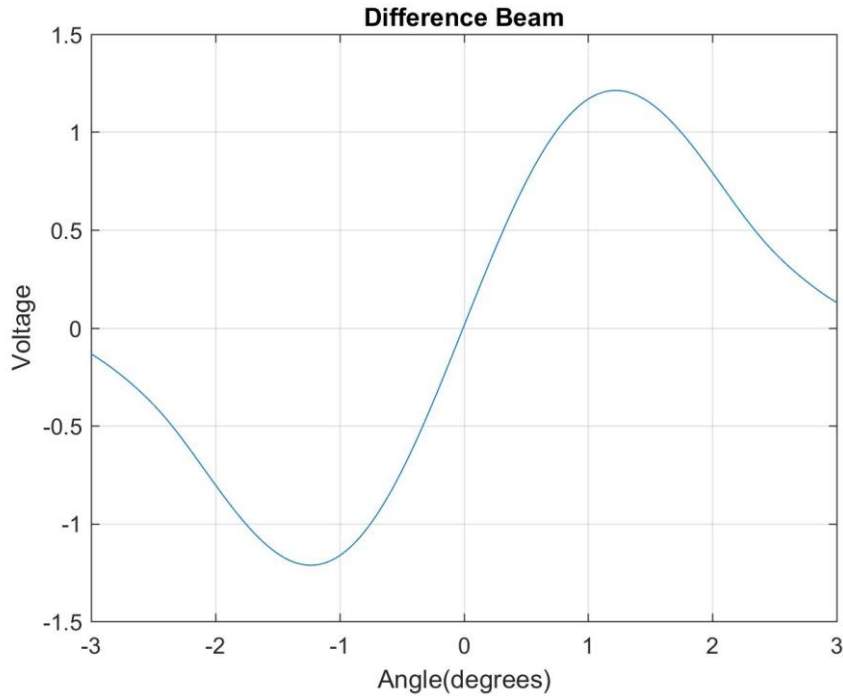


Fig 5-20. Difference pattern ($\theta_i = 1.3^\circ$)

Additional simulations of the monopulse reflector antenna employing the dual-horn feed arrangement are performed across a chosen range of feed tilts, between 1.4 to 1.7 degrees and in increments of 0.1 degrees, from which the properties of the pair of off-axis beams produced and the crossover point between the main lobes at the antenna boresight for each of the feed tilt applied are evaluated. Based on the radiation pattern of the pair of off-axis beams simulated, the corresponding sum and difference patterns in the horizontal plane are obtained for each feed tilt applied and are evaluated to determine the optimum feed tilt that is most suitable to the antenna requirements. The properties of the simulated pair of off-axis lobes produced for each value of feed tilt applied, θ_i , are presented in Table 5-2.

Feed tilt (deg) (θ_i)	Beam deflection angle (deg) (θ_r)	Azimuth -3 dB BW (deg)	Sidelobe level (dB)	Elevation -3 dB BW (deg)	Sidelobe level (dB)	Gain (dB)	Crossover point (dB)
1.3	1.14	1.6	-13.1	6.1	-22.9	34.4	-7.6
1.4	1.21	1.6	-12.9	6	-22.4	34.4	-8.6
1.5	1.28	1.6	-12.3	6	-21	34.4	-10.2
1.6	1.35	1.6	-12.3	5.9	-19.7	34.4	-11.7
1.7	1.42	1.6	-12.2	5.8	-18.2	34.4	-13.5

Table 5-2. Radiation properties of the beams produced corresponding to each feed tilt

The simulation results for the values of θ_i applied shows that the radiation properties of the pair of beams produced from the truncated parabolic reflector are also very similar to one

another, which indicates that incrementing the feed tilt applied by 0.1 degrees has nearly insignificant difference on the properties of the beams produced.

A family of sum and difference patterns obtained across the range of feed tilts applied (1.3 to 1.7 degrees) are presented in Figure 5-21 and 5-22, respectively. The plots shown in the respective figures are based on the sum and differencing of the simulated pair of off-axis beams produced by the antenna, with each plot corresponding to each feed tilt applied.

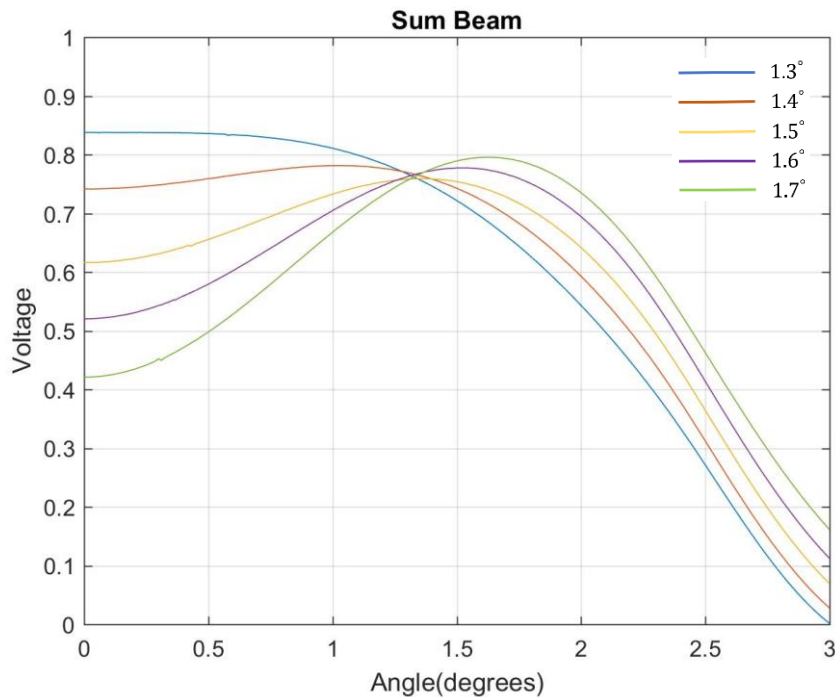


Fig 5-21. Simulated sum pattern across the range of feed tilt applied

The properties of the sum pattern obtained determines the detection sensitivity of the monopulse antenna. At smaller feed tilts the crossover point between the pair of off-axis lobes produced is closer to its respective peak due to the smaller deflection angle of the respective lobes. The high crossover point between the pair of lobes causes the sum pattern to exhibit a narrower beamwidth and a higher on-axis voltage, or gain, which enables the antenna to have superior detection sensitivity. Consequently, applying a larger feed tilt causes the crossover point between the pair of lobes to occur at a lower point due to the larger deflection angle of the lobes, which corresponds to an increase of the sum pattern beamwidth and decrease of the on-axis voltage gain. The family of sum patterns obtained corresponding to each feed tilt applied indicates this, whereby the sum pattern beamwidth and gain decreases and increases, respectively, with decreasing squint angle. With this dual feed arrangement, the smallest possible feed tilt that can be applied is 1.3 degrees, from which the sum pattern gain and resolution performance is maximized as compared to the other feed tilts applied. Hence, if the

detection sensitivity of targets is prioritized, the feed arrangement should be modelled to ensure that the squint angle between the pair of lobes produced from the parabolic reflector is as small as possible to form a sum pattern with the highest gain and narrowest beamwidth achievable.

When an angular displacement of 1.3 degrees is applied on the pair of feed horns the normalized on-axis sum voltage is 0.837 and the sum pattern beamwidth is 3.77 degrees. In comparison to the azimuthal beamwidth of the beam produced from the original center-fed reflector antenna (1.6 degrees) the sum pattern beamwidth is wider by 2.36 times. This infers that the angular resolution of the monopulse antenna is in fact just approximately 40 percent the resolution capability of the original reflector antenna, and therefore the clutter footprint within the signal received from the sum channel output is approximately 2.4 times higher. Moreover, the on-axis gain of the sum beam is also approximately 1.6 dB lower than the gain of the beam produced from the center-fed reflector antenna (34.4 dBi). This is, however, not a serious issue since the sum pattern is only used for identifying the presence of a target visible to the radar and the gain is still sufficiently high and suitable for most long-range applications. Thus, a sum pattern with a high angular resolution is often not critical.

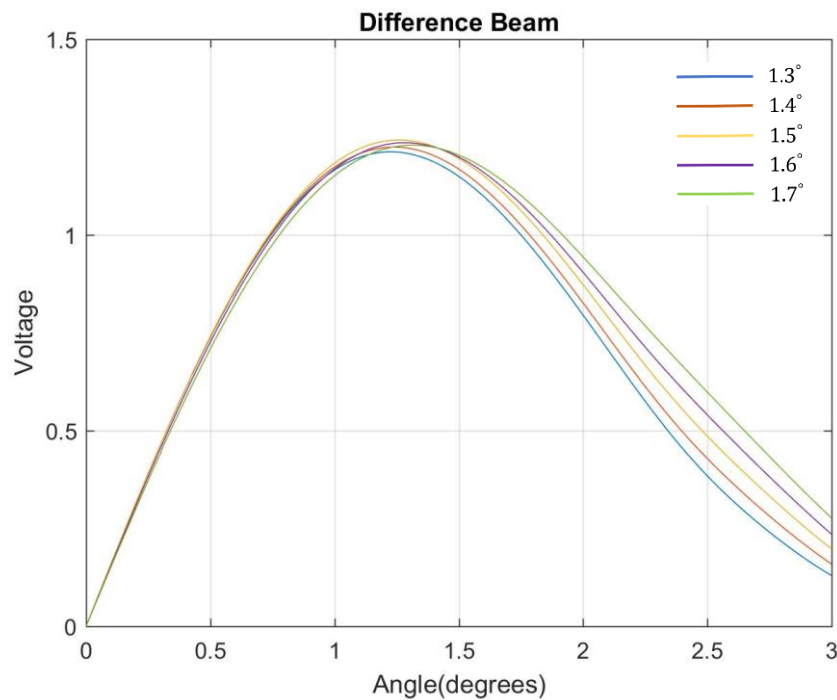


Fig 5-22. Simulated difference pattern across the range of feed tilt applied

The on-axis slope of the difference pattern determines the angle-error sensitivity (angular accuracy) of the monopulse antenna for measuring the positional information of targets that are positioned on or near the antenna boresight axis, which provides the angle-error of a target's position relative to the antenna boresight. Hence, producing a difference pattern with a

large on-axis slope is critical in achieving a higher angular accuracy for accurate target imaging and/or tracking. As mentioned, applying a larger feed tilt causes the crossover point between the pair of off-axis lobes to be lowered due to the larger squint angle of the respective lobes. If we had assumed the properties of the beam produced from the reflector were to remain unchanged as the feed tilt is increased over several tenths of a beamwidth, the on-axis difference slope is expected to increase substantially with the squint angle formed until it reaches a maximum (i.e. in this case between 1.3° to 1.4°), which would be the same feed tilt at which the sum pattern changes from a maximum to a minimum, before gradually decreasing at angles larger than this. This suggests that a large squint angle is usually more suitable to optimize the difference pattern, at least for active targets on or near boresight, for applications that prioritizes on achieving a high angular accuracy over its detection sensitivity.

However, in practice, given the dual-horn feed arrangement proposed, gradually increasing the feed tilt applied by only a tenth of a beamwidth causes broadening of the main lobe produced. Hence, despite the larger squint angle of the pair of beams and a lower crossover point between the main lobes when larger feed tilts are applied, the variation in the on-axis slope of the family of difference patterns obtained (Figure 5-22) becomes minimal due to it being offset by the variation in properties of the lobes produced with increasing feed tilt applied. Thus, the angular accuracy of the monopulse antenna would be very similar to one another across the range of feed tilt simulated (k_d in Table 5-3). The sharp null or the large on-axis slope of the difference pattern obtained infers that the angular accuracy of the monopulse antenna is enormously superior as compared to that of the original center-fed reflector antenna, which provides the operator with the positional information of the tracked target relative to the boresight axis that is accurate to within a small fraction of a beamwidth of the off-axis beam.

Figure 5-23 is a magnified version of the family of difference pattern shown in Figure 5-22 to observe the small variation in on-axis slope of the respective difference patterns obtained. It shows that the on-axis slope of the difference pattern increases until the feed tilt applied is 1.4 degrees, after which the on-axis slope starts to decrease when feed tilts larger than 1.4 degrees is applied.

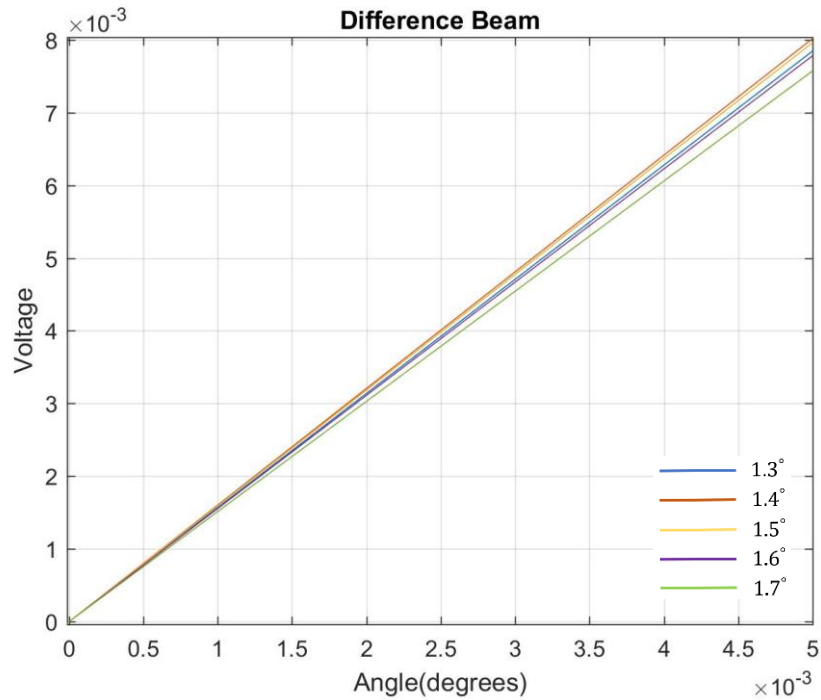


Fig 5-23. Zoom in on-axis difference pattern

Nonetheless, the amplitude of the difference signal does not only depend on the angular position of the target but also on the target range and RCS. To remove the dependency of the error signal on external factors and, therefore, accurately determine the angle error of an off-axis target relative to the boresight axis of the antenna, the IF signals from the difference channel is normalized with respect to the IF signal from the sum channel by performing the ratio of the echo amplitude of the difference to sum signal. The corresponding difference-to-sum ratio (error) voltage output is independent of signal strength and linear against the angle error over a wide range of angles [35]. The angle-error-detector output allows the exact direction of arrival of the target to be identified solely based on the target displacement from the boresight axis to within a fraction of a beamwidth. As mentioned in Section 2.2.1.3, this ratio can be obtained using an Automatic Gain Control (AGC) circuit that operates on the difference channel itself and is driven by the output of the sum channel, or by division after detection in a digital tracker [34]. The difference-to-sum ratio pattern of the monopulse antenna for a feed tilt of 1.3 degrees is presented in Figure 5-24. The slope of the difference-to-sum ratio pattern is also known as the monopulse slope, or error slope, which has a constant on-axis angle error sensitivity.

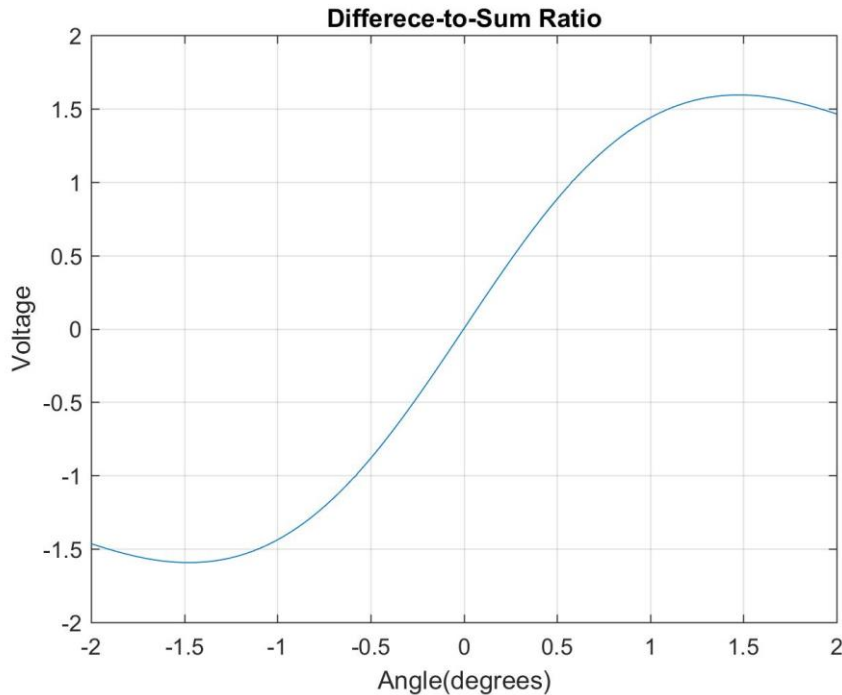


Fig 5-24. Difference-to-sum ratio pattern ($\theta_i = 1.3^\circ$)

5.1.3.1.1 Factors Influencing Optimization of Feed Tilt

Considering the case where the monopulse antenna is used for both transmission and reception, the criterion for optimization of the squint angle depends on the radar function that is to be optimized (i.e. prioritizing detection or accuracy capability) and whether the type of target detected is an active (i.e. a beacon) or passive (i.e. one that merely scatters or reradiates the power incident on it) one. For the detection of both active and passive targets, the modelling of the monopulse reflector antenna shows that the feed tilt, or corresponding squint angle formed between the pair of off-axis lobes, must be as small as possible ($\theta_i = 1.3^\circ$) if the detection sensitivity of the antenna is prioritized.

If the objective of implementing monopulse is prioritized on optimizing the angular accuracy of an existing antenna instead for steady targets on or near the boresight, evaluating the corresponding difference pattern formed in each case and identifying the optimum feed tilt is of greatest interest. However, unlike the optimization of the detection sensitivity of a monopulse antenna, the optimum squint angle required to optimize the angular accuracy for a passive and an active target may differ slightly, and will be discussed individually.

For the detection of a passive (skin) target that merely scatters or reradiates the power incident on it, the transmission-pattern gain of the radar antenna has an effect on the antenna accuracy due to sources of errors introduced, such as thermal noise, which is a dominant source of error especially under low SNR conditions. The following shows that the angular accuracy

of the monopulse antenna for detection and tracking of a passive target is optimized by identifying the feed tilt that maximizes the product of on-axis difference slope and on-axis sum voltage [38]. The approximate formula derived for the single-pulse error due to the effect of thermal noise, which is a dominant source of monopulse angle error measurement, for a steady target on or near the axis is given by [38]:

$$\sigma_{\theta} = \frac{\theta_{bw}}{k_m \sqrt{2S/N_d}} \quad (5-10)$$

where σ_{θ} is standard deviation of angle error, in the same units as θ_3 of an off-axis lobe

θ_{bw} is sum pattern 3dB beamwidth

k_m is normalized monopulse slope

S is sum-signal power

N_d is average noise power in difference channel

Let the on-axis difference slope and on-axis sum voltage on any of the plots shown in Figure 5-21 and 5-22, respectively, be denoted by k_d and s_o , respectively, which have been normalized to the peaks of the off-axis lobes produced from the parabolic reflector. The normalized monopulse (error) slope k_m of any of the plots shown in Figure 5-24 is the ratio of k_d to s_o , expressed in terms of the sum half-power beamwidth θ_{bw} , given by [38]

$$k_m = \frac{k_d \theta_{bw}}{s_o} \quad (5-11)$$

The monopulse slope is the slope of the difference pattern at an angle θ , in volts per sum-pattern beamwidth, divided by the sum voltage at angle θ , in volts. Usually, only the on-axis value of k_m is of concern. k_d and k_m are normalized to the peak of an individual off-axis beam and the peak of the sum beam, respectively, and for k_m the unit of angle is the beamwidth of the sum beam.

For the detection of passive targets, assuming the sum pattern is used for transmission and reception, as it normally is in a radar, the on-axis sum power S is proportional to s_o^4 . Hence, σ_{θ} is given by

$$\sigma_{\theta} = \frac{s_o}{k_d \theta_{bw}} \frac{\theta_{bw}}{s_o^2} = \frac{1}{k_d s_o} \quad (5-12)$$

To minimize the angle error σ_{θ} the term to be maximized is $k_d s_o$ which is the product of the on-axis difference slope and on-axis sum voltage of the difference and sum patterns, respectively.

The values of the figure of merit $k_d s_o$ are calculated based on the simulated sum and difference patterns of the modelled reflector antenna for each of the chosen feed tilts applied. The results presented in Table 5-3 show that the maximum value of $k_d s_o$ occurs when an angular displacement of ± 1.3 degrees is applied on the respective feed horns.

θ_i	k_d (volts/deg)	s_o (volts)	$k_d s_o$
1.3	1.569	0.837	1.313
1.4	1.603	0.742	1.189
1.5	1.592	0.616	0.981
1.6	1.556	0.52	0.809
1.7	1.514	0.421	0.637

Table 5-3. The figure of merit $k_d s_o$ across the range of feed tilt applied

Moreover, the simulation results also show that with the proposed dual feed-horn arrangement for this type of reflector outline, by applying a feed tilt of 1.3 degrees it is possible to optimize the detection sensitivity (highest s_o) and angular accuracy (highest $k_d s_o$) of the antenna simultaneously, that is, the monopulse patterns, when dealing with passive targets.

Consequently, when dealing with an active target, such as a beacon or transmitting source, or when the radar is used in a receive only mode, the transmission-pattern gain of the radar antenna has no effect on the angular accuracy. Hence, the factor s_o^2 in the numerator of the left side of (5-12) is replaced with s_o and the right side of the equation is simply reduced to be the reciprocal of k_d . Thus, applying the feed tilt that maximizes the on-axis slope of the difference pattern is desirable to minimize the angular error measurement for tracking of an active target that is on or near the off-axis beam from the boresight axis of the antenna. This condition, based on the family of difference patterns plotted across the range of feed tilts simulated (Figure 5-22 and 5-23), is achieved when the feed tilt applied is 1.4 degrees. Nonetheless, the on-axis slope of the respective difference patterns obtained has nearly negligible difference from one another, which infers that the angular accuracy of the monopulse antenna for each of the feed tilt applied is very similar.

In general, the design of conventional monopulse radars are optimized for accurate angular tracking of either an active or passive target since it is unlikely for a radar to minimize the angle error measurement σ_θ for both types of target simultaneously. This is observed in radars where the squint angle that produces the highest value of k_d and $k_d s_o$ differs considerably from one another, and therefore, the optimization of the angular accuracy for both

types of target cannot be simultaneously achieved. Nonetheless, it is evident that with the proposed dual feed-horn arrangement it is almost possible to optimize the angular accuracy for both types of targets simultaneously, by applying a feed tilt of 1.3 degrees, since the variation of the on-axis slope of the respective difference pattern obtained are negligible across the feed tilt applied. The simulated patterns presented in this section will be verified by the measured radiation patterns of the manufactured monopulse reflector antenna, which are presented in Section 6.3.2.

5.2 Signal Processing Technique

A significant factor concerning the performance of a surveillance radar is its detection capability, which relies heavily on the resolution and gain characteristics of the radar antenna. In FMCW radars, the desired range resolution can be achieved by modulating the transmitted signal over a wide range of frequency (bandwidth) within a specified sweep time or can be readily achieved with “chirp” or pseudo-noise modulation, whereas the SNR of the radar antenna can be increased by increasing the transmit power of the radar. The angular resolution of a radar system operating at a specific frequency, on the other hand, cannot be easily increased by simply altering radar parameters, but instead requires physical modifications to be done on the antenna design. The angular resolution depends on the antenna beamwidth and worsens with increasing operating range. When a radar is used for target detection in long range applications, the deteriorating angular resolution characteristics of the antenna at long range would prevent the radar from distinguishing two or more targets individually when the targets are within the beamwidth of the antenna. Moreover, in a scanning radar, the extent of a target image in range is usually significantly less than that in azimuth. This limits the azimuth resolution, which could prevent the detection of significant closely-spaced targets due to the presence of clutter within the large footprint that buries it. In rough sea condition, the maximum detection range of small targets is limited by sea clutter, and this range is inversely proportional to the ratio of the target radar cross section to the echo’s generally much larger azimuth footprint. Since the effect of spreading losses on a target and clutter are equal, an n-fold reduction of that ratio would cause an n-fold increase in maximum clutter-limited detection range for a given signal to clutter ratio [87]. Hence, methods of scaling down the azimuthal echo footprint and/or beamwidth of the detected response corresponding to a target is often necessary to effectively improve the resolution performance of an existing radar.

In a conventional parabolic reflector antenna, a major enhancement in angular resolution can only be achieved using an impractically large reflector to produce a beam with a narrow azimuth beamwidth. The angular accuracy of the antenna, however, can be

significantly improved by implementing amplitude monopulse on the center-fed reflector antenna, as shown in Section 5.1, as an alternative to using a large dish. Maximizing the angular accuracy of the radar system introduces a very accurate and effective way of target tracking using the monopulse difference pattern. However, the implementation of monopulse actually degrades the resolution and increases the clutter footprint within the signal received as the beamwidth of the sum beam, which is used for target detection, is usually a few times wider than the individual squinted beams used in a monopulse antenna, or the beam produced from a center-fed reflector antenna in azimuth. Moreover, implementing monopulse on an existing reflector antenna requires modifications to be performed on the feed used to illuminate the reflector (extra horn antenna) and on the radar hardware (extra receiver for difference channel), which effectively increases the complexity of the RF hardware circuitry and overall cost of the radar system. In this section, a novel beam sharpening technique that is aimed to provide a considerable enhancement in the angular resolution and clutter resilience of the radar through sharpening of the video output, or detected target response, of an existing radar is proposed and evaluated.

5.2.1 Pattern Selective Differential Processing

This section introduces a one-dimensional and non-coherent post-detection signal processing technique named Pattern Selective Differential Processing (PSDP) that simulates beam sharpening on the detected output of a new or existing radar system. The differential video processing scheme proposed is a simple and cost-effective processing technique that artificially sharpens the final appearance of the detected target response on the PPI display by processing the non-coherent data using priori information of the antenna far-field radiation pattern, that is, exploiting prior knowledge of the transmit and receiving properties of the antenna pattern to sharpen the target response detected within the signal received from the output of a radar system before it is presented on the radar display. Hence, this proposed method is considered as an artificial technique that has credibility in improving the angular resolution of the antenna, which also transforms the original video output of a radar to have a sharper appearance providing that the target still remains within the sharpened beamwidth or resolution cell. Depending on the characteristics of the transmit and receive antenna pattern, the proposed signal processing technique is capable of realizing a modest improvement of at least 20 percent or more (by as much as 60 percent) on the angular resolution and clutter-limited detection range of an existing radar system without requiring any modification on the existing radar hardware. Although the enhancement in angular accuracy, which is received as a minor-by-product of the enhanced angular resolution of the radar system, is significantly less attractive as compared to that from

the performance of a monopulse antenna, the enhancement that can be achieved on any existing antenna at a very low cost and complexity will prove to be of great value and demand.

In practice, the processing technique operates on the raw video signal obtained from the radar output and therefore the concept can ideally be implemented by means of a simple hardware, such as a digital processing box, that is connected between the radar output and its display. The processed, or sharpened, target responses will be observed instead of the original target responses on the radar display. Hence, the benefit of the concept can be realized on any existing radar system, and particularly for navigational or surveillance radar systems it is likely to make a significant positive involvement to safety at sea. However, the processing of raw video data is expected to result in a small delay, which is the time taken for the antenna to move one beamwidth, before the processed video appears on the display. Nonetheless, the delay would only be a matter of milliseconds since the rotation period of a scanning navigational radar is usually only a few seconds long. Hence, the delay in information provided is not critical to the requirements of a typical navigational radar that are usually tasked for monitoring of slow moving objects.

This thesis demonstrates the application of the differential processing technique in the angular domain of the received waveform to enhance the angular resolution performance of a radar system for improved target detection accuracy. Although the implementation of the technique in the time domain will not be discussed, the concept of applying the technique in both time and angular domain are similar to one another. To evaluate the advantages of the technique on the detection performance of several radar systems, each with a different antenna pattern, the technique is applied individually on the several antenna patterns simulated, with each pattern exhibiting its own unique properties, from which the most suitable antenna characteristic that would benefit the most from the processing technique can be identified. The principles of the signal processing technique is extensively described before it is applied on various simulated radar outputs of existing systems employing a line source antenna of several common aperture field distributions, since their far-field patterns are simple to model and also provide very close representation of typical antenna radiation patterns. The effect of the differential processing on antennas with other aperture shapes are not covered in this thesis, although the principles are the same. Beforehand, the theory for linear apertures and the relationship between the several aperture distributions and their corresponding far-field pattern are discussed and provided in Section 5.2.1.1.

5.2.1.1 Aperture Theory for a One-dimensional (Linear) Aperture

The aperture surface of an antenna comprises of a finite opening in an infinite plane. Several approximate methods are used to generally determine the electric and/or magnetic fields in the

aperture region of the antenna, while the fields are assumed to be zero elsewhere. As a first approximation, the distant radiated fields can be obtained from the calculated fields on the aperture surface alone. Thus, the steps involved in the analysis of aperture antennas are first to calculate the electromagnetic fields over the aperture due to the sources on the rearward side of the infinite plane and to use these field distributions as the basis for the prediction of the distant fields in the forward half-space [51]. As will be shown based on the derivation provided, the relationship between the excitation of an antenna aperture and the far-field directional pattern may be expressed in terms of the Fourier Transform [50]. The calculations here are presented for a line source antenna, which has a one-dimensional (linear) aperture, but can clearly be extended to a planar geometry, or for the analysis of more practical two-dimensional rectangular apertures (i.e. rectangular horns).

The exact EM fields in the aperture plane of an antenna is rarely determined although approximate distributions of the aperture plane can be found through several methods. The most suitable method of approximation is dependent on the type of antenna. For example, illustrated below, the induced current method is a popular choice for one-dimensional aperture antennas, which is based on approximating the electric current distribution on the aperture surface. The diagram in Figure 5-25 shows an aperture of length a excited with a current/voltage/field varying along the length of the aperture according to the function $f(x)$. The field at some point P may then be calculated on the basis of the elemental contributions, $f(x)$, integrated over the length of this aperture, taking account of the phase change due to propagation through free space [50].

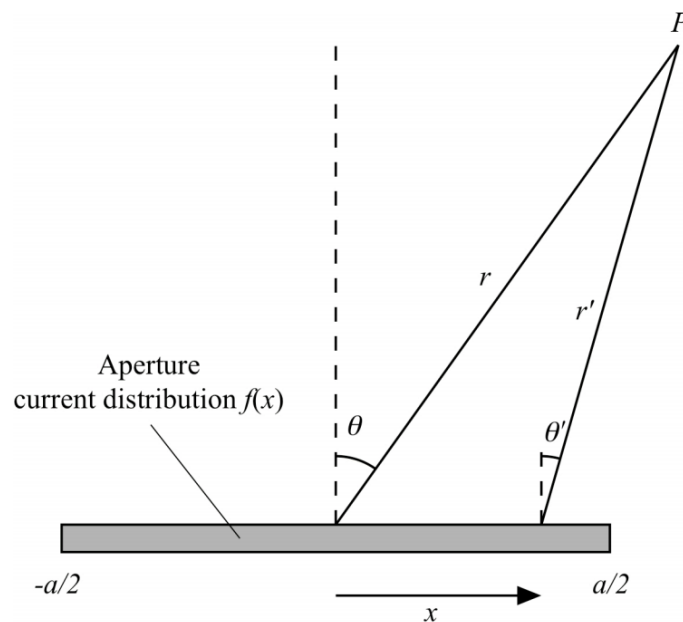


Fig 5-25. Construction to calculate field at point P from a linear aperture [50]

The field contribution, dE , at point P , distance r from the centre of the aperture, due to an element of width dx is thus given by (5-13) where $f(x)$ is the current variation along the aperture, which is a complex quantity in general.

$$dE = \frac{r}{r'} f(x) \cdot dx \cdot \exp j \left[\omega t - \frac{2\pi r r'}{\lambda} \right] \quad (5-13)$$

For high and even moderate gain antennas the radiation pattern is largely focused into a small range of angles in the far-field region. Where $r \gg a$, the geometry simplifies such that $\theta' \rightarrow \theta$ and $r' \rightarrow r - x \sin \theta$, so the total field due to the aperture may be written as [50]

$$E(\theta, t, r) = \int_{-\frac{a}{2}}^{\frac{a}{2}} f(x) \cdot \exp j \left[\omega t - \frac{2\pi r}{\lambda} + \frac{2\pi x \sin \theta}{\lambda} \right] dx \quad (5-14)$$

$$E(\theta) = \int_{-a/2}^{a/2} f(x) \cdot \exp j \left[\frac{2\pi x \sin \theta}{\lambda} \right] dx \quad (5-15)$$

The time dependence and $\exp j(\frac{2\pi r}{\lambda})$ constant phase term are of little significance and can be omitted, (5-15) shows that the Fourier transform relationship exists between the far fields and the tangential aperture field. The directional pattern can now be redefined in terms of the variable $u = -(\sin \theta)/\lambda$ and the integration limits extended, giving the familiar Fourier transform pair (on a $\sin \theta$ scale) [50]

$$G(u) = \int_{-\infty}^{\infty} f(x) \cdot \exp(-j2\pi u x) dx \quad (5-16)$$

$$f(x) = \int_{-\infty}^{\infty} G(u) \cdot \exp(j2\pi u x) du \quad (5-17)$$

This shows that the far-field radiation pattern of an aperture (on a $\sin \theta$ scale) is given by the Fourier Transform of the aperture illumination profile (field distribution). Both the far-field pattern and aperture distribution may be complex quantities due to the variation in amplitude and phase. Providing the aperture concept can be applied on any given antenna and an approximate aperture field distribution can be established, the radiated far-field directional pattern can be formulated based on the Fourier transform relationship between the aperture field and the corresponding far-field pattern. Thus, the Fourier transform relationship is vital in determining the expression for the radiated fields which is extremely important since it utilizes all the properties of the Fourier transform theory for the analysis and synthesis of aperture antennas. Increasingly complex aperture distributions cannot be solved by analytical solutions and are usually solved numerically (i.e. numerical integration). However, the increasing power

and lower costs of the digital computer have made it a conventional tool for antenna designers to calculate complex field distribution of an antenna.

5.2.1.1.1 Far-field Patterns of Line Source Distributions

This section covers the far-field patterns of several common line source distributions. The line source is a one-dimensional aperture where the field radiates from a source, length a , along the x axis. The source is positioned in a ground plane of infinite extent. The simplest distribution of field across the aperture is when the electric field is constant (uniform distribution). This model is simple and yet the analysis gives results which illustrate the main features of the more practical two-dimensional apertures [51].

The far-field patterns $G(u)$ of several common line source distributions $f(x)$ are presented in Table 5-4. In general, it will be seen that the use of tapered distributions enables better patterns to be obtained, with lower sidelobe levels and broader beamwidths. The cosine squared profile most resembles a Gaussian and produces the lowest sidelobe levels [50]. Other aperture shapes, such as rectangular and circular, are often used where the geometrical tapering acts to reduce sidelobe levels. However, these aperture shapes are not covered in this thesis.

Name	$f(x)$	$G(u)$	3 dB beamwidth $a\Delta u$	Max. sidelobe
Rectangular	1	$a \cdot \frac{\sin(\pi au)}{\pi au}$	0.9	21.7 % -13.3 dB
Triangular	$1 - \frac{2 x }{a}$	$a \cdot \frac{1 - \cos(\pi au)}{(\pi au)^2}$	1.3	4.7 % -26.5 dB
Cosine	$\cos\left(\frac{\pi x}{a}\right)$	$(\pi a / 2) \cdot \frac{\cos(\pi au)}{(\pi / 2)^2 - (\pi au)^2}$	1.2	7.0 % -23 dB
Cosine-squared	$\cos^2\left(\frac{\pi x}{a}\right)$	$(a / 2) \cdot \frac{\sin(\pi au)}{\pi au} \cdot \frac{\pi^2}{\pi^2 - (\pi au)^2}$	1.45	2.6 % -31 dB

Table 5-4. Common aperture distributions of linear aperture and their Fourier Transforms [50]

5.2.1.2 Principles and Concept of PSDP

The underlying principle of the differential processing technique introduced will be demonstrated on Matlab, whereby the technique is applied on several simulated line source antenna of various aperture distributions. It will be shown that the reduction in beamwidth of

the sharpened point-target response provided, or the enhancement in angular resolution of the radar, is influenced by the characteristics of the antenna pattern and the extent of beam sharpening applied, which can be varied. As will be observed, applying the proposed technique enables a radar to have improved detection performance due to the enhancement provided from the proposed technique on top of the existing resolution performance of the original system. Implementation of the technique would allow the radar system to better distinguish two or more partially overlapping targets of different sizes and also have a higher success in discriminating targets against background clutter as it continuously scans for them.

5.2.1.2.1 Dealing with Point-target Operation

In signal processing, it is vital to recognize the shape of the desired signal and to be able to identify it within the received radar returns. The pertinent information that optimizes the discrimination of closely-spaced targets (resolution) is the amplitude gradient of the detected response, which is most accurately extracted by matching the gradient profile to that of the antenna response. Likewise, the detection of the presence of a signal is based on its amplitude, which is best detected by correlation of the amplitude profile of the received signal waveform with the known amplitude profile of the TX/RX antenna response. Hence, prior knowledge of the antenna response pattern of the echoes sought within the received radar returns, and that ideally being the two-way antenna propagation response for a monostatic radar, is significant in achieving the above. The processing technique proposed would give considerable improvement in radar performance as it is designed to make optimum use of the prior information. The algorithm used to apply the processing technique, which is described in this section, implements this.

To demonstrate the proposed signal processing method on the received signal of a radar, a monostatic radar employing a line source antenna with a uniform aperture distribution will be considered first. Since the same antenna is used for transmission and reception the radar antenna response is simply given by the antenna pattern squared. If two different antennas are used to transmit and receive respectively, such as in a bistatic arrangement, the antenna response is the product of the far-field patterns of Antenna 1 and Antenna 2. The far-field radiation pattern of a line source antenna with a uniform aperture distribution is represented by a sinc function. In a monostatic radar, the round-trip (TX/RX) antenna response is of the form

$$G(\theta) = \text{sinc}^2(a\theta) \quad (5-18)$$

The underlying principle and concept of the proposed technique is most easily understood when applied to a simulated video signal of a radar containing a single point-target in the absence of noise and clutter. Hence, a noise and clutter-free signal will be assumed first.

The process of the signal processing technique applied on the received signal of a radar is illustrated in Figure 5-26, where the y-axis represents the signal amplitude and the x-axis represents angle in degrees for all the plots presented.

In a practical system, the point-target response observed within the received signal is differs from the known antenna response due to the presence of noise and distributed clutter within the signal received. In this case, the pertinent information required to identify the presence of a point-target within a noisy signal is by extracting the amplitude gradient and matching the gradient profile to that of the known antenna response. This is achieved by creating the difference functions of both the point-target and antenna responses. However, in the absence of noise and clutter, assuming the case where the radar echoes received contains the detection of a point-target that falls on the center of the scanning beam, the target response would be easily identified within the received signal as it is identical to the antenna response, whereby the azimuthal shape of the beam is replicated by the envelope of several pulses within the received echo. In this case, the gradient profile of the detected point-target and antenna responses is identical to one another, as shown in Figure 5-26.

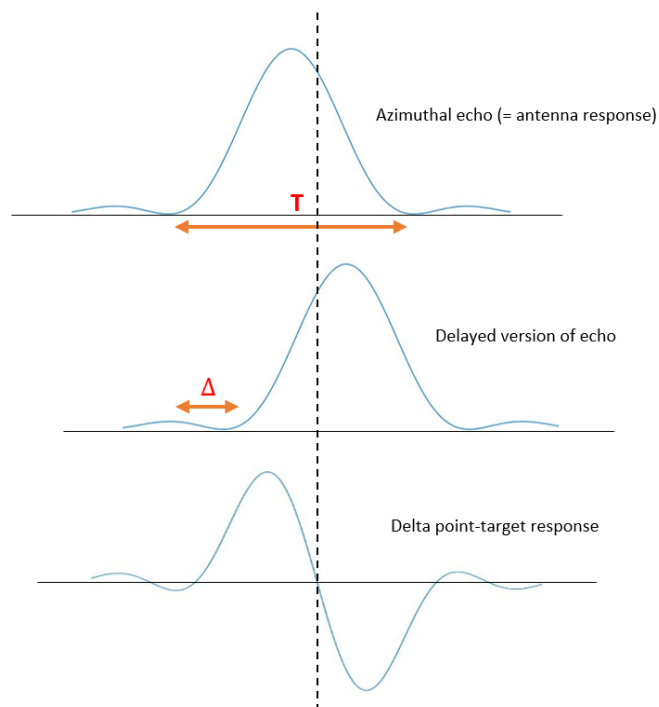


Fig 5-26. Differencing to create Δ point-target response and the correlation reference pattern

In both ideal and real-life scenarios, prior to differencing of the antenna and point-target response functions from their respective delayed versions, the separation Δ between the original and delayed versions of the point-target response is identical to the chosen separation

Δ between the original and delayed versions of the radar antenna response, which is determined based on the separation required to produce the chosen peak amplitude of the delta antenna response. Since the duplicated versions of the point-target and antenna responses are both delayed by an equal amount prior to differencing to create the respective difference functions, the delta antenna response function is also referred to as the correlation reference pattern.

The rising and falling edges of the original detected point-target response are extenuated when the delayed version is subtracted from it, which yields a positive peak followed by a negative peak, respectively, that contributes equally to the combined power within the difference function of the point-target response. Upon receiving at least one beamwidth worth of information, the operator can analyse these data from a single pulse as a line of constant bearing based on prior knowledge of the pattern of the echoes sought. However, for the gradient profile of the point-target response to be observable the SNR must be larger than one. This would also benefit the radar to effectively discriminate the presence of a valid target against weaker echoes that do not conform to the amplitude gradient, or shape, of the antenna response pattern, thereby avoiding false detections due to antenna sidelobes or background clutter. Nonetheless, the consideration of pattern acceptance is directly proportional to the chosen fraction of the gradient profile of the target response that matches the correlation reference pattern. Hence, the probability of false alarm would also largely depend on this choice. In Figure 5-27, since the illustration assumes the absence of noise and clutter, the difference function of the point-target response and antenna response (correlation reference pattern) is identical to one another.

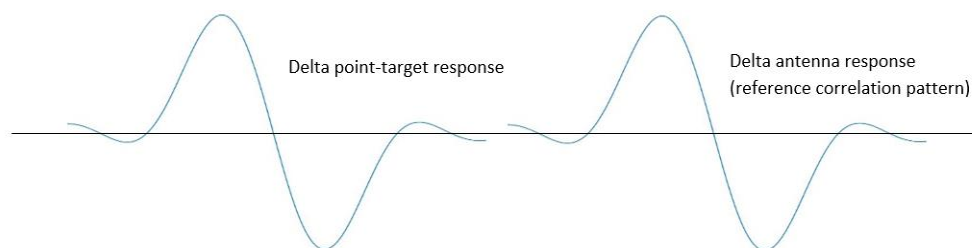


Fig 5-27. Δ point-target response equals the correlation reference pattern in the absence of clutter

Differencing of the point-target response prior to correlation with a replica of itself in an ideal noise free case, or with a similar waveform in real-life conditions, effectively converts the blunt top of the main lobe of the point-target response into a considerably sharper peak (i.e. beam sharpening). Differencing, before correlation, is a form of spectral weighting of the beam shape that favours the high-frequency components. Replica correlation (i.e. match filtering) may be applied directly to the full, undifferentiated pulse. However, correlation for the full

pulse would only provide the matched filter benefit of looking for echoes of known shape, in both SNR and precision, but it does not improve the angular resolution and clutter resilience of the radar. Hence, correlation can be applied directly if the properties of the point-target response waveform is already optimum for resolution.

The resulting correlation function is essentially a sharpened version of the original point-target response. This function is referred to as the sharpened response which corresponds to the same target. Hence, the presence of a signal is best detected by correlating the difference function of the point-target response with the known difference function of the antenna response (correlation reference pattern), or a replica of itself in a noise and clutter free case. Unlike conventional systems, the signal processing method does not depend on a high SNR to achieve a very low probability of false alarm. As shown in Figure 5-28, in addition to the more compact main lobe within the sharpened point-target response, the autocorrelation of the difference functions also generates a pair of fundamental pre-cursor and post-cursor -6 dB sidelobes that flanks both sides of the main lobe.

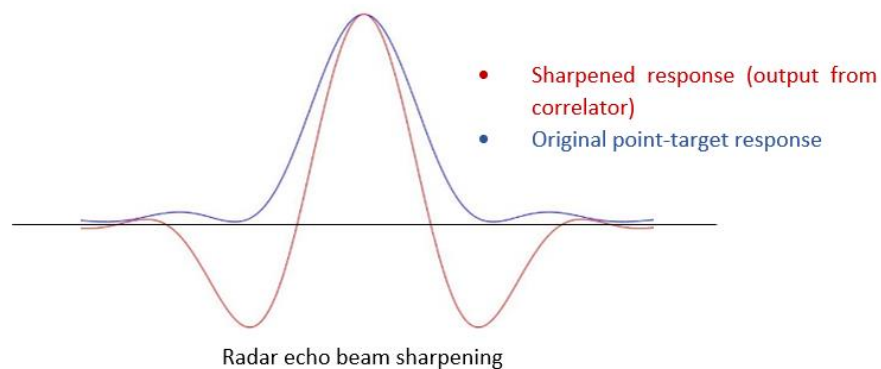


Fig 5-28. Output of correlator in the angle-domain

Assuming only the horizontal plane of the radar response is of interest, applying the processing technique would substantially reduce the azimuthal echo footprint received due to the beam sharpening of the point-target response. The sharpened response produced exhibits a narrower beamwidth that corresponds to a modest improvement in the angular resolution of the radar at all ranges. The beamwidth of the sharpened response is n times the beamwidth of the original target response, which corresponds to a radar with an angular resolution that is $1/n$ times higher than the original system. The reduction in beamwidth of the sharpened response is by $1-n$ times the beamwidth of the original response and, therefore, the angular resolution and clutter footprint within the sharpened echo is increased and decreased by $1-n$ times, respectively, since the decrease in clutter footprint relative to the target signal is proportional to the reduction in beamwidth of the original response.

Providing that the point-target remains within the beamwidth, or resolution cell, of the sharpened response in a specific plane, the proposed processing technique is effective as not only does it improve the detection capability for targets that the radar seeks to detect but it also increases the target signal to clutter ratio (SCR) at a given range, which increases the much needed clutter resilience of the radar by the same amount, since both are affected equally by spreading losses and, therefore, the SCR decreases inversely with the increasing azimuthal clutter footprint (i.e. inversely with range). Hence, the clutter-limited maximum detection range of the radar is increased by $1/n$ times. The analysis on the effect of the technique on the SNR of a noisy radar signal received is provided in Section 5.2.1.5, where the technique is applied on a simulated noisy signal. Nonetheless, the effect of noise on the received signal is likely to be minimal as the system is likely to be clutter limited.

The extent of beam sharpening can be effectively varied according to the requirement of the application in hand, and this allows the technique to be applied for various radar applications involving different target sizes and operating ranges. The term describing the different levels of beam sharpening can be categorized into minimum, intermediate, and maximum sharpening. For a given antenna pattern, the extent of beam sharpening is dependent on the separation, or overlap, between the original antenna and point-target responses with their duplicate versions prior to differencing and correlation of the respective difference functions. An analysis on the enhancement in resolution performance of the sharpened response for different levels of beam sharpening is provided in Section 5.2.1.3.

5.2.1.3 Effect of Overlap on Enhancement in Resolution Performance

In a coastal surveillance radar, the resolution of the radar system in the plane in which the technique is applied is prioritized. This section simulates different levels of pulse sharpening with the sharpened response by varying the overlap between the original video pulse and the delayed version of the pulse prior to differencing of the two functions, and, for each case, to analyze the effect that the amount of overlap has on the level of sharpening achieved with the sharpened response. To demonstrate this the differential processing technique is first applied on the output of a line source antenna with a uniform aperture distribution that has a far-field antenna pattern represented by a sinc function.

To specify the properties of the radar antenna response (TX/RX antenna pattern), $G(\theta)$, the scale factor a in (5-18) must be defined to model the desired half-power beamwidth of $G(\theta)$. The scale factor is parameterized according to the specific function and is unique to itself. The analysis for a sinc squared function is provided, as an example, to determine the appropriate scale factor of this function.

At the -3 dB points, $G(\theta) = 1/\sqrt{2}$. By iteration, this occurs at

$$a\theta = \pm 1.0 \text{ (to 2 s. f.)} \quad (5-19)$$

Thus, for a sinc squared function, a is a function of the beamwidth by

$$a \approx \frac{2}{BW} \quad (5-20)$$

A scale factor of 0.5 is required to simulate a sinc squared function that has a beamwidth of 4 degrees. Figure 5-29 presents this antenna response function, which will be used for the remaining simulations presented in this chapter.

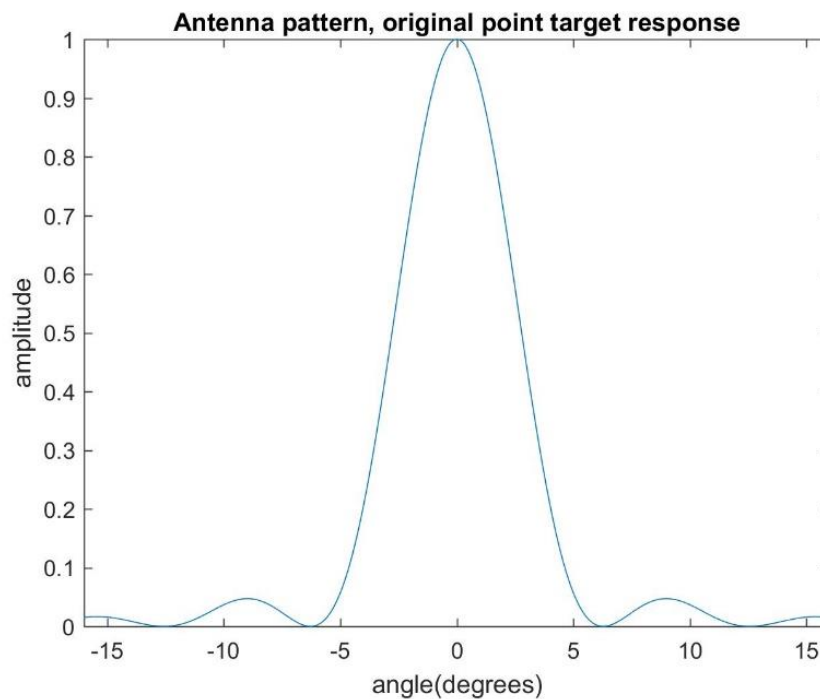


Fig 5-29. Antenna response pattern - far-field pattern of uniform line-source distribution

A significant overlap, or small separation, between the original and delayed versions of the antenna response prior to differencing of the two functions corresponds to a correlation reference pattern that has a narrow positive and negative peak, each of a small amplitude or a substantially reduced power within the function. A small overlap, on the other hand, would correspond to a correlation reference pattern with a wide positive and negative peak, each of a considerably larger amplitude that is close to the peak amplitude of the original function. Thus, the extent of overlap between the two functions can be measured by means of the peak amplitude of the correlation reference pattern relative to the peak amplitude of the original function, A .

The differential processing technique is applied at various extent of overlap between the two functions, such that the peak amplitude of the correlation reference pattern lies within $0.2 \leq A \leq 0.8$, in intervals of 0.2, to analyse the extent of beam sharpening on the sharpened response. To identify the separation of the normalized antenna response and its delayed version (two identical sinc squared functions) such that the peak amplitude of the correlation reference pattern is 'A' of the peak amplitude of the original function, the value of $\Delta(a\theta)$ in (5-21) must be determined such that

$$\max \{ \text{sinc}^2(a\theta) - \text{sinc}^2(a\theta - \Delta(a\theta)) \} = A \quad (5-21)$$

again by iteration, the appropriate value of $\Delta(a\theta)$ for the desired value of A to be achieved is evaluated. Thus, the required angular spacing ($\Delta\theta$) between the original and delayed versions of the antenna response for the peak amplitude of the difference function to be of the desired value (A) is given by

$$\Delta\theta \approx \frac{\Delta(a\theta)}{a} = \frac{\Delta(a\theta)BW}{2} \quad (5-22)$$

This separation required between the two functions prior to differencing is calculated according to the known properties of the radar antenna response (i.e. antenna beamwidth).

Assuming the absence of clutter within the received signal and noise at the radar output, the properties of the sharpened response corresponding to various extents of beam sharpening are summarized in Table 5-5. The data provides an analysis on the effect of the chosen separation, or overlap, between the azimuthal echo and the delayed version of the echo has, prior to differencing and correlation of the difference functions, on the level of sharpening achieved with the sharpened response. The level of sharpening, nonetheless, is measured based on the reduction in beamwidth (angular resolution enhancement) of the sharpened response as compared to the original point-target response.

Amplitude of Difference function (A)	BW of Original response (deg)	BW of Sharpened response (deg)	Fractional BW (%)	Sharpening improvement factor
0.2	4	2.99	74.7	1.34
0.4	4	3.02	75.5	1.32
0.6	4	3.08	77	1.3
0.8	4	3.2	80	1.25

Table 5-5. Original and sharpened response for different extent of beam sharpening

For maximum pulse sharpening ($A = 0.2$) of a detected point-target response the enhancement in resolution performance of the radar is realized through a modest reduction of

25.3 percent in beamwidth (from 4 to 2.99 degrees), or target size, between the original and sharpened response, thereby effectively increasing the angular resolution of the radar by 33.8 percent. The effective echo footprint within the sharpened response is also reduced by the same amount, which relates to a proportional increase in the target SCR (increased maximum clutter-limited range) as compared to the original response.

The sharpening effect of the technique on an antenna with a far-field pattern approximated by a sinc function is not substantial because although the rising and falling edges of the function are considerably steep (sharp roll-off), the pattern has a rounded shape rather than a flat top. The optimum beam pattern of the antenna that would benefit the most from the technique is discussed in Section 5.2.1.6. The routine shown in the simulation above is unique to the chosen antenna far-field pattern and would be different for any other random arbitrary antenna pattern. Figure 5-32 illustrates the process that demonstrates maximum beam sharpening ($A = 0.2$), and in Figure 5-33 for reduced beam sharpening ($A = 0.8$), associated with fuller exploitation of the pulse energy. The amplitude of the plots shown were normalized to the peak of the original point-target response.

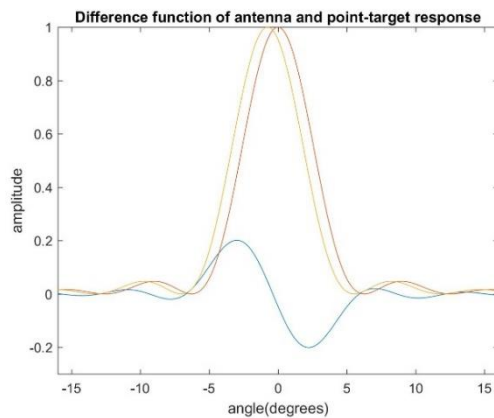


Fig 5-30. Maximum overlap ($A = 0.2$)

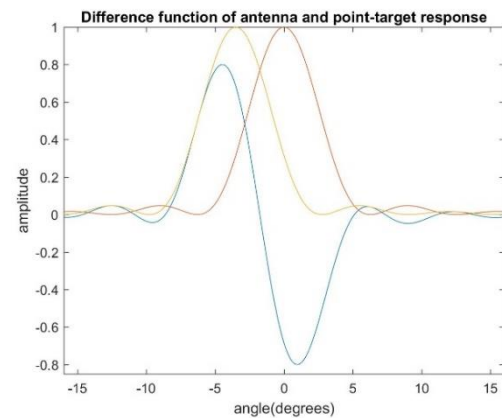


Fig 5-31. Minimum overlap ($A = 0.8$)

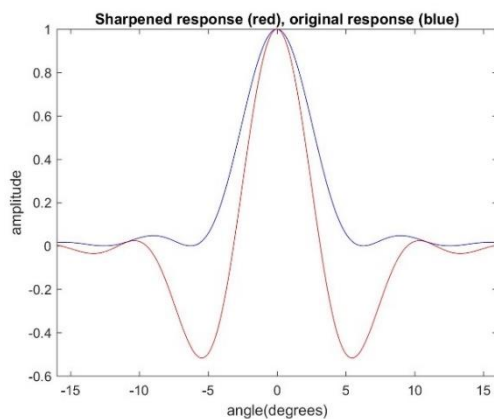


Fig 5-32. Maximum pulse sharpening

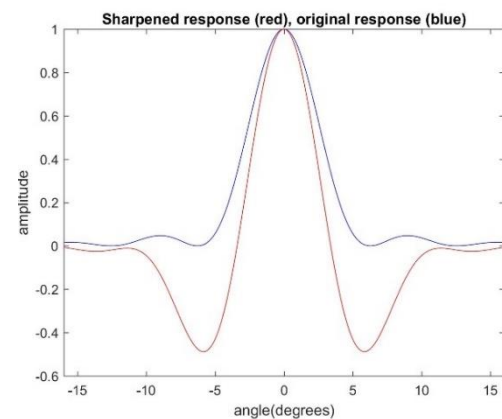


Fig 5-33. Reduced pulse sharpening

This section had evaluated the effect that the chosen overlap has on the extent of beam sharpening realized for a given antenna pattern. The following section provides an analysis on the influence that the characteristics of the antenna far-field pattern has on the sharpening effect of the processing technique achieved for a given overlap specified beforehand. To present this, the sharpening technique is also applied on a simulated received signal of a radar that has an antenna far-field radiation pattern represented by the far-field pattern of several other chosen line source antennas of common aperture distributions.

5.2.1.4 Resolution Enhancement on Common Aperture Distributions

This section demonstrates the effect of the processing technique on the output signal of radar systems employing line source antennas with several types of common aperture distributions, given that the same set of assumptions applied in the simulation performed thus far are retained. The objective is to evaluate the improvement in angular resolution between the original and sharpened response for each case, and to compare and identify the optimum characteristics of the antenna far-field pattern that would maximize the enhancement in resolution performance achieved with the sharpened response.

The far-field pattern of several common line source aperture distributions are given by the functions, $G(u)$, shown in Table 5-6. These functions are Fourier transforms of each of the aperture distributions and are approximate representation of typical antenna far-field patterns.

Name	$f(x)$	$G(u)$
Rectangular	1	$a \cdot \frac{\sin(\pi au)}{\pi au}$
Triangular	$1 - \frac{2 x }{a}$	$a \cdot \frac{1 - \cos(\pi au)}{(\pi au)^2}$
Cosine	$\cos\left(\frac{\pi x}{a}\right)$	$(\pi a / 2) \cdot \frac{\cos(\pi au)}{(\pi / 2)^2 - (\pi au)^2}$
Cosine-squared	$\cos^2\left(\frac{\pi x}{a}\right)$	$(a / 2) \cdot \frac{\sin(\pi au)}{\pi au} \cdot \frac{\pi^2}{\pi^2 - (\pi au)^2}$

Table 5-6. Far-field pattern of common aperture distributions [50]

In Section 5.2.1.2 and 5.2.1.3, the differential processing technique was simulated on the output of a radar employing a line source antenna with a uniform aperture distribution. The simulation demonstrating the processing technique is repeated in this section for several other antenna far-field radiation patterns, each of which is represented by the far-field pattern of a specified line source distribution. These several other common aperture distributions are triangular, cosine and cosine-squared. Assuming point-target operation, the differential processing technique is simulated on a section of the received signal containing a point-target, that is, a point-target response within the output signal that is equivalent to the antenna response $(G(u))^2$ for a monostatic radar) in a noise and clutter-free case. For each of the antenna far-field pattern $G(u)$, the scale factor a of the radar antenna response, which defines the beamwidth of the response, is unique to itself, and the same applies for the parameterization required to produce a correlation reference pattern with a peak amplitude that is chosen to be half of the antenna response ($A = 0.5$), as shown in the examples in this section.

The effect of the differential processing technique observed on the respective point-target responses are presented in Table 5-7. An analytical comparison of the properties of the sharpened responses corresponding to each antenna pattern simulated allows the ideal characteristics of the antenna radiation pattern that would most benefit from the sharpening effect of the technique to be determined, which is particularly based on the greatest reduction in beamwidth of the corresponding sharpened point-target response. The effect of the processing technique on antennas with other aperture shapes is not provided in this thesis.

Aperture Distribution	Original -3 dB BW (deg)	Sharpened -3 dB BW (deg)	Fractional BW	Reduction in BW (%)	Sharpening Factor
Rectangular	4	3.04	0.76	24.1	1.32
Triangular	4	3.19	0.8	20.2	1.25
Cosine	4	3.17	0.79	20.8	1.26
Cosine squared	4	3.2	0.8	20.1	1.25

Table 5-7. Effect of the sharpening technique on different far-field distributions

Apprehending the simulation results shown in Table 5-7 indicates that the largest sharpening effect is observed on the point-target response represented by a sinc squared function. The processing technique is most suitably applied on an antenna with a uniform aperture distribution, which is expected due to the elevated shape and sharper roll-off of the function as compared to the other patterns presented. Applying the processing technique on the detected point-target response (sinc squared function) observes a 24.1 percent reduction in beamwidth on the sharpened target response, thereby theoretically producing an antenna

whereby the angular resolution and maximum clutter-limited detection range of the radar is 32 percent higher than the original radar system.

5.2.1.5 Effect of Sampling Interval on SNR of Received Signal

In the simulations performed thus far we have assumed that the detected signal from the radar output imagines as a point-target at the center of the beam in the absence of noise and clutter. In a real system, however, received radar signals are always infiltrated with clutter, which is masking as noise, and receiver noise. Hence, an analysis on the effect of the differential technique on the SNR of a radar signal is vital.

This section demonstrates this by applying the differential technique on a simulated radar signal that is infiltrated with noise. An artificial detected signal is simulated by adding random Additive White Gaussian noise (AWGN) on the ideal modelled noise free signal (equivalent to the antenna response) shown in Figure 5-29, assuming for a point target operation. The SNR of the simulated noisy signal is 20 dB.

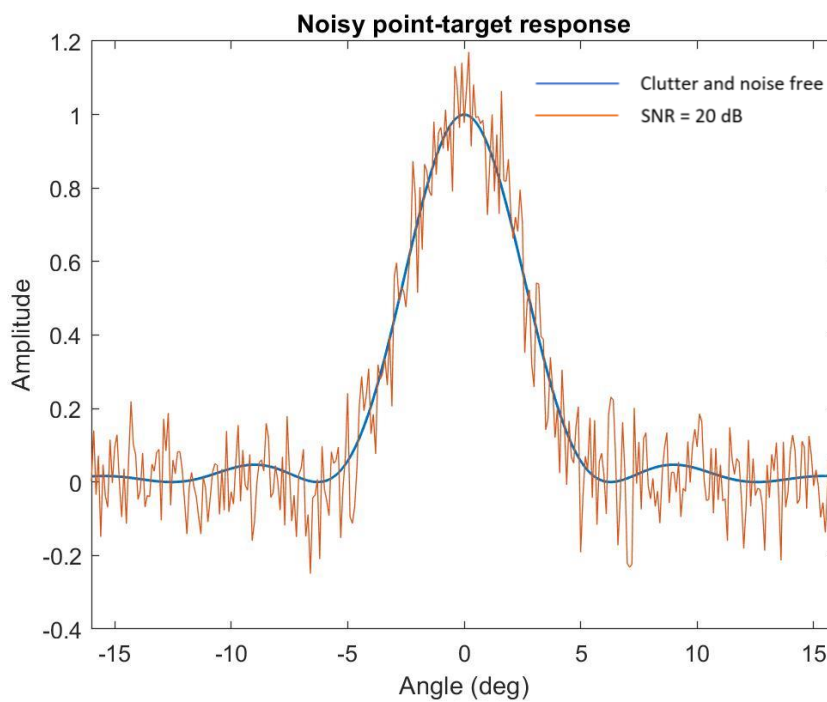


Fig 5-34. Noisy point-target response (SNR = 20 dB)

The effect of the differential technique on the SNR of the original response is analysed by comparing the difference between the SNR of the original noisy signal and that of the sharpened response. To analyse this, two parameters are considered when applying the differential technique on the simulated noisy signal – the number of sample points, or sampling interval, of the measured data, which is related to the scan period plus duration and time of

flight, and the peak amplitude of the correlation reference pattern, that is correlated with the difference function of the target response to produce the sharpened target response.

The simulated point-target response shown in Figure 5-34 has a sampling interval of 0.1 degree. The differential processing technique is applied on the noisy target response for $0.2 \leq A \leq 0.8$, where A is the peak amplitude of the correlation reference pattern relative to the peak amplitude of the normalized antenna response. In this case, for all values of A the peak amplitude of the correlation reference pattern and of the difference function of the target response will not be the same due to the presence of clutter and noise within the received radar signal. Nonetheless, the noise within the difference function of the point-target response is effectively averaged out when it is cross-correlated with the correlation reference pattern, which tends to the differential of the antenna response, because correlation is effectively an averaging process. Hence, as the amplitude of the difference function A tends to zero, the noise of the target response is filtered by a nearly perfect differentiator (favouring higher frequencies) and the random noise present on the processed signal is almost eliminated entirely (Figure 5-36). Figure 5-35 presents the original and sharpened point target response, for $A = 0.2$.

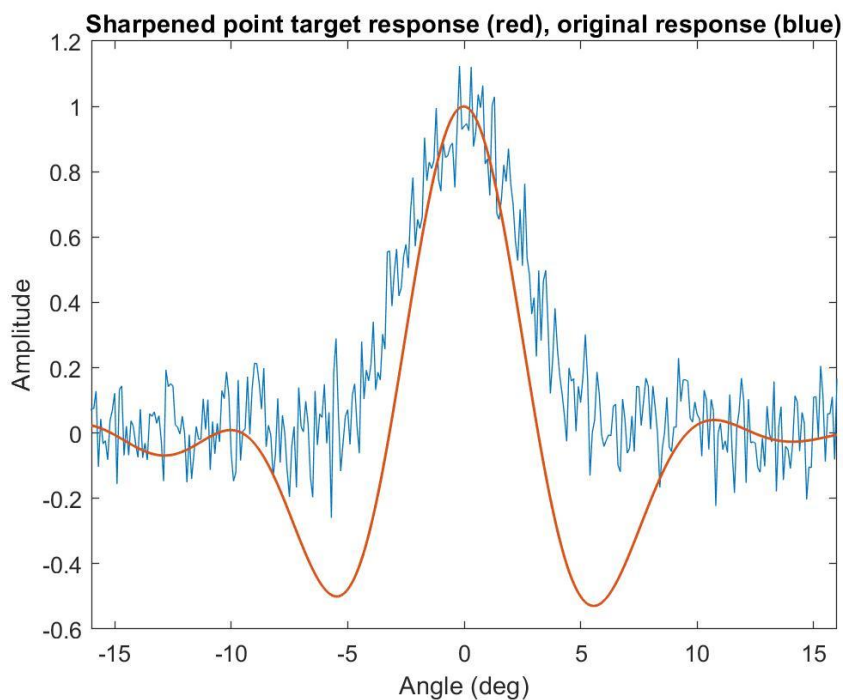


Fig 5-35. Original and sharpened point-target response

To calculate the SNR of the sharpened point-target response the noise within the signal must be identified. The noise that remains within the sharpened target response is generated by subtracting the sharpened response of the noise-free case from the noisy case, or the difference in signal amplitude of the two signals. This example is illustrated below.

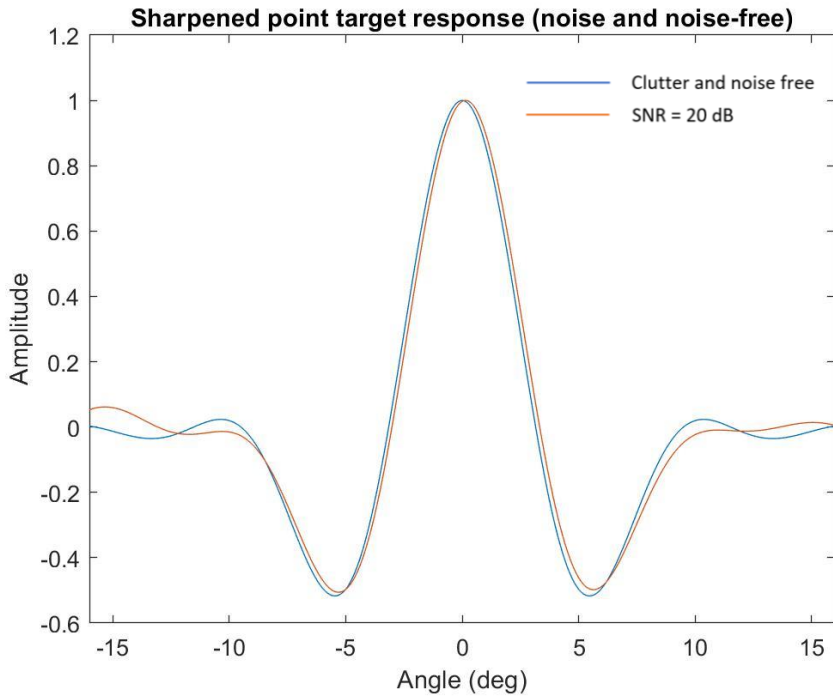


Fig 5-36. Sharpened response (noise and noise-free)

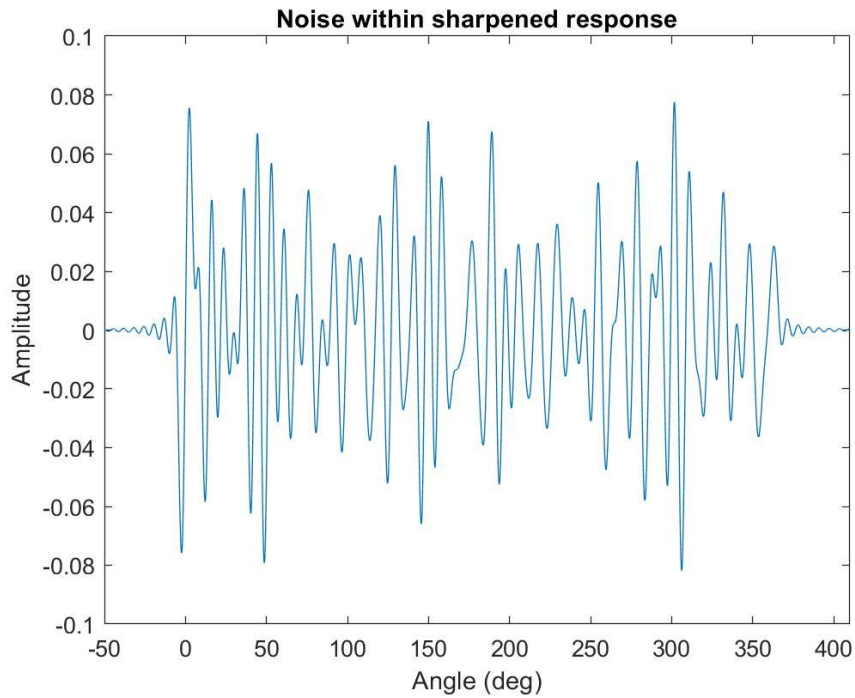


Fig 5-37. Noise within the sharpened point-target response

The SNR of the sharpened point-target response obtained is 32.1 dB, for $A = 0.2$. This corresponds to an SNR improvement of 12.1 dB given that the SNR of the original point-target response is 20 dB. The impression of an improved SNR of the sharpened target response benefits from the effect of correlating a smooth but noisy function (difference function of point-

target response) with a priori knowledge of the underlying shape, or a known version of the point target response, which significantly reduces the random noise within the originally received radar signal. Hence, the differential technique not only improves the maximum clutter-limited detection range of the radar but also improves its noise-limited detection range, despite the effect of noise on the received signal to be minimal since coastal surveillance radar systems are likely to be clutter-limited.

The process is repeated across the other chosen values of A . Table 5-8 provides the SNR of the sharpened point-target response and the change in SNR between the original and sharpened response for each value of A simulated.

Amplitude of Difference function (A)	Sampling interval	SNR of Original response (dB)	SNR of Sharpened response (dB)	SNR improvement (dB)
0.2	0.1	20	32.1	12.1
0.4	0.1	20	31.9	11.9
0.6	0.1	20	32.1	12.1
0.8	0.1	20	32.6	12.6

Table 5-8. SNR of sharpened point-target response for increasing values of A

The SNR of the sharpened response remains unchanged across the values of A simulated and, therefore, the improvement in SNR realized is independent of the peak amplitude of the correlation reference pattern, if not only has minimal effect. This is expected as noise within the difference function of the point-target response reduces proportionally with decreasing A . Hence, the value of A only influences the extent of beam sharpening realized with the sharpened response. For this reason, a small value of A is preferred to optimize the resolution performance of the sharpened response since in most cases it does not present a trade-off with the enhancement of SNR achieved from the processing technique.

The following parameter to consider is the sampling interval of the detected point-target response. Since the processing technique is an averaging process, the SNR improvement of the detected target response is expected to be related to the real sampling interval of the data. To analyze the effect that the chosen sampling interval has on the SNR change between the original and sharpened point-target response, the original point-target response shown in Figure 5-29 is re-simulated with several sampling intervals, from which the differential processing technique is applied individually on each target response and the SNR of the corresponding sharpened responses are calculated. Table 5-9 provides the SNR of the sharpened point-target response and the SNR change between the original and sharpened response for different sampling rates, or intervals, used to simulate the detected point-target response.

Amplitude of Difference function (A)	Sampling interval	SNR of Original response (dB)	SNR of Sharpened response (dB)	SNR improvement (dB)
0.2	0.01	20	41.8	21.8
0.2	0.05	20	35	15
0.2	0.1	20	31.9	11.9
0.2	0.5	20	24.7	4.7

Table 5-9. SNR of sharpened point-target response for increasing sampling interval

As shown in Table 5-9, the smallest possible sampling interval is preferable to maximize the enhancement on the SNR of the sharpened response. The sampling interval can be made arbitrarily small in the MATLAB simulation, but in practice it is unlikely for it to be smaller than 0.1 degrees. For samples every 0.1 degree a substantial c. 11.9 dB SNR improvement is realized. The sharpened target response achieved at this sampling interval has a very good visual appearance (Figure 5-36). On the other hand, at an interval of 0.5 degrees, for instance, although the sharpened target response still appears to be noise-free (due to the small point spacing and because the noise is very smooth) and a modest (c. 4.7 dB) SNR improvement is achieved, the visual appearance is deteriorated due to the lower sampling rate.

Referring to the results shown in Table 5-9, a sampling interval of 0.1 degrees is an ideal choice in evaluating the effect of the technique on the SNR of the original target response as this is a realistic sample rate that can be implemented. The simulation has demonstrated that the SNR of the processed signal varies only with the number of samples and not the peak amplitude of the correlation reference pattern (A value). Hence, a suitable value of A would be chosen to achieve maximum beam sharpening.

5.2.1.6 Optimum Beam Pattern

The simulations performed thus far has shown that the enhancement in resolution performance of an existing radar system from the implementation of the differential processing method proposed is based on two characteristics of the antenna response function: the steepness of the roll-off and the flatness of the pattern, from which a greater improvement in resolution is observed on antennas that radiates a pattern exhibiting a flat top and steep sides. Indeed, the technique offers zero improvement in resolution performance for antennas with ultra-sharp waveforms since these types of functions directly realizes the optimum resolution potential of their beamwidth, and therefore does not observe any beneficial improvement from differential processing. Hence, to achieve maximum benefit of the beam sharpening the antenna aperture must be designed to have a substantially uniform distribution, rather than tapering markedly towards its edges. Figure 5-38 illustrates the processing technique on a suitable multi-pulse

azimuthal echo that possesses the desirable characteristics required to take full advantage of the sharpening effect of the technique proposed.

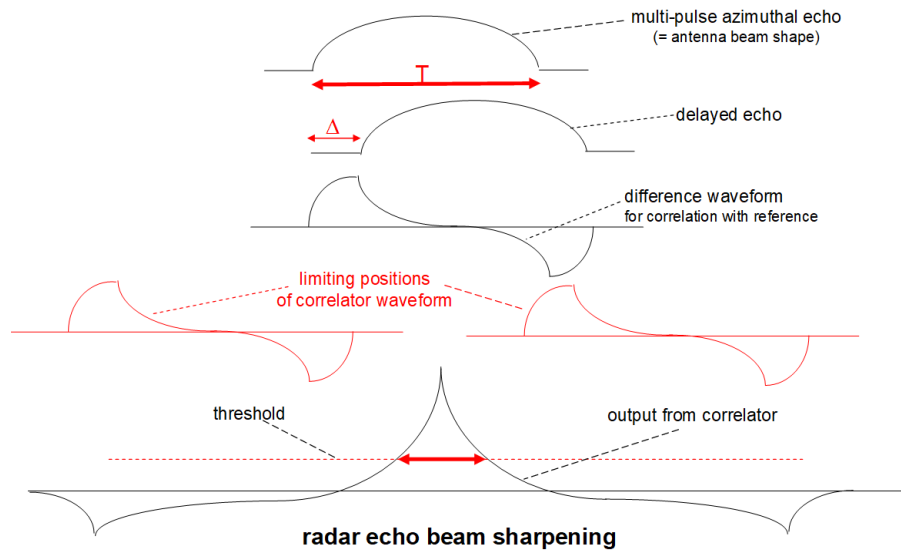


Fig 5-38. Optimum beam pattern for PSDP

The example in Figure 5-38 shows that, with a suitable antenna response function, applying the technique on the echo received could produce a sharpened beam with a beamwidth that is a tenth of the beamwidth of the original response, which corresponds to enhancing the angular resolution performance of the antenna by as much as ten times. Although the ideal antenna pattern to operate with the proposed technique is one that has a sharp roll-off and a rather flat top, such as the pattern used in the example shown above, the radiation pattern of most antennas does not exhibit these properties. To observe the maximum sharpening capability of the differential processing on an existing video output of a radar, methods of designing the aperture field distribution of an antenna to produce a far-field radiation pattern with the desired properties can be focused on as future work.

5.2.2 Sidelobe Reduction Technique

Implementing pattern selective differential processing would considerably enhance the detection capability of a target against clutter and an improvement in the resolution performance of an existing radar system. However, in addition to generating a more compact echo within the sharpened response is a pair of fundamental sidelobes that flanks both sides of the main lobe. The formation of the pair of sidelobes are undesirable especially in complicated situations where there are several closely spaced targets as the sidelobe of a large target could partially, if not completely, obscure the detection of a much smaller target. The issues arising

from the formation of large sidelobe within the sharpened response of a point-target are discussed in Section 5.2.2.1, and a signal processing method that will significantly reduce the pair of -6 dB sidelobes is introduced in Section 5.2.2.2. This proposed technique is known as sidelobe reduction technique, which effectively redistributes the energy within the original -6 dB sidelobes across several smaller sidelobes that are formed to replace the original sidelobes within the newly sharpened response.

5.2.2.1 Issues with Sidelobes of a Point-target Response

Applying the differential processing technique on the received signal of a continuously scanning antenna containing the detection of a point-target produces the signature shown in Figure 5-41. In a stationary radar, the presence of the negative pre-cursor and post-cursor sidelobes within the sharpened response could detect unwanted targets and provide a false interpretation of target detection in terms of direction and target size. In a mechanically scanning radar, the issue can get more complicated as the pair of sidelobes could interfere with the main lobe of a response belonging to a neighbouring target.

In situations where there are multiple targets present the operator will supposedly observe multiple scaled versions, or amplitude, of that shape, whose amplitude would correspond to the target size, but in different positions or in different angles of rotation. For closely spaced targets the response of each target could partially overlap one another. When this happens, the sidelobes within the response of a real target could accurately coincide and substantially reduce the amplitude of the main lobe of a neighbouring target response by the sidelobe amount. The worst case is realized when the detection of a much smaller target is prevented due to it being completely masked by the negative sidelobes of a large neighbouring target. Hence, a small target may completely fail to be detected should it accurately coincide with a larger sidelobe belonging to the response of a nearby target. Although the probability of this occurring is significantly less than that of a small target being undetected due to the merging of the two echoes in the absence of resolution sharpening benefited from the differential processing technique this would be detrimental as the detection of the obscured target within that rotation scan is prevented, for at least the duration of the target remaining in the sidelobe.

Figure 5-39 illustrates the above-mentioned situation; there are two closely spaced point-targets which we will name ‘Target 1’ and ‘Target 2’, respectively. In the example provided, the size of Target 2 is half of Target 1 and therefore the amplitude of the response corresponding to the smaller target is assumed to be half of the larger target in the absence of noise and clutter. The resulting waveform at the video output is given by the green plot, which is the sum of the two point-target responses.

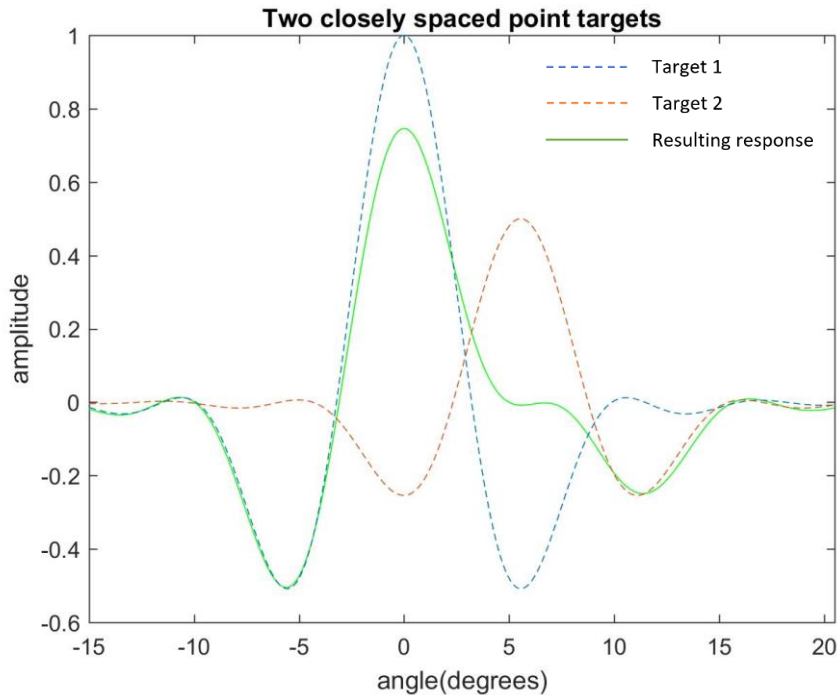


Fig 5-39. Corresponding response of two closely spaced targets

From the resulting waveform produced, the peak amplitude of Target 1 is reduced by approximately 25 percent due to the pre-cursor sidelobe within the response of Target 2 coinciding with it. Likewise, the peak amplitude of Target 2 is completely obscured by the post-cursor sidelobe of Target 1, which at this point prevents the scanning radar from detecting Target 2 as a valid target. Although the inability of the radar to detect a valid target should only be temporary as it is unlikely to remain in the sidelobe of a neighbouring target for long, the presence of sidelobes within the response of a point-target can be detrimental especially in applications involving the surveillance of many closely spaced targets. Hence, it is vital to eliminate, if not suppress, the pair of sidelobes to prevent the deterioration in radar performance.

A processing technique is proposed to suppress the pair of sidelobes generated within the sharpened response and, therefore, to minimize the probability of a smaller target from being obscured by a larger sidelobe, so that a smaller target would still be detected by the radar although its true size is altered and, therefore, inaccurate. The technique achieves this by suppressing the amplitudes of the negative sidelobes within a sharpened target response into several sidelobes of smaller amplitude. The proposed technique that effectively suppresses the original -6 dB sidelobes into several smaller ones is known as sidelobe reduction processing, and is a measure taken against such unnecessary losses that can be minimized. The technique is described in depth and will be simulated on an existing sharpened point-target response. An

analysis of the sidelobe suppression method will be provided in Section 5.2.2.2 based on the simulations performed.

5.2.2.2 Principles and Concept of SRT

As observed in Figure 5-38, the leading edge of the difference function comprises of its own convex leading edge followed by a concave trailing edge, whereas the trailing edge of the difference function comprises of a concave leading edge followed by a convex trailing edge. Since the extra component pulses of the extended correlation reference pattern have to correlate with these equally, the best shape of the extra pulses in the leading and trailing edge of the correlation reference pattern is the mean of these two (i.e. a symmetrical linear rising and falling edges that is bridged by a short and slightly curved flat top). By adding one or more of these positive pre-cursor and negative post-cursor pulses, or lobes, to the leading and trailing-edges of the correlation reference pattern, respectively, prior to correlation of the extended reference pattern with the difference function of the target response corresponding to a detected point-target, the largest sidelobe within the newly sharpened response would be significantly smaller than the pair of -6 dB sidelobes within the original sharpened response. Hence, for point-target operation in an ideal noise and clutter-free scenario, correlation of the extended correlation reference pattern with the difference function of the target response would effectively reduce the amplitude of the original precursor and post-cursor negative sidelobes by replacing itself with n sidelobes, respectively, within the newly sharpened response. In other words, the proposed technique redistributes the energy of the original sidelobes across the newly formed n sidelobes, each of a significantly smaller amplitude.

As demonstrated in Figure 5-30 and 5-31, the amplitude and shape of the positive and negative peaks within the correlation reference pattern is justified by the separation between the known antenna response and a delayed version of itself prior to differencing of the two functions. In the example shown, the separation between the two sinc squared functions was chosen to generate a correlation reference pattern with an amplitude that is half the peak amplitude of the antenna response. Figure 5-40 shows the correlation reference pattern with a peak amplitude of ± 0.5 .

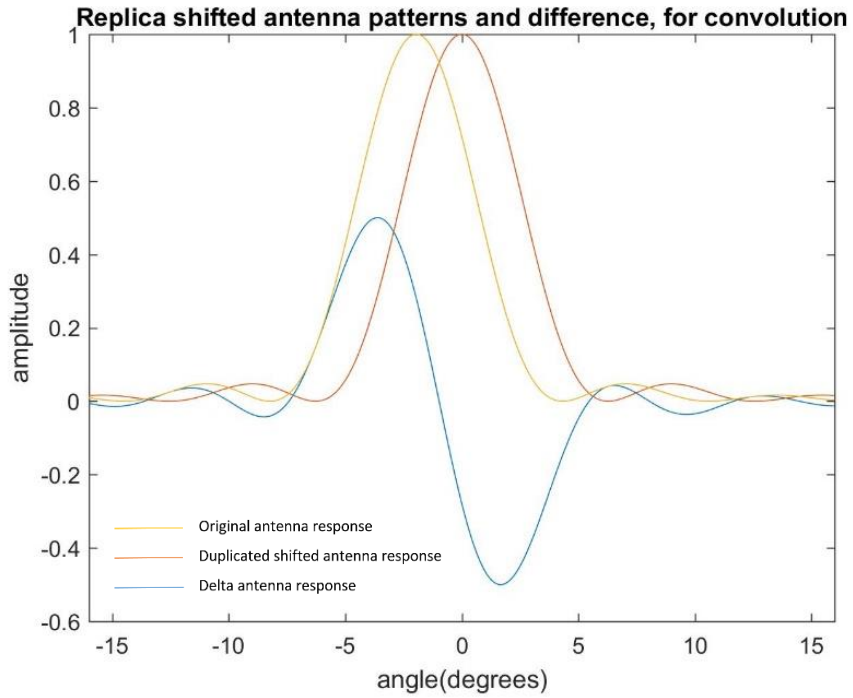


Fig 5-40. Correlation reference pattern ($A = 0.5$)

For point target operation, the sharpened response produced from the differential processing technique applied on the radar output of a line source antenna with a uniform aperture distribution (sinc function far-field pattern) is shown in Figure 5-41.

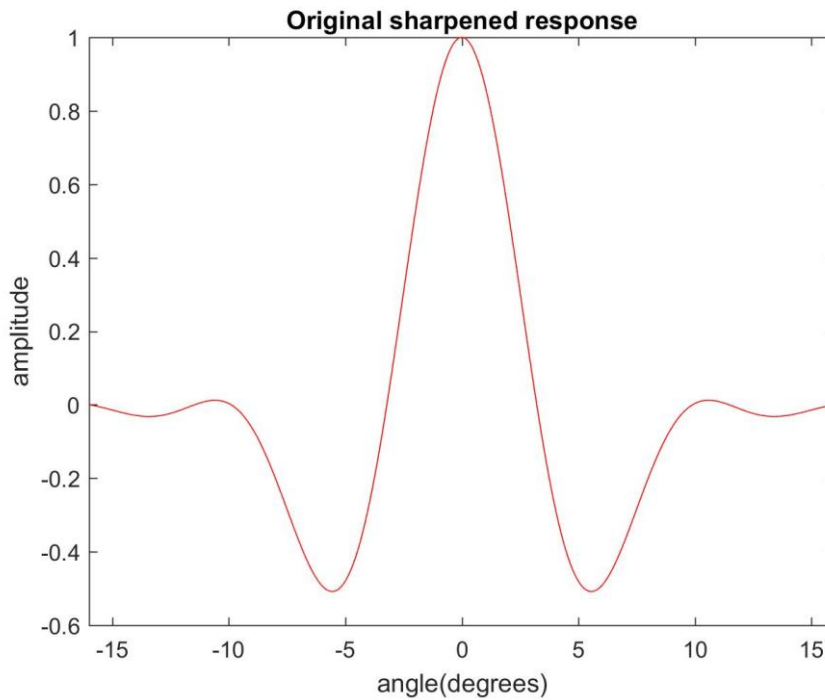


Fig 5-41. Sharpened response with -6 dB negative precursor and post cursor sidelobes

The pair of -6 dB sidelobes generated within the sharpened response of a real target are fundamental properties of the response arising from replica correlation of the difference function of the target response and the correlation reference pattern. Applying sidelobe reduction technique replaces each of the -6 dB sidelobe with n sidelobes of significantly lower amplitude within the newly sharpened response, which effectively reduces the original sidelobe amplitude by a considerable amount. Figure 5-42 presents the newly sharpened response of a point-target after sidelobe reduction technique is applied, for $n=2$.

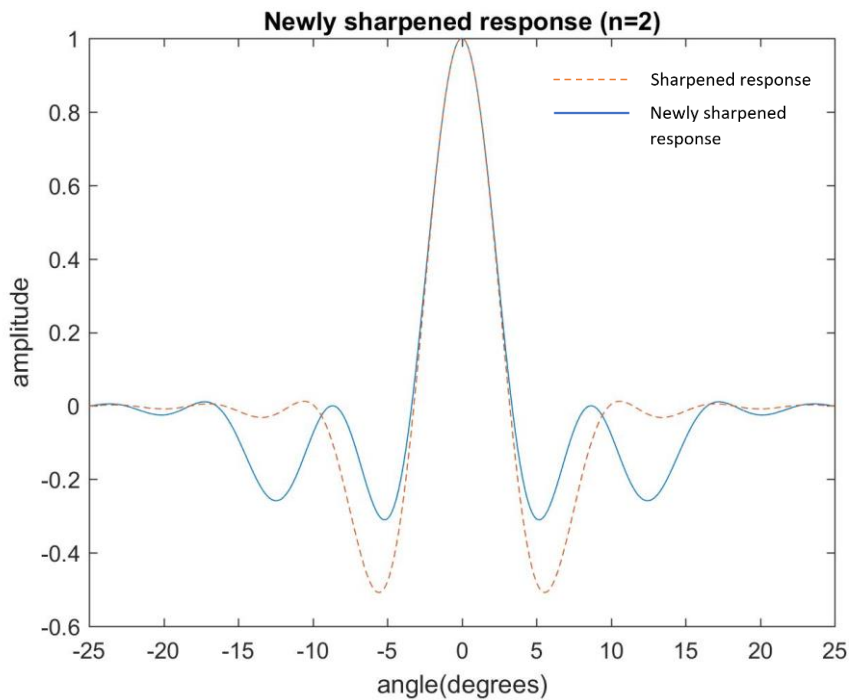


Fig 5-42. Newly sharpened point-target response, for $n = 2$

In the example shown in Figure 5-42, an extra pre-cursor and post-cursor lobe was added to the correlation reference pattern, at pulse length spacing, prior to correlation with the difference function of the target response. The newly sharpened response generates two pre-cursor and post-cursor sidelobes that flanks the unchanged main lobe. The amplitude of the highest sidelobe is reduced from -6 dB to -10.1 dB after the sidelobe reduction technique is applied, while the amplitude and beamwidth of the main lobe echo is unaffected and therefore retains the same degree of sharpening on the original point-target response, with and without sidelobe reduction technique applied.

The amplitude of the sidelobes produced within the newly sharpened response is dependent on the number of extra precursor and post-cursor lobes ($n-1$) introduced into the correlation reference pattern prior to correlation with the difference function of the target response. In the example shown above ($n=2$), the energy of the original pre-cursor and post-

cursor sidelobes are each redistributed almost evenly across the two new sidelobes formed on each side of the main lobe. Hence, for increasing values of n , or $n-1$ extra pulses introduced to the reference pattern, the technique effectively redistributes the energy of the original precursor and post-cursor -6 dB sidelobe across the n smaller sidelobes and, thus, the amplitude of the largest sidelobe decreases with increasing number of (n) pre-cursor and post-cursor sidelobes formed within the newly sharpened response.

The following section provides an analysis on the relationship between the number of pre-cursor and post-cursor lobes added into the correlation reference pattern, prior to correlation with the difference function of the target response, and the amplitude of the largest sidelobe formed in the newly sharpened response. Thus, the extent of suppressing the original -6 dB precursor and post-cursor sidelobes of the sharpened response upon applying the sidelobe reduction technique for different values of n can be observed by measuring the amplitude of the largest sidelobe of the newly sharpened response for the values of n simulated.

5.2.2.3 Effect of n Number of Pulses on the Extent of Sidelobe Reduction

The amplitude of the largest sidelobe flanking the positive lobe of the newly sharpened response is dependent on the equal number ($n-1$) of positive pre-cursor and negative post-cursor pulses introduced into the leading and trailing-edge of the correlation reference pattern prior to correlation with the delta target response. The number of pre-cursor and post-cursor pulses added alongside the leading and trailing-edge pulse of the correlation reference pattern are identical, each of $n-1$ similar pulses respectively, and separated from one another at pulse-length spacing. However, with increasing values of n , the drawback of the extra pre-cursor and post-cursor lobes introduced within the extended reference pattern is the inclusion of samples of ambient clutter. Nonetheless, since this includes equal numbers of positive and negative samples, this may not be a serious issue, provided the clutter is reasonably uniform.

To apply the sidelobe reduction technique on the original sharpened response, the leading-edge pulse of the correlation reference pattern will be preceded by $n-1$ similar precursor lobes, whose amplitude increases from one lobe to the next by $1/n$ of the amplitude of the positive pulse. Based on the original correlation reference pattern shown in Figure 5-40, the amplitude of the lobes added rises from $1/n$ to $(n-1)/n$ of the peak amplitude (+0.5), in intervals of $1/n$ of the peak amplitude between the n successive positive pulses, and then an amplitude of +0.5 for the true leading-edge pulse of the original reference pattern. Similarly, the trailing-edge pulse with an amplitude of -0.5 is followed by the $n-1$ similar postcursor pulses introduced, whose amplitude decreases from one pulse to the next by $1/n$ of the amplitude of the negative pulse. Thus, from the true trailing-edge pulse with an amplitude of -0.5, the amplitude of the lobes added declines from $-(n-1)/n$ to $-1/n$ of the peak amplitude (-0.5) in intervals of $1/n$ of the

peak amplitude between the n successive negative pulses. Hence, the extended correlation reference pattern consists of $n-1$ extra lobes in the leading and trailing-edge of the function, respectively.

Figure 5-43 illustrates an extended correlation reference pattern for $n=3$. In the leading-edge of the extended correlation reference pattern, two extra positive pulses, separated at pulse-length spacing, is followed by the already existent leading-edge pulse. The amplitude of the three positive pulses rises by $1/3$ of the amplitude of the existing leading-edge pulse consecutively, from $1/3$ of 0.5 (0.167) to 0.5 . Likewise, in the trailing-edge pattern, the already existent trailing-edge pulse is followed by two extra negative pulses. The amplitude of the three negative pulses increases by $1/3$ of the absolute amplitude of the existing trailing-edge pulse consecutively, from -0.5 to $-1/3$ of -0.5 (-0.167). Hence, apart from its polarity, the amplitude of the family of pulses in the leading and trailing-edge pattern will be the same for all values of n chosen.

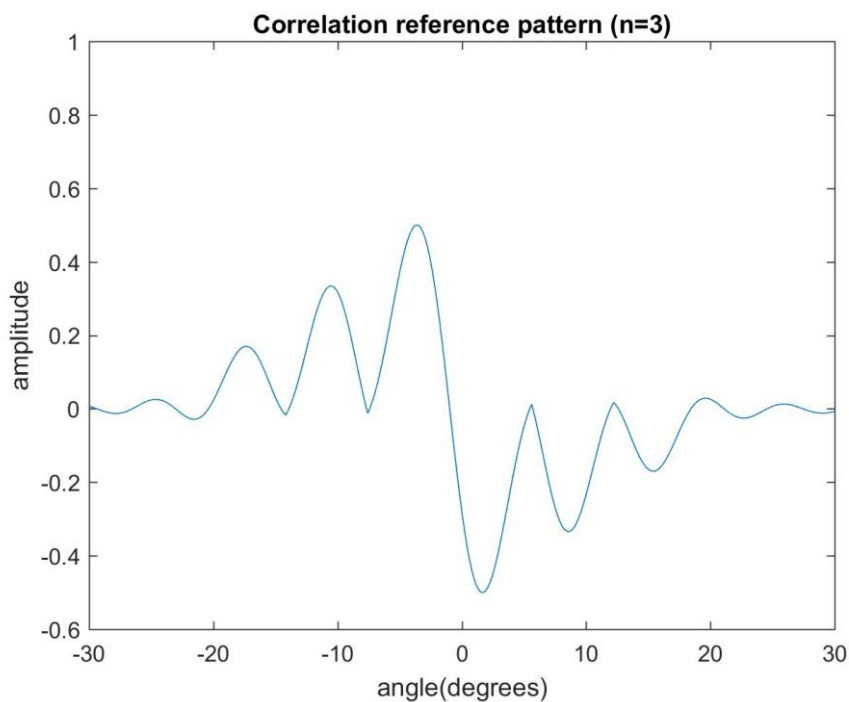


Fig 5-43. Extended correlation reference pattern, for $n=3$

The newly sharpened response produced (Figure 5-44) is a result of the correlation between the extended reference pattern (Figure 5-43), for $n=3$, and the difference function of the point-target response. As shown, suppressing the pair of original -6 dB sidelobes does not affect the main lobe shape for all values of n chosen.

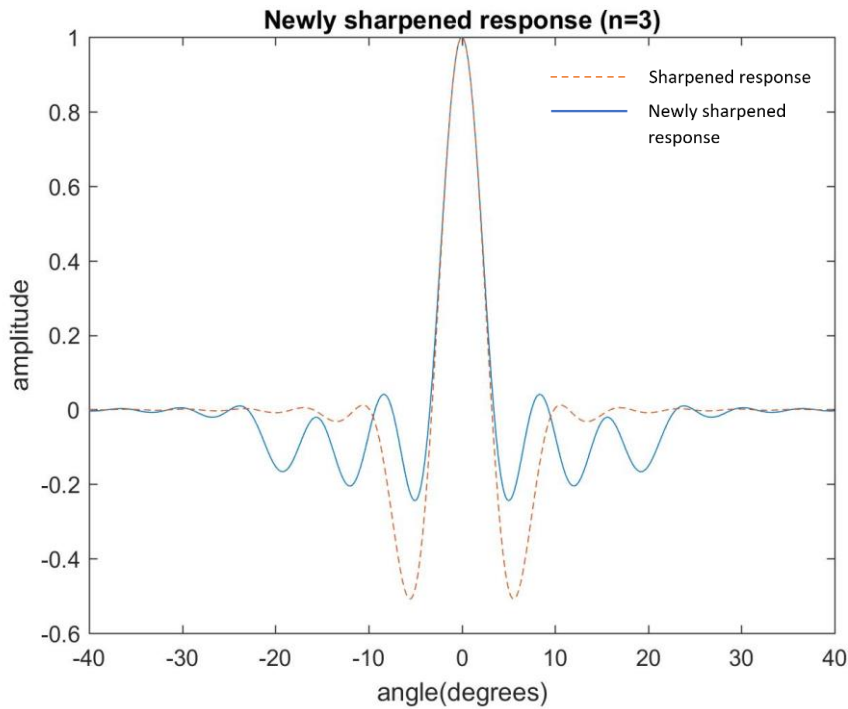


Fig 5-44. Newly sharpened response with three precursor and postcursor sidelobes

Due to the conservation of energy the mean square value of the energy within the sidelobes of the original sharpened response and the newly sharpened response must be the same. Hence, in an ideal case, the energy within the sidelobes of the original sharpened response is equivalent to the sum or total energy within the suppressed sidelobes of the newly sharpened response. For $n=3$, the energy within the -6 dB sidelobe is redistributed across the three sidelobes of the newly sharpened response. The largest sidelobe of the newly sharpened response is considerably suppressed to -12.2 dB.

The sidelobe reduction technique is applied on the original sharpened point-target response for different values of n . Based on the newly sharpened response produced for each value of n , the amplitude of the largest sidelobe within each of the newly sharpened response produced is identified, and an analysis of the effect of the technique on the sidelobe suppression achieved is presented in Table 5-10.

n	Sidelobe Level (dB)
1 (Original Response)	-6
2	-10.1
3	-12.2
4	-13.6
5	-14.5
6	-15.1
7	-15.6
8	-16

Table 5-10. Sidelobe level of the newly sharpened response for each value of n

The pair of sidelobes of the original sharpened response is increasingly suppressed as the number of lobes in the leading and trailing-edge of the correlation reference pattern is increased prior to correlation with the difference function of the point-target response. For instance, for $n=8$, the sidelobe amplitude of the newly sharpened response is reduced from $1/2$ to $1/6$ of the main lobe amplitude, from which the largest suppression of the -6 dB sidelobes of the original sharpened response is achieved. This improvement is worthwhile and adequate in most circumstances. Nonetheless, a suitable number of extra lobes to be added into the correlation reference pattern is dependent on the sidelobe requirements of the application in hand, or the maximum sidelobe level that can be tolerated. For instance, given the simulated example, if the maximum sidelobe level requirement is -15 dB, applying the sidelobe reduction technique for $n=6$ is ideal to fulfil the requirement. The technique demonstrated has shown its importance in minimizing the issues arising from the presence of the sidelobes within the sharpened response, or otherwise would imminently shadow the supposed improvement in detection performance of the antenna introduced from the differential processing applied on the received signal.

5.2.3 Application of PSDP to Surveillance Radar

Pattern selective differential processing provides beam sharpening on the detected output of any type of radar system purely through signal processing, although the improvement in resolution performance of an existing radar is dependent on certain radar characteristics and therefore may differ from one another. Thus, the technique can be implemented on various types of radar focusing on a wide range of applications. This section focuses on the benefits of the processing technique particularly on existing surveillance and navigational radar systems,

which are frequently mounted on land or on-board the deck of a suitable ship for providing sea and coastal surveillance.

The principal cause of clutter within the echo footprint and, more importantly, the limitation to picture quality of the radar is due to the poor angular resolution of the radar, which is naturally far inferior to its range resolution when operational at long ranges. This primarily serves as a limitation towards the accurate discrimination of targets and the clutter-limited detection range of a radar. The presence of clutter at various detection range would often mask the detection of small boats, buoys, and such critical targets that a radar seeks to detect despite the sufficient amount of power supplied to the radar system. Hence, resolution enhancement is critical for the detection performance of a radar system, especially for coastal surveillance radars that is clutter limited when operating in rough sea conditions.

With the implementation of monopulse on an existing reflector antenna the angular accuracy of the radar for target tracking is significantly improved as the positional information of the target is provided through the sharp null of the difference beam of the monopulse antenna, which is obtained from the differencing of the respective feed-horn outputs. Pattern selective differential processing, on the other hand, provides an extra stage improvement in addition to the existing resolution capability of the radar system. It is equivalent to a final stage image sharpening technique as it is a non-coherent post-detection process. Applying the technique to the detected radar response not only improves the resolution of the antenna through beam sharpening in the chosen plane, but also provides a substantial increase in the maximum clutter-limited detection range of the radar. Hence, any improvement in radar resolution that can be incorporated into navigational radar systems through an economic and simple external add-on box without requiring any modification on the radar hardware, such as an extra antenna and receiver (i.e. monopulse system), is of great value. The simplicity of implementing it on the video output of any existing radar is the main benefit of the technique. For future work, the algorithm implementing the differential processing technique would be generalized to cater for any arbitrary antenna response of a radar. The main benefits and much lesser drawbacks of the differential processing technique on typical surveillance radars mentioned above are summarized in Table 5-11.

Advantages	Disadvantages
<p>Azimuth sharpening is crucial for 2D resolution, especially when performance is clutter-limited</p> <p>Improved clutter resilience results in an increase in clutter-limited detection range</p> <p>SNR of the sharpened response is improved compared to the SNR of the original response</p> <p>Exploits knowledge of the radar beam pattern (p priori knowledge)</p> <p>Low cost implementation by means of a simple digital-processing box</p> <p>Can be easily implemented on new and existing radar systems</p>	<p>Processing of data is expected to incur a small delay on the data provided at the video display</p> <p>Unable to distinguish two targets that overlaps one another significantly</p> <p>Formation of fundamental precursor and postcursor sidelobes</p>

Table 5-11. Pros and cons of differential processing on surveillance radars

5.2.4 Application of PSDP on Sum Pattern of Monopulse Antenna

For a monopulse radar, the sum beam is used for the detection of targets while the difference beam is used to identify the angular position of a detected target that is usually accurate to within a fraction of a beamwidth of the main lobe, and for target tracking. As discussed in Section 5.1.3.1, the optimization of the sum and difference patterns is dependent on the requirements of the application in hand, whether it is to prioritize the detection sensitivity or angular accuracy of the monopulse antenna.

The detection sensitivity of a monopulse antenna is determined by two properties, that is, the gain (on-axis voltage) and beamwidth of the sum pattern, whereby a narrow sum pattern beamwidth and high gain corresponds to a higher detection sensitivity of the antenna towards target detection. On the other hand, for the detection of passive, or skin, targets, the angular accuracy of the monopulse radar is optimized when the product of the on-axis slope of the difference beam and on-axis voltage of the sum pattern is maximized. Evidently, the modeling of any feed design of a monopulse reflector antenna would be heavily influenced by the radar function that is to be prioritized.

The modelling of the dual-horn feed arrangement in Section 5.1.3 for the monopulse reflector antenna had shown that applying an angular displacement of ± 1.3 degrees on the pair of feed enables the sum and difference patterns to be optimized simultaneously for the detection of passive targets, where the on-axis voltage gain and -3 dB beamwidth of the sum pattern is the largest and smallest, respectively, and the product of the on-axis slope of the difference pattern and on-axis voltage of the sum pattern is maximized as compared to the other feed tilts

that were simulated (Table 5-3). The angular accuracy of the monopulse antenna is significantly improved as compared to that of a center-fed reflector antenna, which is vital for accurate target tracking, but on the other hand, the angular resolution of the monopulse antenna is considerably degraded and this causes an increase in clutter footprint within the signal received at the sum channel receiver due to the larger beamwidth of the sum pattern produced, which is generally several times wider than the beam produced by a center-fed reflector antenna in azimuth, as shown in Figure 5-21. Although the properties of the sum beam is less critical in a tracking radar as it is only used to provide a reference signal to the difference channel and for the detection of the presence of a valid target, the differential processing technique can be applied on the output signal of the sum channel to enhance the angular resolution of the monopulse antenna, thereby providing the operator with an improved capability of distinguishing two or more closely spaced targets that is within the same beamwidth of the original antenna response (sum pattern squared). This section implements this, whereby the processing technique will be applied on the sum beam of the monopulse antenna to achieve an improvement in detection sensitivity of the antenna.

The monopulse reflector antenna consists of a dual-horn feed arrangement that illuminates the reflector about the vertex. The modelling of the dual-horn feed arrangement identifies the optimum feed tilt on the individual feed to be ± 1.3 degrees from which the optimum detection sensitivity (sum pattern) and angular accuracy (difference pattern) of the monopulse antenna are simultaneously achieved. Referring to the sum pattern shown in Figure 5-21, the sum pattern beamwidth of the monopulse antenna is 3.77 degrees, which is 2.36 times wider than that of the beam produced by the center-fed reflector antenna (1.6 degrees). Thus, in this case, the azimuth resolution and the maximum clutter-limited detection range of the monopulse antenna is, in fact, deteriorated by 2.36 times as compared to resolution performance of the center-fed reflector antenna designed in Section 4.4. In a monostatic radar, where the sum pattern is used for transmission and reception, the round-trip (TX/RX) response of the monopulse antenna is given by the sum pattern squared. The monopulse antenna response is presented in Figure 5-45. The y-coordinates of the graph is the voltage gain which are normalized to the peaks of the individual off-axis beams of the monopulse antenna.

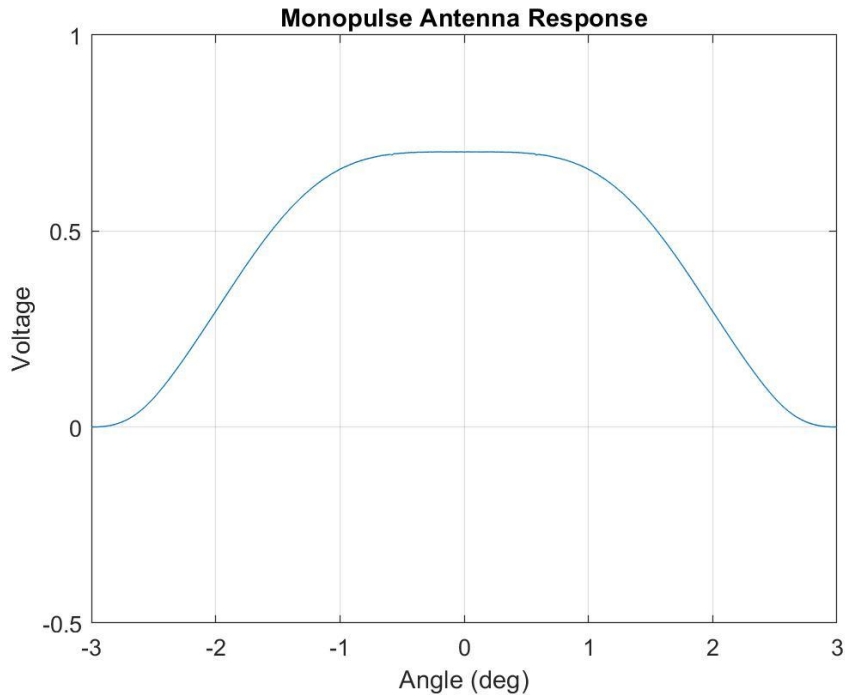


Fig 5-45. Monopulse antenna response – sum pattern squared

Assuming point target operation and the field strength of the echo wave arriving at the antenna is constant in amplitude, the detected target response within the received signal of the radar would be identical to the antenna response in a noise and clutter free scenario. Hence, in this example a point target response is identical to the monopulse antenna response shown in Figure 5-45. Various extent of beam sharpening is applied on the detected target response by varying the overlap between the original and delayed versions of the beam function prior to differencing of the two functions, and correlation of the difference function with a replica of its own. In the absence of noise at the radar output, the amount of overlap required between the two functions are chosen to yield a difference function with a peak amplitude that is ‘A’ of the peak amplitude of the original function. For each value of A, within the range of $0.2 \leq A \leq 0.8$, the effect of the amount of overlap applied on the properties of the sharpened response produced, and particularly on the level of sharpening achieved, is summarized in Table 5-12.

Amplitude of Difference function (A)	BW of Original response (deg)	BW of Sharpened response (deg)	Fractional BW (%)	Sharpening improvement factor	Sidelobe level (dB)
0.2	3.13	1.28	40.9	2.44	-6.2
0.4	3.13	1.33	42.5	2.35	-6.1
0.6	3.13	1.42	45.4	2.2	-6.1
0.8	3.13	1.58	50.5	1.98	-6.1

Table 5-12. Properties of original and sharpened response for various beam sharpening

From the set of simulations performed, maximum pulse sharpening ($A = 0.2$) achieves a significant enhancement in detection performance of the radar through a substantial reduction of 59.1 percent in beamwidth (from 3.13 degrees to 1.28 degrees), or target size, between the original and sharpened response, thereby effectively reducing the clutter footprint within the signal received by 59.1 percent and achieving an angular resolution that is 144% higher than the original system. In fact, upon applying the differential processing technique on the sum channel output (sum squared pattern) the beamwidth of the sharpened point-target response is narrower than the beamwidth of the individual off-axis lobes produced from the reflector. Applying the differential technique on the output of the radar sum channel, for $A = 0.2$, produces the sharpened point-target response presented in Figure 5-46.

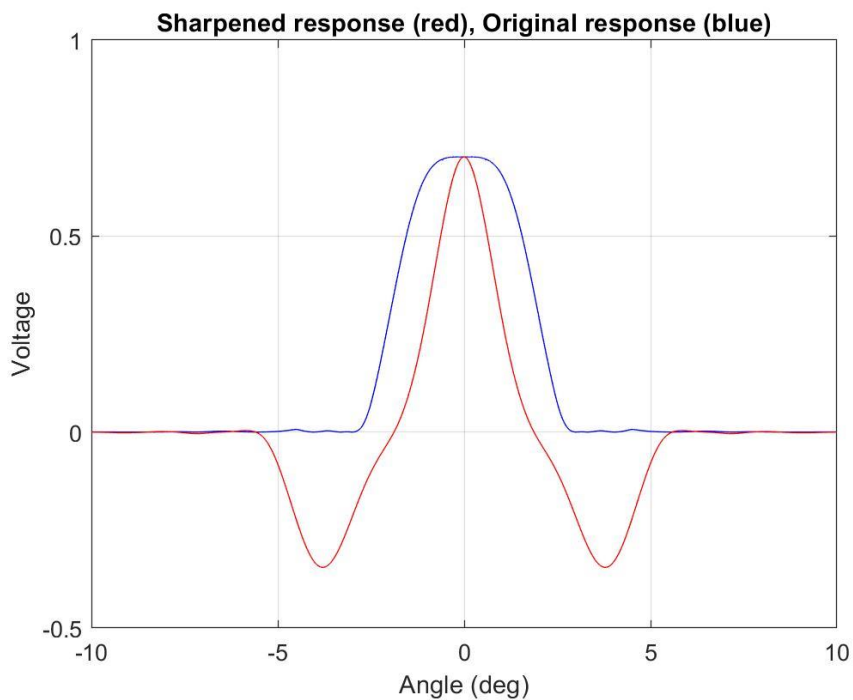


Fig 5-46. Sharpened response for maximum pulse sharpening ($A = 0.2$)

Table 5-13 provides a comparison of the sharpening effect of the technique, for maximum pulse sharpening ($A = 0.2$), on the output signal of two types of antenna, that is, a line source antenna with uniform aperture distribution and the sum pattern of a monopulse antenna, respectively.

Antenna Pattern	BW of Original response (deg)	BW of Sharpened response (deg)	Fractional BW (%)	Sharpening improvement factor	Sidelobe level (dB)
Sum beam of monopulse antenna	3.13	1.28	40.9	2.44	-6.2
Line source antenna with uniform distribution	4	2.99	74.7	1.34	-5.7

Table 5-13. Properties of sharpened response for two types of antenna

The sharpening improvement factor realized on the monopulse antenna (144 percent) is significantly larger than on a line source antenna with uniform distribution (34 percent). Moreover, the fundamental side lobes produced within the sharpened response of the monopulse antenna is lower by 0.5 dB. Thus, as expected, the benefit of the processing technique is significantly more pronounced on the received signal of the monopulse antenna as compared to the line source antenna. The desirable properties of the sharpened response of the monopulse antenna, as compared to that of the line source antenna, is attributed due to the much flatter top and steeper rising and falling edges (roll-off) of the antenna response function.

5.3 Summary

This chapter has described the implementation of amplitude monopulse on the azimuthal plane of the existing reflector antenna that was modelled in Section 4.4. Following the proposed dual-horn feed arrangement presented in Section 5.1.3, the modelling of the monopulse feed on CST has shown the optimum feed tilt about the vertex of the reflector that simultaneously optimizes the detection sensitivity (on-axis voltage gain of sum pattern) and angular accuracy (product of the on-axis slope of difference pattern with on-axis voltage gain of sum pattern) of the monopulse antenna to be ± 1.3 for the detection of a passive target, which is generally the type of target that is of interest.

Section 5.2.1 has outlined the principles of the proposed signal processing technique prior to demonstrating it on the radar output of an existing antenna. The processing technique was simulated on line source antennas of various common aperture distributions, from which the simulation results have shown the technique to be most effective, in terms of the enhancement in angular resolution achieved, on antenna with a radiation pattern exhibiting a flat top and steep roll-offs. In addition, for a given antenna pattern, the simulation results have shown that the smallest possible sampling interval of the received radar returns is preferred in order to maximize the enhancement in SNR of the sharpened point-target response.

The large interest for any potential improvements that can be observed on the detection performance of surveillance and similar navigational radar systems have led for the remaining of Chapter 5 to discuss and evaluate the importance of the technique on coastal surveillance activities, or similar navigational applications, and the benefits that are offered from it at the expense of a very low cost and complexity (Table 5-11).

Chapter 6

Experimental Measurements and Discussion of Results

This chapter consists of three sub-section. Section 6.1 provides the measurement and optimization of the RF performance of the sectoral horn antenna designed in Section 4.3. The measurements allow the transition design of the WR90 adapter that achieves the most desirable antenna performance to be identified, from which the results will also be used to validate the modelling and CST simulation results of the adapter transition design provided in Section 4.2.

Section 6.2 evaluates some of the most common methods of manufacturing reflectors of varied sizes before discussing the chosen method of fabrication of the reflector designed in Section 4.4.2, which prioritizes on manufacturing the reflector from a low cost and weight perspective. This is followed by a cost and weight analysis on the manufactured reflector and the construction of the feed and reflector support using an alternative profile system that is cost effective, lightweight and portable.

Section 6.3 provides the far-field radiation pattern measurements of several types of antennas that were designed earlier in this thesis, and in particular, the measurement results will be used to validate the modelling of the dual-horn monopulse feed arrangement that was proposed in Section 5.1.3, which was based on CST simulations, to create a amplitude monopulse reflector antenna.

6.1 Measurement and Validation of Horn Antenna Performance

Prior to measuring the far-field radiation pattern of the modelled center-fed and monopulse reflector antenna, the RF performance of the horn antenna is measured to verify the optimum transition design of the adapter that optimizes the horn antenna performance at an operating

frequency of 9.2 GHz. The measurement results provided in this section will also be used to validate the simulated RF performance of the WR90 adapter that was provided in Section 4.2.

The Antenna Under Test (AUT) is the pair of E-plane sectoral horn antenna manufactured according to the design shown in Section 4.3. The pair of horns were CNC machined and therefore were manufactured to a very high precision. As demonstrated in Section 4.2, the optimization of the RF performance of the horn antenna is performed by measuring the return loss of the horn across a range of different probe lengths extending into the WR90 adapter, with a constant back-short distance of 7 mm (ideal length for X-band operation). Prior to the analysis of the recorded measurements obtained, the measurement plan and test equipment used (Vector Network Analyser) to measure the RF performance of the antenna under test (AUT) is described.

6.1.1 Vector Network Analyzer

The test equipment used to measure the RF performance (S_{11}) of the horn antenna is a Vector Network Analyser (VNA). A VNA is a precision measuring tool that tests the electrical performance of high frequency components, in the radio frequency (RF), microwave, and millimeter-wave frequency bands. It is a stimulus response test system, composed of an RF source and multiple measurement receivers, that is designed specifically for the measurement of the forward and reverse reflection and transmission responses, or S-parameters, of RF components [88]. Hence, the linear RF performance of a high frequency device under test can be characterized in terms of both the magnitude and phase component of the S-parameters.

The network analyzer hardware is optimized for speed, yielding swept measurements that are much faster than those obtained from the use of an individual source and an individual receiver, such as a spectrum analyzer [88]. The measurement accuracy of a VNA is highly dependent on the measurement errors within the system. By correcting for the systematic errors in the instrument through calibration of the test system, the characteristics of cables, adapters and test fixtures, a VNA achieves the highest level of accuracy for measuring RF components. Hence, the accuracy of VNAs can be significantly improved by identifying the cause of these persistent measurement errors and, more importantly, how to correct for them within the measured data collected.

Calibrated VNAs are unique among RF instrumentation because they have the potential to provide exceptional accuracy when calibrated. Few RF instruments can match the measurement performance of better than ± 0.1 dB and ± 0.1 degree that most VNAs deliver [89]. The VNA used to perform the measurements is a product of ROHDE-SCHWARZ (R&S® ZNB Vector Network Analyzer) that has a frequency range from 9 kHz to 40 GHz [90].



Fig 6-1. R&S® ZNB Vector Network Analyzer [90]

6.1.1.1 Sources of Measurement Errors

The measurement errors are categorized into 3 different types: drift errors, random errors and systematic errors. The sources of measurement error for each type of error are briefly discussed, and how to monitor these error terms and successfully remove some of them through user calibration of the test equipment are described in Section 6.1.1.2.

6.1.1.1.1 Drift Errors

Drift errors are due to the instrument or test-system performance changing after a calibration has been done. This type of error is primarily caused by thermal expansion characteristics of interconnecting cables within the test set and conversion stability of the microwave frequency converter. The error can be removed by re-calibrating, although the time frame over which a calibration remains accurate is dependent on the rate of drift that the test system undergoes, which is influenced by the test environment [91]. Hence, drift can be controlled and minimized by providing a test environment with a stable ambient temperature.

6.1.1.1.2 Random Errors

Random errors are not only unpredictable, but are also unable to be removed through user calibration. The three main sources of random errors are instrument noise errors, switch repeatability errors and connector repeatability errors, each of which are highlighted below. However, the impact of each source of random error on the measurement accuracy can be minimized, but usually not removed, in certain ways.

Unwanted electrical disturbances generated in the components of the VNA are known as instrument noise. The noise generated gives rise to instrument noise errors that affects the

measurement accuracy of the VNA. These disturbances include low level noise due to the broadband noise floor of the receiver, and high-level noise or jitter of the trace data due to the noise floor and the phase noise of the LO source inside the test set. The noise errors could be reduced by doing one or more of the following: increasing the source power to the device being measured (only reduces low-level noise), narrow the IF bandwidth and apply several measurement sweep averages [91].

The second type of random error is known as switch repeatability error. Mechanical RF switches are used in the analyzer to switch the source attenuator settings. Switch repeatability error arises when the mechanical RF switches are activated and the contacts close differently from when they were previously activated [91]. When this occurs the measurement accuracy of the VNA could be degraded. Preventing the operator from switching attenuator settings during a critical measurement would reduce, if not prevent, the error from occurring

The final type of random error is due to the wear and tear of the connector being used. This type of error is known as connector repeatability errors, which causes changes in electrical performance [91]. Practicing good connector care methods significantly reduces the chances of creating this error.

6.1.1.1.3 Systematic Errors

Limitations in the analyzer and test setup results in systematic errors, which are non-random, repeatable errors that can be measured and removed mathematically. These errors include errors from the network analyzer itself, connector interface, imperfections in the calibration standards, plus all of the interconnecting test cables, and/or probes that are between the analyzer and the Device Under Test (DUT) [91]. Assuming no residual errors are generated due to limitations in the calibration process, systematic errors can be characterized during the calibration process and mathematically removed after subsequent measurements. The major systematic errors associated with VNA measurements are shown in Figure 6-2.

For reflection and transmission measurements of a two-port device there are two errors each relating to signal leakage, signal reflections and frequency response of the receivers, respectively, which corresponds to a total of six systematic errors for a forward measurement. The two errors related to signal leakage are directivity and crosstalk (isolation error), whereas the two errors related to signal reflections are source and load mismatch, and the final class of errors related to the frequency response of the test system receivers are called reflection and transmission tracking. The term “tracking” is used because S-parameter measurements are ratioed measurements between a test and a reference receiver RI (i.e. ratios A/RI for reflection measurement and B/RI for transmission measurement).

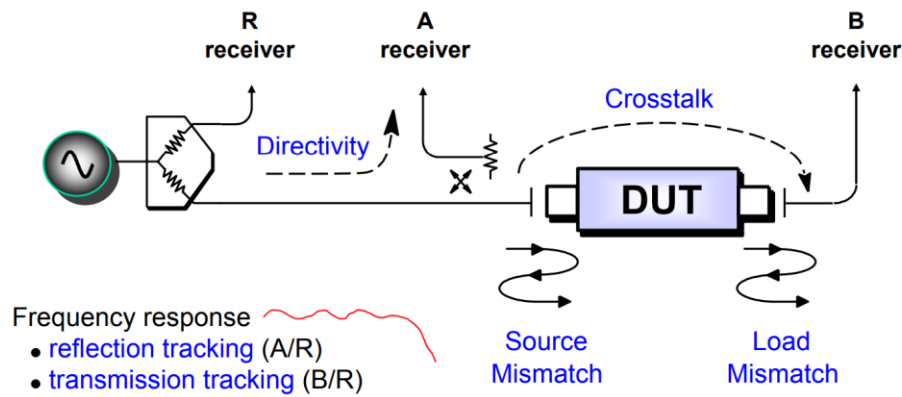


Fig 6-2. Major systematic errors associated with VNA measurements [91]

For two-port devices, the full two-port error model includes all six of these systematic error terms for the forward direction and the same six in the reverse direction, for a total of twelve systematic error terms. Therefore, a two-port calibration would mathematically remove the twelve-term errors from subsequent reflection and transmission measurements. Error models for test systems with more than two test ports consists of more than twelve error terms, although they consist of the same error terms. Whereas for test systems with only one test port (one-port devices), since only reflection measurements can be performed a one-port error model only includes three of the six of these terms for the forward direction.

A one-port calibration (S_{11} or S_{22} , but not both) of the VNA is sufficient since the VNA will only be used for the return loss measurement of the horn antenna. Therefore, it will be the chosen calibration method to provide both amplitude and phase information of each of the error terms. Unless the gain measurement of the DUT is of interest, a comprehensive two-port calibration is necessary. Reflection measurements generate the following three systematic errors: directivity, source mismatch and frequency response reflection tracking, with each error briefly described below. All three errors can be characterized and reduced by the analyzer through user calibration. A one-port calibration of a VNA is described in Section 6.1.1.2.

Directivity error limits dynamic range for reflection measurements. All network analyzers make reflection measurements using directional couplers or bridges. With an ideal coupler, only the reflected signal from the DUT appears at the A receiver. In reality, a small amount of incident signal leaks through the forward path of the coupler and directly into the A receiver. This leakage path, and any other path that allows energy to arrive at the A receiver without reflecting off the DUT, contributes to directivity error [91]. Source mismatch errors result from interactions between the test system's source match and the input match of the DUT [88]. Ideally in reflection measurements, all of the signal that is reflected off of the DUT is measured at the A receiver. In reality, some of the signal reflects off the DUT, and multiple

internal reflections occur between the analyzer and the DUT. These reflections combine with the incident signal and are measured at the *A* receiver, but not at the *R* receiver [91]. This measurement error is called source match error. Frequency response reflection tracking error is due to imperfect tracking between the test and reference receivers. Reflection measurements are made by comparing signal at the *A* receiver to signal at the *RI* receiver. For ideal reflection measurements the frequency response of the *A* and *RI* receivers would be identical. In reality, frequency response reflection tracking error are generated due to a discrepancy between the frequency response of the *A* and *RI* receivers. Reflection tracking errors is the vector sum of all test variations in which magnitude and phase change as a function of frequency, which includes variations contributed by: signal-separation devices, test cables, adapters and variations between the reference and test signal paths [91].

6.1.1.2 VNA Calibration

VNAs provide high measurement accuracy by calibrating the test system using a mathematical technique called vector error correction, or also known as user calibration [88]. User calibration refers to the periodic calibration performed by the operator before making a measurement, and is not the same as the yearly instrument calibration performed by the manufacturer to ensure that the instrument is functioning properly and meeting its published specifications [88]. Performing periodic calibration on a VNA test system ensures that the systematic measurement errors in the test-system are accounted for in the measurement results of the DUT. Hence, user calibration eliminates the largest source of measurement uncertainty (systematic errors) and is therefore crucial in ensuring the accuracy and repeatability of the VNA measurements and for it to provide real performance of the DUT. The VNA sources of systematic errors for a one-port device were highlighted in Section 6.1.1.1. Optimizing the accuracy of VNA measurements is nearly unachievable without proper user calibration.

User calibration is very important to network analysis as manufacturing a perfect test-system is unrealistic and would be very difficult. Furthermore, manufacturing a network analyser that is sufficient to eliminate the need for calibration would be very costly. As with any RF measurement, the accuracy of the RF performance measurement of the DUT is dependent on the quality of the measurement practices used during the calibration process. Since the VNA will only be used to measure the return loss of the horn antenna, only reflection measurements are required. Hence, the type of VNA calibration focused on is the one-port calibration, or often referred to as three-term error correction. Nonetheless, the error terms of a one-port device are a subset of those of a two-port device that was described above, and therefore a one-port calibration is a subset of a two-port calibration.

User calibration is the process of characterizing systematic error terms by measuring each of the known electrical calibration standards [88]. The electrical standards used during the calibration process are found in many commercial calibration kits, which are either mechanical or passive devices. Through a set of defined calibration equations, the VNA computes and compares the measured values with the ideal models of these standards, and any deviation from the expected results (due to systematic errors in the test system) are used to create a correction factor for each frequency point. Once these errors are quantified, the correction factors are applied to the VNA measurements to remove the effects of each error term from subsequent measurements. The calibration process has to measure enough standards to sort out the magnitude and phase of every systematic error described above [88], which are usually expressed as vectors. Calibration measurements, which characterize the test system, are made with all cables and connections in place but without the DUT.

There are several user calibration methods that can be performed on a network analyzer to correct for the systematic error terms mentioned. The VNA user calibrations is divided into three commonly used categories or standards: SOLT (Short, Open, Load, Thru), TRL (Thru, Reflect, Line), and automatic calibration [89]. The differences between the various calibration methods are dependent on the types of electrical standards they use during the calibration process and how the standards are defined. Each calibration methods pros and cons are dependent on the frequency range and the intended application. This is summarized in Table 6-1. Of all VNA calibrations, the SOLT calibration is the easiest to perform and, therefore, will be the user-calibration performed and the only calibration method further discussed.

	SOLT Calibration	TRL Calibration	Automatic Calibration
Ease of Use	Good	Fair	Excellent
Accuracy	Good	Excellent	Good
Repeatability	Good	Excellent	Excellent
Advantages	<ul style="list-style-type: none"> • Familiar method with many variants • Wide broadband of frequencies • Wide variety of calibration kits and connector types • Cost-effective method 	<ul style="list-style-type: none"> • Calibration standards need not be completely defined • Large range of variants for different applications • Effective option for connectorless applications • Cost-effective method 	<ul style="list-style-type: none"> • Ability to mix and match connector types and sexes • Significantly faster speed than manual calibration • Large reduction in human errors • Large improvement in repeatability
Disadvantages	<ul style="list-style-type: none"> • Considerations needed for non-insertable devices • Large number of steps required • Calibration standards must be completely defined 	<ul style="list-style-type: none"> • Less broad band • Requires good design and fabrication for best repeatability • Not as intuitive as SOLT 	<ul style="list-style-type: none"> • Most units support only devices with up to 4 ports • Different frequency ranges require different modules • Higher cost than equivalent manual cal kits • Exclusive use in connectorized applications

Table 6-1. Summary of the various calibration properties [91]

6.1.1.2.1 One-port SOLT Calibration

As its name implies, SOLT calibration is based on shorts, opens, loads, and thus as electrical standards. It is the simplest calibration method available. As the name suggests, this requires access to known standards with a short circuit, open circuit, a precision load (usually 50 Ω) and, only for a two-port SOLT calibration, a through connection. SOLT calibration is very easy to perform and is used in a broad variety of environments. It is the most widely used choice for coaxial measurements, since there are many commercial coaxial calibration kits available to match most connector types. It can also be used with fixtures and probes. SOLT inherently provides a broadband calibration, essentially from DC to the upper frequency limit of the connector type being used [88].

A one-port calibration of the VNA is the suitable method of calibration since the VNA will only be used to measure the return loss of the horn antenna. As mentioned in Section 6.1.1.1, a one-port calibration accounts for the three systematic errors (directivity, source match, and reflection tracking error), analogous to the twelve possible systematic errors for two-port devices, which appears in one-port reflectivity measurements. In a typical one-port reflection calibration of the test equipment, each of the three systematic errors mentioned above are measured and reduced by the analyzer based on the SOLT standards, and this does not apply to other types of calibration. The user measures three known electrical standards, an open, a short and a known load during the calibration process, from which, the systematic errors are accounted for by mathematically removing them from subsequent reflection measurements of the DUT. Prior to measuring the return loss of the horn antenna, the VNA was calibrated to ensure that accurate measurement results are obtained.

6.1.2 Measurement Results

To perform the optimization of the horn antenna RF performance, seven Female SMA connectors were prepared. The probe length of each SMA were within the range of 4 mm to 7 mm, in small intervals of 0.5 mm, and a total of seven measurements of the DUT were performed using the VNA. The return loss of the horn antenna was measured across the frequency range of 6.55 GHz to 12.4 GHz. The lower limit is the cut-off frequency of the adapter and the upper limit is the upper frequency limit of the X-band frequency spectrum. The frequency of interest is the operating frequency of the radar at 9.2 GHz. Hence, the objective is to identify the optimum probe length of the SMA connector that achieves the lowest return loss of the horn antenna at this operating frequency.

The measurements of the antenna return loss were performed starting with a SMA with a probe length of 7 mm connected to the horn antenna. This was replaced with a SMA connector

with a probe length that is shortened by 0.5 mm after each consecutive measurement was completed. The measured return loss of the antenna for several of the SMA connectors used across the X-band frequency spectrum is provided in Figures 6-3 to 6-9. The ripples in the VNA measurements is mostly likely caused by the multiple reflections of the signal travelling within cables, connectors, evaluation board traces, DUT and packages. It may also be due to impedance mismatch at the junctions of these interconnects [89].

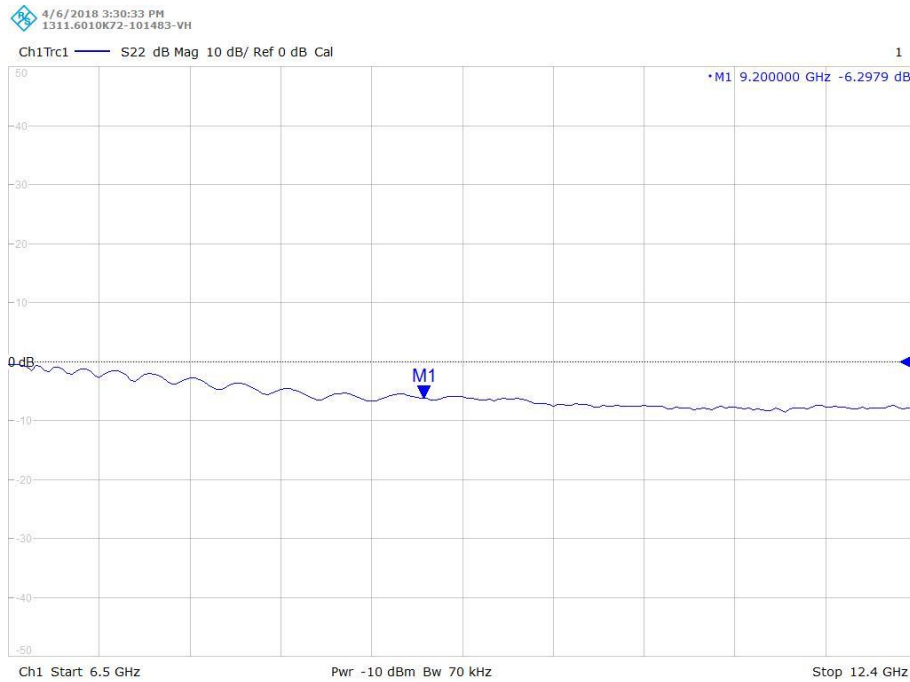


Fig 6-3. S₁₁ measurement for probe length of 4 mm

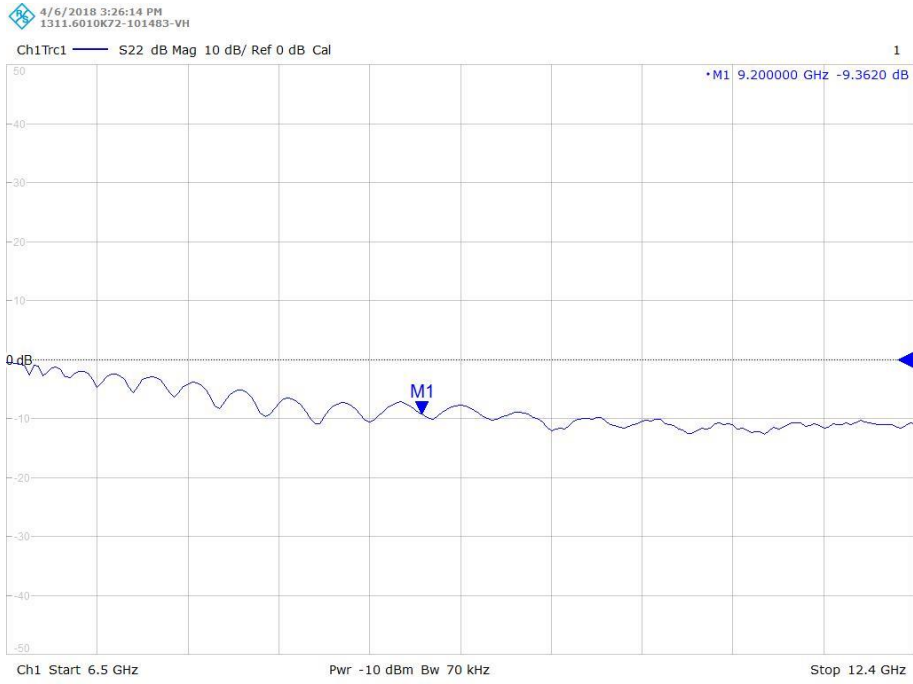


Fig 6-4. S_{11} measurement for probe length of 4.5 mm

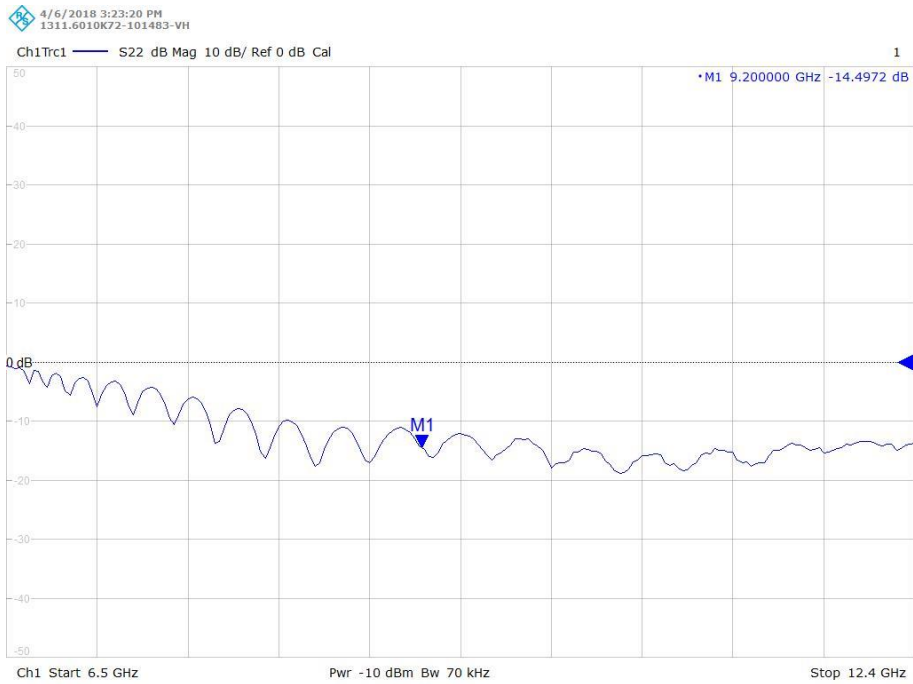


Fig 6-5. S_{11} measurement for probe length of 5 mm



Fig 6-6 S_{11} measurement for probe length of 5.5 mm

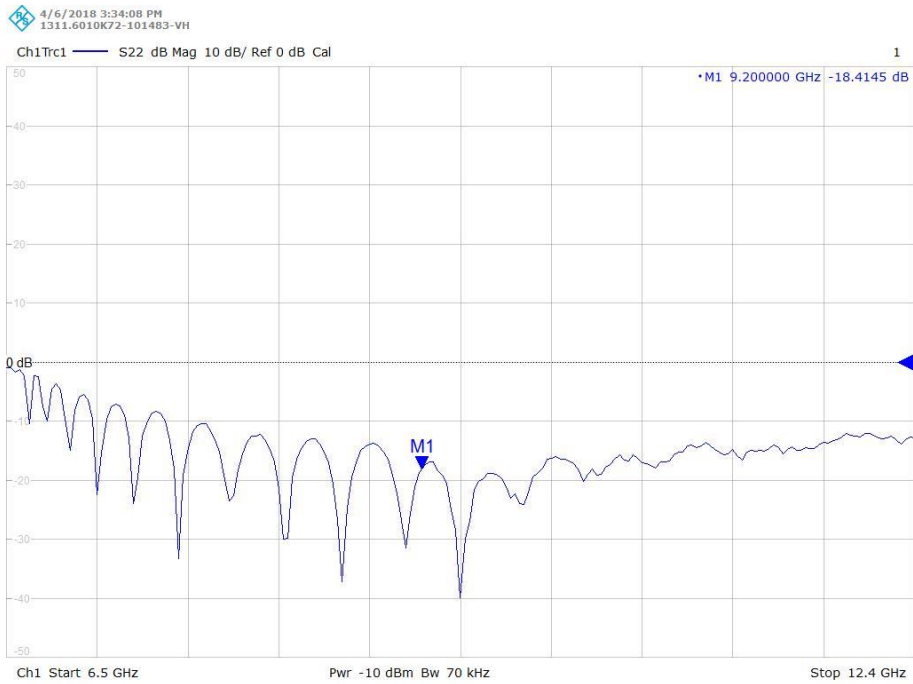


Fig 6-7. S_{11} measurement for probe length of 6 mm

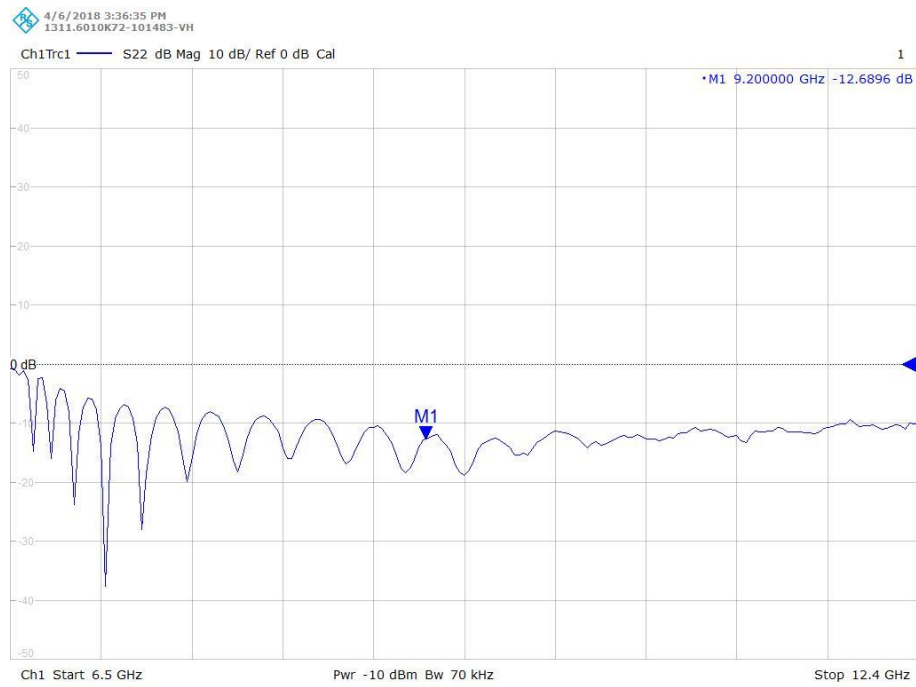


Fig 6-8. S_{11} measurement for probe length of 6.5 mm

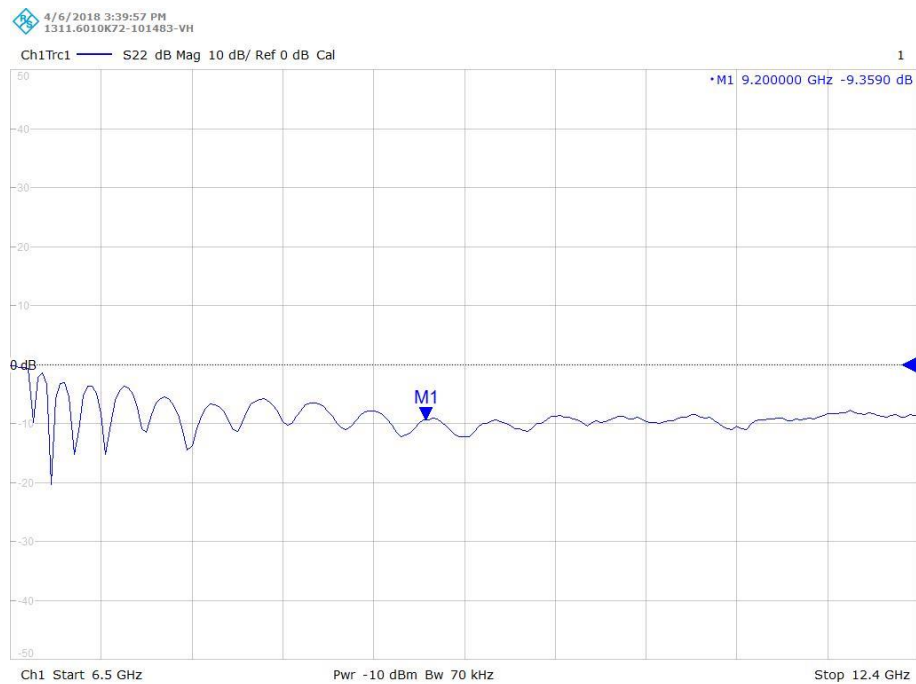


Fig 6-9. S_{11} measurement for probe length of 7 mm

The RF performance of the horn antenna is generally acceptable when a return loss of -15 dB is achieved across the operating frequency band. Based on the antenna return loss measurements corresponding to the probe length of each SMA connector, the range of suitable probe lengths that fulfils the criteria of an efficient antenna is between 5 to 6 mm.

The marker ‘M1’ in each of the above-mentioned figures indicate the return loss of the horn antenna at 9.2 GHz. The measurements show that the centre frequency of the antenna return loss gradually shifts from the upper limit towards the lower limit of the frequency band as the probe length is gradually increased. The measured return loss at 9.2 GHz for each case is presented in Table 6-2.

Probe Length (mm)	Measured S ₁₁ (dB) at 9.2 GHz	Simulated S ₁₁ (dB) at 9.2 GHz
4	-6.3	-5
4.5	-9.36	-8.2
5	-14.5	-13.1
5.5	-36.65	-21.2
6	-18.41	-15.4
6.5	-12.69	-10.8
7	-9.36	-8.2

Table 6-2. Simulated and measured S₁₁ of sectoral horn for varying probe lengths

The probe length of the SMA connector that optimizes the RF performance of the horn antenna at 9.2 GHz is 5.5 mm, in which the return loss of the horn antenna is -36.65 dB and the corresponding VSWR is 1.03:1. Moreover, the center frequency of the return loss also occurs close to this operating frequency. Since the wall thickness of the horn antenna is 1.27 mm, the length of the probe extending into the inner top wall of the adapter is 4.23 mm.

A comparison of the simulated and measured return loss of the RF devices is presented in Table 6-2. The recordings obtained from the return loss measurement of the horn antenna closely agrees with the simulation results of the WR90 adapter, which confirms that the optimum probe length of the SMA connector used for the horn antenna will be 5.5 mm with a back-short distance of 7 mm. The measured far-field radiation pattern of the E-plane sectoral horn antenna, which was performed in QinetiQ’s far-field measuring range in Funtington, is provided in Section 6.3.

6.2 Reflector Construction

The size of a reflector aperture, depending on the application it is used for, may range from centimeters up to 100 meters in length. The reflector used in mechanical surveillance radars employing reflector antennas is usually relatively large, ranging from one to tens of meters. For reflector antennas that are used in a typical coastal surveillance radar system, manufacturing a

large metallic reflector can cost up to tens of thousands of pounds, especially for those requiring high surface accuracies at high operating frequencies of the radar. Ideally, the method of constructing a small reflector (i.e. smaller than one meter) and a large reflector (i.e. larger than 3 meters) is not the same. Depending on the size of the reflector, there are several fabrication techniques that uses a range of suitable materials. The reflector fabricated for this project is discussed in Section 4.4.2; the reflector is a vertically truncated parabola that has a height and width of 120 cm and 30 cm respectively. The dimensions of the reflector considers it to be of a small to medium sized dish. Since this project focuses on the design and manufacturing of a reflector antenna that utilizes a reflector that extends over a meter wide, this section aims to evaluate the various existing methods and potentially novel economical methods of fabricating a reflector of a similar sizes that would considerably reduce the manufacturing cost and weight of the reflector while still fulfilling the surface accuracy requirements and possess the properties of a metallic material. Although existing fabrication techniques are not explained in great depth, and the less popular materials and methods of reflector construction are not mentioned, the purpose is to provide an understanding of the existing methods used and a comparison between the conventional fabrication techniques discussed along with the proposed method of reflector fabrication undertaken in this project. Section 6.2.3 also discusses the design of the proposed feed and reflector support of the antenna, whereby optimizing the weight, rigidity and stability of the support are prioritized to maintain the respective positions of each component.

The existing platform of the *Guidance Marine* radar, which measures at approximately 50 cm in diameter, is used as the base to the reflector antenna and, therefore, the reflector must be fabricated using a suitable material that minimizes the overall weight of the antenna to prevent exerting excessive torque on the radar base while scanning. Although the objective is to manufacture the reflector as cost-effective and light as possible, the quality of the reflector, and therefore its performance, must be retained. Hence, this section proposes viable manufacturing alternatives that would optimize its cost and weight, while ensuring that the reflector surface accuracy requirements are fulfilled.

For the measured radiation pattern of the beam produced from the reflector antenna to be similar to its theoretical simulated pattern, it is critical for the surface accuracy, or shape, of the manufactured parabolic reflector to conform closely to a parabola to ensure that the aperture excitation is co-phased and that the reflecting surface possesses the properties of a Perfect Electric Conductor (PEC). The total reflection of the radiation pattern of the feed off the reflector surface to yield the secondary radiation pattern consists of two components, that is from a specular component and a scattered or diffuse component, the former is the desirable reflection whereas the latter is the undesirable one contributed due to the deviation of the reflector surface from a perfect one, which produces additional side lobe levels and causes a

reduction of overall gain. By ‘additional side lobe level’ it is meant that the relative power of the side lobes due to reflector inaccuracies will be added to the relative power of whatever side lobes would be present if the reflector were perfect [27]. Determining a suitable surface accuracy of a reflector according to the required specifications of the application in hand will be discussed in Section 6.2.2.

The cost of manufacturing a parabolic reflector of a given size is significantly dependent on the material and fabrication technique used. Most large radar manufacturing companies do not prioritize cost, and in many cases where the weight of the antenna is not a significant factor of consideration, it is common for reflectors that are several meters wide to be made of a large block, or a thick single solid sheet, of aluminum using very accurate but highly time-consuming and costly fabrication techniques that would optimize the radiation properties of the beam produced from the reflector. The most common technique of fabricating reflectors up to approximately 3 meters in diameter from a solid sheet of metal is achieved by spinning or stretching the metal on a solid form of the suitable shape, which may be made of wood by standard wood-working techniques, and using a parabolic template to check the shape [92]. The template, which can be made of any stiff material, is in the form of a parabolic curve in accordance to the equation of a parabola, given by $x^2 = 4fz$, for the desired value of the chosen focal length, f [92]. This ensures that the reflector produced conforms as closely as possible to the shape of a parabola with a specified f/D ratio. Whereas for small reflectors measuring less than 1 meter in diameter, or those requiring a very precise surface, it is preferred for the reflector to be fabricated by metal casting and then machining it individually at the expense of a higher production cost, before the fabricated reflector is attached to a suitably designed support. As for most methods in engineering, a compromise between the cost and performance of a reflector antenna frequently exists. Nonetheless, the specification of the reflector, particularly the surface accuracy requirement, may vary according to the requirement of the application in hand. Alternative methods of construction for medium sized reflectors that measures between 1 to 3 meters in diameter, which could offer a substantial reduction in cost and weight of the reflector while still fulfilling the radar requirements without compromising its performance, are analysed and evaluated accordingly.

6.2.1 Alternative Methods of Construction for Medium-sized Reflector

Although dishes of this size are generally made of aluminum, it can be made of other metals or any other suitable rigid material with suitable properties. Using alternative materials instead of solid blocks of metal would be the preferred choice to reduce the fabrication cost and weight of the reflector, which are factors prioritized in this project. Several existing and novel methods

of manufacturing a reflector with the two mentioned factors taken into significant consideration are discussed and evaluated in this section. Nonetheless, it is important to also perform an economic and performance analysis of the antenna system beforehand, especially in cases where the application has a commercial interest.

An alternative method of reflector construction is for the surface of the reflector to be solely made of perforated metal sheets, or a metallic mesh in the form of panels of a suitable size, instead of a solid sheet of metal [27]. The fabrication technique used to construct the reflector would be the same as the one described above; the mesh is molded onto a former to produce the lattice structure that conforms to the shape of a parabola with the appropriate f/D ratio. Using a local mesh to construct the reflector in the form of a lattice structure is an attractive and popular alternative since it significantly reduces the total weight of the dish and the amount of force applied on the reflector by the wind approaching from the direction opposite to the rotating direction of the scanning radar. Thus, wind loading is an unlikely issue with this type of reflector as most of the wind approaching it would not be caught by the reflector. However, it is unlikely to manufacture a reflector with very high surface accuracy using this method of reflector construction. Hence, this method is more suitable for applications prioritizing the use of light reflectors, instead of a reflector with very high surface accuracy requirements.

Another factor of great importance is the rigidity of the reflector (re-enforced by a strong support frame), which contributes to the resistance of the reflector from deformation due to wind or gravitational forces. In such scenarios, the strength of the reflector can be substantially increased by attaching the lattice mesh structure to a molded plastic of an identical shape over a layering of electric conductive paint. This is particularly useful for large reflectors that are subject to strong windy conditions. Consequently, a large reflector made of solid sheet of metal is usually vulnerable under such conditions due to the drag imposed on it, which to some extent, could deform the reflector from its original shape and directly affect the direction and properties of the secondary lobe produced. The net effect of reflector surface inaccuracies and reflector and feed-support deformation can be separated into two parts. One is a deterioration of the pattern produced, such as an increase of sidelobe level and reduction of gain, while the other is a potential shift in the main beam direction, which would cause angle-measurement errors in a radar system unless the shift is known and corrected in interpretation of data.

Although the effect of large wind forces can be reduced through the methods mentioned above, the most serious consideration of providing measures is to prevent an antenna from being overturned under such extreme weather conditions, or steering motors from being unable

to overcome an opposing wind force in mechanically scanning radars. Hence, on top of reflector inaccuracies due to manufacturing, the distortion of the reflector by wind forces can also be serious, such that if left unattended large amount of air resistance encountered by the reflector could significantly affect the performance and detection accuracy of the radar. A metallic mesh reflector is shown in Figure 6-10.



Fig 6-10. Reflector dish manufactured out of mesh panels [93]

Apart from the significantly lower wind resistance encountered by the reflector, a significant reduction on the total weight of the reflector antenna is also achieved. Providing sufficient space is available the weight reduction can also be utilized to design a substantially larger reflector that is capable of producing a narrower beamwidth and higher gain. Typically, the perforations or mesh openings must be small as compared to the wavelength, preferably less than $1/16$ wavelength in the direction perpendicular to the polarization of the radiation if the polarization is linear [27]. In the other direction the opening size is noncritical. Additionally, in cases of manufacturing larger reflectors in the form of multiple panels it would be necessary to provide electrical bonding at the edges of adjacent panels unless the size of each panel is large as compared to the operating wavelength of the radar system, although it is always mechanically more desirable to do so [27]. Hence, the manufacturing cost of the reflector itself could be reduced for certain radar applications where a high surface accuracy is not required. This type of reflector is suitable and therefore often considered especially for mechanically scanning radars employing a medium-sized reflector prioritizing cost and weight.

Nonetheless, the revolution that wireless communication has experienced over last decades has increased the need of antennas where performances such as lightweight, rapid manufacturing and portability run in parallel with their electric performance [94]. To move towards this direction, instead of using the conventional fabrication methods described above, the use of 3D printing technology to fabricate a cost effective and lightweight reflector within a short turnover period is an area to be further investigated. This method of fabrication is proposed in this project. The simulated and measured monopulse reflector antenna performance are presented in Section 4.4 and 6.3, respectively, and a comparison of results allows the performance of the proposed antenna to be validated and then evaluated.

6.2.1.1 3D Printing Technology for Reflector Fabrication

Since the appearance of commercial 3D printers, its performance has been increasing while its unitary and operational costs have continuously been decreasing with advancements within the field [95]. This makes them common tools across a wide range of areas, such as research and education. During the last few years the antenna sector has begun to explore towards the use of this new technology with interests in achieving lower cost and weight performance in traditional antenna technology. Nonetheless, to present times most contributions from 3D technology towards the antenna field have mostly been related to only low profile antennas [96] - [98], and there are not many contributions related to 3D manufacturing of electrically larger antennas [99] [100]. As a matter of fact, contributions related to electrically large and non-planar antennas operating at microwave frequencies is limited since they would require the assembly of different large radiating structures such as horn and reflector antennas. This project, nonetheless, presents a reflector antenna that is fabricated through 3D printing technology.

The 3D model of the reflector designed in Section 4.4.2 is exported from CST in a .STL file. This format can be processed using a slicing software, and the generated GCODE is fed to the 3D printer in an SD card, from which the reflector is manufactured accordingly with the highest achievable surface accuracy from the chosen material. The vertically truncated reflector is fabricated using a STRASYS FDM® uPrint SE Plus™ 3D printer that has a build area of 250 by 250 by 300 mm. The specifications of the FDM® 3D printer used is provided in Appendix C.2. Given that the horizontal diameter of the reflector is 1.2 meter, the inability of the 3D printer to directly manufacture the reflector as a single structure arises the necessity of fabricating the reflector in five individual parts, or panels, of equal size. Outsourcing the fabrication of the reflector to a larger printer in order to fabricate the reflector in a single piece would have significantly increased the manufacturing cost. The individual parts of the reflector was designed with a T-section joint (i.e. a tool used for panel jointing), using a CAD tool called

SolidWorks (Figure 6-11), in order to ensure that the physical panels located accurately together. This was also required to allow the designer to identify the dimensions of each panel.

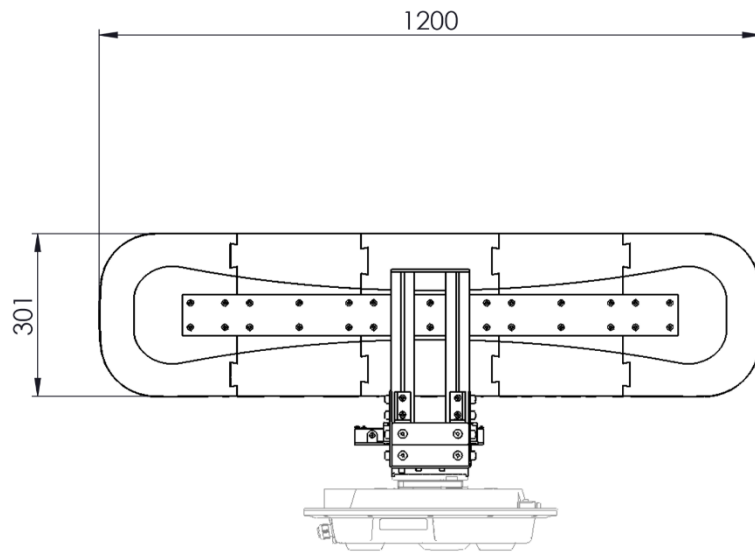


Fig 6-11. Rear view of parabolic reflector comprising of five joint panels

For the application in hand, the fabrication method is able to fulfil the minimum surface accuracy requirements of the reflector, which will be discussed in Section 6.2.2. The machining of the reflector panels according to the reflector design is shown in Figure 6-12.

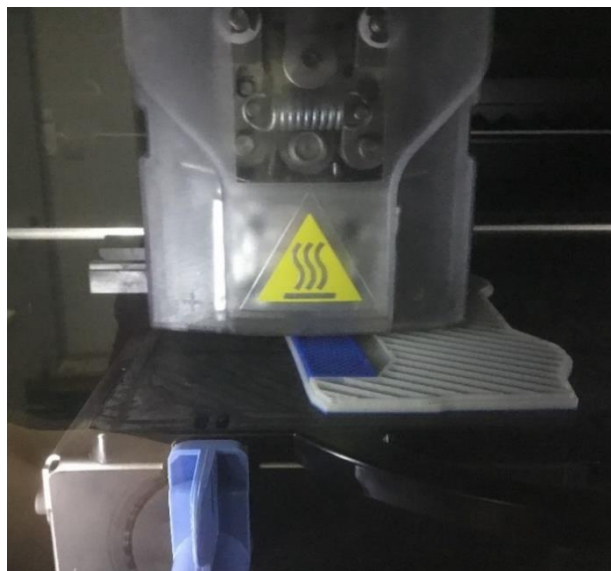


Fig 6-12. Machining process of the individual reflector parts

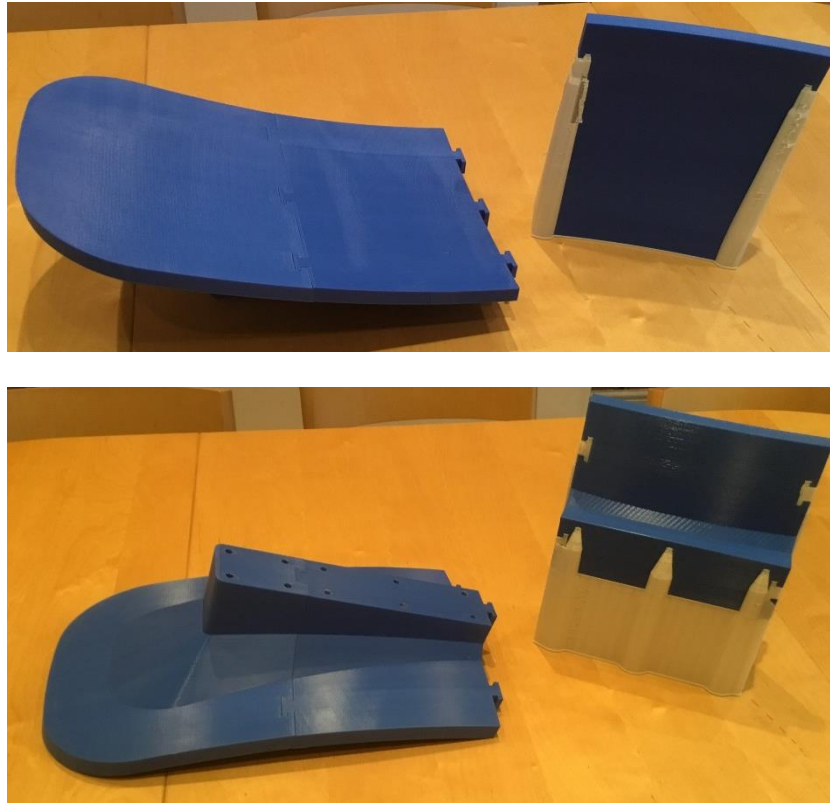


Fig 6-13. The first 3 of 5 parts of the 3D printed reflector

The material used to fabricate the reflector is a type of plastic known as Acrylonitrile-Butadiene-Styrene (ABS). ABS is an opaque thermoplastic polymer material made from the monomers Acrylonitrile, 1,3-Butadiene and Styrene [101]. The material has a strong resistance to corrosive chemicals and/or physical impacts and is considered as a very strong and rigid material, which makes it a true production-grade thermoplastic that is durable enough to have the same performance as standard production parts. It has a low melting temperature that makes it particularly simple to use in injection molding manufacturing processes and is very easy to machine when used in conjunction with FDM® printers, undoubtedly making the material ideal for building 3D structural prototypes in an office environment. The properties of the materials (ABS) used to manufacture the reflector is provided in Appendix C. The reflector was measured and checked for accuracy after the reflector panels were assembled and aligned. This was followed by solvent welding of the five panels together to form the truncated parabolic reflector.



Fig 6-14. Rear view of the 3D printed reflector attached to support frame

The issues concerning the cost and weight of a conventional reflector is significantly reduced given that it is manufactured from plastic and the metallic properties of the 3D printed reflector is achieved by coating a metallic compound on its collecting surface. The two most common metals used within the radar industry are copper and aluminum. Although both materials are very popular conductors with desirable characteristics, the properties of each metal, such as conductivity, tensile strength, weight and environmental exposure, are different and some are more desirable than the other. With the exception of silver, copper is the most conductive metal and has become the international standard. The International Annealed Copper Standard (IACS) was adopted in 1913 to compare the conductivity of other metals to copper. Relative to other metals, commercially pure annealed copper has a conductivity of 100 percent IACS. In addition to its superior conductivity, the metal contains great tensile-strength, thermal-conductivity and thermal-expansion properties [102]. Even though copper has a long history as the material of choice for conducting electricity, aluminum has certain advantages that make it attractive for specific applications. Aluminum has 61 percent of the conductivity of copper, but has only 30 percent of the weight of copper. Aluminum also sees usage where its low-weight properties are important, such as aircraft and future applications in automobiles. Aluminum is generally more inexpensive when compared to copper conductors [102]. A brief comparison between the general properties of copper and aluminum for the same application are provided in Table 6-3.

Comparison of XHHW-2 Properties	AA-8000 Series Aluminum	Copper
AWG size for 60 A at 75°C	6	8
Weight per 1,000 ft.	39 lb.	65 lb.
Nominal diameter	0.26 in	0.23 in
Maximum pulling tension	157 lb.	132 lb

Table 6-3. Comparison of Copper and Aluminum properties [102]

The metallic properties of the reflector is achieved by coating a silver copper screening compound on the reflecting surface of the dish. Copper is the preferred material solely due to its higher conductivity as compared to aluminum, and given that it is applied by coating means that the weight comparison of the two conductors is irrelevant. The coating of the ABS reflector is applied evenly using a copper compound spray (RS 427-4251) produced by RSPRO®. The compound is a silver-plated copper shielding coating that is designed to give low resistance even in thin layers. It is an extremely efficient EMI/RFI shielding compound that adheres to a wide variety of substrates. The product is of industrial grade and shows excellent environmental ageing ability with superior scratch and corrosion resistant [103]. The specifications of the copper compound spray used is provided in Appendix C.3

As a safe approximation, the thickness of the copper coating on the reflector surface must be at least 10 times the skin depth of copper at the intended operating frequency to ensure that the radiation of the feed is not absorbed by the reflector as the electromagnetic waves reflects off the illuminated surface. The skin depth is a measure of how closely electric current flows along the surface of a material, it refers to how deeply an RF signal can penetrate a material, which is dependent on the frequency as well as the material's properties [104]. The skin depth of a conductive material is given by

$$\delta = \sqrt{\frac{\rho}{\pi f \mu}} \quad (6-1)$$

Where δ is the skin depth of a material at a given frequency

f is the frequency of the current

ρ is the resistivity of the material (Ohms/meter)

μ is the permeability of the material

The skin depth of all conductive materials decreases with increasing frequency, and thus, at RF frequencies (>10 MHz) the electric current only propagates through the surface of the material. Given the values of ρ and μ for copper is 17.24×10^{-9} and 1 respectively, the skin depth of copper at an operating frequency of 9.2 GHz is approximately $0.68 \mu\text{m}$. The required minimum thickness of the coating applied on the reflector surface is $6.8 \mu\text{m}$.

The precise thickness of the coating applied was not specified although it was ensured to be greater than $6.8 \mu\text{m}$. A single can of the compound spray can cover a surface area of 1.2 m^2 at $50 \mu\text{m}$ dry film thickness. Given that the surface area of the reflector is 0.36 m^2 (1.2 m by 0.3 m), the coating applied on the reflector surface will be approximately $170 \mu\text{m}$ thick, which represents coating over the surface area of the reflector with one full can. In radar

applications operating at very high frequencies (~ 50 GHz), it is critical that the coating is evenly applied throughout the reflector aperture to minimize surface deviations and inaccuracies due to the small operating wavelength. The operating wavelength is quite large (3.26 cm) at 9.2 GHz, and thus, spraying layers of the compound on the reflecting surface of the reflector in even vertical and horizontal passes to maintain an even coating is sufficient. The surface accuracy requirements of a reflector and its significance on the performance of the reflector antenna is discussed in Section 6.2.2. The 3D printed reflector coated with a copper compound spray is shown in Figure 6-15.



Fig 6-15. Front view of the 3D printed reflector attached to support frame

6.2.1.1.1 Reflector Cost and Weight Analysis

The weight of the manufactured reflector is 5.4 kilograms. The density of the material used (ABS (Injection Grade)) to fabricate the reflector is 1.05 g/cm^3 , which is several times less than the density of aluminium (2.7 g/cm^3). Hence, manufacturing the same reflector by machining it entirely out of solid blocks or sheets of aluminium, or through other conventional fabrication methods, would produce a reflector that weighs approximately three times heavier. The reflector manufactured for this project is considered to be a very lightweight reflector considering its large size.

The cost of manufacturing the reflector through 3D printing technology is significantly lower than if it was to be manufactured through conventional fabrication methods due to two factors. Firstly, the 3D printer fabricates the modelled structure from raw materials until the final product is produced. Hence, unlike machining of a large metallic reflector, it is a very simple and relatively quick process that only requires minimal labour for assembly. Secondly,

the cost of ABS that is compatible with standard commercial 3D printers is approximately £90 to £100 per 2 kg, which is the cost of a single cartridge [105]. The total material cost of the reflector shown in Figure 6-15 is approximately £320, which would be significantly cheaper as compared to the any other type of conventional metal that can be used. The cost of manufacturing a metallic reflector of this size would typically be in excess of a thousand pounds, with a substantial portion of the figure contributed from the high labour costs.

The use of 3D printing technology to fabricate large antennas has been proven to be very advantageous and attractive especially from the cost and weight perspective of the components produced. Hence, if the reflector antenna manufactured in this project exhibits desirable performance, this method of fabrication can be more seriously considered in the future for not only small antennas, but also larger ones.

6.2.2 Surface Accuracy Requirements

The surface of the molded reflector must first adapt to the shape of a true parabolic curve described by the parabolic equation of $x^2 = 4fz$ to an accuracy of within a fraction of a wavelength in order to produce the desired plane wavefront of the reflected radiation at the aperture plane. In practice, the acceptable deviation is generally between 1/32 to 1/16 of a wavelength [50]. Thus, the surface accuracy requirement increases with the operating frequency and the irregularity of a given reflector surface effectively determines the maximum acceptable frequency at which the reflector can be used successfully. Furthermore, it is notable that the requirements of the reflector surface accuracy is also dependent on special patterns requirements, such as very low side lobes and/or back lobe. The surface accuracy requirement of the reflector is higher at higher operating frequencies due to the smaller operating wavelength of the EM waves. Thus, the surface accuracy requirement of very small dishes tends to be significantly higher as compared to standard sized dishes as they are more frequently used in high frequency applications. This explains the need for very small dishes to be manufactured using more complex methods.

It has been proven experimentally that the existence of wide and random deviations of the shape of the reflector surface from a true parabolic dish due to either tolerancing errors or to surface roughness will result in phase errors in the aperture plane, which causes diffuse reflection that increases the sidelobe level and reduces the directive gain of the antenna pattern. As illustrated in Figure 6-16, the magnitude of these phase errors can be easily estimated by considering a deviation from the ideal parabola δr that is measured from the focus [50].

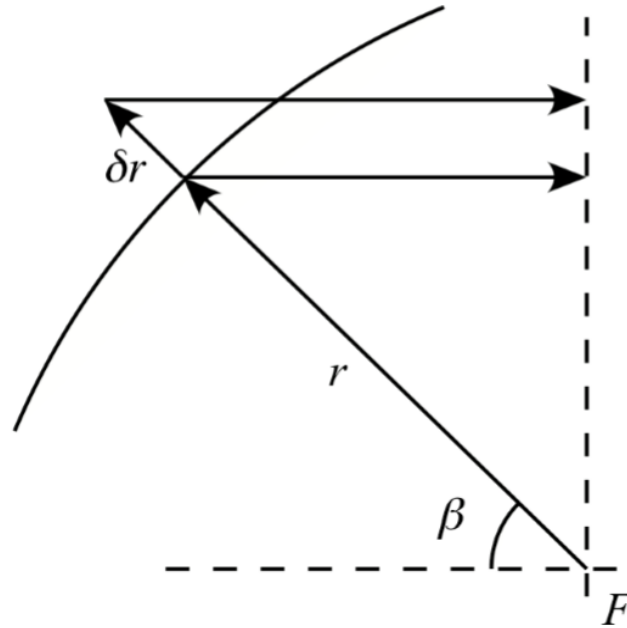


Fig 6-16. Illustration of surface errors in a reflector antenna [50]

The path length from the plane containing the focus to the focus is $r(1 + \cos \beta)$. Considering an error in the shape of the reflector of δr at β , the difference in path length is

$$\delta L = \delta r(1 + \cos \beta) = 2\delta r \cos^2(\beta/2) \quad (6-2)$$

which is very similar to the amplitude taper expression. The phase error due to this surface error is therefore

$$\delta \phi = \frac{2\pi \delta L}{\lambda} = \frac{2\pi \delta r}{\lambda} \cos^2(\beta/2) \quad (6-3)$$

This expression indicates that the worst phase errors occur due to surface errors around the vertex, however this is the region of the reflector which is easiest to control in shape. For a focal-plane feed, assuming a maximum phase error of $\pi/4$ is tolerable, the surface must be accurate to at least $\lambda/16$ at the vertex $\lambda/8$ at the edge of the reflector [50].

An analysis performed by RUZE (1966) [106] on this matter had also quantitatively shown how these effects are related to the rms deviation of the reflector from the exactly correct surface. He showed that a given rms deviation has a greater effect on sidelobe level in a small reflector than in a large one, and also that the effect depends on the correlation interval (statistical concept) of the irregularities. If the individual “bumps” of the surface extend over a small area, the correlation interval is small. If they extend over a larger area, as would be true of a “wavy” rather than a “bumpy” surface, the correlation interval is larger. In terms of these

concepts, [106] showed that a given magnitude of rms deviation from the true surface causes a greater increase of sidelobes and reduction of gain when the correlation interval is large than when it is small [27].

For the application in hand, given that the operating frequency of the radar is at 9.2 GHz, which corresponds to an operating wavelength of 32.6 mm, a suitable surface accuracy of the reflector must be at least 2 mm at the vertex and 4.1 mm at the edge of the reflector. Fabricating the dish using the proposed method described above according to the surface accuracy requirement can be easily fulfilled. However, at scenarios where very high performance is required from a radar system that operates at high frequency bands, the fabrication of a perfect parabolic surface is difficult to achieve and is likely to increase the manufacturing cost of the reflector significantly. Thus, a reflector that perfectly conforms to the shape of a parabola with a perfect surface accuracy is not commonly required since phase errors of a certain extent is frequently tolerable. Depending on the application of the radar system, it is therefore important to identify the maximum degree of surface inaccuracy that can be tolerated without imposing a realizable degradation on the properties of the secondary lobe produced, or on the performance of the reflector antenna. Fabricating the reflector using a 3D printer is unlikely to be suitable for applications where very small phase error is permitted, as this would correspond to a reflector with very high surface accuracy requirements.

6.2.3 Feed and Reflector Support-frame and Antenna Assembly

In addition to placing the feed at the appropriate position along the focal line of the reflector to optimize the performance of the radar, ensuring that the feed will remain at the correct position when subjected to various stresses that may occur due to wind, gravity, and so forth, is critical in maintaining the desired characteristics of the beam produced. An obvious method that accomplishes this requirement is to support the feed with a strong and rigid mechanical structure. However, the challenge with a center-fed reflector antenna is to prevent the feed support from blocking a substantial amount of the reflected rays, and therefore minimizing the supports used is vital in the design.

The feed and reflector support-frame are designed and constructed using a T-slot aluminium profile system by Valufame®. Valufame® focuses on providing an aluminium profile system suitable for economical frame building, which assists in designing a light and economic framework using hollow aluminium tubes. The key feature of the aluminium extrusion from Valufame® is that it could be easily connected to one another using the various connecting elements produced by them. The fast and simple connection and disconnection of the aluminium extrusions, as opposed to welded fabrications and other aluminium extrusion

systems, reduces the cost, complexity and time required to construct the support-frame of the feed and reflector [107]. This feature introduces many advantages of the profile system as compared to other profile framework systems. The advantages of Valuframe® T-slotted aluminium profile system are summarized in Table 6-4.

<u>Advantages of T-slotted Aluminium Profile System (Valuframe)</u>	
○	No welded joints – Once assembled the aluminium extrusions can still be shifted and repositioned accordingly.
○	Unskilled and safe – No health and safety issues associated with welding, dressing, painting and other engineering operations as they are not required.
○	Simple and quick assembly – The aluminium extrusions can be easily and quickly assembled accordingly.
○	Adaptability – The connecting elements are small and handy to use.
○	Recyclable – Aluminium extrusions can be re-used for another purpose if the framework is temporary.

Table 6-4. Advantages of T-slotted aluminium profile system [107]

The proposed feed and reflector support-frame constructed using Valuframe® aluminium profile system, which consists of their aluminium extrusions and connecting elements, is shown in Figure 6-17 to 6-19. The design of the feed and reflector support is rather simple for this reflector antenna since the direction of the beam produced from the reflector is always towards a fixed point, which permits the feed and reflector support to be attached to the antenna base rather than directly to the dish. The respective supports were designed to be as narrow as possible to minimize reflections of the propagating EM waves with the aluminium extrusions. This is to minimize the undesirable effects of feed and support blockages on the beam produced from the reflector. The support framework uses a single aluminium extrusion to firmly support the feed and reflector, and a strong and rigid base to hold the individual aluminium extrusion at a fixed position. Mounting brackets were also designed to firmly attach the horn antenna and reflector to their respective supports. The feed and reflector are positioned according to the reflector antenna designed in Section 4.4.3 and 5.1.3, that is, for a center-fed reflector antenna and a monopulse reflector antenna, respectively.

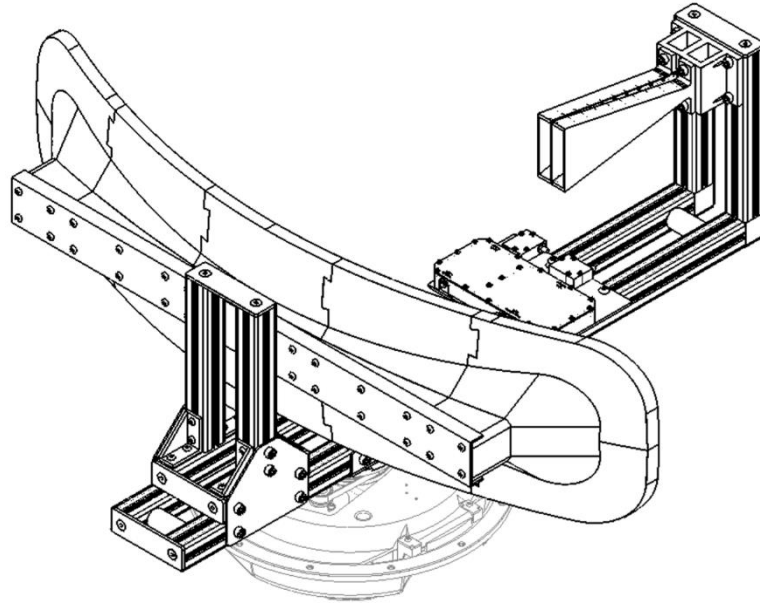


Fig 6-17. Perspective view - Aluminium profile system of radar employing reflector antenna

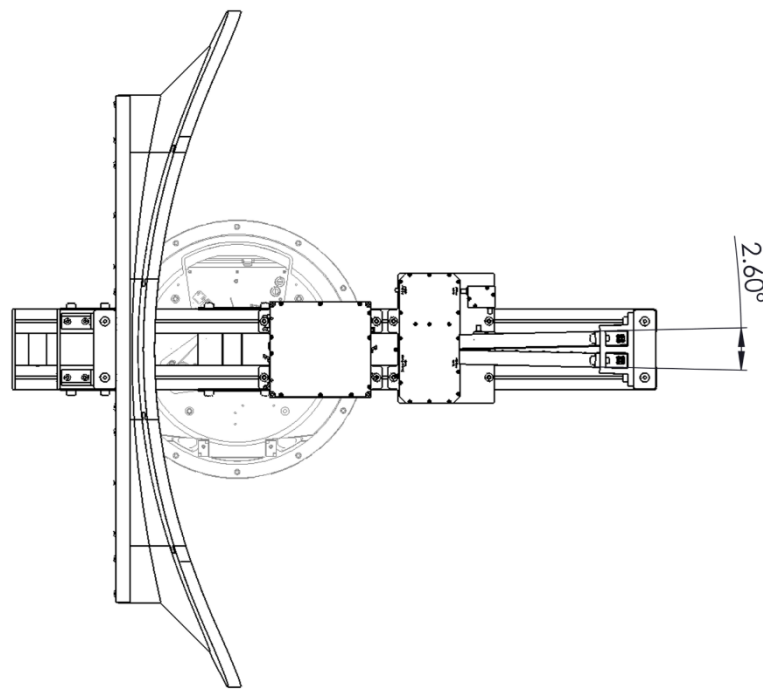


Fig 6-18. Top view - Aluminium profile system of radar employing reflector antenna

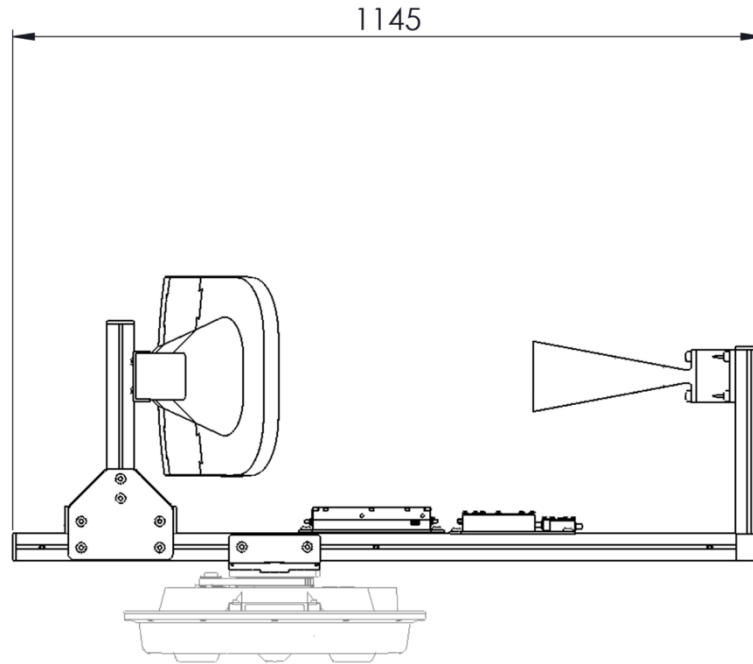


Fig 6-19. Side view - Aluminium profile system of radar employing reflector antenna

The assembly of the reflector and feed with their respective support structures that is based on the modelled aluminium profile system shown above forms the reflector antenna system, which is shown in Figure 6-20. Moreover, with appropriate tools, the framework can be dismantled and assembled easily within a short period, which makes the reflector antenna a highly portable one.

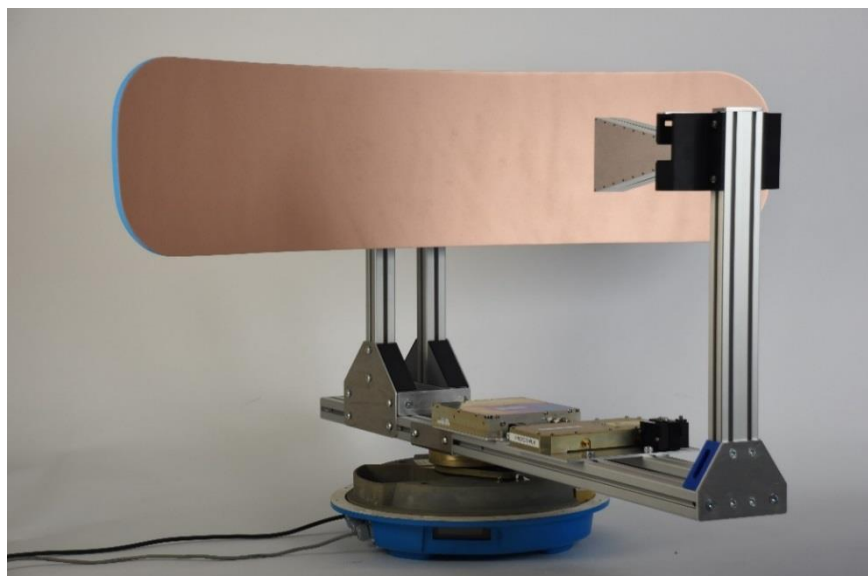


Fig 6-20. Monopulse feed and reflector attached to the designed supports

The aluminium extrusion used in the profile system is not painted but finished with an anodized finish. It therefore has the same manufacturing tolerances and quality as other more expensive aluminium profile framework systems available in the market. Hence, the framework used would still match the versatile strength and attractive appearance of welded aluminium or steel frameworks, and fabrications, and of other similar, yet more expensive, conventional profile systems used in large antennas. The aluminium profile system used to construct the feed and reflector support are, therefore, ideal cost-effective alternatives to welded steel fabrications and the more established and expensive aluminium profile systems available. The properties of the T-slotted aluminium profile system used is provided in Appendix C.1.

Upon assembling the reflector antenna, the critical dimensions of the antenna such as the focal length of the reflector and the position of the feed relative to the reflector are measured and verified to ensure that they are identical to the reflector antenna design. The antenna far-field pattern measurements of the constructed reflector antenna are presented, analysed and compared to the simulated performance of the antenna model in Section 6.3.

6.3 Antenna Under Test (AUT) Far-field Pattern Measurements

The aim of manufacturing the monopulse reflector antenna according to the antenna modelled on CST is to measure the antenna performance and to validate the EM simulations of the designed antenna using the measured patterns. Ideally, the measured far-field radiation pattern of the monopulse antenna is expected to be identical to that of the simulated patterns presented in Section 5.1.3. In practice, they are expected to conform closely to one another due to several discrepancies in measurement conditions. This section describes the method undertaken and the facility used to measure the far-field radiation pattern of the monopulse antenna, and is followed by an analysis on the measured patterns and a comparison with the simulated performance of the antenna on CST.

6.3.1 Antenna Characterization Range (X-Band)

An anechoic chamber is a popular test facility used to measure the near and far-field radiation pattern of mainly small to medium sized antennas. To successfully measure the far-field pattern of the monopulse reflector antenna in such a facility, which, as calculated by (3-10), has a large far-field region of 89 meters, this would require a chamber than can perform a conversion of the measured antenna pattern from the near-field to far-field region. However, due to the large size of the antenna some issues were encountered with the near-field to far-field transformation,

and therefore the most ideal solution is to perform the antenna far-field pattern measurements on a far-field X-band antenna characterization range test facility.

Most large antennas with a wide far-field region are measured on an outdoor test range, where a proper far-field measurement of the antenna can be performed in a large open facility and the most accurate far-field antenna measurements can be achieved. It is by far the most popular type of test facility and is frequently the only type that is practical for large antennas. The measurements of the antenna far-field pattern were carried out on an outdoor X-band elevated antenna range at QinetiQ Funtington (Figure 6-21). The range is 397 meters long and runs approximately west-to-east with the transmission source site located at the western end of the range. All measurements were conducted at 9.2 GHz vertical polarization.



Fig 6-21. X-band antenna measurement range

The transmit, or source, and receive antenna is positioned at site A and B, respectively, and the separation between the antennas is 397 meters. The transmit antenna used was a 1.8 meter parabolic dish with a 1 degree beamwidth in both principal planes, at a height of 12 meters and a look-down angle of 1 degree. The transmit antenna is circled in red, as shown in Figure 6-22.



Fig 6-22. Transmit parabolic reflector antenna

The antenna under test (AUT), or the receive antenna, whose far-field pattern will be measured in both principal planes, is mounted on a 1.2 meter support to the antenna positioning system. The AUT was clamped to the antenna support to ensure that it remained stationary as it is rotated in both planes, one after another, through the positioning system, while the antenna pattern measurements are recorded.

The measurements of the antenna pattern were performed individually in the horizontal plane followed by the vertical plane. Hence, the principal plane patterns will be provided for each type of antenna measured in the test range facility. For azimuth measurements, the antenna was rotated clockwise with 0 degree corresponding to electrical boresight. Whereas for elevation measurements, the antenna was rotated up and then down, or vice versa, with 0 degree corresponding to electrical boresight. The positive and negative angles for elevation measurements correspond to the antenna looking up and down, respectively.

The drawback with the antenna pattern measurements is the limited maximum number of sampling points of the recorded data permitted for each measurement performed. Thus, a trade-off between the angular range and resolution, or sampling interval, of the data recorded (x-axis) is required to be specified for each antenna pattern measurement. The angular range in which the antenna pattern is measured across in azimuth and elevation, and its corresponding

resolution, will be specified accordingly for each antenna measurement performed in the test range facility.



Fig 6-23. 1.2-meter antenna support



Fig 6-24. AUT mounted on antenna support

The main devices of the antenna measurement system comprise of a Vector Network Analyzer (VNA), synthesizer and an antenna positioning system. A schematic diagram of the antenna measurement system is shown in Figure 6-25.

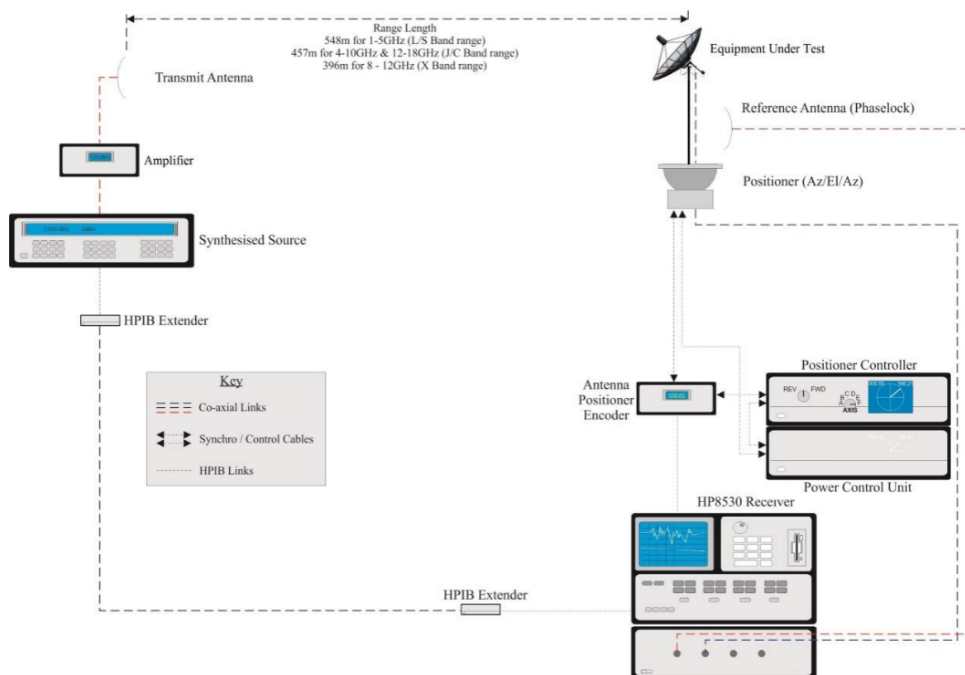


Fig 6-25. Schematic of the antenna measurement system

The antenna radiation pattern measurements are calibrated to provide gain relative to an isotropic radiator. The system will be calibrated for gain prior to the pattern measurements using the substitution method. Hence, the first measurement is of a *Narda 640 standard gain horn* which was used to calibrate the RF measurement system. The measurements of the AUT is commenced upon calibration of the RF system.

6.3.2 Antenna Far-field Pattern Measurements

The components used for the antenna measurements performed in the antenna range test facility (QinetiQ – Funtington) comprises of two E-plane sectoral horn antennas and a vertically truncated parabolic reflector. A single horn antenna and the reflector are initially assembled to create a center-fed reflector antenna (Section 4.4), and this is followed by the addition of a second horn antenna to create an amplitude monopulse reflector antenna (Section 5.1.3). Both types of reflector antennas were manufactured and constructed identically according to their respective modelled designs.

The allocated time available to occupy the antenna range test facility was limited to half a day (approximately five hours between 9:00 to 14:00). Within this duration we were able to obtain the required measurements of the various antenna types according to the measurement plan prepared prior to the scheduled test date. All the antenna far-field pattern measurements presented in this section are in the form of a cartesian plot, whereby, the y-coordinates is the antenna gain on a dBi scale and is relative to power and x-coordinates is the angle of rotation, or target angle, in degrees. The antenna measurements have been conducted according to QinetiQ Work Instruction *Ref: ENG/W499/MS/1.0*.

6.3.2.1 Measurement Plan and Results

The antenna pattern measurements of three different types of antennas were performed in the antenna range test facility. Measurements of the antenna systems are carried out to verify the corresponding modal analysis and the simulation results of the respective antennas. The first far-field pattern measurement is of an E-plane sectoral horn antenna, followed by a center-fed reflector antenna, and lastly a monopulse reflector antenna that is illuminated by a dual-horn feed arrangement across a range of angular displacement applied on the pair of feed. The pattern measured for each antenna is presented and analysed in individual sections. The final objective of the experiments performed is to prove that the proposed dual feed horn arrangement is a suitable method of producing a one-coordinate monopulse reflector antenna, and to achieve this, the measured performance of the monopulse reflector antenna must conform closely to the corresponding EM simulation results. Thus, the properties of the measured antenna patterns

will be analysed and compared to their corresponding simulated counterparts. This also allows the validation of the antenna patterns that were simulated on CST, for each type of antenna that was designed in this project.

6.3.2.1.1 E-plane Sectoral Horn Antenna

The E-plane sectoral horn antenna is used as the feed of the reflector antenna. It is critical that the measured far-field pattern of the E-plane sectoral horn antenna must conform closely to the simulated pattern of the horn presented in Section 4.3, since the dimensions and shape of the reflector was designed according to the illumination of the reflector aperture by the simulated pattern of the feed horn. Hence, the first and most significant EM simulation measurement to be validated is the far-field pattern of the manufactured E-plane sectoral horn antenna in both principal planes.

The setup arrangement for the AUT shown in Figure 6-26 is for the measurement of the far-field pattern of the E-plane sectoral horn antenna.



Fig 6-26. AUT – E-plane sectoral horn antenna

Figure 6-27 presents the plot of the measured radiation pattern of the horn antenna in the horizontal and vertical plane, respectively. The far-field pattern of the horn antenna was measured across an angular range of ± 90 degrees in azimuth and from ± 30 degrees in elevation, with a sampling interval of 0.225 degree and 0.1 degree, respectively. Hence, the

angular resolution, or accuracy, of the plot denoting the measured antenna pattern in the vertical plane is greater than that in the horizontal plane, albeit at the expense of a smaller angular range.

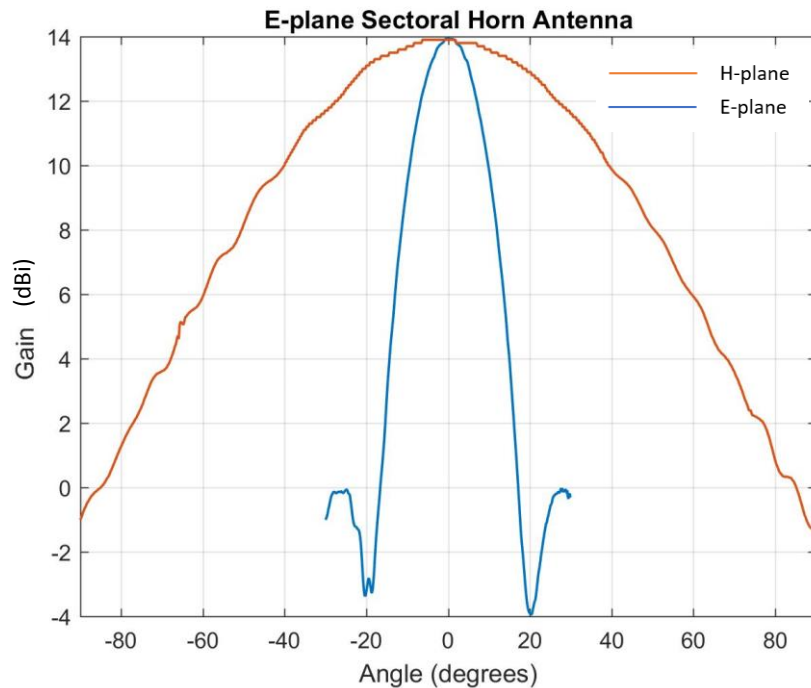


Fig 6-27. Measured principal plane pattern of E-plane sectoral horn antenna

The -3 dB azimuth beamwidth of the measured antenna pattern is 71.1 degrees. The highest sidelobe in the horizontal plane was not measured as it was beyond the angular range measurement. The -3 dB elevation beamwidth is 16.8 degrees with a sidelobe level of -14 dB in the vertical plane. The measured gain of the sectoral horn antenna is 14 dBi.

The measured (Figure 6-28) and simulated (Figure 6-29) far-field patterns of the E-plane sectoral horn antenna in azimuth and elevation are each plotted on the same axis. A comparison of the properties of the corresponding antenna far-field patterns in both principal planes shows that the results conform very closely to one another, with a deviation less than 0.3 dB (Table 6-5).

Radiation Properties	Azimuth BW (deg)	Sidelobe Level (dB)	Elevation BW (deg)	Sidelobe Level (dB)	Gain (dB)
Measurement	71.1	NA	16.77	-14	13.96
Simulation	70.9	-25.3	17.17	-13.9	14.22

Table 6-5. Far-field radiation pattern – E-plane sectoral horn antenna

Simulated and Measured Azimuth Pattern (E-plane Sectoral Horn Antenna)

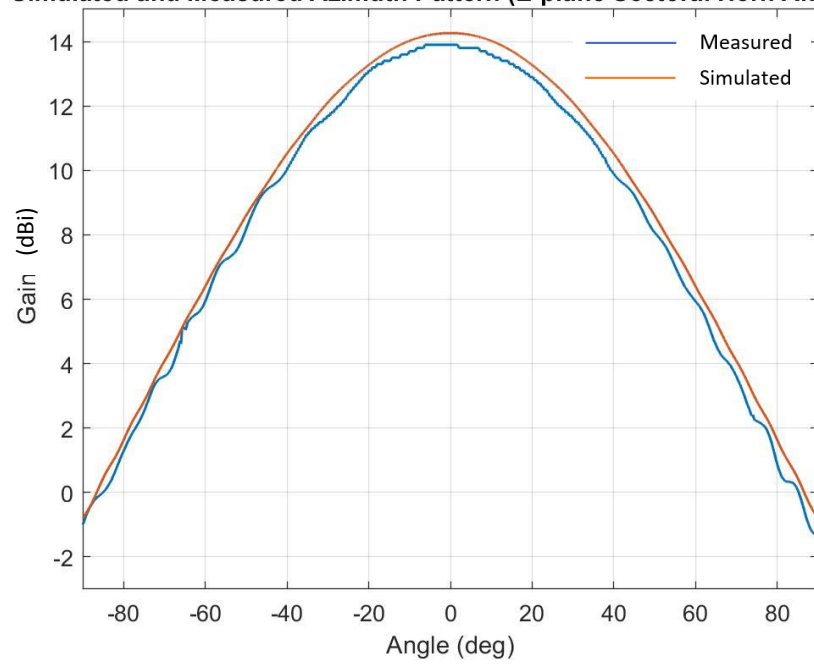


Fig 6-28. Simulated and measured azimuth pattern – Sectoral horn antenna

Simulated and Measured Elevation Pattern (E-plane Sectoral Horn Antenna)

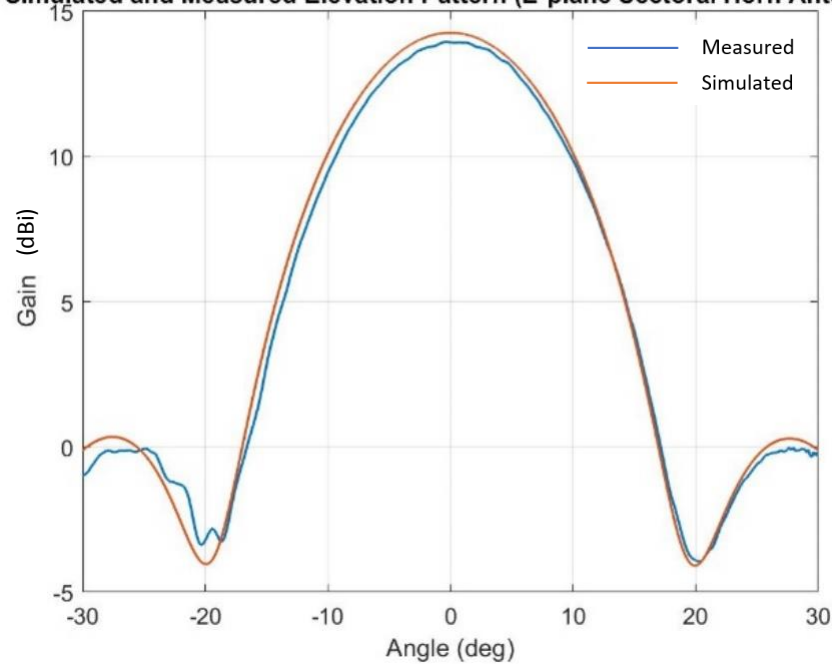


Fig 6-29. Simulated and measured elevation pattern – Sectoral horn antenna

6.3.2.1.2 Center-fed Reflector Antenna

The test proceeds with the principal plane pattern measurements of a center-fed parabolic reflector antenna to verify the modelling of the reflector antenna calculated in Section 4.4. Since the measured and simulated principal plane patterns of the feed horn matches one another, the

feed is expected to illuminate the manufactured reflector with an illumination taper of approximately -10 dB across the reflector aperture in both planes.

The setup arrangement for the AUT shown in Figure 6-30 is for the far-field pattern measurement of the center-fed reflector antenna.



Fig 6-30. AUT – Center-fed reflector antenna (side)



Fig 6-31. AUT – Center-fed reflector antenna (perspective)

The antenna far-field pattern is measured between an angular range of ± 10 degrees (Figure 6-32) and ± 90 degrees (Figure 6-33) in azimuth, and between ± 10 degrees in elevation (Figure 6-32). Two measurements are performed in the horizontal plane. The sampling interval of the first measurement is 0.1 degrees – this is a considerably small interval which provides a high resolution, or accuracy, of the measured antenna pattern around the boresight axis of the main lobe, in the expense of a smaller angular range (± 10 degrees). The second measurement measures the antenna pattern across half of a complete rotation (± 90 degrees) in the horizontal plane, which exhibits important properties of the antenna pattern of the reflector antenna extending away from the main lobe and first few sidelobes. However, the sampling interval is 2.25 times wider than the first measurement performed, at 0.225 degrees, which corresponds to a resolution that is 2.25 times poorer than that of the first measurement.

Figure 6-32 presents the plot of the measured principal plane far-field pattern of the center-fed reflector antenna between an angular range of ± 10 degrees.

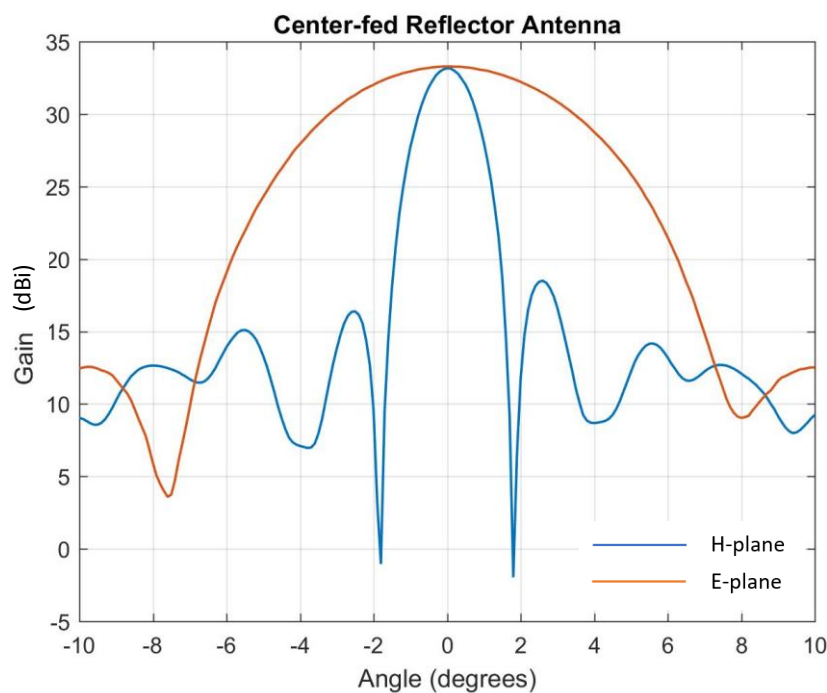


Fig 6-32. Measured pattern of center-fed reflector antenna in both principal planes

An additional far-field pattern measurement in azimuth between an angular range of ± 90 degrees is presented in Figure 6-33.

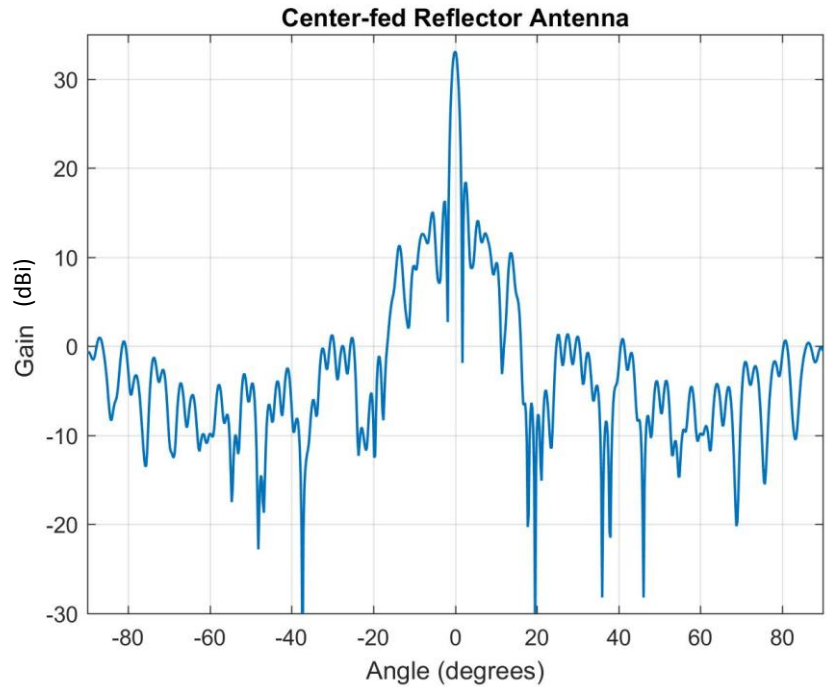


Fig 6-33. Measured pattern of center-fed reflector antenna in horizontal plane

The -3 dB azimuth beamwidth of the measured antenna pattern is 1.54 degrees with a sidelobe level of -15.8 dB in the horizontal plane, and a -3 dB elevation beamwidth of 6.4 degrees with a sidelobe level of -20.8 dB in the vertical plane. The measured gain of the center-fed reflector antenna is 33.2 dBi.

The measured and simulated far-field patterns of the center-fed reflector antenna in azimuth and elevation are each plotted on the same axis (Figure 6-34 and Figure 6-35, respectively) between an angular range of ± 10 degrees. A comparison of the properties and shape of the corresponding antenna patterns shows that they conform very closely to one another, with a deviation that is less than 1.3 dB in both principal planes (Table 6-6). The measured radiation pattern of the reflector antenna also verifies the chosen method of manufacturing the reflector to be an acceptable one.

Radiation Properties	Azimuth BW (deg)	Sidelobe Level (dB)	Elevation BW (deg)	Sidelobe Level (dB)	Gain (dB)
Measurement	1.54	-15.8	6.38	-20.8	33.16
Simulation	1.6	-18.9	6.12	-22.7	34.45

Table 6-6. Far-field radiation pattern – Center-fed reflector antenna

Simulated and Measured Azimuth Pattern (Center-fed Reflector Antenna)

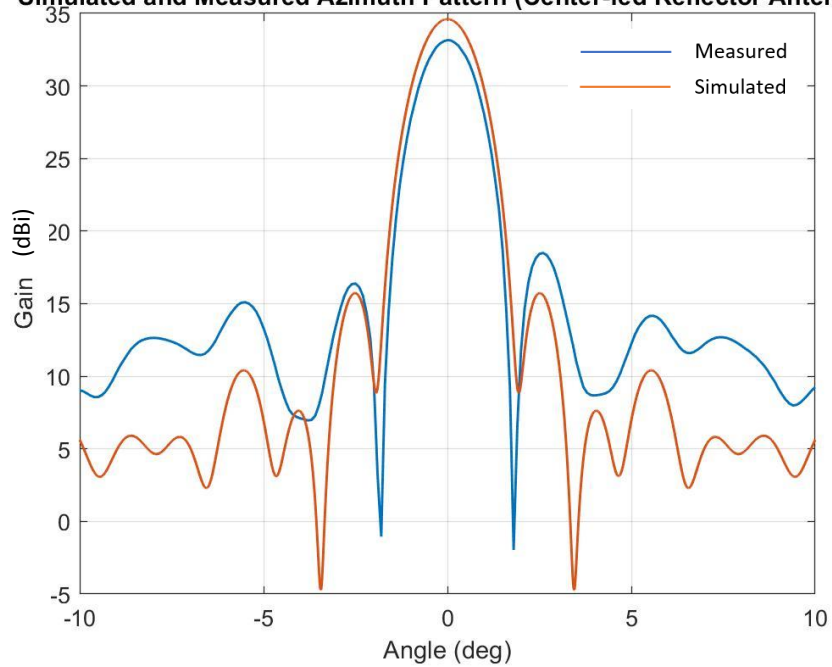


Fig 6-34. Simulated and measured azimuth pattern – Reflector antenna

Simulated and Measured Azimuth Pattern (Center-fed Reflector Antenna)

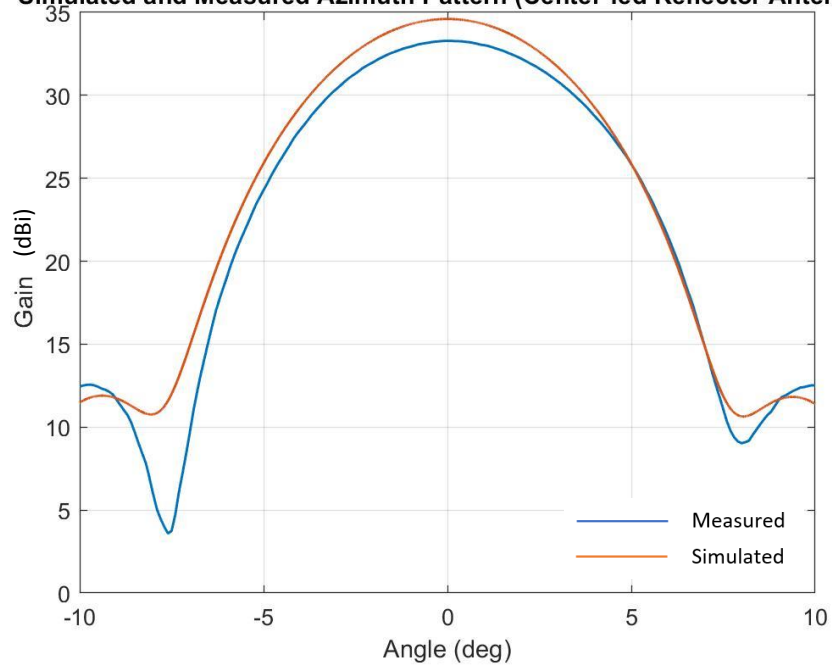


Fig 6-35. Simulated and measured elevation pattern – Reflector antenna

6.3.2.1.3 Monopulse Reflector Antenna

The final set of antenna pattern measurements are of the amplitude monopulse reflector antenna that utilizes the same reflector, but is illuminated about the vertex using a pair of E-plane sectoral horn antennas. The AUT shown in Figure 6-36 is for the far-field pattern measurement

of the amplitude monopulse reflector antenna. The far-field radiation pattern of the pair of off-axis beams produced from the reflector were measured individually for feed tilts between 1.3 to 1.7 degrees, from which the corresponding sum and difference patterns of the monopulse antenna were directly obtained for each feed tilt applied. The family of sum and difference patterns are used to verify the optimum feed tilt to be applied, and therefore the design of the monopulse reflector antenna shown in Section 5.1.3, which is based on the properties of both patterns, each corresponding to a feed tilt applied, that is most suitable to the requirement of the application in hand.



Fig 6-36. AUT – Monopulse reflector antenna

The mounting bracket that attaches the pair of feed horn to the aluminium extrusion, or feed support, was designed to accurately align the position of the dual-horn feed when an angular displacement is applied on the pair of feed about the vertex of the reflector. The bracket ensures that the position of the pair of feed relative to the reflector is accurate for feed tilts in between ± 5 degrees, and the distance from the apparent phase center of each feed to the vertex is constant across the range of angles. It ensures that the constructed monopulse reflector antenna would replicate the antenna arrangement designed across the feed tilts applied. The numbers marked on the mounting bracket indicates the angular separation of the respective feed horn from the original position of the feed in a center-fed reflector antenna, and therefore it allows the position of the pair of feed horn to be easily adjusted by sliding the position of the horn across the numbers on the mounting bracket. Hence, the mounting bracket used in a center-fed and monopulse reflector antenna are different, where the design of the latter is significantly

more complicated than the former. The mounting bracket used in the monopulse reflector antenna is circled in red, as shown in Figure 6-37.



Fig 6-37. Mounting bracket of dual-horn feed of a monopulse reflector antenna

Due to time constraints we were only limited to three measurements of the monopulse reflector antenna. This was allocated for the measurement of the antenna pattern when three angular displacements are applied on the pair of feed horn (1.3, 1.5 and 1.7 degrees). For each of the chosen feed tilt applied, the antenna pattern is measured between an angular range of ± 5 degrees in azimuth with a sampling interval of 0.02 degrees. The plot of the pair of off-axis beams produced from the reflector presents the properties of the main lobe and first sidelobe, and its corresponding sum and difference patterns, to a very high accuracy in the expense of a smaller angular range. Since the monopulse technique is implemented in azimuth only, the radiation pattern in elevation were not measured for all monopulse feed configurations. Nonetheless, the measured antenna pattern in elevation for all three dual feed horn arrangements are expected to have negligible difference from another, and from its simulated counterpart, since there is zero feed displacement in this plane.

The AUT comprises of two feed horns. The received signals from the output of each feed horn were measured separately, one after another, in terms of the signal amplitude and phase (i.e. voltage real and imaginary parts). Since the outputs of the individual feed horns are accessible, the sum and difference patterns can be directly obtained from the measured squinted beam patterns (Section 3.6.1.2). The squinted patterns include the effects of mutual coupling among the horns. They are not quite the same as the patterns that would be obtained from each horn or pair of horns if the others were removed, but those patterns are of no interest for our

purpose, since coupling is always present with this dual-horn feed arrangement proposed [38]. The sum and difference monopulse patterns are derived from the post addition and subtraction of the pair of off-axis beams produced from the reflector, which is obtained from the measured output data of each feed horn, respectively. The sum and difference patterns are given by (6-4) and (6-5), respectively, in terms of gain on a dBi scale and is relative to power.

$$\text{Sum gain} = 20 \log \left(\sqrt{(AM1 + AM2)^2 + (PH1 + PH2)^2} \right) \quad (6-4)$$

$$\text{Difference gain} = 20 \log \left(\sqrt{(AM1 - AM2)^2 + (PH1 - PH2)^2} \right) \quad (6-5)$$

where $AM1$ and $AM2$ is the amplitude and $PH1$ and $PH2$ is the phase of the received signal from the left horn (Horn 1) and right horn (Horn 2), respectively.

Figure 6-38, 6-39 and 6-40 presents on the same axis the measured radiation far-field patterns of the pair of off-axis beams produced from the reflector (denoted by dashed lines) and the corresponding sum and difference patterns (denoted by solid lines) obtained in the horizontal plane when a feed tilt of 1.3, 1.5 and 1.7 degrees is applied, respectively, about the vertex of the reflector.

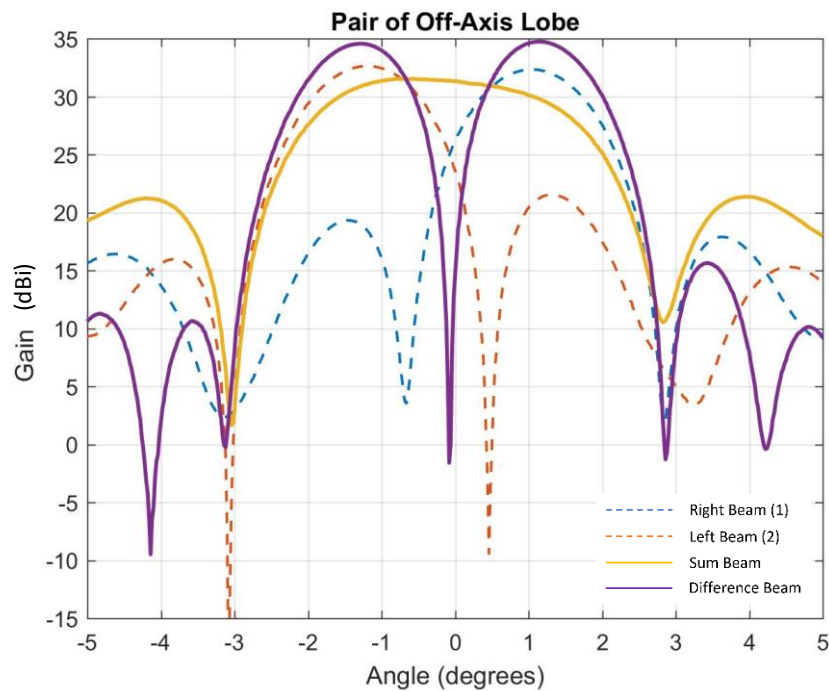


Fig 6-38. Measured off-axis beams, sum and difference patterns ($\theta_i = 1.3^\circ$)

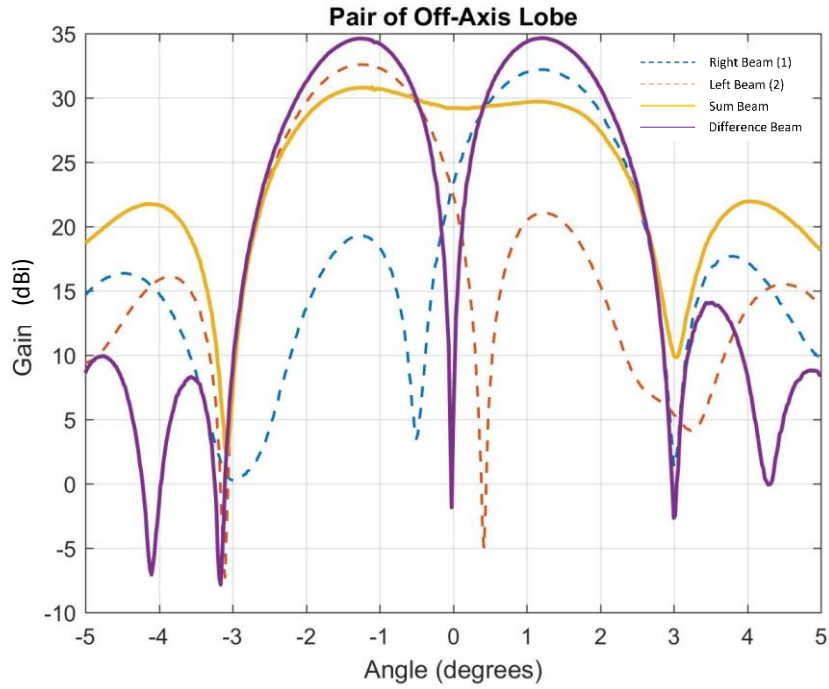


Fig 6-39. Measured off-axis beams, sum and difference patterns ($\theta_i = 1.5^\circ$)

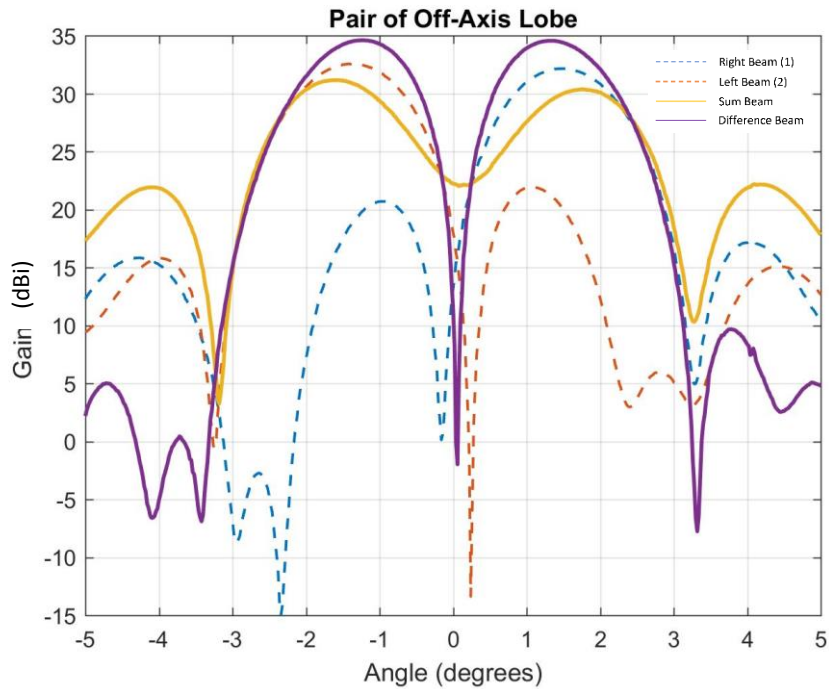


Fig 6-40. Measured off-axis beams, sum and difference patterns ($\theta_i = 1.7^\circ$)

Evaluating the properties of the measured sum and difference pattern obtained in azimuth corresponding to the individual feed tilts applied enables the optimum feed tilt that is most suitable to the requirements of the application in hand to be determined. The properties of the optimum sum and difference pattern obtained will also be used to validate the proposed

monopulse feed system by comparing it with the simulated performance of the monopulse reflector antenna in Section 5.1.3 (Figure 5-21 and 5-22).

A family of sum and difference patterns obtained across the feed tilts applied are plotted on the same axis (Figure 6-41). Only the negative bearing is plotted in order to condense the horizontal axis. These plots are based on the sum and differencing of the measured pair of off-axis beams produced from the reflector antenna using (6-4) and (6-5), respectively.

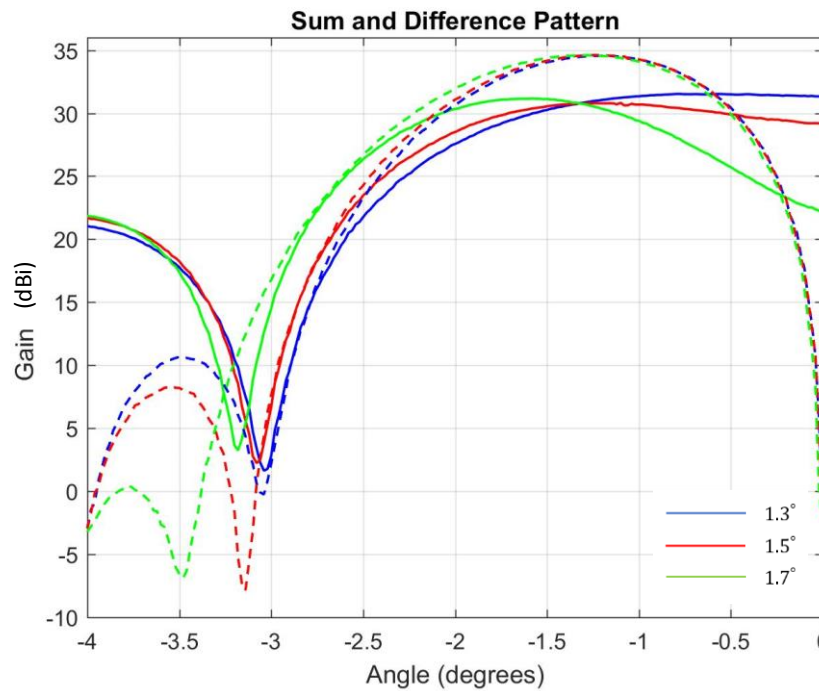


Fig 6-41. Measured sum and difference patterns across the range of feed tilt applied

The properties of the sum pattern obtained corresponding to the feed tilts applied are provided in Table 6-7. In agreement with the trend of the family of sum patterns obtained from the simulation of the monopulse antenna provided in Section 5.1.3, the sum pattern on-axis gain and beamwidth decreases and increases, respectively, with increasing squint angle.

Sum Beam Properties	1.3 deg	1.5 deg	1.7 deg
On-axis Gain (dB)	31.5	29.2	22.1
Beamwidth (deg)	3.36	4.04	4.7

Table 6-7. Measured sum beam properties across the range of feed tilt applied

The sum pattern gain and beamwidth (resolution performance) of the monopulse antenna is optimized when a feed tilt of 1.3 degrees is applied. This would be the optimum

choice if the detection sensitivity of the radar for identifying targets is prioritized. Applying this feed tilt produces a sum beam with a measured beamwidth of 3.36 degrees and an on-axis gain of 31.5 dB. The sum beam exhibits desirable properties as it deviates from the simulated properties of the sum pattern shown in Figure 5-21 by an acceptable margin of 15%. Nonetheless, it is worth noting that the discrepancy between the measurement and simulated properties of the antenna performance are also contributed due to several factors, which are outlined and described in Section 6.3.2.2. The measured and simulated properties of the sum pattern produced when a feed tilt of 1.3 degrees is applied are presented in Table 6-8.

Sum Beam Properties	On-axis Gain (dB)	Beamwidth (deg)
Measurement	31.5	3.36
Simulation	32.8	3.77

Table 6-8. Sum beam properties corresponding to a feed tilt of 1.3 degrees

Based on the antenna measurements obtained, the sum pattern beamwidth is 2.15 times wider than the azimuthal beamwidth of the center-fed reflector antenna (1.56 degrees), which infers the angular resolution of the monopulse antenna to be 2.15 worse than the resolution of the center-fed reflector antenna. Subsequently, the on-axis gain is approximately 1.7 dB lower than the gain of the measured center-fed reflector antenna (33.2 dBi). Nonetheless, as mentioned, this is usually not an issue providing the gain is still sufficiently high (>30 dBi) for most operational detection range. Moreover, since its sole purpose is for identifying the presence of a target that is visible to the radar, a high angular resolution is often not required.

On the other hand, the family of difference pattern in Figure 6-41 shows that the on-axis difference slope decreases with increasing feed tilt applied, although the slope of the respective patterns has nearly negligible difference from one another. Thus, the angular accuracy of the manufactured monopulse antenna, corresponding to each feed tilt applied, is very similar to one another. The family of difference patterns obtained from the antenna measurements are highly favourable as the properties conforms closely to that of the simulation results presented in Figure 5-22. The sharp null or large on-axis slope of the family of difference pattern obtained infers that the angular accuracy of the monopulse antenna is enormously superior as compared to that of the original center-fed reflector antenna, which is highly critical for accurate target imaging and tracking. This provides the operator with the positional information of the tracked target that is accurate to within a fraction of a beamwidth of the simultaneous lobes produced.

Given that the monopulse antenna is used in transmit and receive modes (i.e. monostatic radar), the criterion for optimization of the squint angle depends if the angular accuracy or detection sensitivity of the radar antenna is prioritized. However, apart from the radar function that is to be optimized, Section 5.1.3.1 has shown that the optimization of the squint angle also depends on the type of target of interest; whether it is an active or passive one. For the detection of both types of target, the monopulse antenna measurements across the range of feed tilts applied shows that the optimum feed tilt that would maximize the detection sensitivity of the monopulse antenna is 1.3 degrees, or the smallest possible feed tilt that can be applied, from which the sum pattern beamwidth is the narrowest and the on-axis gain is the highest achievable.

On the other hand, if optimizing the angular accuracy of an antenna for targets on or near the boresight is prioritized instead, the optimum feed tilt that achieves this may differ for an active and passive type of target, as discussed in Section 5.1.3.1, which is also dependent on the monopulse feed design. For the detection of a passive target that merely scatters or reradiates the power incident on it, the transmission-pattern gain of the radar antenna influences the antenna accuracy primarily due to errors from thermal noise. The angular accuracy of the monopulse antenna for detection and tracking of a passive target located on or near the boresight axis is optimized by identifying the feed tilt that minimizes the single-pulse angle error σ_θ due to thermal noise, which is achieved by maximizing the product of the on-axis difference slope and on-axis sum voltage gain [38], as derived from (5-10) to (5-12). Based on the family of sum and difference patterns obtained (Figure 6-41) this is achieved when a feed tilt of 1.3 degrees is applied since the variation in on-axis difference slope is very minimal across the family of difference patterns obtained, while the on-axis sum gain is considerably higher at this feed tilt as compared to the other feed tilts applied. Consequently, when dealing with an active target the transmission-pattern gain of the antenna has no effect on the angular accuracy. Thus, applying the feed tilt that maximizes the on-axis slope of the difference pattern is desirable to minimize the angular error measurement, which in this case is achieved when a feed tilt of 1.3 degrees is applied.

The measured sum and difference patterns of the monopulse antenna obtained shows that the optimization of the angular accuracy for tracking of active and passive targets is achieved when an angular displacement of 1.3 degrees is applied on the pair of feed horn. Moreover, the results show that the proposed dual-horn feed arrangement enables the detection sensitivity and angular accuracy for both active and passive target types to be optimized simultaneously. The measured monopulse patterns of the monopulse reflector antenna employing the proposed dual-horn feed design closely agrees with the modelling of the antenna provided in Section 5.1.3.

6.3.2.2 Discrepancy Between Measurement and Simulation Results

The discrepancy between the antenna beam properties obtained from the antenna measurements performed in the far-field X-band antenna characterization range (Section 6.3) and the corresponding simulation counterpart in CST (Section 4.4) are due to several notable factors, which will be outlined in this section.

Firstly, the simulation of the antenna performance provided from CST had made a few assumptions on the reflector antenna modelling, which have caused the parametric conditions to differ from that of a practical antenna measurement in a far-field antenna range. In the simulations of the antennas performed using CST, the antenna models were created with the assumption of the material being a Perfect Electrical Conductor (PEC), whereas the manufactured reflector was fabricated through 3D printing technology using ABS plastic and coated with a copper compound spray to achieve the metallic properties. Hence, the reflector surface does not exhibit the properties of a PEC although it has a very high electrical conductivity. Secondly, the reflector created in CST assumed a 100% surface accuracy (i.e. no surface roughness), and therefore the shape of the modelled reflector conformed exactly to a circular parabola. Hence, the simulation did not account for this factor that causes a slight reduction in antenna gain. Finally, although the reflector antenna utilises a very narrow feed and reflector support (i.e. less than 10 cm), these supports were not included in the simulation of the reflector antenna because the support designs were not yet finalised during the modelling stage of the antenna. Hence, the simulation did not account for the minimal additional aperture blockage due to the feed support, which may have affected the antenna beam properties by a very slight amount. These minor assumptions, or differences, between the simulation and measurement conditions causes a slight discrepancy on the antenna beam properties obtained from both measurements, which explains for the more desirable antenna performance obtained from the simulation results.

6.4 Summary

This section has presented the validation of the CST simulations from Chapters 4 and 5 by means of practical measurements of the respective components and physical model of the antennas. In Section 6.1, it has verified the suitable transition design for a WR90 adapter that optimizes the RF performance of the horn antenna at an operating frequency of 9.2 GHz.

In Section 6.2, some of the most common methods of manufacturing medium to large sized reflectors were outlined, from which the pros and cons of each method were described. There is inevitably a trade-off between manufacturing a cost-effective and lightweight reflector

of a certain size and achieving very high surface accuracy. Nonetheless, the vertically truncated reflector designed in this project was manufactured through 3D printing technology and coated with an electrically conductive spray, from which the measurement results of the antenna far-field radiation pattern presented in Section 6.3 has proven it to be a viable method of manufacturing. It has been shown that the use of 3D printing technology allows an easy and highly flexible manufacturing process of large antennas, which is significantly cost-effective and yet produces much lighter systems.

Section 6.3 had discussed the outdoor test range facility used to measure the far-field radiation pattern of a E-plane sectoral horn antenna, a center-fed reflector antenna, and lastly the amplitude-comparison monopulse reflector antenna. Each of the antennas were manufactured according to their respective designs that were provided in Chapters 4 and 5. In particular, the modelling of the dual-horn feed arrangement that was proposed to create a monopulse reflector antenna was successfully validated by the desirable measurement results presented in this chapter.

Chapter 7

Conclusions and Future Work

Improvements in the detection performance of a mechanically scanning reflector antenna, particularly the angular resolution and accuracy of target measurements, without increasing the size of the reflector size is a predominantly complex problem in the early generations of such systems. The vast requirement has initiated decades of research within the radar industry, which have resulted in the emergence of new and innovative angle refinement measuring methods used for imaging and tracking applications within FMCW radars. The research provided in this thesis is a topic requiring continuous research to provide alternative approaches to the issues faced in existing methodologies, and the continuous advancement in feed design configurations and signal processing methods for such antennas are usually based on conventional designs which have previously been shown to limit antenna performance. Most of the work presented in this thesis are supported and justified based on theoretical calculations and simulations performed on CST and MATLAB. Based on these results obtained the proposed monopulse feed design and signal processing technique will be implemented to existing radar systems.

The research topic is initiated based on optimistic ideas to provide alternative antenna systems to current existing radar systems employing large phased array and reflector antenna systems, which are used to provide and fulfil surveillance and security requirements along the Strait of Malacca. These ideas were developed to realistically achievable methods, which are those proposed in this thesis. The improvements on the existing radar systems were to be notably achieved from the perspective of enhancing the resolution and accuracy of a given reflector antenna without increasing the reflector aperture, while simultaneously reducing the cost and weight of the antenna. This chapter highlights the conclusion drawn from the key areas of the project.

There are many potential areas which can be expanded upon using the framework provided within this thesis. A number of following areas could be explored in order to add to

the findings of this research project as future work. These are discussed in Section 7.2 with the aim of providing future researches a starting point.

7.1 Conclusions

This research project has developed a dual-horn feed design through CST based modelling for a monopulse antenna employing a vertically truncated parabolic reflector that achieves significantly enhanced angle sensing capabilities in one-coordinate. The proposed monopulse feed design was developed based on the modelling and corresponding simulations of the properties of the sum and difference patterns obtained from the dual-horn feed configuration, and successful validation of the monopulse antenna design and a number of other simulation results was accomplished through measurements of the antenna far-field radiation pattern, which was performed in QinetiQ far-field antenna characterization range.

The monopulse reflector antenna designed for this project was manufactured through 3D printing technology. The use of this technology for electrically large antennas operating at microwave frequencies has limited exposure due to the various reasons that were mentioned in Section 6.2.1.1. The vertically truncated parabolic reflector manufactured using a 3D printer, fabricated from a type of plastic (ABS) and coated with a silver copper screening compound, has shown to exhibit sufficiently high surface accuracy at the X-band frequency range, conductivity and performance (based on the measured far-field antenna patterns). The assembly of the feed and reflector using specifically designed aluminium profile systems created a framework for the reflector antenna that was very low-cost and low-weight as compared to similar sized reflector antennas that are fabricated entirely out of metal through conventional machining methods.

As part of this research, a novel signal processing technique was introduced to further enhance the resolution performance of new and existing antenna systems. MATLAB codes have been developed to create the algorithm that implements the underlying principles and methods of the proposed differential processing technique (Appendix B). The codes will enable the proposed technique to be applied, or rather simulated, on any given radar output. As demonstrated in this thesis, the processing technique was applied on several functions that are accurate representation of typical antenna far-field patterns in order to evaluate the benefits offered and be able to optimize the positive effects of the technique. Based on simulation results the processed radar output has shown to offer substantial improvements on the resolution performance, the maximum clutter-limited detection range and signal to noise ratio of the radar, although the enhancement in detection performance is dependent on the characteristics of the antenna pattern and sampling interval of the data measured.

7.2 Future Work

New ideas or closely related area of interest supporting the existing work performed will be regarded as an extension of a topic that has been established, and will be briefly discussed in this section. The future work planned to realize the full potential and significance of the proposed research are as follows:

7.2.1 Field Trials of the Developed Radar System

This thesis has provided the modelling and design of the proposed dual-horn feed system for monopulse antennas employing a vertically truncated reflector, from which a prototype of the reflector antenna was manufactured. The measured monopulse patterns of the reflector antenna has proven to successfully validate the simulation of the antenna design on CST. The successive plan of the work is to integrate the antenna system onto the FMCW radar hardware provided by Guidance, from which, in the near future, the prototype of the FMCW radar system employing the proposed monopulse antenna system can be implemented and trialled in one of the more accessible radar sites along the coast of the Strait of Malacca, or the Sunda Strait, to evaluate the monopulse patterns and its detection performance for target imaging and tracking under real conditions. The local authorities have granted permission to perform experimental measurements of the mechanically scanning radar system developed in this project.

7.2.2 Optimizing Scan Rate of Mechanical Scanning Radar

Another interesting concept is the idea of using a rather unique mechanical orientation of the radar system that is suitable for applications, such as coastal surveillance, that only requires to scan over a limited sector of interest (i.e. ± 80 degrees with respect to the nominal axis of the radar), instead of the full complete rotation. Existing mechanical radar systems scans across a complete rotation, and therefore, for applications such as coastal surveillance that is required to monitor only a certain section of the strait, this means that slightly more than half of the scan is not of interest and is essentially wasted. Several methods of implementing a mechanical scanning system that removes the wastage of power while increasing the scan rate of the antenna by a factor of two have been innovated and analysed, which in theory can be implemented without increasing the rotational speed of the scanning antenna and without reducing the lifetime of the antennas rotational movement. From the various unique reflector antenna arrangements evaluated, which have not been elaborated in this thesis, one arrangement in particular has appeared to be a viable proposal that may be implemented successfully for future 2D scanning radars employing a reflector antenna.

The proposed reflector antenna system that can obtain two scan rates in a single rotation is achieved by through the implementation of a two-antenna system that is positioned back to back, one facing forward and the other in the opposite direction (backward). The system functions with two identical antennas, Antenna A and Antenna B, perform one 180 degree scan respectively one after another. A simple illustration of the two-antenna system is presented in Figure 7-1.

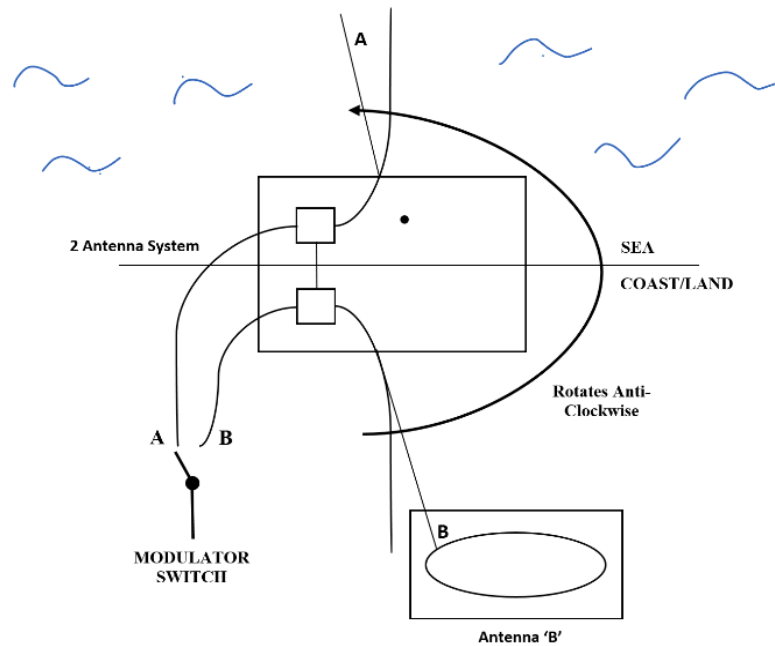


Fig 7-1. Two-antenna system operated by a switch after every half rotation

As the radar base rotates, antenna A would perform the first half of the complete rotation followed by antenna B which would scan the second half. When Antenna A is facing towards the sea, the system is designed to automatically switch into position A of the modulator in order for Antenna A to be active and operate across half a rotation, and likewise for Antenna B as well. Hence, a switch that is in perfect synchronization with the radar system must be used to accurately operate each antenna individually in a consecutive manner between every half of a rotation, such that only one antenna is functional and scanning at any point of time, and neither of the antenna would be transmitting towards the direction facing the coast. Implementing this dual antenna arrangement essentially obtains two scans worth of information within a single rotation. Hence, the system will get two passes in the beam every 360 degrees, that is, successfully providing twice the update rate of conventional scanning radar systems without having to increase the scan period and having to reverse the direction of the rotating radar base after every half rotation.

7.2.3 Pattern Selective Differential Processing in RF Hardware

The algorithm that performs the proposed differential processing technique was created in the form of MATLAB codes which, thus far, has only been simulated and applicable for the detection of a point-target subject to a high SNR (i.e. low sea clutter). Based on the algorithm provided in this thesis, the MATLAB codes can be refined further to become more adaptable to any arbitrary signal it receives from the radar output, which includes the detection of extended and distributed types of target. Once the algorithm is refined, the sequence of pattern selective differential processing may then be adopted directly into RF, such as in the form of a digital signal processing box, so that it can be interposed directly between the radar output and display to realize and evaluate its importance on the detection performance of surveillance and navigation radars, in particular, which is expected to make a major contribution towards the objectives of the application in hand. Due to its great potential and demand for new and existing radar systems, implementing the proposed processing technique in RF can be ventured into as future work. The architecture that implements the algorithm in RF is illustrated by a simple schematic of the hardware (Figure 7-2). Nonetheless, other applications of differential processing may result in requiring a more refined implementation.

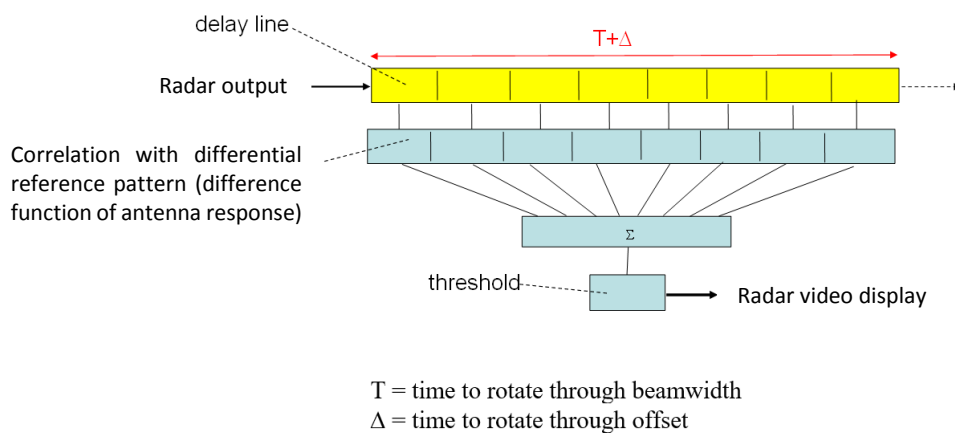


Fig 7-2. Schematic of hardware implementing pattern selective differential processing

Bibliography

- [1] Patrick, W., "Strait of Malacca Is World's New Piracy Hotspot". *NBC News*, Mar. 14, 2017.
- [2] "Malay Archipelago". *The Maritime Heritage Project*. Mar. 14, 2017.
- [3] *Freeman, D. B., The Straits of Malacca: Gateway or Gauntlet?*. McGill-Queen's-University Press., 2003.
- [4] Tarrant, B., "Balancing powers in the Malacca Strait," *Reuters News Agency*, Mar. 7, 2010.
- [5] "*International - U.S. Energy Information Administration (EIA)*". Nov. 22, 2014.
- [6] "*Strait of Malacca - World Oil Transit Chokepoints*", Energy Information Administration, U.S. Department of Energy, Aug. 1, 2017.
- [7] Gran, S., "MALACCA: The Impact of Transportation on Wildlife in the Malacca Straits," *Trade Environ. Database Case Studies*, vol. 9, no. 3, p. 573, Sep. 1999.
- [8] Chen, T. P., "Prevention Measures in the South East Asia Region," in *Proc. SPILLCON, Aust. Inst. Petroleum Conf.*, Melbourne, Australia, 2000.
- [9] Anderson, S. J., "A Parametric Wave Spectrum Model for HF Radar Applications," *Australian Defence Sci. Technol. Org.*, Edinburgh, SA, Australia, Tech. Rep., 2012.
- [10] Hancock, B., "Singapore Raises Terror Alert on Malacca Strait, one of the World's Most Important Shipping Lanes," *Christian Sci. Monitor*, Mar. 5, 2010.
- [11] Raymond, Catherine (2009). "Piracy and Armed Robbery in the Malacca Strait: A Problem Solved?". *Naval War College Review*. 62: 31–42 – via Proquest.
- [12] "*Piracy down 3rd year in row: IMB report.*", *Journal of Commerce*, Jan. 23, 2007.
- [13] Brandon, J. J., "Reducing Piracy in Southeast Asia," *The Asia Foundation*, Aug. 2009.

- [14] Hoffman, E., "Piracy in Asia: Background report", *Bergen Risk Solutions*, Bergen, Norway.
- [15] Posada, M., Greidanus, H., Alvarez, M., Vespe, M., Cokacar, T. and Falchetti, S., "Maritime Awareness for Counter-Piracy in the Gulf of Aden," *European Comiision – Joint Research Center*, Ispra, Italy., 2011.
- [16] Coastal Surveillance. <https://saab.com/security/maritime-traffic-management/coastal-surveillance/coastal-surveillance/>. [Online] [Accessed Feb 2016].
- [17] Coastal Surveillance Radar. <https://www.kelvinhughes.com/maritime/coastal-surveillance-radar>. [Online] [Accessed Feb 2016].
- [18] Anderson, S. J., "Optimizing HF Radar Siting for Surveillance and Remote Sensing in the Strait of Malacca," *IEEE Transactions on Geoscience and Remote Sensing*, vol. 51, pp. 1805-1815, no. 3, Mar. 2013.
- [19] "Drastic Drop in Piracy in Malacca Straits," *MaritimeSecurity.Asia*, Apr. 21, 2011. <http://maritimesecurity.asia/free-2/piracy-2/drastic-drop-in-piracy-in-malacca-straits/>. [Online] [Accessed Feb 2016].
- [20] Cornwall to communicate with MARS: Goonhilly will host the world's first commercial communications station that can track deep space missions. <https://www.dailymail.co.uk/sciencetech/article-5421677/Cornwall-host-deep-space-communications-station.html> [Online] [Accessed Jan 2017].
- [21] Iran Unveils Advanced Radar System, *Tasnim News Agency*, Nov. 27, 2017. <https://www.tasnimnews.com/en/news/2013/11/27/204234/iran-unveils-advanced-radar-system>. [Online] [Accessed Jan 2017].
- [22] Parsa, A. and Hansen, N. H., "Comparison of Vertically and Horizontally Polarized Radar Antennas for Target Detection in Sea Clutter – An Experimental Study," *R&D Department, Rutter Inc.*, Newfoundland and Labrador, pp. 0653-0658, 2012.
- [23] Thao, L. Q., Loc, D. Q. and Tuyen, N. X., "Study Comparative of Parabolic and Phased Array Antenna," *VNU Journal of Science: Mathematics – Physics*, Vol. 30, No. 3 (2014) 31-36, Sept. 2014.
- [24] Mahafza, B. R., *Radar Systems Analysis and Design using Matlab*, Chapman & Hall/CRC Press, 3rd ed., 2013.
- [25] Skolnik, M. I., *Radar Handbook*, New York: McGraw Hill, 3rd ed., 2008.

- [26] Jayaprakash, A., Reddy, G. R. and Prasad, N. S. S. R. K., "Small target detection within sea clutter based on fractal analysis," *ICETEST - 2015*, Procedia Technology, Vol. 24, pp. 0988-0995, 2016.
- [27] Blake, L. V. and Long, M. W., *Antennas Fundamentals, Design, Measurement*, SciTech Publishing, Inc., 3rd ed., 2009.
- [28] Kirkpatrick, G. M., "Aperture Illumination for Radar Angle-of-Arrival Measurements," *Trans. IRE Professional Group on Aeronautical and Navigational Electronics*, Vol. PGAE-9, pp. 20-27. Sep. 1953.
- [29] Blair, W. D., Richards, M. A. and Long, D. A., *Principles of Modern Radar: Basic Principles*, Institution of Engineering and Technology, 2010.
- [30] Skolnik, M. I., *Introduction to Radar System*, New York: McGraw Hill, 3rd ed., 2001.
- [31] Leonov, A. I. and Formichev, K. I., *Monopulse Radar*, Norwood: Artech House, 1986.
- [32] IEEE Standard 100, *The Authoritative Dictionary of IEEE Standards Terms*, 7th ed., New York: IEEE Press, 2000.
- [33] Bonefacic, D., Jancula, J. and Majuree, N., "Model of a Monopulse Radar Tracking System for Student Laboratory," *Radioengineering*, University of Zagreb (Croatia) & University of Massachussetts (USA), vol. 16, no. 3, pp. 062-067, Sep. 2007.
- [34] Angle Tracking. <http://www8.cs.umu.se/research/ifor/dl/Sensors/radar/Tracking.pdf>. [Online] [Accessed Apr 2018].
- [35] Griffiths, H. D. and Woodbridge, K., *MSc Module Lecture Notes: Radar Systems*, University College London, 2016.
- [36] Gilson, W. H., "Relationships Between Average Radar Power and Steady-State Track Accuracy," *Department of the Navy under Air Force Contract F19628-90-C-0002*, pp. 24-25. 1991.
- [37] Alimenti, R. J., Fox, D. P. and Kenton, J., *FAA Technical Center Letter Report*, U. S. Department of Transportation. Jul. 1982.
- [38] Sherman, S. M. and Barton, D. K., *Monopulse Principles and Techniques (Second Edition)*, Norwood: Artech House, 2011.
- [39] Chotaliya, B. M. and Polara, S., "The Comparison of Two Monopulse Tracking Systems: Four-Horn and Multimode (based on the simulation results of HFSS),"

International Journal of Computer Trends and Technology (IJCTT), vol. 4, issue 9, Sep. 2013.

- [40] Darwish, M. M, Ahmad, H. N. and El-Tager, A. M., "Multimode Antenna Feed System for an X-Band Monopulse Radar," *IEEE Radar Conference (2009)*., Pasadena, USA, May. 26, 2009.
- [41] Darwish, M. M., "Modal Analysis of an Antenna Feed System for a Multimode Monopulse Radar," *The 2009 International Symposium on Antennas and Propagation (ISAP 2009)*., Bangkok, Thailand, Oct. 20-23, 2009.
- [42] Petrie Meyer, Christopher A Vale, Werner Steyn, "On the design of waveguide devices using multiple propagating modes,". 6th International Conference on Telecommunications in Modern Satellite, Cable and Broadcasting Service, TELSIKS 2003.
- [43] EA3462 X-Band Antenna. <https://www.easat.com/products/ea3462>. [Online] [Accessed Mar 2016].
- [44] Automatic Range Tracking. http://www1.labvolt.com/publications/Exercises/38545-00_3.pdf. [Online] [Accessed Sep 2017].
- [45] Balanis, C.A., *Antenna Theory: Analysis and Design*, New Jersey: Wiley & Sons, 3rd ed., 2005.
- [46] Volakis, J. L., *Antenna Engineering Handbook*, New York: McGraw Hill, 4th ed., 2007.
- [47] Wentworth, S. M., *Fundamentals of Electromagnetics with Engineering Applications*, New Jersey: Wiley & Sons, 2004.
- [48] Christodoulou, C. G. and Wahid, P. F., *Fundamentals of Antennas: Concepts and Applications*, Washington: SPIE Press, 2001.
- [49] Saunders, S. R. and Aragon-Zavala, A., *Antennas and Propagation for Wireless Communication Systems*, Chichester: Wiley & Sons, 2nd ed., 2007.
- [50] Brennan, P., *MSc Module Lecture Notes: Antennas and Propagation*, University College London, 2016.
- [51] Rudge, A. W., Milne, K., Olver, A. D. and Knight, P., *The Handbook of Antenna Design - Volume I*, London: Peter Peregrinus Ltd, 1982.
- [52] Silver, S., *Microwave Antenna Theory and Design*, London: Peter Peregrinus Ltd, 1997.

- [53] Bansal, R., *Fundamentals of Engineering Electromagnetics*, Florida: Taylor and Francis Group, 2006.
- [54] Wentworth, S. M., *Fundamentals of Electromagnetics with Engineering Applications*, New Jersey: Wiley & Sons, 2004.
- [55] Besser, L. and Gilmore, R., *Practical RF Circuit Design for Modern Wireless Systems – Volume I*, Massachusetts: Artech House, 2003.
- [56] Milligan, T. A., *Modern Antenna Design*, New Jersey: John Wiley & Sons, 2nd ed., 2005.
- [57] Fusco, V. F., *Foundation of Antenna Theory and Techniques*, Essex: Pearson, 2005.
- [58] Collin, R. E., *Antennas and Radiowave Propagation*, McGraw Hill, 1985.
- [59] Tirro, S., *Satellite Communication Systems Design*, New York: Plenum Press, 1993.
- [60] Evans, B. G., *Satellite Communication Systems*, London: The IET, 3rd ed., 2008.
- [61] Drabowitch, S., Papiernik, A., Griffiths, H. D., Encinas, J. and Smith, B. L., *Modern Antennas*. Netherlands: Springer, 2nd ed., 2005.
- [62] J. S. Seybold, *Introduction to RF Propagation*, John Wiley and Sons, pp. 55–58, 2005.
- [63] *Electronic Warfare and Radar Systems Engineering Handbook*. Avionics Department AIR-4.5, Washington, D.C., Apr. 1999.
- [64] Nikolova, N. K., *Lecture 18: Horn Antennas (Rectangular horn antennas. Circular apertures.)*, McMaster University, pp. 10-15, 2016.
- [65] Love, A. W., “Horn Antennas,” *Antenna Engineering Handbook*, McGraw-Hill, pp. 15-6, 1993.
- [66] Antenna Gain Formulas.
<http://user.engineering.uiowa.edu/~ece195/2006/docs/AntennaFormulas.pdf>. [Online] [Accessed Jul 2016].
- [67] Kingsley, S. and Quegan, S., *Understanding Radar System*, SciTech Publishing, Inc., 1999.
- [68] Adams, R. J. and Kelleher, K. S., “Pattern Calculation for Antennas of Elliptical Aperture,” *Proceedings IRE*, vol. 38, pp. 1052, Sep. 1950.
- [69] Dobricic, D., “3D Corner Reflector Antenna as an Efficient Feed for Offset Parabolic Antennas for 5.8 GHz,” *antenneX Online*, Issue 126, Oct. 2007.

- [70] Pozar, D. M., *Microwave Engineering*, Reading: Addison-Wesley, 1993.
- [71] CST STUDIO SUITE® 2014 – 3D Electromagnetic Simulation Software. <https://files.vogel.de/vogelonline/vogelonline/companyfiles/7128.pdf>. [Online] [Accessed Nov 2015].
- [72] “Broadband Radar,” *RYA*, 2017.
- [73] Patel, A., “Signal Generation for FMCW Ultra Wide-band Radar,” University of Kansas School of Engineering, Jan. 2009.
- [74] Vijayachitra, S., *Communication Engineering*, Tata McGraw-Hill Education, 2013.
- [75] Watts, S., “Optimum Radar Polarization for Target Detection in Sea Clutter,” *IEEE Colloquium on Polarization in Radar*, pp. 4/1-4/5, 1996.
- [76] Pace, P. E., *Detecting and Classifying Low Probability of Intercept Radar*, Norwood: Artech House, pp. 101-105, Oct. 2003.
- [77] Lipa, B. J. and Barrick, D. E., *FMCW Signal Processing*, Mirage Systems, California.
- [78] Waveguide to coax transitions. <https://www.microwaves101.com/encyclopedias/waveguide-to-coax-transitions> [Online] [Accessed May 2016].
- [79] Wade, P., “Rectangular Waveguide to Coax Transition Design,” pp. 10-17, Dec. 2006.
- [80] Waveguide Horn Antennas – Sectoral Horn Antennas. <https://www.atmmicrowave.com/waveguide/horn-antenna-sectoral/> [Online] [Accessed May 2016].
- [81] Straw, R. D., *The ARRL Antenna Book*, USA: American Radio Relay League. pp. 18.14, 19th ed., Sep. 2000.
- [82] Cutler, C. C., “Parabolic-Antenna Design for Microwaves.” *Proc. IRE*, vol. 35, No. 11, pp. 1284-1294, Nov. 1947.
- [83] Crompton, J. W., “On the Optimum Illumination Taper for the Objective of a Microwave Aerial.” *Proc. IEEE*, vol. 101, Pt 3, Nov. 1954.
- [84] *Antenna Introduction / Basics*, University of Hawaii at Manoa.
- [85] Lo, Y. T., “On the Beam Deviation Factor of a Parabolic Reflector,” *IRE Trans. on Antennas and Propagation*, vol. 8, pp. 347-349, May. 1960.

- [86] Nessmith, J. T. and Sherman, S. M., "Phase Variations in a Monopulse Antenna," *Record of the IEEE 1975 International Radar Conf.*, Washington, D.C., pp. 354-359, Apr 21-23. 1975.
- [87] Benjamin, R., "Differential Radar or Sonar Video Processing for Clutter Resilience and Enhanced Resolution," 2017.
- [88] Advanced Calibration Techniques for Network Analyzers, *Modern Measurement Techniques for Testing Advanced Military Communications and Radars, 2nd Edition*, Agilent Technologies, Inc. 2006.
- [89] Vector Network Analyzer Calibration – National Instruments. <http://www.ni.com/tutorial/14114/en/#toc3>. [Online] [Accessed Mar 2018].
- [90] R&S® ZNB Vector Network Analyzer. https://www.rohde-schwarz.com/uk/product/znb-productstartpage_63493-11648.html. [Online] [Accessed Mar 2018].
- [91] Measurement Errors in a Vector Network Analyzer. http://na.support.keysight.com/pna/help/latest/S3_Cals/Errors.htm#errsrcmtch. [Online] [Accessed Jan 2018].
- [92] Aluminium Parabolic Antenna Reflectors / Satellite Communication Dishes. <https://www.helandermetal.com/parabolic-antenna-satellite-communication-industry>. [Online] [Accessed Dec 2016].
- [93] *Antenna Mesh AL 7210 (7ft)*, PT. Subur Semesta, Indonesia.
- [94] Lavado, A. R., Munoz, L. E. G., Botello, G. S. and Vargas, D. S., "Low-Cost and Low-Weight Horn and Reflector Antennas through 3D Printing," *Universidad Carlos III de Madrid*, Jul 23. 2018.
- [95] Willis, S., "The maker revolution," in *Computer*, *IEEE Computer Society*, vol. 51-3, pp. 62-64, 2018.
- [96] Kimionis, J., Isakov, M., Koh, B. S., Georgiadis, A. and Tentzeris, M. M., "3D printed Origami Packaging with inkjet-printed antennas for RF harvesting Sensors," *IEEE Transactions on Microwave, Theory and Techniques*, MTT-63, vol. 12, pp. 4521-4532, Dec. 2015.
- [97] Tawk, Y., Chahoud, M., Fadous, M., Constantine, J. and Christodolou, C. G., "The miniaturization of a partially 3D printed quadrifilar helix antenna," *IEEE Transactions on Antennas and Propagation*, TAP 65, vol. 10, pp. 5043-5051, Oct. 2017.

- [98] McKerricher, G., Titterington, D. and Shamim, A., "A fully inkjet printed 3D honeycomb inspired patch antenna," *IEEE Antennas and Wireless Propagation Letters*, AWPL 15, pp. 544-547, 2016.
- [99] Castro, A. T., Babakhani, B. and Sharma, S. K., "Design and Development of a multimode waveguide corrugated antenna using 3D printing technology and its comparison with aluminum based prototype," *IET Microwaves, Antennas and Propagation*, MAP-14, vol. 11, pp. 1977-1984, Nov. 2017.
- [100] Nayeri, P., Liang, M., Sabory-Garca, R. M., Tuo, M., Yang, F., Ghehm, M., Xin, H. and Elsherbeni, A. Z., "3D printed dielectric reflectarrays: low cost high gain antennas at submillimeter waves," *IEEE Transactions on Antennas and Propagation*, TAP62, vol. 4, pp. 2000-2008, Apr. 2014.
- [101] Boustead, I., *Acrylonitrile-Butadiene-Styrene Copolymer (ABS)*, Plastics Europe, Mar. 2005.
- [102] Copper vs. Aluminum Conductors. https://www.anixter.com/en_uk/resources/literature/wire-wisdom/copper-vs-aluminum-conductors.html [Online] [Accessed Sep 2017].
- [103] RS PRO 247-4251 Copper Compound Spray. <https://www.ie.rs-online.com/mobile/p/shielding-aerosols/2474251/> [Online] [Accessed Mar 2018].
- [104] Skin Depth Calculator. <https://www.pasternack.com/t-calculator-skin-depth.aspx> [Online] [Accessed Oct 2016].
- [105] Price compare – 3D printing materials – Filament:. <https://www.3ders.org/pricecompare/?o=Diameter&sc=UK&cg=Blue&m=ABS> [Online] [Accessed Mar 2018].
- [106] J. Ruze, "Antenna tolerance theory—a review", *IEEE*, vol. 54, pp. 633-640, Apr. 1966.
- [107] Valuframe – The Economy Aluminium Profile Systems. <http://www.valuframe.co.uk/> [Online] [Accessed Dec 2017].
- [108] Harre, I., "Experimental study of the radar cross section of maritime targets," *Electronic Circuits and Systems*, Vol. 2, No. 4, 2004.

Appendix A

Radar Transmit Power Budget Analysis

Ship RCS Table
(Source: Williams/Cramp/Curtis: Experimental study of the radar cross section of maritime targets, Electronic Circuits and Systems, Vol. 2, No. 4, July 1978, amended by I. Harre, 2004)

Target Ship			Median radar cross section of target vessel, m ²								approx. min. RCS	approx. max. RCS
Type	Overall length (m)	Gross tonnage	10	100	1,000	10,000	100,000	1,000,000	10,000,000			
Inshore fishing vessel	9	5	■							3	10	
Small coaster	40-46	200-250		■	■					20	800	
Coaster	55	500		■	■					40	2,000	
Coaster	55	500			■	■				300	4,000	
Coaster	57	500			■	■				1,000	16,000	
Large Coaster	67	836-1,000			■	■				1,000	5,000	
Collier	73	1,570			■	■				300	2,000	
Warship (frigate)	103	2000*				■	■			5,000	100,000	
Cargo liner	114	5,000				■	■			10,000	16,000	
Cargo liner	137	8,000				■	■			4,000	16,000	
Bulk carrier	167	8,200			■	■				400	10,000	
Cargo	153	9,400			■	■				1,600	12,500	
Cargo	166	10,430			■	■				400	16,000	
Bulk carrier	198	15,000-20,000			■	■				1,000	32,000	
Ore carrier	206	25,400			■	■				2,000	25,000	
Container carrier	212	26,436**			■	■				10,000	80,000	
Medium tanker	213-229	30,000-35,000			■	■				5,000	80,000	
Medium tanker	251	44,700			■	■				16,000	1,600,000	

* Displacement
 ** Considerable deck cargo

S = stern on
 Q = quarter
 B = broadside
 BW = bow
 BWO = bow on
 n = near

Table A-1. Ship RCS table [108]

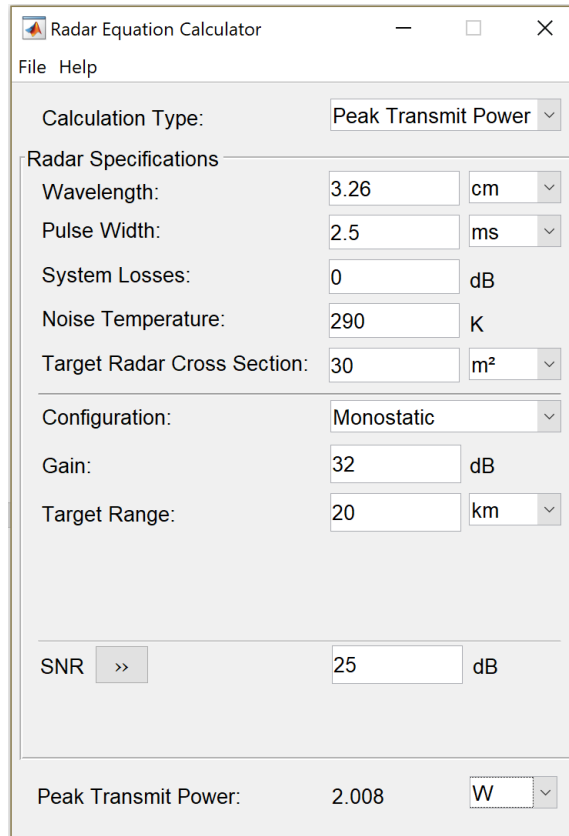


Table A-2. MATLAB Radar Equation Calculator

Target Range (km)	Transmit Power (W)	SNR (dB)	Target RCS (m2)
10	3	25	1.3
20	3	25	20
30	3	25	100
40	3	25	320
50	3	25	780

Table A-3. Radar transmit power budget analysis

Appendix B

MATLAB Based Algorithm of the Signal Processing Techniques

B.1 Pattern Selective Differential Processing

The following code has been simplified to apply the differential processing technique to a received signal concerning the detection of a point-target. The example shown simulates the far-field patterns, or antenna responses, of several line source antennas with common linear aperture distributions, notably rectangular, triangular, cosine and cosine squared.

```
clear all
close all

deltatheta=0.01;
theta=-180:deltatheta:180-deltatheta;

BW=4; %set antenna response beamwidth to 4 deg.

% Parameters to define -3 dB beamwidth and spacings (for 50% peak
difference) of the far-field antenna patterns corresponding to each
linear aperture distribution.
a=2/BW; %rectangular
a=2.86/BW; %triangular
a=2.67/BW; %cosine
a=3.23/BW; %cosine squared

% Creating far-field pattern of several linear aperture distributions.
antpattern=sinc(a*theta/pi); %rectangular
antpattern=(1-cos(a*theta))./((a*theta).^2); %triangular
antpattern=cos(a*theta)./((pi/2)^2-(a*theta).^2); %cosine
antpattern=((sin(a*theta)*pi^2)./((a*theta).*(pi^2-(a*theta).^2)));
%cosine squared

% Simulating antenna response for any antenna pattern (TX/RX pattern).
antsquared=antpattern.^2;
antsquared=antsquared/max(antsquared);
antsquared(length(theta)/2+1)=1; % avoid divide-by-zero
```

```

figure
plot(theta,antsquared)
title('Antenna pattern, original point target response')
xlabel('angle(degrees)')
ylabel('amplitude')

% Assuming the absence of noise and clutter, the detected point-target
response is equivalent to the antenna response.
detsig=antsquared; %point-target response = antenna response
OriginalBeamwidth=deltatheta*sum(1+sign(antsquared-1/sqrt(2)))/2

% Creating the correlation reference pattern corref.
% Setting the max. amplitude of correlation reference pattern to 0.5.
deltaatheta=1.95; %rectangular
deltaatheta=2.91; %triangular
deltaatheta=2.69; %cosine
deltaatheta=3.31; %cosine squared

spacing=deltaatheta/a/deltatheta;
spacing=round(spacing/2); %/2 because pattern is shifted by ±spacing

corref(1:length(theta))=0;
antsquaredposshift(1:length(theta))=0;
antsquaredposshift(1:length(theta)-
spacing)=antsquared(spacing+1:length(theta));
antsquarednegshift(1:length(theta))=0;
antsquarednegshift(1:length(theta)-
spacing)=antsquared(1:length(theta)-spacing);
corref=antsquaredposshift-antsquarednegshift;
peakdifference=max(corref);

figure
plot(theta,deltaantsquared,theta,antsquarednegshift,theta,antsquaredp
osshift)
axis([-4*BW +4*BW,-0.6,1])
title('Correlation reference pattern')
xlabel('angle(degrees)')
ylabel('amplitude')

% Make detected signal difference function.
% Since the detected target response is assumed equal to the antenna
response, deltadetsig = corref.
spacing=round(spacing/2); % /2 because pattern is shifted by ±spacing
deltadetsig(1:length(theta))=0;
deltadetsig(1:length(theta)-spacing)=-detsig(1:length(theta)-
spacing)+detsig(spacing+1:length(theta));
deltadetsig(length(theta))=0;

figure
plot(theta,deltadetsig)
axis([-4*BW 4*BW,-0.6,1])
title('Detected point target difference function')
xlabel('angle(degrees)')
ylabel('amplitude')

% Cross-correlation of reference pattern and difference function of
point-target response to create sharpened point-target response (z).

```

```

z=xcorr(deltadetsig,corref);
z=z/max(z);
z(2*length(theta))=0;

figure
plot(theta,detsig,'b')
hold on

theta(length(theta)+1:2*length(theta))=theta+360;
plot(theta-180,z,'r')
axis([-4*BW 4*BW,-0.6,1])
title('Sharpened response (red), original response (blue)')
xlabel('angle(degrees)')
ylabel('amplitude')

SharpenedBeamwidth=deltatheta*sum(1+sign(z-1/sqrt(2)))/2; %BW of
sharpened response
fracBW=SharpenedBeamwidth/OriginalBeamwidth;
sharpeningimprovementfactor=1/fracBW; %Sharpening factor of processed
response achieved

```

B.2 Sidelobe Reduction Technique

The following code has been simplified to apply sidelobe reduction technique, for $n = 3$, on an arbitrary function. In the following example, the code applies sidelobe reduction technique on the sharpened point-target response produced in the previous section. Hence, the following code is a continuation of the above and uses the same parameters.

```

% Applying SLRT for n=3 (demonstrated on antenna with rectangular
distribution - 'sinc squared' antenna response).

% Creating the appropriate correlation reference pattern for n=3. The
reference pattern is called corref3.
% Continuing from the existing code shown above:

[a,b]=max(corref);
[c,d]=min(corref);

peakdiff=abs(1.25*(d-b));
halfway=round((b+d)/2);
L=length(corref);

% for n=3, two extra lobes are introduced into both sides of the
original reference pattern, each separated at pulse length spacing in
intervals of 1/3rd the amplitude of the peak amplitude.
corref3=zeros(1,L);
corref3(1:halfway-peakdiff)=-corref(peakdiff+1:halfway);
corref3(halfway+peakdiff:L)=-corref(halfway:L-peakdiff);
corref3=corref-0.47*corref3;

theta2=-180:deltatheta:180-deltatheta;

figure
plot(theta,corref3)

```

```

axis([-4*BW 4*BW,-0.6,1])
title('Modified correlation reference pattern to reduce sidelobes')

% Cross-correlation of new reference pattern and difference function
of point-target response to produce sharpened point-target response
(zz) with suppressed sidelobes.
zz=xcorr(corref3,deltadetsig);
zz=zz/max(zz);
zz(length(theta))=0;

figure
plot(theta-180,zz,'g',theta-180,z,'r')
axis([-4*BW 4*BW,-0.6,1])
title('Sharpened response with sidelobe reduction (green), original
sharpened response (red)')
xlabel('angle(degrees)')
ylabel('amplitude')

```

Appendix C

Data Sheets

C.1 ValuFrame®

Support Frame (ValuFrame®):

- **Process:** Extruded
- **Material:** Aluminium
 - Alloy Al Mg Si 0,5 F25
 - Mechanical Details
 - Min. tensile strength Rm 20 N/mm².
 - 0,2% Min. yield point Rp 0,2 200 N/mm².
 - Elongation at rupture 10%.
 - Modulus of elasticity E approx. 70,000 N/mm².
 - Brinell hardness approx. 75 HB.
 - Surface
 - Natural colours, matt (E6/EV1).
 - Scratch and corrosion resistant.
 - Minimum layer thickness 12 µm.
 - Layer hardness 250 - 350 HV.